Investigating the mechanistic role of Ykt6 in Wnt Trafficking and Cell cycle progression

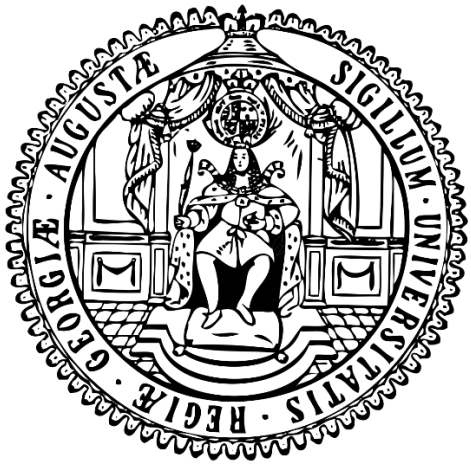

Dissertation

for the award of the degree “Doctor rerum naturalium”

of the Georg-August-Universität Göttingen

within the doctoral program Molecular Medicine

of the Georg-August University School of Science (GAUSS)

submitted by

Pradhipa Karuna M

from Coimbatore, India

Göttingen, 2021

Thesis Committee:

Prof. Dr. Julia Christina Groß

Health and Medical University Potsdam & Institute for Developmental Biochemistry

Haematology and Oncology, University Medical Center Göttingen

Prof. Dr. Holger Bastians

Institute of Molecular Oncology, University Medical Center Göttingen

Prof. Dr. Blanche Schwappach-Pignataro

Centre for Molecular Neurobiology, Universitatsklinikum Hamburg Eppendorf, Hamburg

Members of the Examination board:

Prof. Dr. Julia Christina Groß

Health and Medical University Potsdam & Institute for Developmental Biochemistry

Haematology and Oncology, University Medical Center Göttingen

Prof. Dr. Holger Bastians

Institute of Molecular Oncology, University Medical Center Göttingen

Further Members of the Examination board:

Prof. Dr. Gregor Bucher

Department of Evolutionary Developmental Genetics, Georg-August-University Göttingen

PD. Dr. Laura Zelarayán-Behrend

Institute of Pharmacology and Toxicology, University Medical Center Göttingen

Prof. Dr. Dieter Kube

Haematology and Oncology, University Medical Center Göttingen

Date of Oral Examination: 15.09.2021

This thesis is dedicated to my Parents Moureen (Amma) and Manivannan (Appa).

Acknowledgements

I would like to express my sincere gratitude to my supervisor Prof. Dr. Julia Christina Gross for providing me with the opportunity to work in her lab. I would like to thank her for her continuous support, motivation and guidance throughout these years. She is not only a great supervisor but also a mentor who always encouraged my research ideas, provided me with opportunities to collaborate and inspired me to pursue research every day. She is always available to discuss any difficulties or challenges that I faced during my PhD journey and helped me grow as a scientist with her positive spirit. I am extremely grateful and honoured to do my PhD under her guidance.

This thesis would have not been successful without the help and support of my thesis committee members Prof. Dr. Holger Bastians and Prof. Dr. Blanche Schwappach. Their in-depth knowledge and expertise in the field along with timely criticism and suggestions helped to shape my project. I would further like to thank Prof. Dr. Gregor Bucher, Prof. Dr. Dieter Kube and PD. Dr. Laura Zelarayán-Behrend for being a part of the extended thesis committee. I would like to thank the Department of Biochemistry for the productive work environment. I would like to thank the Wnt SFB1324 consortium for their funding, support and collaborations which has contributed significantly to my thesis.

I cannot thank my lab members Dolma, Leonie, Karen and Mona enough for being constantly supportive during the ups and downs of my PhD life. The morning coffee conversations have played a tremendous role in uplifting my mood and stimulated me to brainstorm ideas. I thank them for always helping me with research questions, experiments and giving me a pep talk whenever needed. I am so grateful to work with such a friendly and supportive team. I would like to thank Sabnam, Adi and Robert for contributing to significant parts of my thesis. I would further like to thank my friends Roshan, Siva, Priya, Vasan, Yaamini and Pratheebha who have made my life enjoyable in Goettingen outside of work.

I would like to extend my heartfelt gratitude to the most important people in my life, my parents and my sister Nancy who have always believed and supported me in every possible way despite the long distance. I would like to thank my greatest friend Krishnan Unni, who has been a constant pillar of support this entire journey and for always hearing me out patiently. I would like to thank my grandparents, Ralph uncle and my extended family for always motivating me to follow my dreams. My stay in Germany would not have been possible without their love, emotional comfort and encouragement every single day.

Last but not the least, I would like to thank my partner Anand, who has been with me during the best and the worst days and helped me grow every day. He has always made me feel confident in my abilities and has been by my side with his open arms.

Affidavit

I hereby declare that my doctoral thesis entitled “Investigating the mechanistic role of Ykt6 in Wnt Trafficking and Cell cycle progression” has been written independently with no other sources and aids than quoted.

Date	Signature

Declaration

I, Pradhipa Karuna M, hereby declare that the following doctoral thesis is organized into four chapters, a general abstract, introduction, results and discussion. The ‘results’ chapter consists of manuscripts either published or are in preparation for immediate submission in peer-reviewed journals.

Date	Signature

Abstract

Ykt6 is an evolutionarily conserved R-SNARE that mediates vesicle fusion events at diverse cellular compartments of secretory, endocytic and autophagy pathways. It is known to be required for the secretion of Wnts on small extracellular vesicles termed exosomes. However, the exact molecular mechanism of Ykt6 in exosomal Wnt sorting remains unclear. Employing proximity labelling, *in vivo* genetics and biochemical approaches, we identified that Ykt6 acts at the level of sorting endosome where it trafficks Wnts to the PM for extracellular Wnt release. Ykt6 is a unique SNARE that lacks a transmembrane domain and cycles between cytosol and membranes to initiate fusion events. Strikingly, blocking acidification led to an increased association of Ykt6 with membranes. Thus, it is plausible that Ykt6 gets recruited to de-acidified endosomal compartments to traffic Wnt proteins. The exact mechanism that governs this conformational switch of Ykt6 from closed, cytosolic form to open, membrane-bound form is unknown. We identified putative phosphosites in the SNARE domain, that triggers the conformational switch, thereby regulating its membrane recruitment and activity. Furthermore, we identified PDK1 to phosphorylate Ykt6 *in vitro* and successfully confirmed PDK1 to regulate its membrane recruitment. PDK1, a nutrient-sensing axis, could sense upstream metabolic cues, which in turn recruits Ykt6 to traffic Wnts. Ykt6 is an essential gene in yeast and lack of Ykt6 leads to growth defects *in vivo*. Ykt6 is highly upregulated in aggressive and metastatic tumours. Furthermore, we identified that Ykt6 KD leads to a delay in cell growth and proliferation in human colon cancer cells, which in turn leads to a delay in cell cycle progression. By single-cell transcriptomics, we identified novel Ykt6-regulated genes involved in membrane trafficking, cell cycle, and polyamine metabolism. Polyamines – putrescine, spermidine and spermine are indispensable for cell growth and proliferation. Remarkably, Ykt6 KD led to reduced expression levels of a key metabolic enzyme that acts as a global polyamine rheostat: SAT1. Concordantly, metabolomic profiling revealed lower levels of polyamines and precursor amino acids upon Ykt6 KD cells and one of the polyamines, putrescine, partially rescued the growth defects of Ykt6 KD. In conclusion, this study elucidates a hitherto unknown function of Ykt6 in modulating polyamine homeostasis during cell cycle progression, possibly via the trafficking of polyamine transporters. This fits with the previously established role of Ykt6 in the trafficking of nutrient transporters to PM and growth factors such as Wnt proteins onto exosomes. Taken together, we propose that Ykt6 acts as a valve that adapts Wnt and metabolite levels required for cell growth and therefore, a proper cell cycle progression.

Table of Contents

List of Figures

(Overall Introduction and Discussion)

1. Introduction

1.1 Cancer

Genetic alterations in our healthy body cells and tissue lead to cancer. Cancer cells are regular cells, that grow and divide continuously. While there are many drivers of genetic alternations, the major mutations implicated in the onset of cancer are proto-oncogenes and tumour suppressor genes. Proto-oncogenes are activated by mutations that cause the genes to be highly active in promoting growth and proliferation (Bishop, 1988). Tumour suppressor genes usually help to keep the growth under control and are often mutated in cancer cells by loss of function, leading to uncontrollable growth (Sager, 1986). Cancer inducing factors that occur based on exposure to the environment, chemicals, radiations during one's lifetime are called carcinogens. However, these mutations can also be inherited along the germline. Most of the cancers arise from carcinogens or errors in copying and repair mechanisms. More often, a series of mutations leads to a clone of altered cells that rapidly proliferate, escaping the regular growth checkpoints. Eventually, these cells grow into a tumour if they are not cleared by the immune system. The tumour cells migrate from their primary site and adapt to a new microenvironment through metastasis that leads to a secondary tumour at a distant site. Metastasis is a cascade of events, where the tumour cells lose cellular adhesion, increase motility, enter the circulatory system, facilitate angiogenesis and eventually colonize the secondary tissue (Fidler & George, 1980; Gupta & Massagué, 2006; Stephen Paget, 1889). Cancer cells escape immune surveillance, hijack cell cycle checkpoints and harness important signalling pathways to promote uncontrollable proliferation and metastasis. Many of these cancer-causing mutations map to signalling pathways that determine crucial processes governing the cell fate, such as cell growth, proliferation, survival, apoptosis and cell motility.

Signal transduction pathways determine the growth and development of an organism by controlling the expression of specific genes at certain stages. When extracellular molecules such as growth factors or amino acids bind to their respective cell surface receptors, the pathway is stimulated in the target cells in an autocrine or paracrine fashion. The pathways are regulated by a cascade of feedback mechanisms based on physiological responses, and aberrations in these pathways or the feedback mechanisms make them oncogenic. Most often, hyperactivation (e.g. gene amplification) and oncogenic mutations (e.g. point mutations, truncations and fusions) in these pathways fuel cancer progression (Sever & Brugge, 2015). For example, mutations in negative regulators of pathways such as PTEN and APC lead to constitutive activation of PI3K/Akt and the Wnt pathway respectively (Huang et al., 1996; Lengauer, Kinzler, & Vogelstein, 1997; Li et al., 1997). The cancer genome atlas (TCGA)

analysed somatic alterations in ten canonical pathways and 89% of the tumours had an alteration in at least one of these pathways. These include Hippo, Myc, Notch, Nrf2, PI3K/Akt, Rtk-Ras, TGF-β, p53, Cell cycle and Wnt signalling pathways (Sanchez-Vega et al., 2018).

1.2 Cell cycle

The cell division cycle is the fundamental means of propagation in all living organisms. The duration of the cell cycle differs between different species, where the cell cycle of *Drosophila* takes only 8 minutes, in contrast to a mammalian cell that takes about 24 hours. The cell division cycle comprises chromosome replication followed by their segregation to daughter cells with proper order and high fidelity (Alberts et al., 2002). The cell cycle is a precisely regulated process coordinated by various cyclins and cyclin-dependent kinases that oscillate during cell cycle progression and are cell-cycle stage-specific. The cell cycle is traditionally divided into four distinct phases called Gap 1 phase (G1), synthesis phase (S), Gap 2 phase (G2) and Mitosis (M). Briefly, at the G1 phase, the cells grow larger in size, synthesize RNA and proteins and prepare for DNA synthesis and chromosome replication during the S phase. During the S phase, DNA is replicated and the cellular contents are duplicated. At the G2 phase, the cells continue to grow and prepare for cell division. Cell division occurs at the M phase, which is the shortest, yet crucial part of the cell cycle. The M phase consists of nuclear division which includes the four phases prophase, metaphase, anaphase and telophase, followed by the cytoplasmic division phase called cytokinesis (Lodish et al., 2004; P Nurse, 1990). During prophase, the chromosomes condense and by the end of late prophase appear as thin threads called chromatids held together by the centromere. At metaphase, the chromatids line up at the equatorial plate of the mitotic spindle, which comprises microtubules and associated proteins. The kinetochore is present on the centromere region that links the chromatids to microtubule polymers reaching out from the mitotic spindle. The cells transition from metaphase to anaphase by abrupt separation of sister chromatids. Mitosis terminates with telophase which is marked by the reforming of the nuclear envelope around each set of chromosomes. This is followed by the division of cytoplasm through the formation of a cleavage furrow by a process called cytokinesis. This results in two daughter cells that have an identical genetic composition (Reviewed by Paul Nurse, 2000; Rhind & Russell, 2012).

Cell cycle progression is regulated by modulating the synthesis, activity and degradation of the cyclin-CDK complexes at every cell cycle stage. The cyclin-CDK complexes are periodically degraded by ubiquitin ligases that mark them for proteasomal degradation

(Morgan, 1995). At every stage of the cell cycle, the cell constantly monitors various internal cues such as replication errors and external cues such as the availability of growth factors and amino acids, which govern the progression to the subsequent phase. If a cell fails to meet the required criteria, it activates the immediate cell cycle checkpoint and cell cycle progression is halted. The major checkpoints include the G1 checkpoint, G2 checkpoint and mitotic checkpoint. In the event of replication errors, DNA damage or other stresses, the cell cycle checkpoint is triggered, p53 is activated, which in turn causes cell cycle arrest or cell death (Giono & Manfredi, 2006). p53 is a transcription factor and a tumour suppressor gene (Finlay, Hinds, & Levine, 1989). It regulates the expression of several genes and has the ability to induce cell cycle arrest (p21), senescence (p16) or apoptosis based on the encountered stress and cell type (Beauséjour et al., 2003; Chen, 2016). It plays a crucial role at the G1/S checkpoint and G2/M checkpoint (Senturk & Manfredi, 2013). Cell cycle arrest by p53 is mainly mediated by transcriptional activation of p21 which is a cyclin-dependent kinase inhibitor. p21 induces cell cycle arrest by inhibiting cyclin-CDK complexes involved in the G1/S transition (Wade Harper, Adami, Wei, Keyomarsi, & Elledge, 1993). Tumour cells manage to escape such tightly regulated checkpoints to facilitate unsupervised cell division. It is no surprise that the TP53 gene is frequently mutated or deleted in almost 50%-60% of the tumours (Hollstein, Sidransky, Vogelstein, & Curtis, 1991).

The cell cycle progression is also regulated by several signalling pathways. One prominent example is Wnt signalling, as in proliferating cells, Wnt Signaling peaks at the G2/M phase (Acebron, Karaulanov, Berger, Huang, & Niehrs, 2014). The Wnt co-receptor LRP5/6 is a key Wnt signalling transducer and is under cell cycle control (Davidson et al., 2009). Wnt β-catenin pathway and PI3K/Akt signalling pathway upregulate target genes such as cyclin D and c-Myc that promotes the G1/S transition of the cell cycle. Other pathways like mTOR contribute to increased protein synthesis that leads to cell growth during the G1 phase (Fingar, Salama, Tsou, Harlow, & Blenis, 2002). Taken together, several signalling pathways along with the feedback mechanisms co-ordinate with each other and culminate in the progression of the cell cycle.

1.3 PI3K/Akt Signalling

The phosphatidylinositol 3 kinase/ protein kinase B is an important signalling pathway involved in the regulation of several downstream processes such as cell cycle, growth, protein synthesis and proliferation. PI3K belongs to the family of lipid kinases and is activated by ligands binding to tyrosine kinase receptors (RTK). However, it is also known to be activated by various stimuli including growth factors such as Epidermal growth factors, cytokines and

hormones. Once activated, it phosphorylates phosphatidylinositol-4,5-bisphosphate (PIP2) at the 3′ position, generating the second messenger phosphatidylinositol-3,4,5-trisphosphate (PIP3). PTEN dephosphorylates PIP3 and acts as a negative regulator of PI3K. Activated PIP3 recruits other downstream molecules especially the serine-threonine kinases Akt and PDK1 (3-phosphoinositol-dependent protein kinase-1) to the cell membranes. PDK1 subsequently phosphorylates and activates Akt, which in turn regulates a wide range of target proteins that control cell growth and survival as depicted in Figure 1 (Cantley, 2002).

An important downstream effect of the PI3K pathway is the control of cell cycle progression. Activated Akt inhibits GSK3β through phosphorylation, which in turn stabilizes cyclin D and myc, involved in the G1/S transition of the cell cycle. Cell proliferation and cell growth are interlinked, where a large part of the cell growth hugely relies on increased protein synthesis. The mTOR pathway controls protein synthesis, which is dependent on the availability of nutrients and growth factors. mTOR regulates cell growth by activating the ribosomal S6 kinase (S6K1) that stimulates protein translation. By phosphorylating Akt and inhibiting tuberous sclerosis complex-2 (TSC2) in response to growth signals, the PI3K pathway activates mTOR, leading to enhanced protein synthesis (Cantley, 2002).

This PI3K-Akt-mTOR axis is crucial for several oncogenic signalling pathways (Fingar et al., 2002; Luo, Manning, & Cantley, 2003). Aberrant activation of PI3K/Akt signalling is reported in many cancers, especially Akt was found to be an oncogene, activated in ovarian, breast and colon cancers. One of the striking discoveries was PTEN being a tumour-suppressor gene. Several loss-of-function mutations were associated with the PTEN gene and are common among melanomas, prostate cancers, breast cancer (Li et al., 1997; Steck et al., 1997). Since the pathway majorly controls cell growth and proliferation, hyperactivation of the PI3K/Akt pathway most often leads to tumorigenesis.

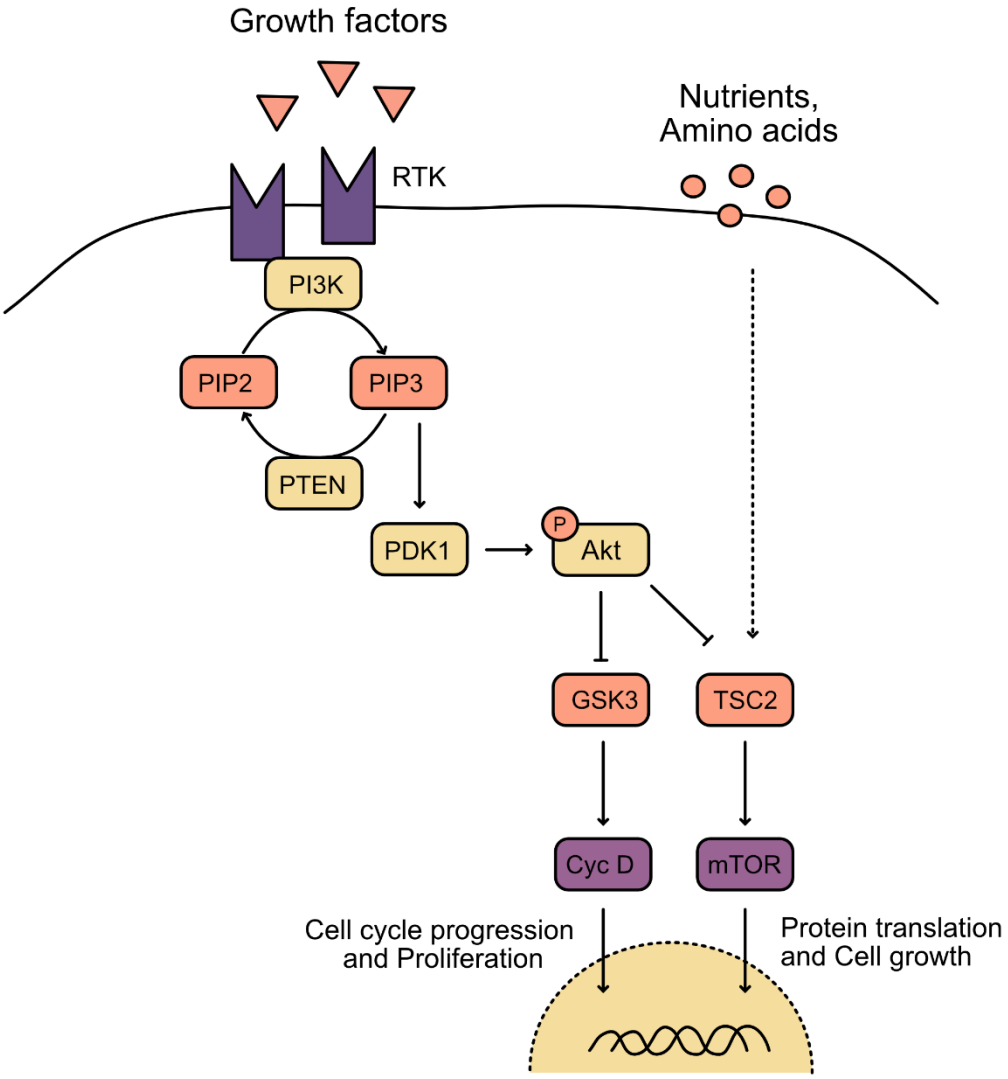

Figure 1: Scheme of the PI3K/Akt Signalling Pathway. Growth factors bind to RTK, which recruits PI3K at the membranes, PI3K phosphorylates PIP2 and converts it to PIP3, which in turn recruits PDK1 and hence Akt. PDK1 phosphorylates Akt which in turn has several downstream targets. Akt regulates cell cycle progression by inhibiting GSK3, which stabilizes cyclin D. Akt also stimulates protein synthesis by activating the mTOR pathway by inhibiting the TSC complex. mTOR can also be activated by nutrients and amino acids upstream. The intermediate steps in this pathway are omitted for clarity.

1.4 Wnt Signalling

Wnts are secreted proteins that mediate cell-cell communication, either in a contact-dependent manner or across a long distance. The Wnt signalling pathway is conserved across evolution and is a fundamental mechanism of intercellular communication used by all multicellular animals. It was initially identified in *Drosophila* termed as Wg (Wingless), necessary of the wing development. Apart from an intricate network of intracellular

components and molecular responses, the 19 different Wnts,10 Frizzled (Fzd) and two low-density lipoproteins (LRP) co-receptor genes in mammalian genomes offer diverse possibilities for promiscuous interactions on the cell surface. Overall, Wnt proteins modulate the generation of cell polarity, determination of cellular fate, maintenance of the pluripotency of stem cells and cellular proliferation by canonical and non-canonical Wnt signalling pathways (Mikels & Nusse, 2006).

Wnt signalling pathways are broadly classified as canonical and non-canonical Wnt pathways. In the canonical β-catenin Wnt pathway, the Wnt3a ligand binds to Fzd and the co-receptor LRP5/6 (He, Semenov, Tamai, & Zeng, 2004), recruits Dishevelled (Dvl) and Axin to the plasma membrane (DeBruine, Xu, & Melcher, 2017). This leads to a series of events that inhibit GSK3β activity and disrupts the protein complex that usually degrades β-catenin. As a result, β-catenin stabilizes and accumulates in the cytosol, translocate into the nucleus and activates TCF/LEF factors (Clevers & Nusse, 2012; Cselenyi et al., 2008). These are transcriptional factors that regulate downstream processes such as cell cycle progression and proliferation. In the absence of Wnts, the degradation complex comprising of Axin, adenomatosis polyposis coli (APC), protein phosphatase 2A (PP2A), casein kinase 1α (CK1α) and glycogen synthase kinase 3 beta (GSK3β) targets β-catenin for degradation (Gordon & Nusse, 2006; Nusse, 2005). Several negative regulators of the pathway serve as a feedback loop, which includes Dickkopf-related protein 1 (Dkk-1) (Glinka et al., 1998) at the receptor level and Axin2 at the cytoplasm (Jho et al., 2002).

The Wnt/LRP6 signalling pathway also has β-catenin independent routes that branch into the Wnt/TOR and Wnt/STOP pathway, which again trifurcates at the level of GSK3β inactivation as depicted in Figure 2 (Acebron & Niehrs, 2016). In the absence of Wnts, GSK3β phosphorylates TSC2 and inhibits it from binding to the TORC1 complex. Wnts block TSC2 and thereby activate the mTOR pathway, which stimulates protein translation during the cell cycle progression. Similarly, Wnts prevent protein degradation by inhibiting GSK3β, which in sum leads to the stabilization of 15% of the cellular proteins by Wnt/STOP signalling (Acebron et al., 2014). Wnt/STOP increases the cell size and stabilizes G1 proteins such as Myc and Cyclin D1, which couple cell cycle progression with cell growth.

Non-canonical Wnt pathways make use of the same core components, but branch into the Wnt/PCP and Wnt/Ca^{2+} pathway at the level of Dishevelled. The non-canonical Wnt Planar cell polarity pathway (PCP) is well studied in *Drosophila* and is known to regulate cell polarity. Epithelial cells possess apical-basolateral polarity and this organization is required in various epithelia, for example in the inner ear, hair follicles and even mesodermal cells during gastrulation. The Wnt PCP pathway regulates the actin cytoskeleton to allow for polarized

cellular organization and cell migration. The Wnt calcium pathway on the other hand stimulates calcium release from the ER and is dependent on G-proteins. Wnt5a and Wnt11 are known to stimulate this pathway that leads to intracellular calcium release and activates several Ca^{2+} sensitive proteins such as Protein Kinase C (PKC) and calcium/calmodulin-dependent kinase II (CamKII). These proteins for example regulate gastrulation in *Xenopus* embryos and heart formation which is a crucial component of the Wnt/Ca^{2+} pathway (Reviewed in (Komiya & Habas, 2008)).

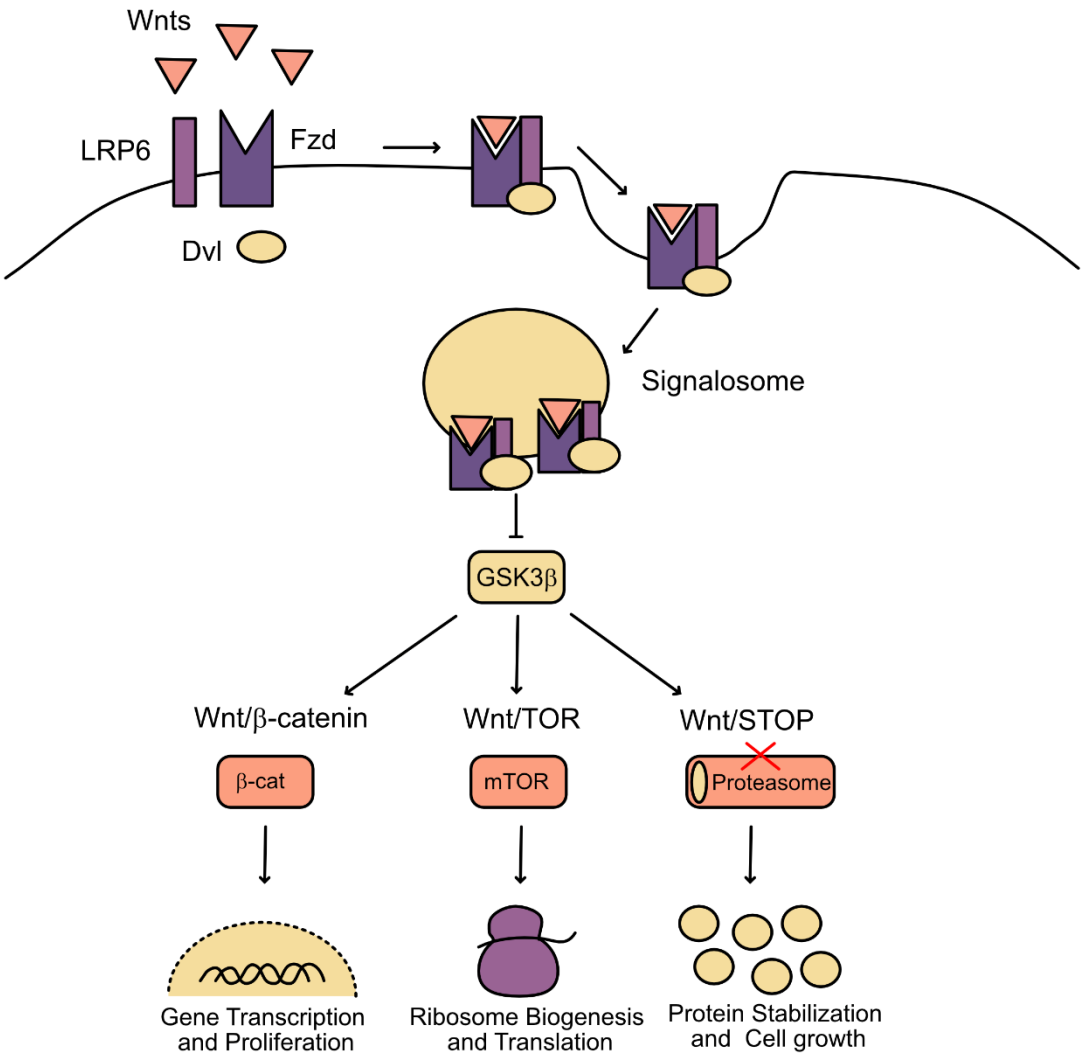

Figure 2: Scheme of the Wnt Signaling Pathway. Wnt ligands form a complex with Fzd and LRP6 that form a cluster along with Dvl. This complex inactivates GSK3β, which triggers several downstream cascades, which are β-catenin dependent and β-catenin independent. These pathways contribute to overall cell growth and proliferation. Inspired by Acebron & Niehrs, 2016.

The Wnt signalling pathway is one of the main regulators for development and adult tissue homeostasis. A mutated Wnt pathway leads to several forms of cancer and growth-related

pathologies. Wnt signalling is not only important during early development, but continues to influence the maintenance of multiple different tissues. In many tumours, the Wnt pathway is hyper activated by dominant mutations in the downstream signalling components, such as APC and β-catenin. However, interesting promising therapeutics have also been discovered in the upstream signalling cascades rather than on events within the receiving cell (Wiese, Nusse, & van Amerongen, 2018)

1.4.1 Wnt Secretion

In Wnt-secreting cells, the O-acyltransferase porcupine (Porcn) is required for lipid modification of Wnts with palmitoleic acids in the endoplasmic reticulum (ER) (Zhai, Chaturvedi, & Cumberledge, 2004). The transport of Wnt proteins from the ER to the Golgi requires members of the p24 protein family. This suggests that p24 proteins might function as early cargo receptors in the secretory route of Wnts (Port, Hausmann, & Basler, 2011). The secretion of Wnt proteins depends on Evi/Wntless(WLS)/Sprinter, a conserved multipass transmembrane protein, that shuttles the lipid-modified Wnts/Wg to the plasma membrane (Bartscherer, Pelte, Ingelfinger, & Boutros, 2006). Evi is then internalized by clathrin-mediated endocytosis which is mediated by AP2, recycled via the retromer complex back to the Golgi and ER (Gasnereau, Herr, Chia, Basler, & Gleeson, 2011). The retrograde transport of Evi from the plasma membrane to the Golgi is required for continuous Wnt secretion and is mediated by the retromer complex SNX3 comprised of the subunits VPS26, VPS29 and VPS35 (Zhang, Wu, Belenkaya, & Lin, 2011). The recycling of Evi from the membrane back to the Golgi is conserved from *C. elegans* to vertebrates (Harterink et al., 2011). Mutation of Evi/WLS leads to surface accumulation of Evi and Wg secretion defects in *Drosophila*. It was discovered that the retromer complex is also required for the retrieval of Evi from the endosomes to the Golgi (Port & Basler, 2010; Port et al., 2008). This suggests that Evi escorts lipidated Wnts to the plasma membrane, where it can be released or endocytosed back into the cell to enter the endocytic pathway (Herr, Hausmann, & Basler, 2012). Wg trafficking into endosomes is required for Wingless signalling in Drosophila wing epithelium (Strigini & Cohen, 2000). Several studies show that Evi and Wnt reach the endosomal compartment together before the secretion of active Wnts. Impairing the early endosomal sorting complexes (ESCRT), which is known to mediate cargo recognition of exosomal proteins, reduces Wg secretion and signalling (Gross, Chaudhary, Bartscherer, & Boutros, 2012).

Wnts are secreted morphogens and lipidated Wnts travel in the extracellular space by forming a short-range or long-range gradient depending on the distance to the target cells.

Wnts are known to be transferred by binding to extracellular matrix components such as heparin sulphate proteoglycans (HSPGs) (Yan & Lin, 2009). They belong to the glypican family and attach to the cells through a GPI anchor. *Drosophila* wing imaginal discs have been widely used to study morphogen gradient formation and Wg signalling where the glypican Dally and Dally like protein (Dlp) is involved in Wnt gradient formation and signalling (Han, Yan, Belenkaya, & Lin, 2005). The morphogens are also transported by forming cell-cell contact sites with the receiving cells, through actin-based filopodial extensions called cytonemes (Hsiung, Ramirez-Weber, David Iwaki, & Kornberg, 2005). The formation of a long-range gradient requires special mechanisms to spread Wnts farther from their source of production, for example, soluble micelles, lipoprotein particles or extracellular vesicles. Wnts are known to be secreted on lipoprotein particles in the *Drosophila* wing epithelium and mammalian cells (Neumann et al., 2009; Panáková, Sprong, Marois, Thiele, & Eaton, 2005). They are also known to be associated with Reggie-1/Flotillin-1 which are components of membrane microdomains in *Drosophila* for long-range spreading (Katanaev et al., 2008). Wnts can also bind to extracellular molecules that act as vehicles that carry Wnts to the target cells. For example, an extracellular Wg binding protein SWIM (secreted Wg interacting molecule), which is a member of the Lipocalin family of transport proteins, was described as a co-factor in long-range Wg signalling (Mulligan et al., 2012). In human cells, a crystal structure revealed that Afamin a glycoprotein is complexed with Wnt and acts as a Wnt carrier (Naschberger et al., 2017). Active Wnts are also secreted on exosomes in human cell lines and *Drosophila* (Gross et al., 2012). The different extracellular forms of Wnts can co-exist and gradient formation is largely dependent on the tissue type and its developmental status.

Exosomes are extracellular vesicles with a size range of 30-100nm and are generated as intraluminal vesicles by inward budding of multi-vesicular bodies. They are formed in the endocytic pathway in an ESCRT-dependent (endosome sorting complex) or ESCRT-independent manner. Based on the machinery involved, exosomes carry specific markers which categorize them into different sub-populations such as CD63, CD81, CD9, Tsg101, Alix or Syntenin bearing exosomes (Van Niel, D'Angelo, & Raposo, 2018). Cytoskeletal proteins, motor proteins, molecular switches such as GTPases and fusion machinery such as SNARE proteins are involved in the release of exosomes (Raposo & Stoorvogel, 2013). An *in vivo* RNAi screen in *Drosophila* identified Ykt6, a SNARE protein to block Wg secretion. Furthermore, Ykt6 is evolutionarily conserved and plays an important role in extracellular transport on Wnt proteins (Gross et al., 2012).

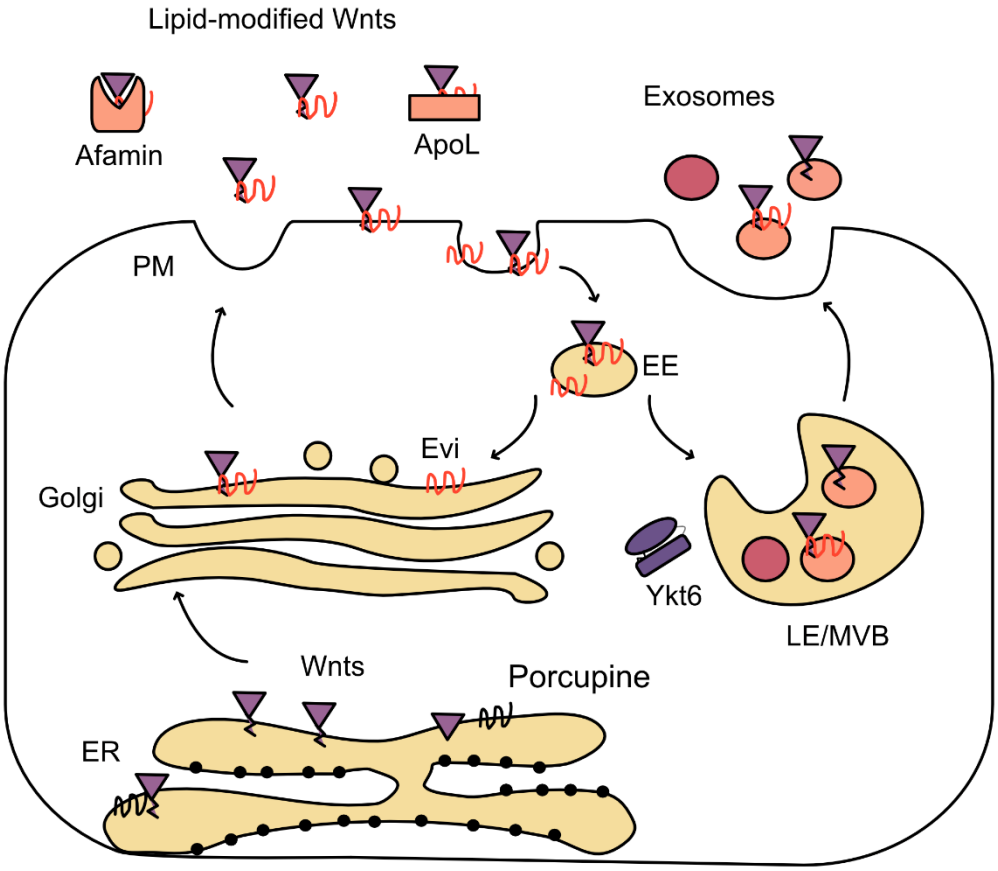

Figure 3: Scheme of Wnt secretion. Wnts are palmitoylated by Porcupine in the ER, transported to the Golgi, where it binds to Evi and subsequently reaches the plasma membrane to be released. It can also be re-endocytosed to enter the endocytic pathway and secreted onto the exosomes. EE: Early endosome; LE: Late Endosome, MVB: Multi-vesicular body. Inspired by Gross et al., 2012.

1.5 SNARE Proteins

Eukaryotic cells have specialized membrane compartments that are segmented to carry out a plethora of functions. One of the most important functions is the transport of molecules between these intracellular compartments as well as the external environment. These movements are mediated by small membrane-bound transport vesicles that bud off from one cellular compartment and fuse with the next compartment and is termed vesicular trafficking. Vesicular trafficking in the endocytic and secretory pathway is facilitated by Rab GTPases (Rab guanosine triphosphate hydrolases), tethering complexes and SNARE proteins (Gonzalez & Scheller, 1999). Inter-compartment communication requires interaction between the targeting molecules on such transport vesicles and the target membranes for cellular compartmentalization and cargo transport. These events are not just unidirectional, where the newly synthesized proteins are transported to the final destination during anterograde

transport. It occurs in the reverse direction as well termed as retrograde transport, which is required for recycling of cargo receptors or recovery of misfolded proteins (Sanderfoot & Raikhel, 1999).

SNARE (Soluble N-ethylmaleimide sensitive factor attachment protein) proteins are evolutionarily conserved and play a central role in vesicle fusion and docking. Understanding the regulation and localization of SNAREs has helped to elucidate both anterograde and retrograde membrane trafficking in the secretory pathway. SNAREs are small proteins that are made of 100-300 amino acids in length and the core complex of SNARE proteins is evolutionarily conserved. They are functionally classified as t-SNAREs and v-SNAREs based on their association with the target membrane or vesicle membrane respectively (Ungar & Hughson, 2003). The assembled SNARE complexes form a four-helical bundle that has several layers of interacting amino acids which make them fusion-competent (Sutton, Fasshauer, Jahn, & Brunger, 1998). The middle of the bundle consists of hydrophilic residues characterized as a zero ionic layer that consists of either Glutamine (Q) or Arginine (R) residues, which led to their structural classification as Q-SNAREs or R-SNAREs respectively (Fasshauer, Sutton, Brunger, & Jahn, 1998). SNARE complexes are usually formed between three Q-SNAREs and one R-SNARE. SNAREs are additionally categorized based on their N-terminal domain and Ykt6 belongs to the category called longin SNAREs (Rossi et al., 2004).

1.5.1 Ykt6 Structure

Ykt6 is a 23 kDa R-SNARE that lacks a transmembrane domain. It is conserved from yeast to humans and is ubiquitously expressed in a variety of tissues (Catchpoole & Wanjin, 1999). It has an N-terminal longin domain and a C-terminal SNARE domain. The resolved N-terminal structure of Ykt6 reveals that it has a profilin-like structure, where Ykt6 adopts a folded back closed conformation. This autoinhibitory conformation was facilitated by the interaction of the N-terminal profilin domain with the C-terminal SNARE domain (Tochio, Tsui, Banfield, & Zhang, 2001). The C-terminal SNARE domain has a consensus CAAX motif, that contains two conserved cysteine residues. This motif is conserved in several other proteins such as Ras, Marcks and Rac-1. The closed, inactive, soluble Ykt6 is only farnesylated at the second cysteine residue (Cys195) and farnesylation alone is not sufficient to anchor the protein to the membrane (Fukasawa, Varlamov, Eng, Sollner, & Rothman, 2004; Veit, 2004). It was later discovered that Ykt6 palmitoylation at the first cysteine residue (Cys194) leads to strong membrane attachment (Lars E.P. Dietrich et al., 2005). In yeast studies, it was proposed that Ykt6 goes through a cycle of palmitoylation/depalmitoylation during the vacuole fusion

reaction. This gives Ykt6 an exclusive ability to cycle between cytosol and membranes, where a large pool of Ykt6 exists cytoplasmically in its inactive form and gets recruited to membranes to initiate vesicle fusion events. Membrane recruitment of Ykt6 is controlled by its N-terminal domain which interacts with the C-terminal SNARE domain to keep Ykt6 in its inactive closed conformation. Palmitoylation is a common reversible post-translational modification and is required for membrane localization and protein sorting (L. E P Dietrich & Ungermann, 2004). It was also reported that Ykt6 mediates protein palmitoylation of Vac8 through its acyltransferase activity in yeast vacuoles (Lars E.P. Dietrich, Gurezka, Veit, & Ungermann, 2004). Another study, further highlights that depalmitoylation of Ykt6 is required for its recycling and entry into the endosomal pathway (Meiringer, Auffarth, Hou, & Ungermann, 2008). Taken together, Ykt6 is a promiscuous SNARE that dynamically regulates the intracellular trafficking by localizing to diverse membrane compartments.

Extensive research has been done in understanding the mechanism of membrane recruitment of Ykt6 and its regulatory mechanism. Regulation of Ykt6 can occur via its longin domain that controls the Ykt6 conformation and localization. It was proposed that Ykt6 exists in a soluble closed conformation, where the longin domain is locked in place and acts as a lipid chaperone masking the hydrophobic residues. The longin domain interacts with the SNARE domain via intramolecular protein-protein interactions and with the masked lipid groups at the C terminus via protein-lipid interactions, thereby preventing the SNARE from binding to promiscuous targets. Once the longin domain retracts, it weakens the interactions with the SNARE motif which would then open up to form complexes with potential partners to modulate vesicle fusion events. Thus, the protein-lipid interaction facilitates the closed conformation of the SNARE to regulate its targeting and activity (H. Hasegawa, 2004). Another study based on circular dichroism spectroscopy revealed that farnesylated Ykt6 is more stably folded than the non-lipidated variant (Pylypenko et al., 2008). Along these lines, NMR (Nuclear magnetic resonance) studies revealed that Ykt6 adopts multiple interconverting conformational states, where farnesylation shifts the conformation from a semi-closed to a dominantly closed stable conformation. Therefore, the Ykt6 SNARE and longin domain mutually cooperate to keep the farnesylated, unpalmitoylated Ykt6 protein in its soluble closed conformation. When Ykt6 is palmitoylated, the partition co-efficient increases that shifts a portion of the protein from cytosol to membranes (Weng, Yang, & Wang, 2015). Even though several studies have reported Ykt6 to be palmitoylated at Cys194, a recent study reported that Ykt6 is a substrate for geranylgeranyltransferase type III (GGTase-III), that recognizes farnesylated Ykt6 and attaches a geranylgeranyl group at the Cys194 position. This leads to a doubly prenylated Ykt6 that is soluble, however, since prenylation is irreversible, perhaps a

different mechanism might regulate the open/closed conformation of the doubly prenylated Ykt6 (Shirakawa et al., 2020).

Another well-known regulatory mechanism that controls the activity of SNAREs is phosphorylation, which is considered a general inhibitory mechanism for SNAREs to suppress membrane fusion. A study on non-neuronal SNAREs such as VAMP8 revealed conserved phosphorylation residues within the SNARE domain in fungi, plant and animal kingdoms. Phosphorylation or mutation of these sites allowed the docking of these SNAREs at membranes but prevented the fusion of secretory granules (Malmersjö et al., 2016b). Based on this paper, several studies followed investigating the role of phosphorylation in regulating Ykt6 activity by mutating these conserved phosphorylation sites in the Ykt6 SNARE domain. In *Drosophila* studies, the phosphomimicking mutant led to wing notches in the adult flies, leading to the development of melanotic tumours (Linnemannstöns et al., 2020). Similar effects were observed in a human cell culture system where phosphorylated Ykt6 gets recruited to membranes but prevents vesicle fusion events. Phosphorylated Ykt6 has dominant-negative effects and cannot revert to its closed conformation which leads to membrane stabilization (Pradhipa Karuna et al., 2020). Phosphorylated Ykt6 also inhibits autophagy flux in yeast (Barz et al., 2020) and prevents the SNARE from binding to its potential partners to form SNARE complexes (McGrath et al., 2021). Several kinases are predicted to phosphorylate Ykt6, including the PKC family of kinases (Malmersjö et al., 2016b), PDK1 (Pradhipa Karuna et al., 2020), protein kinase C iota type (PRKci) (McGrath et al., 2021) and Atg1 kinase during autophagy (Barz et al., 2020). These kinases could differentially modulate the activity of Ykt6 based on the organelle and the processes involved. In a nutshell, Ykt6 is regulated via a two-step process, where the phosphorylation of the SNARE recruits it to the membranes, but an additional dephosphorylation step, that could for example be calcineurin-dependent (McGrath et al., 2021), is required to make it fusion-competent. Hence, phosphorylation of Ykt6 regulates its function in the secretory and autophagy pathway.

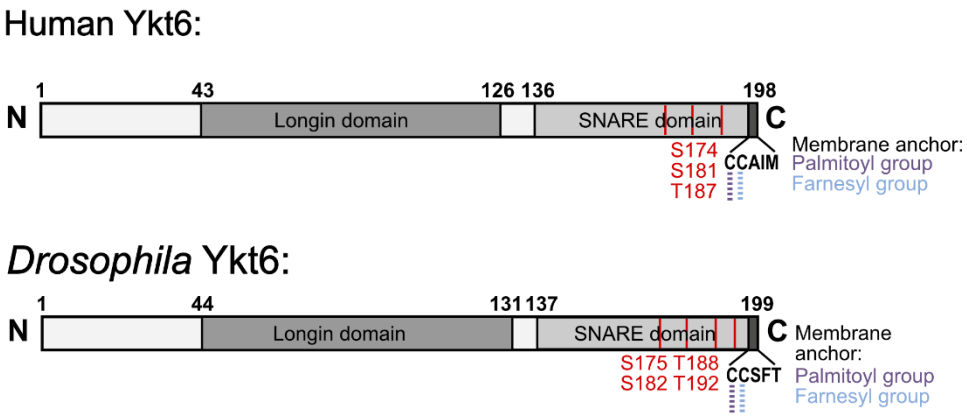

Figure 4: Scheme of human and *Drosophila* Ykt6. Ykt6 with predicted phosphorylation sites in human and *Drosophila*. It consists of the N-terminal longin domain and C-terminal SNARE domain. The SNARE domain has a conserved CCAIM motif, where the cysteine residues at positions 194 and 195 are palmitoylated and farnesylated respectively.

1.5.2 Ykt6 Functions

Ykt6 has been implicated in several steps of trafficking in the endomembrane system. One of the earliest elucidated functions of Ykt6 is in ER- Golgi transport (McNew et al., 1997) and Golgi retrograde transport (Lupashin, Pokrovskaya, McNew, & Waters, 1997). Ykt6 is essential for yeast cell viability and it was known to be involved in homotypic vacuole fusion (Ungermann et al., 1999) in yeast. Later, Ykt6 was shown to be involved in post-Golgi membrane trafficking and cells lacking Ykt6 are blocked at an early Golgi stage in the secretory pathway (Grinnell, 2002). A recent study revealed that Ykt6 is an essential SNARE for the structural and functional organization of the Golgi apparatus (Shirakawa et al., 2020). This suggests that Ykt6 is a multi-functional SNARE that is involved in several membrane trafficking fusion events in the secretory pathway.

Ykt6 is involved in a plethora of functions, however, a major discovery unfolded the role of Ykt6 in the Wnt signalling pathway. Ykt6 was identified as a gene to block Wg secretion in *Drosophila* where depletion of Ykt6 in Wg-producing cells reduced the expression of the Wg target gene senseless in the neighbouring target cells, leading to an adult wing notch phenotype consistent with defective Wg signalling. Furthermore, Ykt6 is required for the extracellular vesicular transport of Wnt proteins (Gross et al., 2012). Complementing these studies, Ykt6 acts via Rab4 recycling endosomes to transport Wnts to the cell surface and is involved in fine-tuning Wnt secretion from endosomes (Linnemannstöns et al., 2020).

Not until recently, another novel function of Ykt6 in autophagy was discovered. In *Drosophila* fat cells, Ykt6 acts as a non-conventional regulatory SNARE to initiate autophagosome-lysosome fusion. It competes with VAMP7 and forms a SNARE complex with Syx17 and Snap29 and is present in the lysosomes and autophagic vesicles (Takáts et al., 2018). Ykt6 also forms a complex with Stx17 and Snap29 in Hela cells for autophagosome-lysosome fusion. Interestingly, here, the longin domain regulates the recruitment of Ykt6 to autophagosomes, as a C-terminal mutant was unable to localize to the Golgi, but was still present on autophagosomes (Matsui et al., 2018). An *in vitro* reconstitution assay in yeast revealed the role of Ykt6 in autophagosome-lysosome fusion, where it forms complexes with the Q-SNAREs Vam3, Vam7 and Vti1 on the vacuole (J. Gao, Reggiori, & Ungermann, 2018; Rossi et al., 2018). This further emphasizes a differential recruitment mechanism for Ykt6 to autophagic membranes.

Another striking study has highlighted yet another function of Ykt6 in adapting to nutritional stress levels in ER^+ breast cancer cell lines: Ykt6 forms a trimeric complex with LLGL2, scaffolding protein and SLC7A5, a leucine transporter to promote leucine uptake in response to nutrient stress. It is therefore proposed as a part of the LLGL2-SLC7A5 pathway to facilitate membrane fusion at the cell surface levels (Saito et al., 2019). Apart from being involved in the transport of leucine, Ykt6 was reported as a potential regulator of GLUT4 trafficking in human cells (Morris et al., 2020).

Ykt6 acts at the cross-road of essential pathways such as secretory, endocytic and autophagy pathways. Diseases such as cancer could harness Ykt6 to their advantage to facilitate tumorigenesis. In fact, Ykt6 is implicated as a key molecule in the regulation of exosome release from lung cancer cell lines (Ruiz-Martinez et al., 2016). Ykt6 overexpression also leads to an increased mitotic index in rat kidney cells (Thayanidhi et al., 2012). Furthermore, Ykt6 is upregulated in p53-mutated breast tumours (Ooe, Kato, & Noguchi, 2007) and plays a role in tumour metastasis (Kluger et al., 2004). Apart from cancer, Ykt6 also plays a role in neurodegenerative disorders such as Parkinson's disease: In neuronal cells, α-synuclein binds to and deactivates Ykt6, which disables the lysosomal stress response and facilitates protein accumulation in patients. Activating Ykt6 restores lysosomal stress clearance activity by enhancing hydrolase trafficking during stressful situations and restores protein homeostasis (Cuddy et al., 2019). The doubly prenylated Ykt6 is not only essential for the Golgi organization, but also critical for lysosomal hydrolase trafficking (Sakata, Shirakawa, Goto, Trinh, & Horiuchi, 2021).

Taken together, Ykt6 is a promiscuous SNARE involved in crucial processes in the cell. It is no surprise that cancer cells or neuronal cells harness the SNARE to their advantage to

induce cancer metastasis or protein accumulation in neurodegenerative disorders. Although it acts in diverse cellular processes, it remains unclear if Ykt6 has a dedicated function or if it's a multifunctional SNARE that acts as a stress sensor. Ykt6 exists in a closed, inactive form and open the active form. Even though there have been several studies investigating the mechanisms that activate Ykt6, the exact molecular mechanism involved in its membrane recruitment and regulation remains unclear.

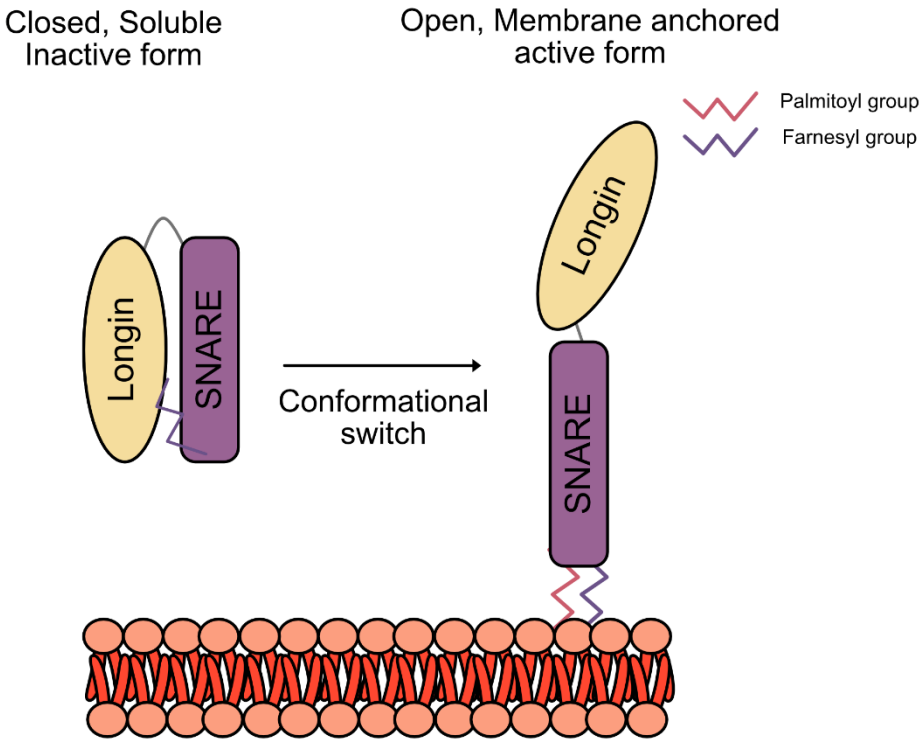

Figure 5: Schematic representation of membrane recruitment of Ykt6. Ykt6 exists in an inactive, soluble closed form. A conformation switch triggers Ykt6 to be anchored to membranes to initiate vesicle fusion events. Inspired by Daste et al., 2015.

2. Aim of the thesis

2.1 Elucidating the molecular mechanism of Ykt6 in Wnt secretion

Ykt6 is a promiscuous SNARE required for Wnt secretion on exosomes. It lacks a transmembrane domain and cycles between cytosol and membranes to initiate vesicle fusion. The first aim of the thesis is to investigate the mechanism of the cytosol to membrane cycling of Ykt6 in fine-tuning the extracellular Wnt levels. An *in vivo* genetic analysis in the *Drosophila* model system, combined with *in vitro* biochemical analysis and proximity-dependent proteomics in human cells was performed to understand this molecular mechanism.

2.2 Deciphering the mechanistic role of Ykt6 phosphorylation in regulating its membrane recruitment and activity

Ykt6 has evolutionarily conserved phosphorylation sites in its SNARE domain. It acts at multiple fusion events in the secretory, endocytic and autophagy pathways. How the phosphorylation of the SNARE regulates its conformational switch to attach to the membranes and what are the kinases involved in phosphorylation remains unclear. The second aim of the thesis is to decipher how phosphorylation of Ykt6 determines its membrane recruitment and hence its activity. An *in vitro* kinase screen assay, membrane fractionation and proximity-dependent proteomics was performed to understand the mechanism of membrane recruitment.

2.3 Characterization of Wnt-bearing small extracellular vesicles

Wnts are secreted morphogens that are loaded onto exosomes for long-range signalling. Even though several studies highlight the role of exosomal Wnts during development and tissue homeostasis, it is still unclear if there is a specific sub-population of exosomes that carry Wnt. The third aim of this thesis is to identify and characterize the Wnt-bearing small extracellular vesicles otherwise called exosomes. Electron microscopy, lipidomics and proteomics were performed to identify and characterize the exosome subtypes that carry Wnt.

2.4 Investigating the function of Ykt6 in cell cycle progression and the signalling pathways involved

Ykt6 is an essential gene in yeast and knockdown of Ykt6 causes growth defects *in vivo*. The fourth aim of the thesis is to investigate the function of Ykt6 in cell cycle progression and to determine the signalling pathway involved in this regulation. Using cell cycle synchronization, flow cytometry, single-cell transcriptomics and metabolomics, novel Ykt6-dependent expression patterns in a cell cycle-dependent manner were elucidated.

3. Results

3.1 Manuscript I: Ykt6-dependent endosomal recycling is required for Wnt secretion in the *Drosophila* wing epithelium

Citation

Karen Linnemannstöns[1,2], Leonie Witte[1,2], Pradhipa Karuna M[1,2], Jeanette Clarissa Kittel[1,2], Adi Danieli[1,2], Denise Müller[1,2], Lena Nitsch[1,2], Mona Honemann-Capito[1,2], Ferdinand Grawe[3,4,5], Andreas Wodarz[3,4,5] and Julia Christina Gross[1,2,*]

Development (2020) 147 (15): dev185421. https://doi.org/10.1242/dev.185421

https://journals.biologists.com/dev/article/147/15/dev185421/143917/Ykt6-dependent-endosomal-recycling-is-required-for

Individual contributions to published article:
Applicant name: Pradhipa Karuna M (third author)

1. **Main and Supplementary Figures/Tables** (actively performed experiments and/or analyzed data)

   Main: 2C, 5C, 5F, 5G, 5H, 5I,
   Supplementary: S2A, B, Table S2

2. **Writing and Intellectual Contributions**

   - Contributed to writing significant parts of the manuscript such as results, figure legends and methods corresponding to the above mentioned figures in association with Prof. Dr. Julia Gross and Karen Linnemannstöns.
   - Contributed to the revision experiments, mass spectrometry data analysis and proof-reading of the manuscript.

© 2020. Published by The Company of Biologists Ltd | Development (2020) 147, dev185421. doi:10.1242/dev.185421

RESEARCH ARTICLE

Ykt6-dependent endosomal recycling is required for Wnt secretion in the *Drosophila* wing epithelium

Karen Linnemannstöns[1,2], Leonie Witte[1,2], Pradhipa Karuna M[1,2], Jeanette Clarissa Kittel[1,2], Adi Danieli[1,2], Denise Müller[1,2], Lena Nitsch[1,2], Mona Honemann-Capito[1,2], Ferdinand Grawe[3,4,5], Andreas Wodarz[3,4,5] and Julia Christina Gross[1,2,*]

ABSTRACT

Morphogens are important signalling molecules for tissue development and their secretion requires tight regulation. In the wing imaginal disc of flies, the morphogen Wnt/Wingless is apically presented by the secreting cell and re-internalized before final long-range secretion. Why Wnt molecules undergo these trafficking steps and the nature of the regulatory control within the endosomal compartment remain unclear. Here, we have investigated how Wnts are sorted at the level of endosomes by the versatile v-SNARE Ykt6. Using *in vivo* genetics, proximity-dependent proteomics and *in vitro* biochemical analyses, we show that most Ykt6 is present in the cytosol, but can be recruited to de-acidified compartments and recycle Wnts to the plasma membrane via Rab4-positive recycling endosomes. Thus, we propose a molecular mechanism by which producing cells integrate and leverage endocytosis and recycling via Ykt6 to coordinate extracellular Wnt levels.

KEY WORDS: Wnt secretion, Wnt signalling, Endosomal sorting, Morphogen trafficking

INTRODUCTION

Cell behaviour and growth is coordinated at the tissue level by morphogen signalling to provide context-specific information in a space-, time- and dose-dependent manner. One such morphogen that forms a concentration gradient across a developing tissue is Wnt. Wnts act on neighbouring and distant target cells to activate Wnt signalling pathways, which play a central role in stem cell maintenance, differentiation in development and adult homeostasis (Nusse and Clevers, 2017). Within the source cells, Wnt trafficking through the secretory pathway is highly regulated to fine-tune extracellular signal distribution. First, Wnts are lipidated in the ER by Porcupine (Kadowaki et al., 1996; Tanaka et al., 2000). This modification is required for their activity and secretion, and is essential for p24 protein-dependent Wnt exit from the ER (Buechling et al., 2011; Port et al., 2011). Here, the cargo receptor Evi [also referred to as Wntless (Wls)] recognizes palmitoleic acid-modified Wnts and escorts them from the ER to the plasma membrane (Herr and Basler, 2012). In the ER, Evi levels depend on Wnt ligands and are regulated by the ERAD pathway (Glaeser et al., 2018). The recycling of Evi from the cell surface to the trans-Golgi network (TGN) enables further transport of newly synthesized Wnts from the TGN to the cell surface. Evi recycling depends both on clathrin-adaptor protein 2 (AP-2)-mediated endocytosis (Gasnereau et al., 2011) and retromer function, because blocking either of these steps leads to a reduction in Wnt secretion (Belenkaya et al., 2008; Harterink et al., 2011; Port et al., 2008; Yang et al., 2008; Zhang et al., 2011). Interestingly, Wnt and Evi only separate in acidified endosomes (Coombs et al., 2010), but the exact routes of post-endocytic trafficking leading to Wnt secretion remain unclear.

Endocytosis into endosomes is required for Wg trafficking, secretion and signalling, as demonstrated in the polarized epithelium of developing *Drosophila* wings (Pfeiffer et al., 2002; Strigini and Cohen, 2000). In addition, there seems to be a dual effect of the endosomal compartment on Wg signalling: impairing early endosomal sorting causes reduction in Wg secretion and signalling (Marois et al., 2006; Seto and Bellen, 2006), whereas blocking endosomal trafficking from late endosome to lysosome increases Wg signalling (Dubois et al., 2001; Seto and Bellen, 2006). Time-course analysis revealed that Wg is first trafficked to the apical membrane and then re-endocytosed before its final secretion. Several hypotheses exist for this postendocytic trafficking: (1) Wg is transcytosed and secreted at the basolateral membrane (Yamazaki et al., 2016); (2) Wg is loaded onto endosome-derived exosomes for export after endocytosis (Gross et al., 2012); and (3) Wg and Frizzled (Fz) receptors meet in endosomal compartments for signalling and degradation (Hemalatha et al., 2016). Therefore, to elucidate the role of Wnt trafficking to endosomal compartments, it is essential to determine whether it is destined for secretion, signalling or degradation.

Previously, we identified the SNARE Ykt6 to be required for the secretion of Wnts on exosomes in *Drosophila* and human cells (Gross et al., 2012). Wnts are secreted on different extracellular vesicles (EVs) such as exosomes (Beckett et al., 2013; Gross et al., 2012; Koles et al., 2012; Menck et al., 2013), e.g. in the context of spermatogenesis and nerve regeneration (Koch et al., 2015; Tassew et al., 2017). Ykt6 is an unusual SNARE, as it lacks a transmembrane domain and therefore cycles between cytosol and membranes (reviewed by Kriegenburg et al., 2019). Ykt6 localizes to different membranes (such as ER, Golgi, endosomal membranes and the plasma membrane) and was found in variable SNARE complexes *in vitro*. In yeast, Ykt6 functions in homotypic fusion of ER and vacuolar membranes, in retrograde Golgi trafficking and in autophagosome formation (Bas et al., 2018; Gao et al., 2018).

[1]Hematology and Oncology, University Medical Centre Goettingen, Goettingen 37075, Germany. [2]Developmental Biochemistry, University Medical Centre Goettingen, Goettingen 37077, Germany. [3]Molecular Cell Biology, Institute I for Anatomy, University of Cologne Medical School, Cologne 50931, Germany. [4]Cluster of Excellence-Cellular Stress Response in Aging-Associated Diseases (CECAD), Cologne 50931, Germany. [5]Center for Molecular Medicine Cologne (CMMC), University of Cologne, Faculty of Medicine and University Hospital Cologne, 50931 Cologne, Germany.

*Author for correspondence (julia.gross@med.uni-goettingen.de)

J.C.G., 0000-0002-8939-5664

Handling Editor: Thomas Lecuit
Received 9 October 2019; Accepted 8 June 2020

Development (2020) 147, dev185421. doi:10.1242/dev.185421

In higher eukaryotes, Ykt6 seems to play a role in non-canonical autophagosome formation under starvation conditions in human cells (Matsui et al., 2018) and *Drosophila* fat body (Takáts et al., 2018). Considering the ability of Ykt6 to adapt to multiple cellular localizations, we investigate it here as a candidate to orchestrate Wnt secretion from endosomes. Combining *in vivo* genetics, proximity-dependent proteomics and *in vitro* biochemical analyses, we found that cytosol-to-membrane cycling of Ykt6 has an evolutionarily conserved function in endosomal Wnt trafficking in *Drosophila* and in human cells. Ykt6 acts via Rab4 in recycling Wnts to the cell surface, and we propose that this is a novel mechanism for fine-tuning of Wnt secretion in endosomes.

RESULTS

Loss of Ykt6 blocks Wnt secretion

To analyse the role of Ykt6 in Wnt secretion, we used the polarized epithelium of *Drosophila* wing imaginal discs (WIDs), a well-established model system to study the secretory pathway of Wingless (Wg), the *Drosophila* homologue of Wnt1 (reviewed by Parchure et al., 2018; Swarup and Verheyen, 2012). RNAi-mediated knockdown of Ykt6 in third-instar WIDs strongly reduced extracellular Wg staining (Fig. 1A; Gross et al., 2012), indicating a block of Wg secretion. We confirmed this RNAi phenotype using two available loss-of-function alleles: $ykt6^{C}$, which has a mutated start codon (M1I); and $ykt6^{A}$, which carries a Q62R exchange in the Longin domain (Haelterman et al., 2014) (Fig. 1B). These alleles are homozygous lethal, confirming the essential role of Ykt6 described in yeast (McNew et al., 1997). GFP-negative $ykt6^{A}$ mutant mitotic clones were small compared with control clones (Fig. S1A), yet Wg accumulated intracellularly within these clones, as observed for RNAi (Fig. 1C). DE-Cadherin staining was unaffected in $ykt6^{A}$ mutant clones, indicating that cargo trafficking from the ER through the Golgi to the plasma membrane is unperturbed (Fig. S1B). This implies that Ykt6 is required for Wg secretion at a post-Golgi step.

To confirm these findings, we next investigated the role of Ykt6 in human cells. Ykt6 knockdown in human Hek293T cells caused intracellular accumulation of overexpressed Wnt3A-GFP (Fig. 1D) and reduced endogenous Wnt5A secretion from SK-BR-3 breast cancer cells (Fig. S1C). Thus, the role of Ykt6 in Wnt secretion appears to be evolutionarily conserved. Proteins of the SNARE family drive membrane fusion by formation of a trans-SNARE complex consisting of four specific v- and t-SNAREs present at vesicle and target membranes. Different trafficking steps are mediated by preferential sets of SNAREs to ensure a directional flow of membranes and cargo (Dingjan et al., 2018). However, Ykt6 has multiple sites of action and it has been shown to interact with different SNARE partners *in vitro* (Tsui et al., 2001). To understand at which step Ykt6 is involved in post-Golgi Wnt trafficking, we undertook a comparative RNAi candidate approach in *Drosophila* WIDs, comparing its knockdown with the knockdown of early and late secretory SNAREs (Fig. 1E, Table S1). First, the adult wings of wgGal4-driven RNAi crosses of all 25 SNAREs were analysed for Wnt signalling defects, i.e. wing notches (Fig. 1E, upper diagram). Owing to the general importance of membrane fusion events for protein secretion (Gordon et al., 2010), 15 of those 25 SNAREs showed notches and one cross was lethal (Table S1). Next, enGal4-driven RNAi of those 16 was analysed in WIDs for Wg secretion defects by comparing and visually scoring Wg staining in the anterior and the posterior compartment (Fig. 1E, lower diagram). Under those conditions, six candidates were lethal and six affected Wg secretion. Golgi SNAREs, such as Syx5 and Bet1, strongly reduced Wg secretion and overall cell survival, and were not further investigated. Sec22 and Vamp7 contain a Longin domain like Ykt6 and, together with Synaptobrevin (Syb), act in plasma membrane fusion of secretory vesicles (Gordon et al., 2017) and Wg secretion (Gao et al., 2017; Li et al., 2015; Yamazaki et al., 2016). Indeed, we observed Wg accumulation and wing notches for Sec22 and Syb, but not for Vamp7 (Table S1). Transverse optical sections clearly showed that Syb RNAi leads to apical accumulation of Wg, similar to the phenotype observed with Ykt6 (Fig. 1F, middle panel). As Ykt6 negatively interacts with Syb and Sec22 in *Drosophila* cells (Gordon et al., 2017), we asked whether Ykt6 knockdown would affect these late secretory SNAREs *in vivo*. Staining for Sec22, Syb and Vamp7 in enGAL4/Ykt6-RNAi WIDs revealed that Ykt6 depletion affects neither localization nor stability of these three SNAREs *in vivo* (Fig. S1D). We further tested for a role for these SNAREs in Wnt secretion and signalling in non-polarized Hek293T cells. In an autocrine Wnt reporter assay, knockdown of Ykt6 and VAMP1 (human Syb homologue) reduced Wnt activity, whereas Sec22B and VAMP7 did not (Fig. S1E). Taken together, these data suggest that Ykt6-mediated trafficking events resemble those of Syb, a SNARE previously described in a post-endocytic step in Wg secretion in WIDs (Yamazaki et al., 2016).

Ykt6 acts on endosomal compartments after apical presentation

To clarify the direction of Ykt6-mediated trafficking events, we used an unbiased BioID approach to label proteins in close proximity (Roux et al., 2012, 2018) and thereby identify potential Ykt6 interaction partners informative of Ykt6 sub-endosomal localization. Ykt6 was N-terminally tagged with the prokaryotic BirA* domain. This promiscuous ligase biotinylates amine groups of neighbouring proteins within a 10 nm radius upon addition of biotin. Wild-type (WT) and mock constructs were expressed in human Hek293T cells in the presence of 50 µM biotin; biotinylated proteins were purified by streptavidin pulldown and subjected to mass spectrometry (Fig. 2A,B). We identified a total of 143 biotinylated proteins enriched over background in cells expressing Ykt6-WT (Table S2). In general, BioID captures weak and transient protein-protein interactions and proximate proteins (Liu et al., 2018). Reactome functional network (Gobert et al., 1996) and Kegg pathway analysis (Kanehisa et al., 2016) of identified proteins connected Ykt6 to processes like vesicle trafficking, metabolic processes and endocytosis (Fig. S2A-C). These connections are in line with the pleiotropic effects observed for Ykt6 in diverse membrane-associated processes such as ER-Golgi traffic (Fukasawa et al., 2004; McNew et al., 1997; Zhang and Hong, 2001), autophagy (Bas et al., 2018; Gao et al., 2018; Matsui et al., 2018; Takáts et al., 2018) and plasma membrane fusion (Gordon et al., 2017). However, we did not identify other SNAREs using the BioID approach, potentially owing to the long labelling time of first generation BioID constructs (Roux et al., 2018).

Interestingly, and supporting the findings from the WID candidate screen, we found nine candidates connected to endocytosis (Fig. 2C). Among them are both early (Clathrin adaptor AP2 complex components and Dynamin2) and late (Alix and Chmp2B) endosomal proteins. We confirmed Ykt6-mediated BioID labelling of AP2A1/2 by immunoblotting of streptavidin pulldown from Hek293T cell lysates (Fig. 2D). Furthermore, knockdown of Dynamin 2, Chmp2B and Alix in Hek293T Wnt reporter cells reduced autocrine Wnt signalling activity (Fig. S2D). Together with the results from the SNARE *in vivo* RNAi approach, this supports a connection between Ykt6 and endosomal sorting in Wnt signalling.

Development (2020) 147, dev185421. doi:10.1242/dev.185421

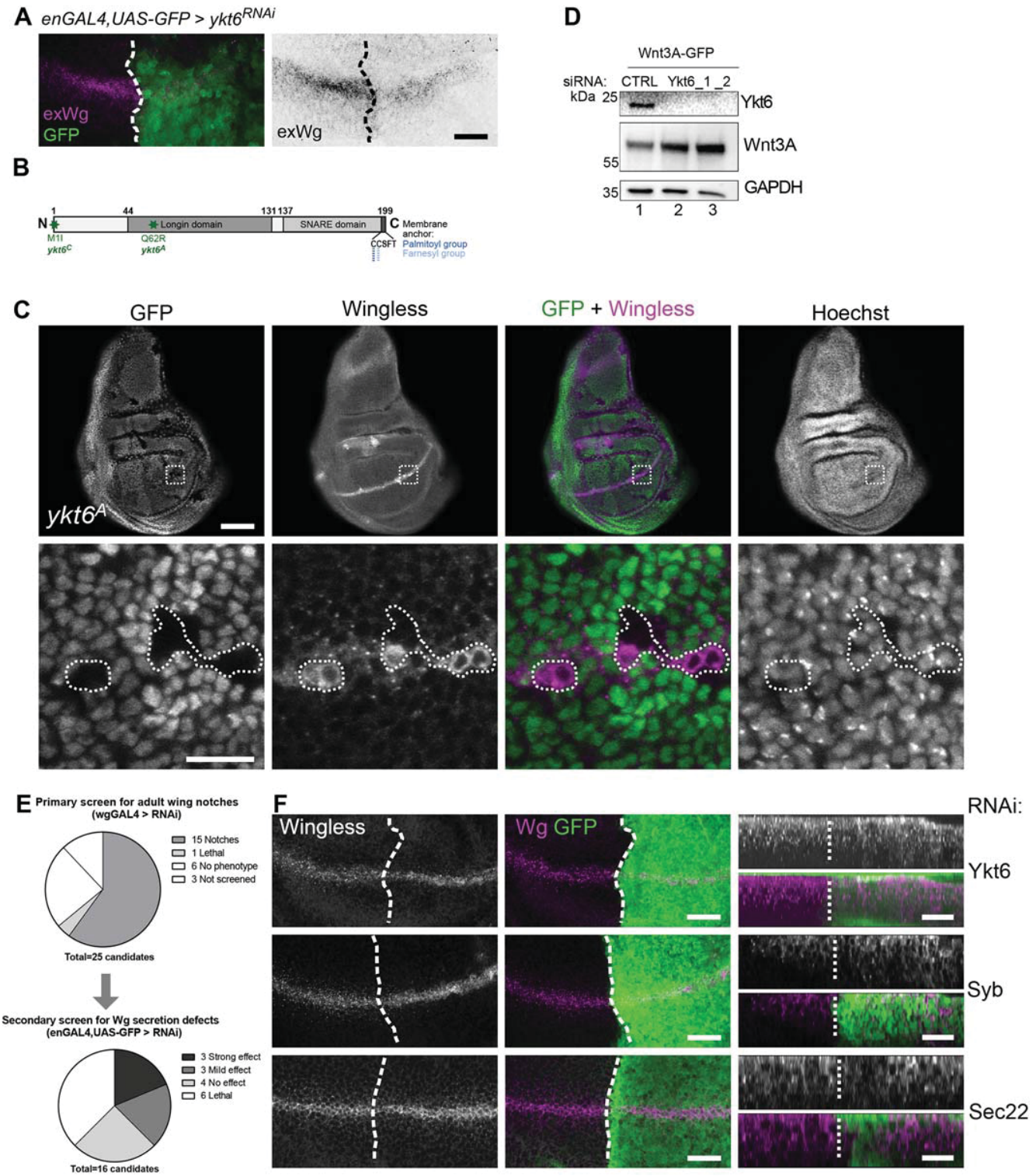

Fig. 1. Loss of Ykt6 blocks Wnt secretion. (A) RNAi-knockdown of Ykt6 in the posterior compartment of third instar WIDs marked by co-expression of GFP (engrailed-Gal4, UAS-GFP/UAS-ykt6RNAi) causes extracellular Wingless reduction. The GFP-negative anterior compartment serves as an internal control. Maximum intensity projection of 20 sections (distance 0.5 µm) depicted for visualization. (B) Scheme of *Drosophila ykt6* mutant alleles. (C) Wingless protein accumulates in *ykt6*^{A} clones marked by the absence of GFP. The lower panels depict enlarged images of the areas outlined in the upper panels. (D) Western blot analysis of intracellular Wnt accumulation in Hek293T cells transfected with control or Ykt6-1 or Ykt6-2 siRNA. (E) RNAi against 25 *Drosophila* SNAREs was screened for Wnt secretion defects in adult wings (wgGAL4) and third instar WIDs (enGAL4) (see also Table S1). (F) Knockdown of Ykt6 and Syb by RNAi in the posterior compartment of third instar WIDs marked by co-expression of GFP leads to intracellular Wg accumulation, whereas Sec22 does not affect Wg distribution. The GFP-negative compartment serves as an internal control. Left panels in F show maximum intensity projections of six (Ykt6), 15 (Syb) and two (Sec22) sections (distance 1 µm) depicted for visualization. Right panels in F show optical transverse sections. Scale bars: 20 µm.

Development (2020) 147, dev185421. doi:10.1242/dev.185421

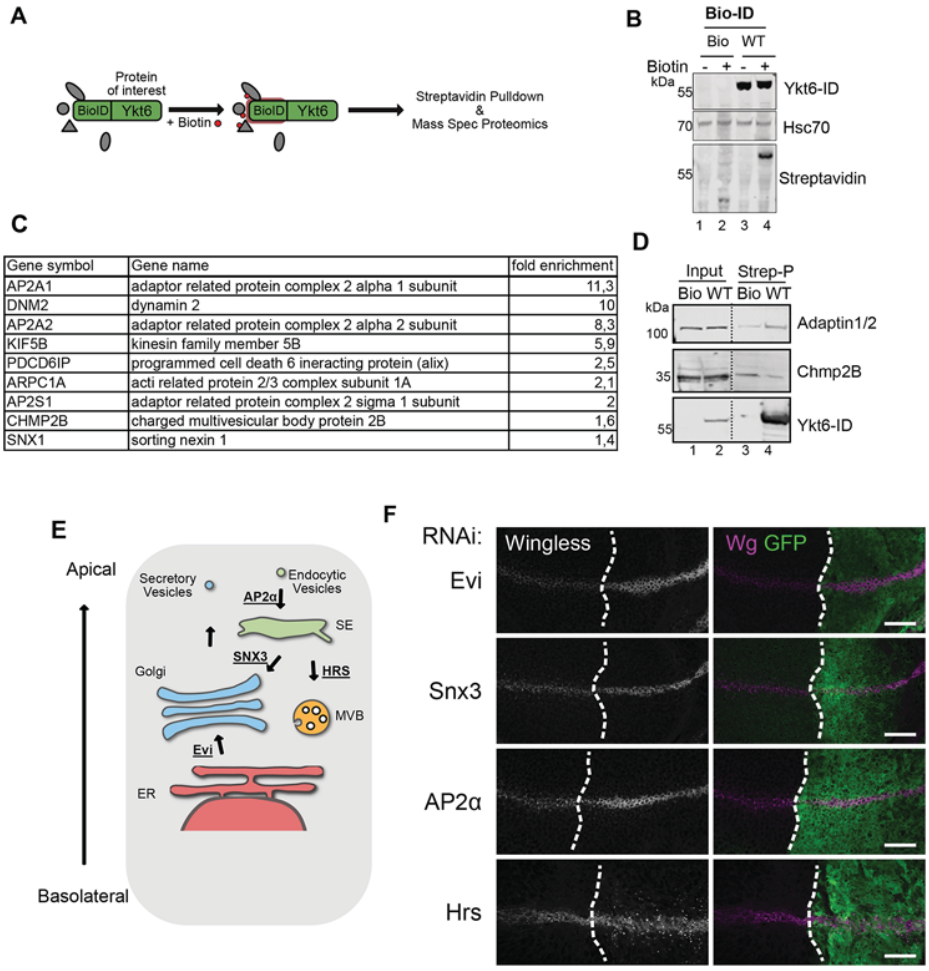

Gene symbol	Gene name	fold enrichment
AP2A1	adaptor related protein complex 2 alpha 1 subunit	11,3
DNM2	dynamin 2	10
AP2A2	adaptor related protein complex 2 alpha 2 subunit	8,3
KIF5B	kinesin family member 5B	5,9
PDCD6IP	programmed cell death 6 ineracting protein (alix)	2,5
ARPC1A	acti related protein 2/3 complex subunit 1A	2,1
AP2S1	adaptor related protein complex 2 sigma 1 subunit	2
CHMP2B	charged multivesicular body protein 2B	1,6
SNX1	sorting nexin 1	1,4

Fig. 2. Ykt6 acts on endosomal compartments after apical presentation. (A) Scheme of BioID labelling in Hek293T cells: Ykt6 was N-terminally tagged with a BioID domain. Upon addition of biotin, a streptavidin pull-down was performed, and control and Ykt6-WT samples were subjected to proteomics identification. (B) Western blot of biotin labelling of Ykt6-BioID and control in the presence of 50 µM biotin. All proteins identified by mass spectrometry in two independent experiments (significance level P=0.003 and 1.3-fold over BioID control samples) are listed in Table S2. (C) Enrichment scores for BioID-identified proteins of the endocytic pathway. (D) Western blot of Ykt6-WT-mediated BioID labelling of AP2A1/2 and Chmp2B. (E) Overview of Wnt secretion components involved after initial apical plasma membrane presentation of Wg. (F) Wg accumulation phenotypes of different factors required for Wg secretion. RNAi against Evi, Snx3 and AP2α expressed with enGAL4, and RNAi against Hrs and Dcr expressed with UAS-Dcr; enGAL4. Images represent a single confocal section and are representative of more than six WIDs per RNAi from three independent experiments. Scale bars: 20 µm.

Last, the identification of AP2 in the BioID approach and the similarity to the Syb phenotype prompted us to compare Ykt6 knockdown with depletion of different Wnt secretion components involved after apical plasma membrane presentation of Wg (Fig. 2E,F). Similar to Ykt6 and Syb RNAi, depletion of Evi, SNX3 and AP2α complex components led to Wg accumulation close to the membrane. In contrast, knockdown of the multivesicular body (MVB) component Hrs displayed punctate accumulation in Wg-secreting and -receiving cells (Fig. 2E,F). We therefore hypothesized that Ykt6 might be either involved in recycling of the transmembrane protein Evi or secretion of Wg from endosomal compartments.

Ykt6 knockdown is not sufficient to block Evi recycling

Similar to Evi knockdown, SNX3 knockdown leads to Wg accumulation. In the absence of all Retromer components (VPS26, VPS35 and SNX3) Evi is lysosomally degraded, instead of retrogradely transported towards the Golgi (Belenkaya et al., 2008; Franch-Marro et al., 2008; Port et al., 2008; Yang et al., 2008). AP2 is crucial for the endocytosis of membrane proteins such as Evi, as AP2α RNAi strongly reduces apical Evi staining (Belenkaya et al., 2008; Franch-Marro et al., 2008; Port et al., 2008; Yang et al., 2008). In contrast, we found that Ykt6 knockdown had only a weak effect on Evi (Fig. 3A-C), thus making a function of Ykt6 in Evi recycling unlikely. This is in line with a model from human cell culture, in which Wnt and Evi separate after reaching acidified endosomes (Coombs et al., 2010). If this is correct, then we expect AP2α and Ykt6 knockdown to differentially affect extracellular Wg. Indeed, staining of non-permeabilized WIDs revealed Wg accumulation at the apical surface in AP2α RNAi, whereas extracellular Wg levels were reduced upon loss of Ykt6 (Fig. 3D-F). Moreover, Wg endocytosis was unchanged in a pulse-chase Wg antibody uptake assay in Ykt6 knockdown compared with control (Fig. S3). Taken together, this demonstrates that Clathrin-mediated endocytosis and Retromer sustain the Evi recycling route. In contrast, Ykt6-dependent trafficking appears to be necessary for postendocytic secondary secretion of Wg independent of Evi.

Ykt6 acts on Wnt trafficking at the level of endosomes

As Ykt6 appears to function after Evi and Wg separate from each other, we hypothesized that it mediates an endosomal fusion event. Upon Ykt6 RNAi, we observed no change in staining for early (Rab5) or late (Rab7) endosomal markers, but a slight increase of Hrs and a slight decrease in staining for Lamp-1, a marker for lysosomes (Fig. 4A,B). Hrs captures ubiquitylated proteins and recruits ESCRT-I to sort cargo into MVBs for degradation or cargo sorting onto exosomes, but recently Hrs was also implicated in promoting the recycling of cargo via WASH-actin (MacDonald et al., 2018). Interestingly, $ykt6^{A}$ and $ykt6^{C}$ homozygous lethality can be rescued by removing one copy of hrs^{D28}, indicating that *ykt6* and *hrs* genetically interact (Fig. S4A). Next, we analysed MVB morphology and the formation of intraluminal vesicles, which can

Development (2020) 147, dev185421. doi:10.1242/dev.185421

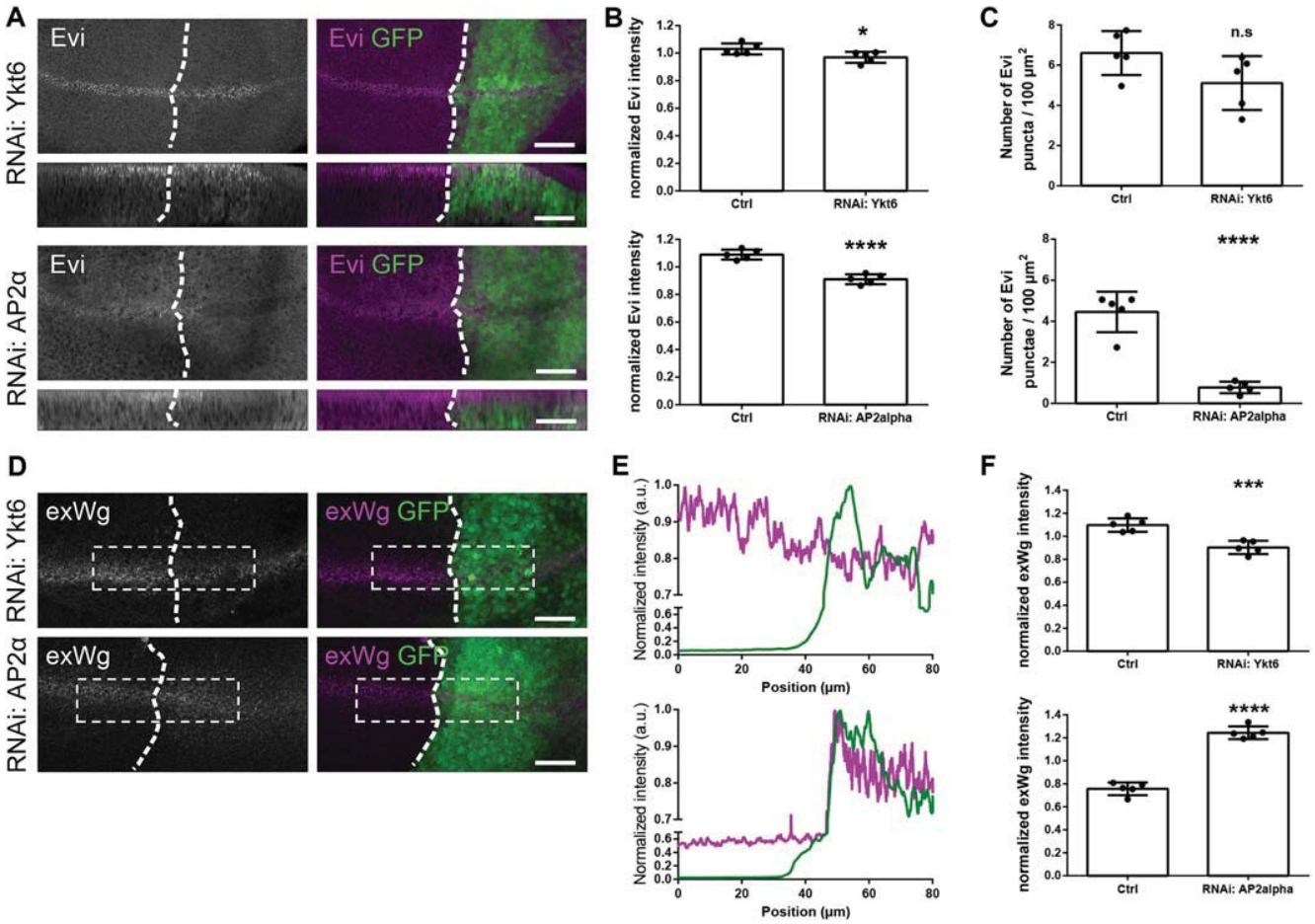

Fig. 3. Ykt6 knockdown is not sufficient to block Evi recycling. (A-C) RNAi against Ykt6 and AP2α was expressed with enGAL4,UAS-GFP, and stained for Evi. (A) The upper panels depict a maximum intensity projection of 15 apical *xy* sections (distance 1 µm); the lower panels are a transverse *xz* section of 20 pixels. (B) Comparison of Evi fluorescence intensity in n=5 biologically independent samples. Data are mean±s.d., *P=0.0425, ****P<0.0001. (C) Quantification of Evi puncta in n=5 biologically independent samples. Data are mean±s.d., ****P<0.0001. (D-F) RNAi against Ykt6 and AP2α was expressed with enGAL4 and stained for extracellular Wg. (D) A maximum intensity projection of all sections covering the entire apico-basal axis is depicted for visualization. (E) Profile of the extracellular Wg staining in the ROI depicted in D of the corresponding average intensity projection. This compares exWg in the anterior (control, no GFP) with the posterior (RNAi, GFP-positive) region for this one representative example. (F) Comparison of exWg fluorescence intensity in n=5 biologically independent samples. Data are mean±s.d., ***P=0.0007, ****P<0.0001. Scale bars: 20 µm.

be secreted as exosomes, a population of small extracellular vesicles, in an ESCRT-dependent and Alix-Syntenin-regulated manner (Baietti et al., 2012). In electron microscopy sections of WIDs, MVBs were of similar sizes in wild-type and Ykt6 RNAi compartments (Fig. 4C,D), and the apical membrane showed no strong morphological defects upon Ykt6 loss (Fig. S4B). This indicates that Ykt6 knockdown does not impair MVB morphology.

Hrs is recruited to endosomes via its Fab1/YOTB/Vac1/EEA1 (FYVE) domain, which interacts with locally generated phosphatidylinositol 3-phosphate (PI3P) (Urbé et al., 2002). To check whether increased binding of Hrs to endosomes in Ykt6 KD cells was due to a change in the composition of PI3P, which is abundant in early endosomes and MVBs, we used 2xFYVE-GFP to mark PI3P-containing endosomes *in vivo* (Wucherpfennig et al., 2003). In larval wing disc cells, 2xFYVE-GFP mostly localizes to Rab7- but not to Rab5- or Rab11-positive endosomes (Abe et al., 2009). In control WIDs, Wg-expressing cells showed a ∼32% colocalization of Wg with FYVE-GFP in puncta, compared with only 16% of Wg in Ykt6 knockdown (Fig. 4E-H). FYVE-GFP structures were smaller in Ykt6 RNAi compared with control and Wg accumulated intracellularly at the plasma membrane (Fig. 4E-H and Fig. S4C), indicating that lack of Ykt6 reduces the pool of late PI3P-containing endosomes.

To check whether Ykt6 mediates an endosome-to-plasma membrane fusion event, we used a constitutively active Rab5 (Rab5Q88L) to enlarge and visualize endosomes (Zhang et al., 2007). WgGal4-driven Rab5Q88L-YFP expression in WIDs led to enlarged endosomes positive for endogenous Wg (Fig. 4I, left panel). In Ykt6-RNAi WIDs, these endosomes were significantly larger and, in addition, Wg was seen outside Rab5Q88L endosomes close to the membrane (Fig. 4I, right panel, J), similar to Ykt6 KD alone (Fig. S4D). Higher resolution using Airyscan imaging revealed that Wg accumulates mainly laterally below junctions as marked with DE-Cadherin (Fig. S4E). Rab5Q88L-YFP expression alone did not impair Wg secretion and signalling, as wings developed normally, but when this was combined with Ykt6-RNAi it resulted in pupal lethality (Fig. S4F). It is noteworthy that we did not find endosomal size alterations in cells that overexpressed a WT version of Rab5-YFP (Fig. S4G,H). Colocalization of Wg- and endogenous Rab5 was significantly decreased in Ykt6 knockdown

Development (2020) 147, dev185421. doi:10.1242/dev.185421

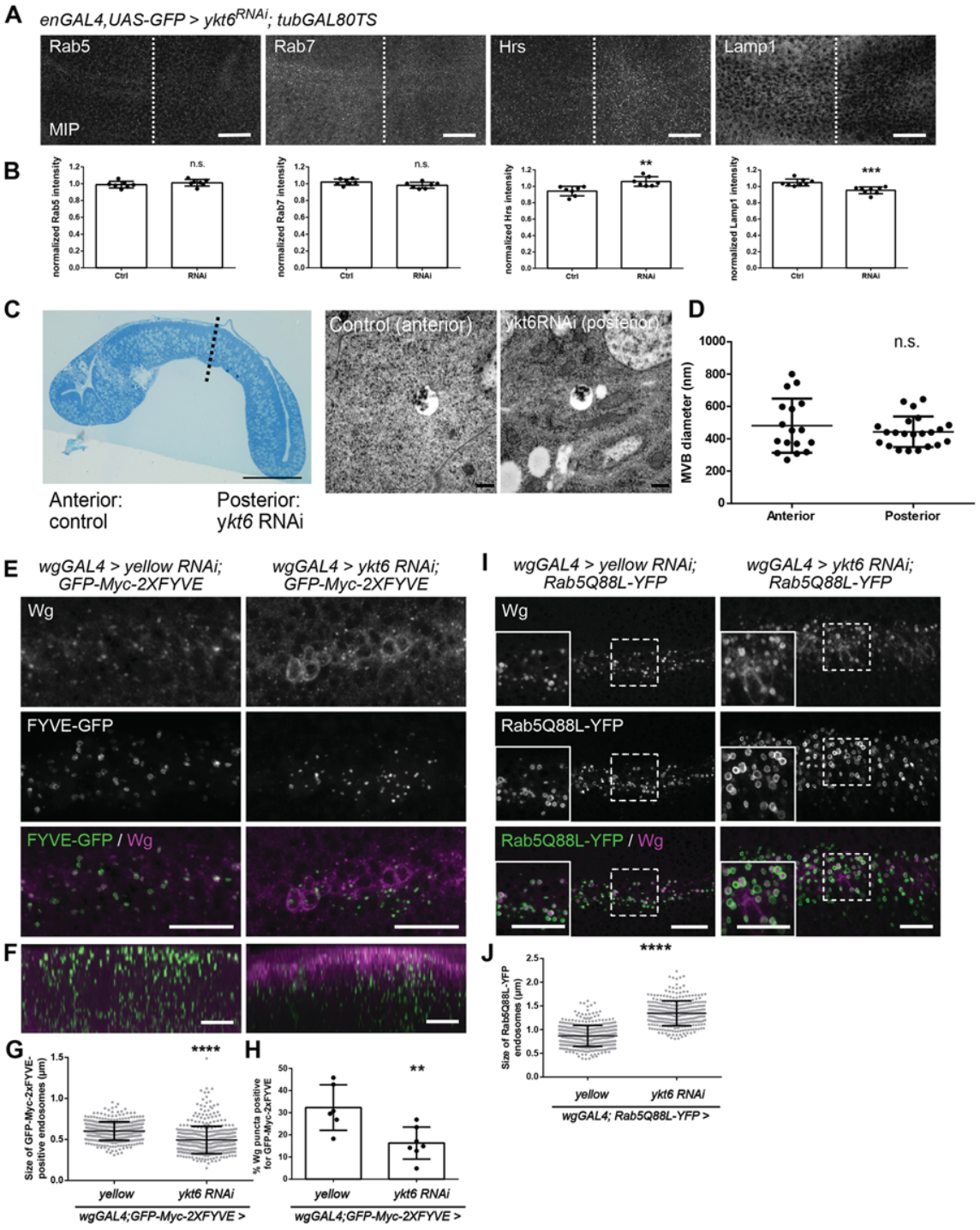

Fig. 4. Ykt6 acts on Wnt trafficking at the level of endosomes. (A) Localization of different organelle markers in wild type (left) and Ykt6 RNAi (right) from enGAL4, UAS-GFP/Ykt6 RNAi WIDs. Maximum intensity projections of 13 (Rab5), seven (Rab7, Lamp1) and nine (Hrs) sections (distance 1 µm) depicted for visualization. Scale bars: 20 µm. (B) Quantification of fluorescence intensity in *n*=7 (Rab5, Rab7 and Hrs) or *n*=8 (Lamp1) biologically independent samples from A. Data are mean±s.d., ***P*=0.0026, ****P*=0.0004. (C) Semi-thin section of a WID (left) and electron microscopy images of MVBs in a WID (right) during time-controlled depletion of Ykt6 by RNAi (engrailed-Gal4, UAS-GFP/UAS-ykt6RNAi; tubGal80-TS/+ larvae reared for 3 days at 29°C). Scale bars: 50 µm (left); 500 nm (right). (D) Quantification of MVB size in electron microscopy images from cells in the anterior (*n*=17) and posterior (*n*=22) compartments of WIDs. (E,F) GFP-Myc-FYVE was expressed with wgGAL4 and yellow (control) or ykt6 RNAi to label PI(3)P-containing endosomes. (E) MIP of six apical sections (distance 0.5 µm). (F) Transverse *xy* section. Scale bars: 10 µm. (G) Quantification of E. The diameter of GFP-Myc-FYVE -positive vesicles with a clear lumen was measured. Four representative WIDs from three biological replicates with in total 394 (yellow RNAi) and 460 (ykt6 RNAi) enlarged endosomes were quantified. Data are mean±s.d., *****P*<0.0001. (H) Quantification of F. The number of Wg puncta positive for GFP-Myc-2XFYVE was quantified. Data are mean±s.d., ***P*=0.0071. (I) Constitutively active Rab5Q88L-YFP was expressed with wgGAL4 and yellow (control) or ykt6 RNAi. Images represent a single confocal section. Scale bars: 10 µm. (J) Quantification of I. The diameter of Rab5Q88L-YFP-positive vesicles with a clear lumen was measured. Five representative WIDs from three biological replicates with, in total, 446 (yellow RNAi) and 326 (ykt6 RNAi) enlarged endosomes were quantified. Data are mean±s.d., *****P*<0.0001.

Development (2020) 147, dev185421. doi:10.1242/dev.185421

(Fig. S4I), further confirming Rab5Q88L results. Taken together, our *in vivo* genetic analyses demonstrate that lack of Ykt6 decreases Wg trafficking to late endosomes, possibly because Ykt6-dependent, endosome-derived vesicles accumulate close to the plasma membrane. Thus, Ykt6 is involved in endosomal Wg trafficking required for Wnt release.

The Ykt6 SNARE domain is required for cycling between compartments

In contrast to SNAREs with a transmembrane domain, Ykt6 is able to cycle from cytosol to membranes and back owing to its reversible C-terminal palmitoylation. Depalmitoylation of Ykt6 was described to prevent its sorting into MVBs and consequently its inactivation (Meiringer et al., 2008). To understand how Ykt6 membrane recruitment mediates Wnt secretion, we mutated the SNARE domain of Ykt6 to prevent interactions with other SNARE partners and therefore fusion events. As shown for VAMP8, mutation of serine/threonine residues to glutamic acid in the SNARE layers facing each other inhibits fusion of secretory granules by sterically blocking the interaction of the SNARE helices (Malmersjö et al., 2016). Within the SNARE layers of human Ykt6, we mutated three serine residues to glutamic acid (Ykt6-3E) and structural modelling showed steric hindrance of these glutamic acids with the auto-inhibited state of Ykt6 (Fig. S5A,B). In this state, the Longin domain binds to the farnesyl group at the C terminus, bringing it into close proximity to the SNARE domain (Tochio, 2001). We therefore investigated the intracellular localization of these Ykt6 constructs in Hek293T cells. Overexpressed Ykt6-WT showed strong cytoplasmic staining partially overlapping with Calnexin, whereas the mutated SNARE Ykt6 (Ykt6-3E) was more punctate at Golgi and the plasma membrane, suggesting accumulation at membranes (Fig. S5C-F). To confirm this biochemically, we separated cytosolic and membrane-bound proteins by differential detergent fractionation (Baghirova et al., 2015). Indeed, overexpressed Ykt6-3E was found in the membrane fraction, whereas overexpressed Ykt6-WT and endogenous Ykt6 was mostly detected in the cytoplasmic fraction (Fig. 5A,B). We hypothesized that Ykt6-3E attached more stably to membranes because it was unable to fold and release the palmitoylation. To address this possibility, we monitored the steady-state level of palmitoylated Ykt6-WT and -3E in a click-palmitate assay (Haberkant et al., 2016). In the pull down of all palmitoylated proteins, Wnt3A, as a positive control, and Ykt6-3E were both detected, whereas Ykt6-WT was below the detection limit (Fig. 5C). This indicates that the majority of Ykt6-WT reverts into its autoinhibited, depalmitoylated form in the cytoplasm, whereas depalmitoylation of Ykt6-3E is hindered and therefore some remains associated with membranes. This is in line with findings in yeast, where the release of Ykt6 from membranes into the cytoplasm depends on a functional Longin domain and its intramolecular interaction with the SNARE domain to fold into a soluble, closed conformation (Fukasawa et al., 2004; Tochio, 2001). Expressing siRNA-resistant, N-terminally-tagged Ykt6 mutant constructs in Hek293T cells, we found that, in contrast to Ykt6-WT and a non-phosphorylatable Ykt6-3A, Ykt6-3E is unable to rescue Wnt secretion (Fig. 5D,E). Mutation of F42 to alanine, a site within the Longin domain and required for the cytoplasmic, closed conformation of Ykt6 (Tochio, 2001), did not reduce Wnt secretion. All these constructs did not affect secretion of secreted GFP (ssGFP; Suzuki et al., 2012), indicating that the SNARE domain is functionally involved in Wnt secretion (Fig. 5D,E).

Endosomes acidify during trafficking towards the perinuclear region (Wallroth and Haucke, 2018), but also during trafficking towards the plasma membrane, as passage through an acidic compartment is required for Wnt secretion (Coombs et al., 2010). To understand how Ykt6 changes from the auto-inhibited soluble form into the membrane-bound active form, we tested how blocking depalmitoylation by Palmostatin B and acidification by Bafilomycin A1, chloroquine or ammonium chloride affect Ykt6 recruitment to membranes. To increase the detection limit of endogenous Ykt6, proteins in membrane and cytoplasmic fractions were methanol precipitated (Wessel and Flügge, 1984). Bafilomycin A1, chloroquine, ammonium chloride and Palmostatin B alone did not significantly increase membrane recruitment of endogenous Ykt6 (Fig. 5F,G). Inhibiting both endosomal acidification and depalmitoylation together significantly increased Ykt6 detection in the membrane fraction (Fig. 5F,G). Next, we checked whether Ykt6 was able to detach from membranes after Bafilomycin A1 release in the presence or absence of Palmostatin B. Bafilomycin-dependent Ykt6 attachment to membranes was reversible only in the absence of Palmostatin B, demonstrating that depalmitoylation is the final step of membrane release (Fig. 5H,I). As Ykt6-3E remains palmitoylated and cannot detach from bound membranes anymore, a functional SNARE domain is required for the turnover of palmitoylation and regulation of membrane detachment.

To confirm the functional role of the Ykt6 SNARE domain *in vivo*, we mutated four serine residues to alanine (Ykt6-4A) or glutamic acid (Ykt6-4E) within the SNARE layers of *Drosophila* Ykt6 (Fig. S5A). Prolonged knockdown or permanent loss of Ykt6 is cell lethal, probably owing to lysosomal dysfunction (Matsui et al., 2018). Time-controlled RNAi of Ykt6 in the posterior compartment of WIDs caused intracellular Wg accumulation compared with the anterior control compartment (Fig. 5J,K). Ykt6 knockdown also suppressed Wnt target gene expression (Fig. S6A) and ultimately led to wing notches in adult flies, indicating blocked Wg secretion and consequently Wnt signalling defects (Fig. 5L; Strigini and Cohen, 2000). The mutated SNARE constructs (Ykt6-4A or Ykt6-4E) and Ykt6-WT were expressed using enGal4 in addition to tubGAL80-mediated time-controlled RNAi of Ykt6 in the posterior WID. Inhibition of Wg secretion and wing notches were rescued by expression of Ykt6-WT and Ykt6-4A (Fig. 5M-O, left and middle panels, Fig. S6B), thus confirming its specificity. However, co-expression of Ykt6-4E resulted in Wg accumulation and adult wing defects (Fig. 5M-O right panel, Fig. S6B). Along these lines, Ykt6-WT and, to some extent, -4A, but not -4E, were able to rescue overall lethality of the mutant alleles $ykt6^{A}$ and $ykt6^{C}$ (Fig. S6C). This indicates that Ykt6 requires a functional SNARE domain for both normal cellular growth and Wg secretion *in vivo*.

Ykt6 recycles Wg via Rab4 endosomes

Based on our findings that Ykt6 is recruited to membranes by endosomal deacidification and genetically interacts with Hrs, we investigated whether Ykt6 recycles Wg from sorting endosomes to the apical surface for secondary, long-range secretion, possibly on cytonemes or extracellular vesicles (Gross et al., 2012; Stanganello et al., 2015). In mammalian cells, Rab4 directs fast recycling from early endosomes to the plasma membrane, whereas Rab11 mediates a slow recycling route from MVBs towards the plasma membrane (De Renzis et al., 2002). In WIDs, localization of the slow recycling endogenously tagged Rab11-YFP, as well as UAS-Rab11-YFP, were not affected upon Ykt6 knockdown (Fig. S6D,E), supporting the previous finding that Ykt6 does not influence MVB biogenesis (Fig. 4C,D). We next analysed the possibility that Wg might be recycled via a fast Rab4-dependent way. Both an endogenously

Development (2020) 147, dev185421. doi:10.1242/dev.185421

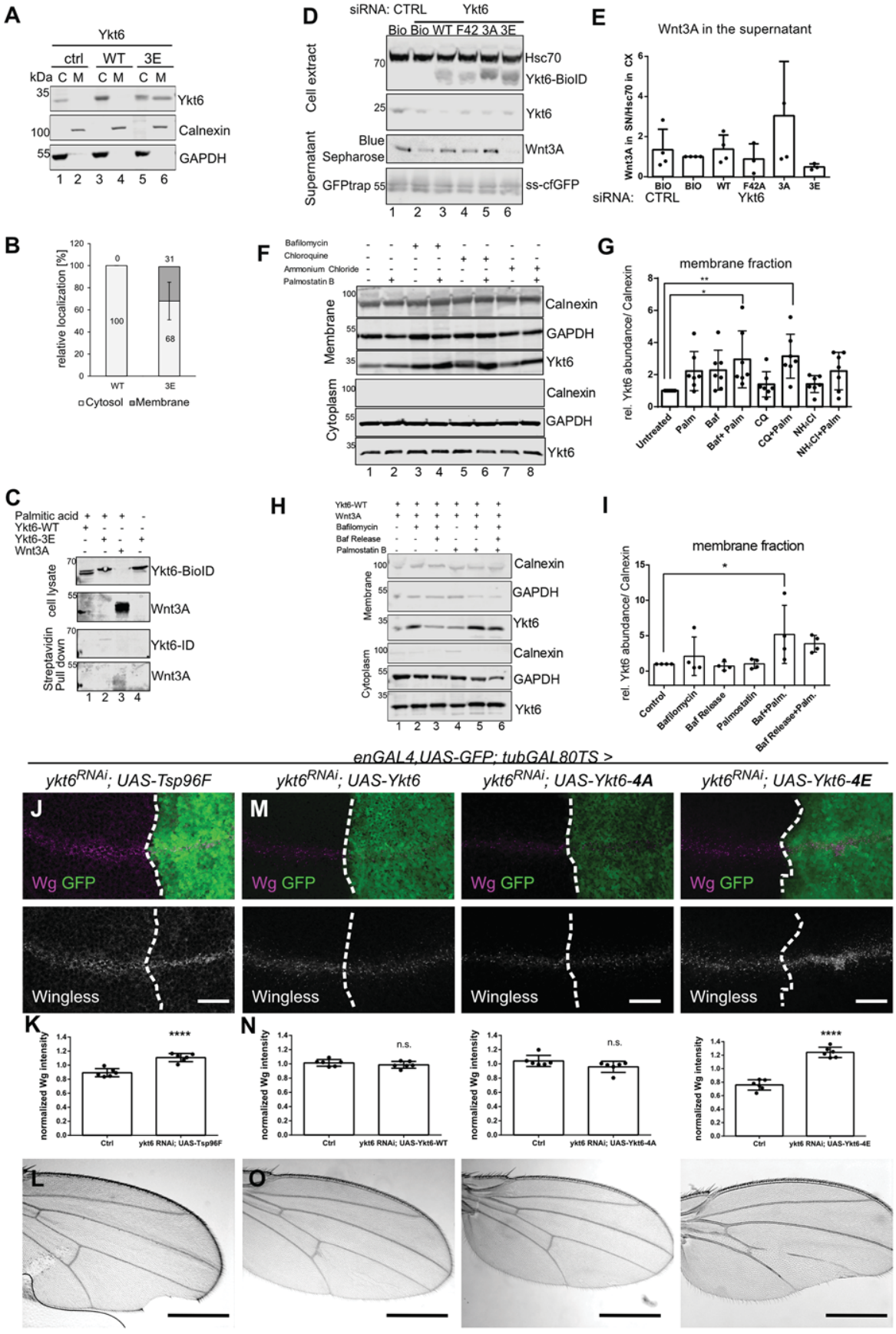

Fig. 5. See next page for legend.

Development (2020) 147, dev185421. doi:10.1242/dev.185421

Fig. 5. A Ykt6 SNARE domain is required for cycling between compartments. (A,B) Representative blot (A) and quantification (B) of detergent fractionation of Hek293T cells transfected with Ykt6-WT and Ykt6-3E constructs. C, cytoplasmic; M, membrane fraction, *n*=3. (C) Click palmitoylation assay of Ykt6-WT and Ykt6-3E; Wnt3A is a positive control. Representative blot of three biological replicates. (D,E) Representative blot (D) and quantification (E) of Wnt3A secretion from Hek293T cells transfected with Ykt6-WT, phosphor-mutant Ykt6-3A and Ykt6-3E, and Longin domain mutant Ykt6-F42 constructs. *n*=4. One-way ANOVA (no significant differences). (F,G) Inhibiting endosomal acidification and depalmitoylation affects Ykt6 subcellular localization. (F) Representative blot of cell fractionation of untagged Ykt6 mutant constructs in Hek293T cells, treated with bafilomycin, chloroquine or ammonium chloride in combination with palmostatin B, stained for Ykt6 and fraction markers. (G) Quantification of Ykt6 in the membrane fraction, *n*=7; **P*=0,01, ***P*=0.005 one-way ANOVA. (H,I) Ykt6 membrane recruitment and release. Blot of cell fractionation of untagged Ykt6 in Hek293T cells treated with bafilomycin and palmostatin B, and release from bafilomycin inhibition stained for Ykt6 and fraction markers. (I) Quantification of H from *n*=4; **P*=0,03, one-way ANOVA. (J-L) Time-controlled depletion of Ykt6 by RNAi (engrailed-Gal4, UAS-GFP/UAS-ykt6RNAi; tubGal80-TS/UAS-Tsp96F larvae reared for 3 days at 29°C) causes intracellular Wg accumulation (J,K) and wing notches (L). (M-O) Time-controlled Ykt6 RNAi-induced block of Wg secretion and adult wing margin notches can be rescued by co-overexpression of wild-type Ykt6 and the SNARE mutant Ykt6-4A (left and middle panels), but not by Ykt6-4E (right panels). (K,N) Quantification of fluorescence intensity in *n*=6 biologically independent samples from J,M. Data are mean±s.d., *****P*<0.0001. (J,M) Projections of six subapical sections (distance 1 µm, J) and six subapical sections (distance 0.5 µm, M). Representative images of more than 10 discs from *n*=3. Scale bars: 20 µm (J,M); 500 µm in adult wing images (L,O).

tagged Rab4-YFP and overexpressed UAS-Rab4-YFP partially colocalize with Wg in puncta under control conditions (Fig. 6A,B). In contrast, both Wg and UAS-Rab4-YFP accumulate together intracellularly at the plasma membrane in Ykt6 RNAi, indicating that Ykt6 mediates Wg trafficking via Rab4 recycling endosomes (Fig. 6B,C, left and middle panels). Co-expression of Ykt6-4E results in Wg accumulating together with Rab4 and does not rescue wing notches induced by impaired Wg secretion (Fig. 6B,C, right panel). In agreement with this recycling route, in RNAi of Rab4, Wg accumulated towards the apical membrane (Fig. 6D,E), similar to Rab5 (Fig. 6D,F). Taken together, our results position Ykt6 function at the level of sorting endosomes, upstream of MVB sorting and ILV formation. Ykt6 cytosol-to-membrane cycling is required in a Rab4 endosomal trafficking step to ensure proper extracellular Wnt levels for Wnt target gene activation.

DISCUSSION

In this study, we have shown that Ykt6 recycles Wg to the membrane via Rab4-positive endosomes to regulate Wnt trafficking in the polarized wing epithelium of *Drosophila*. Counterintuitively, an essential step of this trafficking is Wg endocytosis from the apical membrane before final secondary secretion and subsequent Wnt signal activation. In particular, the SNARE domain of Ykt6 is required for cycling between cytosol and membranes, as Wg/Wnts are trafficked through the secretory pathway. Our results explain how post-endocytic Wnt trafficking and Ykt6 as a valve contribute to adjusting extracellular Wnt levels and proper gradient formation.

Endosomal regulation of Wnt signalling

Early endosomes are a major sorting hub and crossroad for internalized receptors, cargo and membranes (reviewed by Jovic et al., 2010). Interestingly, three Wnt signalling processes converge in and separate from acidified endosomes: (1) separation of Wnt from its trafficking receptor Evi and recycling of Evi via Retromer; (2) Wnt receptor activation; and (3) as we show here, secondary secretion of Wnts. The pool of apically presented and subsequently endocytosed Wg might serve as a signalling reservoir that can be rapidly mobilized by Ykt6-mediated recycling to the membrane. A possible reason for this might be that endosomes sense Wnt signalling levels and fine-tune further Wnt secretion accordingly. In line with this idea, Wg is endocytosed apically, while its receptor Fz2 is internalized from the basolateral side and both meet in acidified endosomes for signal transduction (Hemalatha et al., 2016). Similarly, acidification by V-ATPase activity is required for Wnt receptor activation in vertebrates (Cruciat et al., 2010). MVBs are also important regulatory hubs for non-transcriptional Wnt signalling readout (Acebron et al., 2014; Albrecht et al., 2018; Taelman et al., 2010). We found that, upon Ykt6 depletion, extracellular Wnt levels are reduced, but Evi levels are unchanged. Thus, we excluded a role for Ykt6 in the passage of Evi/Wnt complexes to acidified endosomes and reasoned that Ykt6 is required for an Evi-independent step of Wnt trafficking. We thus propose a model in which Ykt6 is recruited to de-acidified endosomes to re-secrete more Wnts, ensuring proper receptor activation in a feedback loop.

Our finding that Ykt6 acts at the level of early endosomes suggests that it only affects exosomal Wnt sorting indirectly. Ykt6 depletion increases Hrs-positive but reduces FYVE-GFP-positive endosomes and no changes were observed in MVB morphology in WIDs (Fig. 4C,D). This is in line with our previous observation in human cells that Ykt6 depletion affects exosomal CD63 MVB sorting rather than their formation (Gross et al., 2012). Interestingly, Wg endocytosis from the apical side depends on HSPGs (Baeg et al., 2001; Perrimon and Lin, 1999; Selleck et al., 1999), which are also involved in cargo sorting onto exosomes via Alix and Syntenin (Ghossoub et al., 2014).

Our results on Ykt6 membrane recruitment and Rab4 recycling in *Drosophila* indicate that there is an additional level at which Wnt secretion is fine-tuned in the late secretory pathway by Ykt6 cytosol-to-membrane cycling. Wnts and other lipid-modified signalling molecules, such as Hedgehog (Hh), have a common mechanism of intracellular trafficking and secretion (reviewed by Brunt and Scholpp, 2018). In agreement with our findings, two different routes of secretion from WIDs have been proposed for Hh: secretion from: (1) the basolateral membrane on cytonemes/EVs (Bischoff et al., 2013; Gradilla et al., 2014); and (2) from the apical membrane after passage through Rab4 endosomes (D'Angelo et al., 2015). Whether an Ykt6-mediated fusion step via Rab4 is regulating Hh secretion remains to be investigated.

SNARE Ykt6 in endosomal trafficking

A fundamental question in intracellular trafficking is how specificity and directionality can be achieved. Peripheral membrane proteins have an advantage over transmembrane proteins in that their subcellular localization can be rapidly modulated. We identified putative phosphorylation sites within the SNARE domain of Ykt6 that allow membrane recruitment and stabilization. This mechanism is required for Ykt6 membrane-to-cytosol cycling and its function in Wnt secretion. Our rescue experiments show that phosphomimicking mutations stabilize Ykt6 at membranes and fail to rescue Wnt trafficking via Rab4 recycling endosomes. In general, members of the SNARE family are regulated by post-translational modifications such as monoubiquitylation (Syx5) (Huang et al., 2016) or palmitoylation (SNAP25) (Gonzalo and Linder, 1998). A recent study described phosphorylation sites within the SNARE domain of non-neuronal SNAREs conserved over the plant, fungi and animal kingdoms

Development (2020) 147, dev185421. doi:10.1242/dev.185421

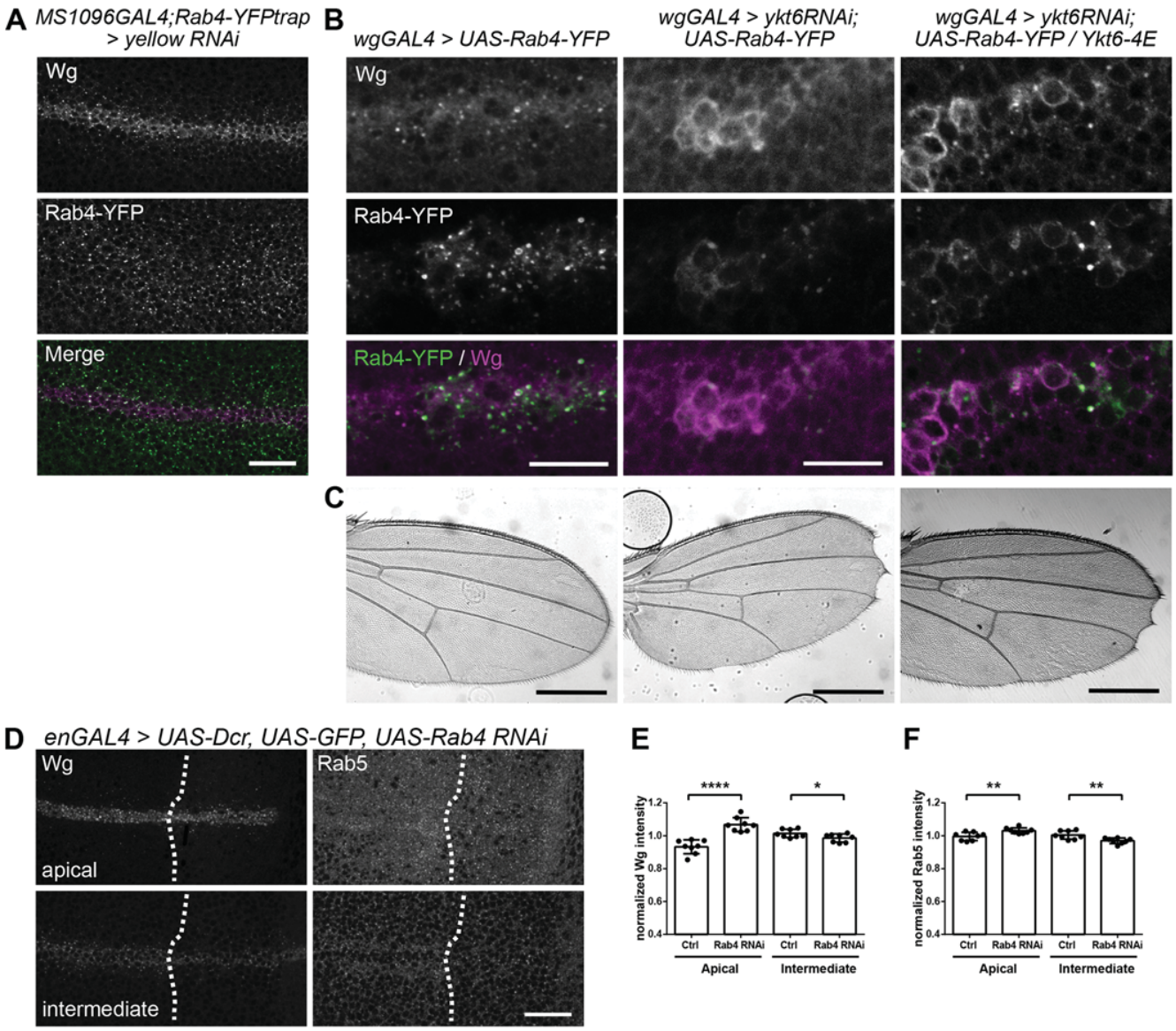

Fig. 6. Ykt6 recycles Wg via Rab4 endosomes. (A) Yellow RNAi was expressed with MS1096GAL4 in the wing pouch in an endogenously tagged Rab4-YFP background. Maximum intensity projection of three sections (distance 0.5 µm) depicted for visualization. Scale bar: 20 µm. (B) UAS-Rab4-YFP was expressed with wgGAL4 alone, in combination with ykt6 RNAi or ykt6 RNAi and Ykt6-4E. A single subapical section is depicted. Scale bars: 10 µm. (C) Adult wings of the crosses from B to show adult wing notches. Scale bars: 500 µm. These wings are representative of more than 10 wings from three independent experiments. (D) RNAi against Rab4 was expressed with enGAL4, UAS-GFP,UAS-Dcr and stained for Wg and Rab5. Maximum intensity projection of three apical (upper panels) and intermediate (lower panels) sections is depicted for visualization. Scale bar: 20 µm. (E) Quantification of Wg apical versus intermediate fluorescence intensity in n=8 biologically independent samples from D. Data are mean±s.d., ****P<0.0001, *P=0.04. (F) Quantification of Rab5 apical versus intermediate fluorescence intensity in n=8 biologically independent samples from D. Data are mean±s.d., **P=0.006.

(Malmersjö et al., 2016). As shown for VAMP8, mutation of these sites inhibits fusion of secretory granules (Malmersjö et al., 2016). Further work will be required to determine which phosphorylation sites of the Ykt6 SNARE domain are physiologically relevant and whether they precede and direct membrane binding or stabilize previous membrane attachment. As a proposed stress sensor in yeast (Dietrich et al., 2004), our results confirm that the majority of human Ykt6 localizes to the cytoplasm, potentially serving as a reserve pool to release trafficking stress at different levels and under specific circumstances.

Our observed trafficking direction towards the plasma membrane oppose recent studies, in which Ykt6 was implicated in non-canonical autophagosome formation under starvation conditions (Kimura et al., 2017; Matsui et al., 2018; Takáts et al., 2018). However, first, we investigated Ykt6 function under normal growth conditions, as Wnt secretion is strongly reduced under starvation (Mihara et al., 2016) and found accumulation of Wg and Rab4 close to the plasma membrane, in combination with an increase in early but a decrease in late endosomal markers. Second, we found a genetic interaction between Ykt6 and Hrs, as Hrs knockout rescued Ykt6 RNAi lethality. These results fit with a re-routing of endosomal trafficking towards the extracellular space. Indeed Matsui and colleagues have proposed that lysosomal dysfunction is the cause of Ykt6 lethality (Matsui et al., 2018). Another Longin

Development (2020) 147, dev185421. doi:10.1242/dev.185421

SNARE, Sec22B, mediates unconventional secretion of cytosolic proteins via autophagosome fusion with the plasma membrane (Kimura et al., 2017). Ykt6 activation via its conformational switch in the SNARE domain raises the interesting possibility of integrating different upstream signalling pathways and determining local activation of Ykt6 and therefore direction of trafficking events. In line with our findings, Ykt6 was shown to increase leucine and isoleucine uptake under starvation conditions by increasing the surface level of their transporters (Saito et al., 2019). Our BioID data confirm that Ykt6 acts proximal to very different cellular processes, such as endocytosis, RNA transport and metabolic signalling pathways, which could contribute to its RNAi-induced cell growth defects. It remains to be determined whether Ykt6 activation is a directional switch in endosomal trafficking towards the plasma membrane or lysosomal degradation.

Taken together, we have shown that Ykt6 cytosol-to-membrane cycling is required for Wnt secretion from endosomes. With its ability to adapt to multiple cellular localizations, Ykt6 is an ideal candidate for orchestrating selected cargo recycling of secreted morphogens such as Wnt, in the endosomal system. Further investigation is required to understand the regulatory networks upstream of Ykt6 endosomal trafficking at the crossroad of secretion and degradation.

MATERIALS AND METHODS

Plasmids and siRNA

The coding region of *Drosophila* Ykt6 was amplified and the PCR product recombined into pDONR221 vector using the Gateway BP Clonase II Enzyme mix (Life Technologies). Point mutations of potential phosphorylation sites (S175, S182, T188 and T192) were introduced by site-directed mutagenesis. For generation of transgenic flies, constructs were subcloned into expression vectors pUASt-attB-rfA-mCherry (a kind gift from Sven Bogdan, Philipps University Marburg, Germany) by LR recombination (Life Technologies). Human Ykt6 was amplified from hYkt6-Myc [C-terminal myc-destination plasmids (DKFZ – Genomics and Proteomics Core Facility)] and the PCR product inserted into pcDNA3.1MycBioID (Addgene 35700). Point mutations for Ykt6-3A (S174A, T181A and S187A), Ykt6-3E (S174E, T187E and S181E), F42A, C194A, C195A and relevant combinations were introduced by site-directed mutagenesis. The MycBioID tag was removed using NheI/XhoI to obtain untagged constructs in pcDNA3.1. The following expression constructs were used: TCF4/Wnt-Firefly Luciferase (Demir et al., 2013), Actin-Renilla Luciferase (Nickles et al., 2012), pCMV-Wnt3A (Gross et al., 2012) and DsRed-Rab5-QL (E. De Robertis, University of California, Los Angeles, USA; Addgene 29688). Dharmacon siRNA SMARTpools are listed in Table S3.

Antibodies

Antibodies were used against Calnexin [1:1000 western blot (WB); rabbit (sc-11397), Santa Cruz); 1:10 immunofluorescence (IF); mouse (Cnx99A 6-2-1), DSHB], CD81 (1.3.3.22) [1:1000 WB; mouse (DLN-09707), Dianova], GAPDH (6C5) [1:5000 WB; mouse (AM4300), Ambion], GFP [1:1000 IF; mouse (A11120) and rabbit (A11122), Molecular Probes], GM130 [1:300 IF; mouse (610823), BD], GM130 [1:500 IF; rabbit (ab30637) Abcam], Hrs [1:10 IF; mouse (Hrs8-2 and Hrs27-4), DSHB], Hsc70 [1:2000 WB; mouse (sc-7298), Santa Cruz], Lamp1 [1:100 IF; rabbit (ab30687), Abcam], mCherry [1:1000 IF; rabbit (ab167453), Abcam], Rab5 [1:500; rabbit (ab31261), Abcam], Rab7 [1:10; mouse (Rab7), DSHB], Sec22, Syb and Vamp7 [IF; 1:250, kind gifts from Andrew A. Peden, The University of Sheffield, UK (Gordon et al., 2017)], Sens [IF; rabbit; 1:1000, a kind gift from Hugo Bellen, Baylor College of Medicine, Houston, TX, USA (Nolo et al., 2000)], Syx1A [1:10; mouse (8C3), DSHB], TSG101 [1:1000 WB; rabbit (HPA006161), Sigma], Wg [1:3 for extracellular and 1:20 for total staining (mouse, 4D4, DSHB)], Wnt3A [1:500 WB; rabbit, Abcam, ab172612), Wnt5A [1:500 WB; rabbit (2530), CST], Evi/Wls [1:500 IF; rabbit, a kind gift from Konrad Basler, University of Zurich, Switzerland), and Ykt6 [1:1000 WB and IF; mouse (sc-365732), Santa Cruz]. Secondary antibodies directed against the species of interest were coupled to Alexa Fluor 488, 568, 594 and 647 (IF, 1:500, Invitrogen), and 680RD and 800CW (WB, 1:20,000, LiCor).

Drosophila stocks and genetics

The following *Drosophila* stocks were used in this study: *en-GAL4, UAS-GFP* (chr. II, a gift from J. Grosshans, Philipps University Marburg, Germany), *wg-Gal4* (chr. II, a gift from S. Cohen, University of Copenhagen, Denmark) and *UAS-GFP-Myc-2XFYVE* (chr. III, a gift from M. Gonzalez-Gaitan, University of Geneva, Switzerland). The following stocks were obtained from Bloomington Drosophila Stock Center: *da-GAL4* (5460), *UAS-Dcr; enGAL4,UAS-GFP* (25752), *tub-GAL80TS* (7108), MS1096-GAL4 (8860), *ykt6^{A}FRT19A/FM7c,Kr-GAL4,UAS-GFP* (57143), *ykt6^{C}FRT19A/FM7c,Kr-GAL4,UAS-GFP* (57142), *His2Av-GFP, hsFlp,FRT19A* (32045), FRT19A (1709), *vas-PhiC31; attP.ZH-86Fb* (24749), AliX TRiP (33417), Hrs TRiP (28026 and 33900), *UAS-Rab4-YFP* (9767), *UAS-Rab5-YFP* (24616), *UAS-Rab5Q88L-YFP* (9773), UAS-Rab11-YFP (50782), Rab4-YFP trap (62542) and Rab11-YFP trap (62549). The following UAS-RNAi stocks were obtained from Vienna Drosophila RNAi Center: ALiX (GD32047), AP-2α (GD15565), Evi (GD5214 and KK 103812), Rab4 (KK106651), Sec22 (KK100766), Snx3 (KK104494), Syb (KK102922) and Ykt6 (KK105648). Additional RNAi lines used for the screens in Fig. 3A are listed in Table S1. UAS-Ykt6 transgenic lines were generated according to standard protocols by ϕC31 integrase-mediated site-specific insertion in the attP landing site at ZH-86Fb (Bischof et al., 2007). We sequenced the *ykt6* mutant allele stocks and realized that the annotation at FlyBase/Bloomington is not correct: *ykt6^{A}* (BL57143), annotated as M1I in fact carries Q62R, the mutation in the Longin domain. *ykt6^{C}* (BL57142), annotated as Q62R in fact carries M1I, the mutation in the start codon.

Fly stocks were kept on standard medium containing agar, yeast and corn flour. Crosses were performed at 25°C except for *tub–Gal80TS* crosses, which were moved to 29°C 3 days before dissection of wing imaginal discs. To generate negatively marked *ykt6* mutant and *FRT* control clones in the wing imaginal disc under the control of *hsFlp*, animals of the appropriate genotype were heat-shocked 4 days after egg laying for 2 h at 37°C on 2 consecutive days and dissected on the next day at the wandering L3 stage.

Cell culture and transfection

Hek293T, HCT116 and SkBr3 cells were maintained in DMEM (Gibco) supplemented with 10% fetal calf serum (Biochrom) at 37°C in a humidified atmosphere with 5% CO_2. Cells were transiently transfected with Screenfect siRNA for siRNA and Screenfect A (Screenfect) for plasmids according to the manufacturer's instructions and checked regularly for mycoplasma contamination and authenticated.

Cell fractionation

Cells were fractionated as described previously (Baghirova et al., 2015), briefly HEK293T cells were seeded and transfected with Ykt6-WT plasmid. At 48 h post-transfection, cells were lysed on ice with 1 ml of Lysis buffer A (150 mM NaCl, 50 mM Hepes, 0.1% saponin, 1 M glycerol and 1% PIC), then centrifuged at 2000 ***g*** for 10 min at 4°C and the supernatant (cytosolic fraction) was transferred to a new tube. The pellet was lysed in 1 ml of Lysis Buffer B (150 mM NaCl, 50 mM Hepes, 1% Igepal, 1 M glycerol and 1% PIC) and incubated by rotating for 30 min at 4°C. It was then centrifuged at 7000 ***g*** for 10 min at 4°C and the supernatant transferred to a new tube (membrane fraction). Proteins in both fractions were precipitated with methanol/chloroform and water as described previously (Wessel and Flügge, 1984).

Blue sepharose precipitation

The relative amount of Wnts secreted into cell culture supernatant was analysed using blue sepharose precipitation as described previously (Glaeser et al., 2016; Willert et al., 2003). Briefly, cells were transiently transfected in 6-well plates with 1 µg of Wnt3A plasmids. At 72 h after transfection the supernatant was collected and centrifuged at 1500 ***g*** to remove cell debris, transferred to a fresh tube and rotated at 4°C for 1 h with 1% Triton X-100 and 40 µl of blue sepharose beads. The samples were washed and eluted from the beads using 2×SDS buffer with β-mercaptoethanol and analysed by immunoblotting.

Development (2020) 147, dev185421. doi:10.1242/dev.185421

Immunostaining, microscopy and image analysis

For IF, cells were reverse transfected with siRNAs, seeded in 6-well dishes or on 8-well microscopic coverslips, transfected 24 h later with indicated plasmids and fixed with 4% paraformaldehyde 48–72 h later. Cells were permeabilized with 0.1% Triton X-100 and blocked in 10% BSA/PBS. Primary antibodies in PBS were incubated for 1 h at room temperature and antibody binding visualized using fluorochrome-conjugated secondary antibodies.

Immunostaining of wing imaginal discs was performed as per standard procedures. Total and extracellular Wg staining were carried out as previously described (Strigini and Cohen, 2000). Staining and microscopy conditions were kept identical for discs used for comparisons. Imaginal discs were mounted in Mowiol and images were taken using a Zeiss LSM780 confocal microscope. *Z* stacks were generated with 0.5-1 µm intervals using a Plan Neofluar 63×/oil NA 1.4 objective. Confocal images were processed with Zen lite (Zeiss), Fiji/ImageJ (NIH) (Rueden et al., 2017; Schindelin et al., 2012; Schneider et al., 2012) and Affinity Designer (Affinity). Quantification of colocalization was performed by calculating Pearson's coefficients of *z*-stacks using the Fiji/ImageJ PlugIn JaCoP (Bolte and Cordelières, 2006). Rab5Q88L and FYVE endosome sizes were quantified manually using Fiji/ImageJ. Details on image analysis are provided in the supplementary Materials and Methods.

Wg endocytosis assay

To monitor Wg endocytosis and intracellular trafficking, WIDs were incubated in mouse anti-Wg (1:5, 4D4, DSHB) for 1 h at 22°C. To remove extracellular antibody signal, WIDs were rinsed three times in PBS and acid washed in 0.1 M glycine-HCl buffer (pH 3.5) for 30 s at room temperature. WIDs were rinsed three more times in PBS before being fixed and stained as described previously (Strigini and Cohen, 2000).

Electron microscopy

Wing imaginal discs were fixed in 2.5% glutaraldehyde in 100 mM phosphate buffer (pH 7.2), washed in 100 mM phosphate buffer and postfixed in 2% osminum tetroxide in phosphate buffer for 1 h on ice. After contrasting en bloc in 2% uranyl acetate, the specimens were dehydrated in ethanol and embedded in araldite using acetone as an intermediate solvent. Thin sections were stained with 2% uranyl acetate and lead citrate. Sections were observed under an EM 109 (Zeiss) microscope at 80 KV. Quantification of MVB diameter was carried out manually in Fiji/ImageJ (NIH) (Rueden et al., 2017; Schindelin et al., 2012; Schneider et al., 2012).

Click palmitoylation assay

Click assay was performed as described previously (Haberkant et al., 2016). In short, HEK293T cells were seeded, then transfected with plasmids (YKT6-WT BioID, YKT6-3E BioID and Wnt3A) in DMEM supplemented with 10% FBS. ω-Alkynyl palmitic acid (Alk-C16) was dissolved in ethanol to a final concentration of 50 mM and stored at −80°C. Alk-C16 was diluted to a final concentration of 100 µM in DMEM supplemented with 5% FBS (fatty acid-free) sonicated for 15 min at room temperature in a water bath and then allowed to precomplex for another 15 min. Alk-C16-containing medium was added to cells and partially replaced after 24 h. At 72 h post-transfection, cells were lysed (PBS with 1% Triton x-100, 0.1% SDS, PIC), then centrifuged at 16,000 ***g*** for 5 min at 4°C. Lysates were then precipitated with Wessel-Flugge Protein precipitation. The click labelling reaction [0.1 mM biotin-azide, 1 mM Tris(2-carboxyethyl)phosphine hydrochloride (TCEP, Sigma-Aldrich) dissolved in water, 0.1 mM Tris[(1-benzyl-1H-1,2,3-triazol-4-yl)methyl]amine (TBTA, Sigma–Aldrich) dissolved in DMSO and 1 mM CuSO4 in water] was incubated by shaking for 2 h at 37°C under dark conditions. After the click reaction, the samples were precipitated with 10× methanol overnight at −80°C, then centrifuged and washed again with ice-cold methanol, The dried pellet was resuspended in 4% SDS. Click-biotinylated proteins precipitated with High Capacity Neutravidin Agarose Resin (Thermo Scientific). Samples were washed with 1% SDS and eluted, then analysed further by immunoblotting.

BioID pull down and mass spectrometry

For large-scale BioID pull down, Hek293T cells were seeded and 24 h later transfected with BioID-WT or mock constructs. At 36 h post-transfection 50 µM biotin was added overnight. Cells were washed with PBS twice and harvested in Ripa Lysis buffer [50 mM Tris-HCl (pH 7.5), 150 mM NaCl, 1% Igepal, 0.5% sodium desoxycholate, 0.1% SDS] containing 1× Complete protease inhibitor (Life Technologies). After centrifugation at 16,500 ***g*** for 10 min, lysates were boiled for 5 min in non-reducing SDS sample buffer [300 mM Tris-HCl (pH 6.8), 12% SDS, 0.05% bromophenol blue, 60% glycerol, 12 mM EDTA], either fully separated or run short-distance (1.5 cm) on a 4-12% NuPAGE Novex Bis-Tris Minigel (Invitrogen). Gels were stained with Coomassie Blue for visualization purposes. Full lanes were sliced into 23 equidistant slices regardless of staining, short runs were cut out as a whole and diced. After washing, gel slices were reduced with dithiothreitol (DTT), alkylated with 2-iodoacetamide and digested with trypsin overnight. The resulting peptide mixtures were then extracted, dried in a SpeedVac, reconstituted in 2% acetonitrile/0.1% formic acid/ (v:v) and prepared for nanoLC-MS/MS as described previously (Atanassov and Urlaub, 2013).

For generation of a peptide library for SWATH-MS, equal aliquots from each sample were pooled to a total amount of 80 µg and separated into eight fractions using a reversed-phase spin column (Pierce High pH Reversed-Phase Peptide Fractionation Kit, Thermo Fisher Scientific). Mass spectrometry analysis protein digests were separated by nanoflow chromatography. Either 25% of gel slices or 1 µg aliquots of digested protein were enriched on a self-packed precolumn (0.15 mm ID×20 mm, Reprosil-Pur120 C18-AQ 5 µm, Dr Maisch, Ammerbuch-Entringen, Germany) and separated on an analytical RP-C18 column (0.075 mm ID×250 mm, Reprosil-Pur 120 C18-AQ, 3 µm, Dr Maisch) using a 30 to 90 min linear gradient of 5-35% acetonitrile/0.1% formic acid (v:v) at 300 nl min^{-1}.

For spectral counting analysis, the eluent was analysed on a Q Exactive hybrid quadrupole/orbitrap mass spectrometer (ThermoFisher Scientific) equipped with a FlexIon nanoSpray source and operated under Excalibur 2.4 software using a data-dependent acquisition method. Each experimental cycle was of the following form: one full MS scan across the 350-1600 m/z range was acquired at a resolution setting of 70,000 FWHM, an AGC target of 1×10e6 and a maximum fill time of 60 ms. Up to the 12 most abundant peptide precursors of charge states 2 to 5 above a 2×10e4 intensity threshold were then sequentially isolated at 2.0 FWHM isolation width and fragmented with nitrogen at a normalized collision energy setting of 25%. The resulting product ion spectra were recorded at a resolution setting of 17,500 FWHM, AGC target of 2×10e5 and a maximum fill time of 60 ms. Selected precursor m/z values were then excluded for the following 15 s. Two technical replicates per sample were acquired.

SWATH-MS library generation was performed on a hybrid triple quadrupole-TOF mass spectrometer (TripleTOF 5600+) equipped with a Nanospray III ion source (Ionspray Voltage 2400V, Interface Heater Temperature 150°C, Sheath Gas Setting 12) and controlled by Analyst TF 1.7.1 software build 1163 (all AB Sciex), using a Top30 data-dependent acquisition method with an MS survey scan of m/z 380–1250 accumulated for 250 ms at a resolution of 35,000 full width at half maximum (FWHM). MS/MS scans of m/z 180–1500 were accumulated for 100 ms at a resolution of 17,500 FWHM and a precursor isolation width of 0.7 FWHM, resulting in a total cycle time of 3.4 s. Precursors above a threshold MS intensity of 200 cps with charge states 2+, 3+ and 4+ were selected for MS/MS; the dynamic exclusion time was set to 15 s. MS/MS activation was achieved by CID using nitrogen as a collision gas and using the manufacturer's default rolling collision energy settings. Two technical replicates per reversed phase fraction were analysed to construct a spectral library.

For quantitative SWATH analysis, MS/MS data were acquired using 100 variable size windows (Zhang et al., 2015) across the 400-1200 m/z range. Fragments were produced using rolling collision energy settings for charge state 2+, and fragments acquired over an m/z range of 180-1500 for 40 ms per segment. Including a 250 ms survey scan, this resulted in an overall cycle time of 4.3 s. Two replicate injections were acquired for each biological sample.

Mass spectrometry data processing

For spectral counting analysis, peaklists were extracted from the raw data using Raw2MSMS software v1.17 (Max Planck Institute for Biochemistry, Martinsried, Germany). Protein identification was achieved using MASCOT 2.5.1 software (Matrixscience, London, UK). Proteins were identified against

the UniProtKB *Homo sapiens* reference proteome (revision 02-2017, 92,928 entries). The search was performed with trypsin as enzyme and iodoacetamide as cysteine blocking agent. Up to two missed tryptic cleavages and methionine oxidation as a variable modification were allowed for. Search tolerances were set to 10 ppm for the precursor mass and 0.05 Da for fragment masses. Scaffold software version 4.4.1.1 (Proteome Software) was used to validate MS/MS-based peptide and protein identifications. Protein and peptide identifications were filtered to 1% FDR using a concatenated forward-and-reverse decoy database approach. Relative quantification of proteins in the samples was achieved by two-sided *t*-tests of normalized spectral counts using a Benjamini-Hochberg-corrected *P* value of 0.05 to judge significance. To allow for the calculation of low abundance protein ratios, a minimum value of three spectral counts was introduced where necessary to avoid division by zero issues.

For SWATH-MS analysis, protein identification was achieved using ProteinPilot Software version 5.0 build 4769 (AB Sciex) at 'thorough' settings. MS/MS spectra from the combined qualitative analyses were searched against the UniProtKB *Homo sapiens* reference proteome (revision 02-2017, 92,928 entries) augmented with a set of 51 known common laboratory contaminants to identify 597 proteins at a false discovery rate (FDR) of 1%. Spectral library generation and SWATH peak extraction were achieved in PeakView Software version 2.1 build 11041 (AB Sciex) using the SWATH quantitation microApp version 2.0 build 2003. Following retention time correction on endogenous peptides spanning the entire retention time range, peak areas were extracted using information from the MS/MS library at an FDR of 1% (Lambert et al., 2013). The resulting peak areas were summed to peptide and protein area values, which were used for further statistical analysis. Reactome functional network analysis (Gobert et al., 1996) was performed with Cytoscape (www.cytoscape.org) and Kegg pathway analysis was performed using David (Huang et al., 2009a,b).

Immunoblot

To analyse total cell lysates using immunoblot, cells were lysed in SDS–PAGE sample buffer and boiled for 5 min. Proteins were separated on 4–12% gradient gels (Bolt Bis-Tris Plus Gels, ThermoFisher Scientific) and transferred to PVDF membrane (Merck). After blocking with 5% (wt/vol) milk-TBST, membranes were incubated with Licor-800nm–conjugated streptavidin (1:20,000, ab7403; Abcam) for 30 min. After detecting biotinylated proteins, membranes were subjected to detection with antibodies against Ykt6, cellular fraction markers already mentioned and Licor680nm–conjugated secondary antibodies.

Ykt6 model prediction

A Ykt6-3E structural model was predicted using RaptorX (Källberg et al., 2012) and is based on the Ykt6 structure (3kyqA) as a template.

Statistics

All experiments were carried out in at least biological triplicates. Error bars indicate s.d. Statistical significance was calculated by carrying out one-way ANOVA with Dunnett's multiple comparison test to compare a control mean with the other means or using an unpaired Student's *t*-test where appropriate. The data that support the findings of this study are available from the corresponding author upon reasonable request.

Acknowledgements

The authors thank the Core Facility Proteomics at the Institute of Clinical Chemistry at UMG, Konrad Basler, Hugo Bellen, Sven Bogdan, Jörg Großhans and Andrew Peden for fly reagents; and Thomas Monecke for helpful comments regarding Ykt6 structural model. We thank Varun Chaudhary and Dolma Choezom for critical reading of the manuscript.

Competing interests

The authors declare no competing or financial interests.

Author contributions

Conceptualization: K.L., J.C.G.; Methodology: K.L., M.H.-C.; Validation: K.L., P.K., A.D., J.C.K., D.M., L.N., M.H.-C.; Formal analysis: K.L., P.K., A.D., J.C.K.; Investigation: K.L., L.W., A.D., J.C.K., D.M., L.N., F.G., J.C.G.; Resources: M.H.-C., F.G., A.W., J.C.G.; Writing - original draft: K.L., J.C.G.; Writing - review & editing: K.L., L.W., P.K., A.D., J.C.K., D.M., L.N., A.W., J.C.G.; Visualization: K.L., L.W., P.K., F.G., J.C.G.; Supervision: J.C.G.; Project administration: J.C.G.; Funding acquisition: J.C.G.

Funding

Research in the lab of J.C.G. is supported by the Deutsche Forschungsgemeinschaft-funded Research Centre SFB1324/1 (331351713 and GR4810/2-1), by the Research program of the University Medical Centre, Georg-August-Universität Göttingen, and by a postdoctoral fellowship to K.L. from the Dorothea Schlözer Program, Georg-August-Universität Göttingen. Deposited in PMC for immediate release.

Supplementary information

Supplementary information available online at
https://dev.biologists.org/lookup/doi/10.1242/dev.185421.supplemental

Peer review history

The peer review history is available online at
https://dev.biologists.org/lookup/doi/10.1242/dev.185421.reviewer-comments.pdf

References

Abe, M., Setoguchi, Y., Tanaka, T., Awano, W., Takahashi, K., Ueda, R., Nakamura, A. and Goto, S. (2009). Membrane protein location-dependent regulation by PI3K (III) and Rabenosyn-5 in Drosophila wing cells. *PLoS ONE* **4**, e7306. doi:10.1371/journal.pone.0007306

Acebron, S. P., Karaulanov, E., Berger, B. S., Huang, Y.-L. and Niehrs, C. (2014). Mitotic Wnt signaling promotes protein stabilization and regulates cell size. *Mol. Cell* **54**, 663-674. doi:10.1016/j.molcel.2014.04.014

Albrecht, L. V., Ploper, D., Tejeda-Muñoz, N. and De Robertis, E. M. (2018). Arginine methylation is required for canonical Wnt signaling and endolysosomal trafficking. *Proc. Natl. Acad. Sci. USA* **115**, E5317-E5325. doi:10.1073/pnas.1804091115

Atanassov, I. and Urlaub, H. (2013). Increased proteome coverage by combining PAGE and peptide isoelectric focusing: comparative study of gel-based separation approaches. *Proteomics* **13**, 2947-2955. doi:10.1002/pmic.201300035

Baeg, G. H., Lin, X., Khare, N., Baumgartner, S. and Perrimon, N. (2001). Heparan sulfate proteoglycans are critical for the organization of the extracellular distribution of Wingless. *Development* **128**, 87-94.

Baghirova, S., Hughes, B. G., Hendzel, M. J. and Schulz, R. (2015). Sequential fractionation and isolation of subcellular proteins from tissue or cultured cells. *MethodsX* **2**, e440-e445. doi:10.1016/j.mex.2015.11.001

Baietti, M. F., Zhang, Z., Mortier, E., Melchior, A., Degeest, G., Geeraerts, A., Ivarsson, Y., Depoortere, F., Coomans, C., Vermeiren, E. et al. (2012). Syndecan–syntenin–ALIX regulates the biogenesis of exosomes. *Nat. Cell Biol.* **14**, 677-685. doi:10.1038/ncb2502

Bas, L., Papinski, D., Licheva, M., Torggler, R., Rohringer, S., Schuschnig, M. and Kraft, C. (2018). Reconstitution reveals Ykt6 as the autophagosomal SNARE in autophagosome–vacuole fusion. *J. Cell Biol.* **217**, 3656-3669. doi:10.1083/jcb.201804028

Beckett, K., Monier, S., Palmer, L., Alexandre, C., Green, H., Raposo, G., Thibault, P., Borgne, R. L. and Vincent, J. (2013). Drosophila Wingless is loaded on exosome-like vesicles but forms a gradient in an exosome-independent manner. *Traffic* **14**, 82-96. doi:10.1111/tra.12016

Belenkaya, T. Y., Wu, Y., Tang, X., Zhou, B., Cheng, L., Sharma, Y. V., Yan, D., Selva, E. M. and Lin, X. (2008). The retromer complex influences wnt secretion by recycling wntless from endosomes to the trans-golgi network. *Dev. Cell* **14**, 120-131. doi:10.1016/j.devcel.2007.12.003

Bischof, J., Maeda, R. K., Hediger, M., Karch, F. and Basler, K. (2007). An optimized transgenesis system for Drosophila using germ-line-specific phiC31 integrases. *Proc. Natl. Acad. Sci. USA* **104**, 3312-3317. doi:10.1073/pnas.0611511104

Bischoff, M., Gradilla, A.-C., Seijo, I., Andrés, G., Rodríguez-Navas, C., González-Méndez, L. and Guerrero, I. (2013). Cytonemes are required for the establishment of a normal Hedgehog morphogen gradient in Drosophila epithelia. *Nat. Cell Biol.* **15**, 1269-1281. doi:10.1038/ncb2856

Bolte, S. and Cordelières, F. P. (2006). A guided tour into subcellular colocalization analysis in light microscopy. *J. Microsc.* **224**, 213-232. doi:10.1111/j.1365-2818.2006.01706.x

Brunt, L. and Scholpp, S. (2018). The function of endocytosis in Wnt signaling. *Cell. Mol. Life Sci.* **75**, 785-795. doi:10.1007/s00018-017-2654-2

Buechling, T., Chaudhary, V., Spirohn, K., Weiss, M. and Boutros, M. (2011). p24 proteins are required for secretion of Wnt ligands. *EMBO Rep.* **12**, 1265-1272. doi:10.1038/embor.2011.212

Coombs, G. S., Yu, J., Canning, C. A., Veltri, C. A., Covey, T. M., Cheong, J. K., Utomo, V., Banerjee, N., Zhang, Z. H., Jadulco, R. C. et al. (2010). WLS-dependent secretion of WNT3A requires Ser209 acylation and vacuolar acidification. *J. Cell Sci.* **123**, 3357-3367. doi:10.1242/jcs.072132

Cruciat, C.-M., Ohkawara, B., Acebron, S. P., Karaulanov, E., Reinhard, C., Ingelfinger, D., Boutros, M. and Niehrs, C. (2010). Requirement of prorenin receptor and vacuolar H+-ATPase-mediated acidification for Wnt signaling. *Science* **327**, 459-463. doi:10.1126/science.1179802

D'Angelo, G., Matusek, T., Pizette, S. and Thérond, P. P. (2015). Endocytosis of hedgehog through dispatched regulates long-range signaling. *Dev. Cell* **32**, 290-303. doi:10.1016/j.devcel.2014.12.004

De Renzis, S., Sönnichsen, B. and Zerial, M. (2002). Divalent Rab effectors regulate the sub-compartmental organization and sorting of early endosomes. *Nat. Cell Biol.* **4**, 124-133. doi:10.1038/ncb744

Demir, K., Kirsch, N., Beretta, C. A., Erdmann, G., Ingelfinger, D., Moro, E., Argenton, F., Carl, M., Niehrs, C. and Boutros, M. (2013). RAB8B is required for activity and caveolar endocytosis of LRP6. *Cell Rep.* **4**, 1224-1234. doi:10.1016/j.celrep.2013.08.008

Dietrich, L. E. P., Gurezka, R., Veit, M. and Ungermann, C. (2004). The SNARE Ykt6 mediates protein palmitoylation during an early stage of homotypic vacuole fusion. *EMBO J.* **23**, 45-53. doi:10.1038/sj.emboj.7600015

Dingjan, I., Linders, P. T. A., Verboogen, D. R. J., Revelo, N. H., ter Beest, M. and van den Bogaart, G. (2018). Endosomal and phagosomal SNAREs. *Physiol. Rev.* **98**, 1465-1492. doi:10.1152/physrev.00037.2017

Dubois, L., Lecourtois, M., Alexandre, C., Hirst, E. and Vincent, J.-P. (2001). Regulated endocytic routing modulates wingless signaling in Drosophila embryos. *Cell* **105**, 613-624. doi:10.1016/S0092-8674(01)00375-0

Franch-Marro, X., Wendler, F., Guidato, S., Griffith, J., Baena-Lopez, A., Itasaki, N., Maurice, M. M. and Vincent, J.-P. (2008). Wingless secretion requires endosome-to-Golgi retrieval of Wntless/Evi/Sprinter by the retromer complex. *Nat. Cell Biol.* **10**, 170-177. doi:10.1038/ncb1678

Fukasawa, M., Varlamov, O., Eng, W. S., Sollner, T. H. and Rothman, J. E. (2004). Localization and activity of the SNARE Ykt6 determined by its regulatory domain and palmitoylation. *Proc. Natl. Acad. Sci. USA* **101**, 4815-4820. doi:10.1073/pnas.0401183101

Gao, H., He, F., Lin, X. and Wu, Y. (2017). Drosophila VAMP7 regulates Wingless intracellular trafficking. *PLoS ONE* **12**, 1-14. doi:10.1371/journal.pone.0186938

Gao, J., Reggiori, F. and Ungermann, C. (2018). A novel in vitro assay reveals SNARE topology and the role of Ykt6 in autophagosome fusion with vacuoles. *J. Cell Biol.* **217**, 3670-3682. doi:10.1083/jcb.201804039

Gasnereau, I., Herr, P., Chia, P. Z. C., Basler, K. and Gleeson, P. A. (2011). Identification of an endocytosis motif in an intracellular loop of Wntless protein, essential for its recycling and the control of Wnt protein signaling. *J. Biol. Chem.* **286**, 43324-43333. doi:10.1074/jbc.M111.307231

Ghossoub, R., Lembo, F., Rubio, A., Gaillard, C. B., Bouchet, J., Vitale, N., Slavík, J., Machala, M. and Zimmermann, P. (2014). Syntenin-ALIX exosome biogenesis and budding into multivesicular bodies are controlled by ARF6 and PLD2. *Nat. Commun.* **5**, 3477. doi:10.1038/ncomms4477

Glaeser, K., Boutros, M. and Gross, J. C. (2016). Biochemical methods to analyze Wnt protein secretion. *Methods Mol. Biol.* **1481**, 17-28. doi:10.1007/978-1-4939-6393-5_3

Glaeser, K., Urban, M., Fenech, E., Voloshanenko, O., Kranz, D., Lari, F., Christianson, J. C. and Boutros, M. (2018). ERAD-dependent control of the Wnt secretory factor Evi. *EMBO J.* **37**, e97311. doi:10.15252/embj.201797311

Gobert, C., Bracco, L., Rossi, F., Olivier, M., Tazi, J., Lavelle, F., Larsen, A. K. and Riou, J.-F. (1996). Modulation of DNA topoisomerase I activity by p53. *Biochemistry* **35**, 5778-5786. doi:10.1021/bi952327w

Gonzalo, S. and Linder, M. E. (1998). SNAP-25 Palmitoylation and plasma membrane targeting require a functional secretory pathway. *Mol. Biol. Cell* **9**, 585-597. doi:10.1091/mbc.9.3.585

Gordon, D. E., Bond, L. M., Sahlender, D. A. and Peden, A. A. (2010). A targeted siRNA screen to identify SNAREs required for constitutive secretion in mammalian cells. *Traffic* **11**, 1191-1204. doi:10.1111/j.1600-0854.2010.01087.x

Gordon, D. E., Chia, J., Jayawardena, K., Antrobus, R., Bard, F. and Peden, A. A. (2017). VAMP3/Syb and YKT6 are required for the fusion of constitutive secretory carriers with the plasma membrane. *PLoS Genet.* **13**, e1006698. doi:10.1371/journal.pgen.1006698

Gradilla, A.-C., González, E., Seijo, I., Andrés, G., Bischoff, M., González-Mendez, L., Sánchez, V., Callejo, A., Ibáñez, C., Guerra, M. et al. (2014). Exosomes as Hedgehog carriers in cytoneme-mediated transport and secretion. *Nat. Commun.* **5**, 5649. doi:10.1038/ncomms6649

Gross, J. C., Chaudhary, V., Bartscherer, K. and Boutros, M. (2012). Active Wnt proteins are secreted on exosomes. *Nat. Cell Biol.* **14**, 1036-1045. doi:10.1038/ncb2574

Haberkant, P., Stein, F., Höglinger, D., Gerl, M. J., Brügger, B., Van Veldhoven, P. P., Krijgsveld, J., Gavin, A.-C. and Schultz, C. (2016). Bifunctional sphingosine for cell-based analysis of protein-sphingolipid interactions. *ACS Chem. Biol.* **11**, 222-230. doi:10.1021/acschembio.5b00810

Haelterman, N. A., Jiang, L., Li, Y., Bayat, V., Sandoval, H., Ugur, B., Tan, K. L., Zhang, K., Bei, D., Xiong, B. et al. (2014). Large-scale identification of chemically induced mutations in Drosophila melanogaster. *Genome Res.* **24**, 1707-1718. doi:10.1101/gr.174615.114

Harterink, M., Port, F., Lorenowicz, M. J., McGough, I. J., Silhankova, M., Betist, M. C., van Weering, J. R. T., van Heesbeen, R. G. H. P., Middelkoop, T. C., Basler, K. et al. (2011). A SNX3-dependent retromer pathway mediates retrograde transport of the Wnt sorting receptor Wntless and is required for Wnt secretion. *Nat. Cell Biol.* **13**, 914-923. doi:10.1038/ncb2281

Hemalatha, A., Prabhakara, C. and Mayor, S. (2016). Endocytosis of Wingless via a dynamin-independent pathway is necessary for signaling in Drosophila wing discs. *Proc. Natl. Acad. Sci. USA* **113**, E6993-E7002. doi:10.1073/pnas.1610565113

Herr, P. and Basler, K. (2012). Porcupine-mediated lipidation is required for Wnt recognition by Wls. *Dev. Biol.* **361**, 392-402. doi:10.1016/j.ydbio.2011.11.003

Huang, D. W., Sherman, B. T. and Lempicki, R. A. (2009a). Bioinformatics enrichment tools: Paths toward the comprehensive functional analysis of large gene lists. *Nucleic Acids Res.* **37**, 1-13. doi:10.1093/nar/gkn923

Huang, D. W., Sherman, B. T. and Lempicki, R. A. (2009b). Systematic and integrative analysis of large gene lists using DAVID bioinformatics resources. *Nat. Protoc.* **4**, 44-57. doi:10.1038/nprot.2008.211

Huang, S., Tang, D. and Wang, Y. (2016). Monoubiquitination of syntaxin 5 regulates golgi membrane dynamics during the cell cycle. *Dev. Cell* **38**, 73-85. doi:10.1016/j.devcel.2016.06.001

Jovic, M., Sharma, M., Rahajeng, J. and Caplan, S. (2010). The early endosome: a busy sorting station for proteins at the crossroads. *Histol. Histopathol.* **25**, 99-112.

Kadowaki, T., Wilder, E., Klingensmith, J., Zachary, K. and Perrimon, N. (1996). The segment polarity gene porcupine encodes a putative multitransmembrane protein involved in Wingless processing. *Genes Dev.* **10**, 3116-3128. doi:10.1101/gad.10.24.3116

Källberg, M., Wang, H., Wang, S., Peng, J., Wang, Z., Lu, H. and Xu, J. (2012). Template-based protein structure modeling using the RaptorX web server. *Nat. Protoc.* **7**, 1511-1522. doi:10.1038/nprot.2012.085

Kanehisa, M., Sato, Y., Kawashima, M., Furumichi, M. and Tanabe, M. (2016). KEGG as a reference resource for gene and protein annotation. *Nucleic Acids Res.* **44**, D457-D462. doi:10.1093/nar/gkv1070

Kimura, T., Jia, J., Kumar, S., Choi, S. W., Gu, Y., Mudd, M., Dupont, N., Jiang, S., Peters, R., Farzam, F. et al. (2017). Dedicated SNAREs and specialized TRIM cargo receptors mediate secretory autophagy. *EMBO J.* **36**, 42-60. doi:10.15252/embj.201695081

Koch, S., Acebron, S. P., Herbst, J., Hatiboglu, G. and Niehrs, C. (2015). Post-transcriptional Wnt signaling governs epididymal sperm maturation. *Cell* **163**, 1225-1236. doi:10.1016/j.cell.2015.10.029

Koles, K., Nunnari, J., Korkut, C., Barria, R., Brewer, C., Li, Y., Leszyk, J., Zhang, B. and Budnik, V. (2012). Mechanism of evenness interrupted (Evi)-exosome release at synaptic boutons. *J. Biol. Chem.* **287**, 16820-16834. doi:10.1074/jbc.M112.342667

Kriegenburg, F., Bas, L., Gao, J., Ungermann, C. and Kraft, C. (2019). The multi-functional SNARE protein Ykt6 in autophagosomal fusion processes. *Cell Cycle* **18**, 639-651. doi:10.1080/15384101.2019.1580488

Lambert, J.-P., Ivosev, G., Couzens, A. L., Larsen, B., Taipale, M., Lin, Z.-Y., Zhong, Q., Lindquist, S., Vidal, M., Aebersold, R. et al. (2013). Mapping differential interactomes by affinity purification coupled with data-independent mass spectrometry acquisition. *Nat. Methods* **10**, 1239-1245. doi:10.1038/nmeth.2702

Li, X., Wu, Y., Shen, C., Belenkaya, T. Y., Ray, L. and Lin, X. (2015). Drosophila p24 and Sec22 regulate Wingless trafficking in the early secretory pathway. *Biochem. Biophys. Res. Commun.* **463**, 483-489. doi:10.1016/j.bbrc.2015.04.151

Liu, X., Salokas, K., Tamene, F., Jiu, Y., Weldatsadik, R. G., Öhman, T. and Varjosalo, M. (2018). An AP-MS- and BioID-compatible MAC-tag enables comprehensive mapping of protein interactions and subcellular localizations. *Nat. Commun.* **9**, 1188. doi:10.1038/s41467-018-03523-2

MacDonald, E., Brown, L., Selvais, A., Liu, H., Waring, T., Newman, D., Bithell, J., Grimes, D., Urbé, S., Clague, M. J. et al. (2018). HRS-WASH axis governs actin-mediated endosomal recycling and cell invasion. *J. Cell Biol.* **217**, 2549-2564. doi:10.1083/jcb.201710051

Malmersjö, S., Di Palma, S., Diao, J., Lai, Y., Pfuetzner, R. A., Wang, A. L., McMahon, M. A., Hayer, A., Porteus, M., Bodenmiller, B. et al. (2016). Phosphorylation of residues inside the SNARE complex suppresses secretory vesicle fusion. *EMBO J.* **35**, 1810-1821. doi:10.15252/embj.201694071

Marois, E., Mahmoud, A. and Eaton, S. (2006). The endocytic pathway and formation of the Wingless morphogen gradient. *Development* **133**, 307-317. doi:10.1242/dev.02197

Matsui, T., Jiang, P., Nakano, S., Sakamaki, Y., Yamamoto, H. and Mizushima, N. (2018). Autophagosomal YKT6 is required for fusion with lysosomes independently of syntaxin 17. *J. Cell Biol.* **217**, 2633-2645. doi:10.1083/jcb.201712058

McNew, J. A., Søgaard, M., Lampen, N. M., Machida, S., Ye, R. R., Lacomis, L., Tempst, P., Rothman, J. E. and Söllner, T. H. (1997). Ykt6p, a prenylated SNARE essential for endoplasmic reticulum-golgi transport. *J. Biol. Chem.* **272**, 17776-17783. doi:10.1074/jbc.272.28.17776

Meiringer, C. T. A., Auffarth, K., Hou, H. and Ungermann, C. (2008). Depalmitoylation of Ykt6 prevents its entry into the multivesicular body pathway. *Traffic* **9**, 1510-1521. doi:10.1111/j.1600-0854.2008.00778.x

Menck, K., Klemm, F., Gross, J. C., Pukrop, T., Wenzel, D. and Binder, C. (2013). Induction and transport of Wnt 5a during macrophage-induced malignant invasion is mediated by two types of extracellular vesicles. *Oncotarget* **4**, 2057-2066. doi:10.18632/oncotarget.1336

Mihara, E., Hirai, H., Yamamoto, H., Tamura-Kawakami, K., Matano, M., Kikuchi, A., Sato, T. and Takagi, J. (2016). Active and water-soluble form of lipidated Wnt protein is maintained by a serum glycoprotein afamin/α-albumin. *Elife* **5**, 1-19. doi:10.7554/eLife.11621

Nickles, D., Falschlehner, C., Metzig, M. and Boutros, M. (2012). A genome-wide RNA interference screen identifies caspase 4 as a factor required for tumor necrosis factor alpha signaling. *Mol. Cell. Biol.* **32**, 3372-3381. doi:10.1128/MCB.06739-11

Nolo, R., Abbott, L. A. and Bellen, H. J. (2000). Senseless, a zn finger transcription factor, is necessary and sufficient for sensory organ development in Drosophila. *Cell* **102**, 349-362. doi:10.1016/S0092-8674(00)00040-4

Nusse, R. and Clevers, H. (2017). Wnt/β-catenin signaling, disease, and emerging therapeutic modalities. *Cell* **169**, 985-999. doi:10.1016/j.cell.2017.05.016

Parchure, A., Vyas, N. and Mayor, S. (2018). Wnt and hedgehog: secretion of lipid-modified morphogens. *Trends Cell Biol.* **28**, 157-170. doi:10.1016/j.tcb.2017.10.003

Perrimon, N. and Lin, X. (1999). Dally cooperates with Drosophila Frizzled 2 to transduce Wingless signalling. *Nature* **400**, 281-284. doi:10.1038/22343

Pfeiffer, S., Ricardo, S., Manneville, J.-B., Alexandre, C. and Vincent, J.-P. (2002). Producing cells retain and recycle wingless in Drosophila embryos. *Curr. Biol.* **12**, 957-962. doi:10.1016/S0960-9822(02)00867-9

Port, F., Kuster, M., Herr, P., Furger, E., Bänziger, C., Hausmann, G. and Basler, K. (2008). Wingless secretion promotes and requires retromer-dependent cycling of Wntless. *Nat. Cell Biol.* **10**, 178-185. doi:10.1038/ncb1687

Port, F., Hausmann, G. and Basler, K. (2011). A genome-wide RNA interference screen uncovers two p24 proteins as regulators of Wingless secretion. *EMBO Rep.* **12**, 1144-1152. doi:10.1038/embor.2011.165

Roux, K. J., Kim, D. I., Raida, M. and Burke, B. (2012). A promiscuous biotin ligase fusion protein identifies proximal and interacting proteins in mammalian cells. *J. Cell Biol.* **196**, 801-810. doi:10.1083/jcb.201112098

Roux, K. J., Kim, D. I., Burke, B. and May, D. G. (2018). BioID: a screen for protein-protein interactions. *Curr. Protoc. Protein Sci.* **91**, 19.23.1-19.23.15. doi:10.1002/cpps.51

Rueden, C. T., Schindelin, J., Hiner, M. C., DeZonia, B. E., Walter, A. E., Arena, E. T. and Eliceiri, K. W. (2017). ImageJ2: ImageJ for the next generation of scientific image data. *BMC Bioinformatics* **18**, 1-26. doi:10.1186/s12859-017-1934-z

Saito, Y., Li, L., Coyaud, E., Luna, A., Sander, C., Raught, B., Asara, J. M., Brown, M. and Muthuswamy, S. K. (2019). LLGL2 rescues nutrient stress by promoting leucine uptake in ER+ breast cancer. *Nature* **569**, 275-279. doi:10.1038/s41586-019-1126-2

Schindelin, J., Arganda-Carreras, I., Frise, E., Kaynig, V., Longair, M., Pietzsch, T., Preibisch, S., Rueden, C., Saalfeld, S., Schmid, B. et al. (2012). Fiji: an open-source platform for biological-image analysis. *Nat. Methods* **9**, 676-682. doi:10.1038/nmeth.2019

Schneider, C. A., Rasband, W. S. and Eliceiri, K. W. (2012). NIH Image to ImageJ : 25 years of image analysis. *Nat. Methods* **9**, 671-675. doi:10.1038/nmeth.2089

Selleck, S. B., Tsuda, M., Kamimura, K., Nakato, H., Archer, M., Staatz, W., Fox, B., Humphrey, M., Olson, S., Futch, T. et al. (1999). The cell-surface proteoglycan Dally regulates Wingless signalling in Drosophila. *Nature* **400**, 276-280. doi:10.1038/22336

Seto, E. S. and Bellen, H. J. (2006). Internalization is required for proper Wingless signaling in Drosophila melanogaster. *J. Cell Biol.* **173**, 95-106. doi:10.1083/jcb.200510123

Stanganello, E., Hagemann, A. I. H., Mattes, B., Sinner, C., Meyen, D., Weber, S., Schug, A., Raz, E. and Scholpp, S. (2015). Filopodia-based Wnt transport during vertebrate tissue patterning. *Nat. Commun.* **6**, 1-14. doi:10.1038/ncomms6846

Strigini, M. and Cohen, S. M. (2000). Wingless gradient formation in the Drosophila wing. *Curr. Biol.* **10**, 293-300. doi:10.1016/S0960-9822(00)00378-X

Suzuki, T., Arai, S., Takeuchi, M., Sakurai, C., Ebana, H., Higashi, T., Hashimoto, H., Hatsuzawa, K. and Wada, I. (2012). Development of cysteine-free fluorescent proteins for the oxidative environment. *PLoS ONE* **7**, e37551. doi:10.1371/journal.pone.0037551

Swarup, S. and Verheyen, E. M. (2012). Wnt/wingless signaling in Drosophila. *Cold Spring Harb. Perspect. Biol.* **4**, a007930-a007930. doi:10.1101/cshperspect.a007930

Taelman, V. F., Dobrowolski, R., Plouhinec, J. L., Fuentealba, L. C., Vorwald, P. P., Gumper, I., Sabatini, D. D. and De Robertis, E. M. (2010). Wnt signaling requires sequestration of Glycogen Synthase Kinase 3 inside multivesicular endosomes. *Cell* **143**, 1136-1148. doi:10.1016/j.cell.2010.11.034

Takáts, S., Glatz, G., Szenci, G., Boda, A., Bor, G., Horváth, V., Hegedűs, K., Ková Cs, A. L., Juhá Sz, G., Horváth, G. V. et al. (2018). Non-canonical role of the SNARE protein Ykt6 in autophagosome-lysosome fusion. *PLoS Genet.* **14**, 1-23. doi:10.1371/journal.pgen.1007359

Tanaka, K., Okabayashi, K., Asashima, M., Perrimon, N. and Kadowaki, T. (2000). The evolutionarily conserved porcupine family is involved in the processing of the Wnt family. *Eur. J. Biochem.* **267**, 4300-4311. doi:10.1046/j.1432-1033.2000.01478.x

Tassew, N. G., Charish, J., Shabanzadeh, A. P., Luga, V., Harada, H., Farhani, N., D'Onofrio, P., Choi, B., Ellabban, A., Nickerson, P. E. B. et al. (2017). Exosomes mediate mobilization of autocrine Wnt10b to promote axonal regeneration in the injured CNS. *Cell Rep.* **20**, 99-111. doi:10.1016/j.celrep.2017.06.009

Tochio, H. (2001). An autoinhibitory mechanism for nonsyntaxin SNARE proteins revealed by the structure of Ykt6p. *Science* **293**, 698-702. doi:10.1126/science.1062950

Tsui, M. M. K., Tai, W. C. S. and Banfield, D. K. (2001). Selective formation of Sed5p-containing SNARE complexes is mediated by combinatorial binding interactions. *Mol. Biol. Cell* **12**, 521-538. doi:10.1091/mbc.12.3.521

Urbé, S., Mills, I. G., Stenmark, H., Kitamura, N. and Clague, M. J. (2002). Endosomal localization and receptor dynamics determine tyrosine phosphorylation of hepatocyte growth factor-regulated tyrosine kinase substrate. *Mol. Cell. Biol.* **20**, 7685-7692. doi:10.1128/MCB.20.20.7685-7692.2000

Wallroth, A. and Haucke, V. (2018). Phosphoinositide conversion in endocytosis and the endolysosomal system. *J. Biol. Chem.* **293**, 1526-1535. doi:10.1074/jbc.R117.000629

Wessel, D. and Flügge, U. I. (1984). A method for the quantitative recovery of protein in dilute solution in the presence of detergents and lipids. *Anal. Biochem.* **138**, 141-143. doi:10.1016/0003-2697(84)90782-6

Willert, K., Brown, J. D., Danenberg, E., Duncan, A. W., Weissman, I. L., Reya, T., Yates, J. R., III, Nusse, R., Yates, J. R. and Nusse, R. (2003). Wnt proteins are lipid-modified and can act as stem cell growth factors. *Nature* **423**, 448-452. doi:10.1038/nature01611

Wucherpfennig, T., Wilsch-Bräuninger, M. and González-Gaitán, M. (2003). Role of Drosophila Rab5 during endosomal trafficking at the synapse and evoked neurotransmitter release. *J. Cell Biol.* **161**, 609-624. doi:10.1083/jcb.200211087

Yamazaki, Y., Palmer, L., Alexandre, C., Kakugawa, S., Beckett, K., Gaugue, I., Palmer, R. H. and Vincent, J.-P. (2016). Godzilla-dependent transcytosis promotes Wingless signalling in Drosophila wing imaginal discs. *Nat. Cell Biol.* **18**, 451-457. doi:10.1038/ncb3325

Yang, P.-T., Lorenowicz, M. J., Silhankova, M., Coudreuse, D. Y. M., Betist, M. C. and Korswagen, H. C. (2008). Wnt signaling requires retromer-dependent recycling of MIG-14/Wntless in Wnt-producing cells. *Dev. Cell* **14**, 140-147. doi:10.1016/j.devcel.2007.12.004

Zhang, J., Schulze, K. L., Hiesinger, P. R., Suyama, K., Wang, S., Fish, M., Acar, M., Hoskins, R. A., Bellen, H. J. and Scott, M. P. (2007). Thirty-one flavors of Drosophila rab proteins. *Genetics* **176**, 1307-1322. doi:10.1534/genetics.106.066761

Zhang, T. and Hong, W. (2001). Ykt6 forms a SNARE complex with Syntaxin 5, GS28, and Bet1 and participates in a late stage in endoplasmic reticulum-golgi transport. *J. Biol. Chem.* **276**, 27480-27487. doi:10.1074/jbc.M102786200

Zhang, P., Wu, Y., Belenkaya, T. Y. and Lin, X. (2011). SNX3 controls Wingless/Wnt secretion through regulating retromer-dependent recycling of Wntless. *Cell Res.* **21**, 1677-1690. doi:10.1038/cr.2011.167

Zhang, Y., Bilbao, A., Bruderer, T., Luban, J., Strambio-De-Castillia, C., Lisacek, F., Hopfgartner, G. and Varesio, E. (2015). The use of variable Q1 isolation windows improves selectivity in LC–SWATH–MS acquisition. *J. Proteome Res.* **14**, 4359-4371. doi:10.1021/acs.jproteome.5b00543

Supplementary information

Table S1: SNARE in vivo RNAi screening results.

Click here to Download Table S1

Table S2: Proteins identified by mass spectrometry from BioID control and Ykt6-WT samples in two biological replicates

Click here to Download Table S2

Table S3: Dharmacon siRNA SMARTpools

Gene Symbol	GENE ID	Gene Accession	GI Number	Sequence
siGENOME Non-targeting Control_5#				UGGUUUACAUGUCGACUAA
AP1S1	1174	NM_057089	148536832	AAUGGUACCUGGCCACUUC
AP1S1	1174	NM_057089	148536832	GCUCGAAAGCCCAAGAUGU
AP1S1	1174	NM_057089	148536832	CAUCGAGGGCCAAGACAAU
AP2S1	1175	NM_021575	70906431	AGACGAAGGUGCUGAAACA
AP2S1	1175	NM_021575	70906431	GGUCUUAAACGAAUAUUUC
AP2S1	1175	NM_021575	70906431	AACAGAAGCUGAUCGAGGA
ARPC1A	10552	NM_006409	22907051	ACGAAGUGCACAUCUAUAA
ARPC1A	10552	NM_006409	22907051	GAAUUAAUCGCGCAGCUAC
ARPC1A	10552	NM_006409	22907051	GUGGCACGAUGGCGAGGAA
ARPC1A	10552	NM_006409	22907051	GGAAGUGGAGCACGACUCA
CHMP2B	25978	NM_014043	40254865	GAAGAUGGCUGGAGCAAUG
CHMP2B	25978	NM_014043	40254865	UAAGGAAGCUUGCAAAGUU
CHMP2B	25978	NM_014043	40254865	GCUCGAAGCUUACCAUCUG
CHMP2B	25978	NM_014043	40254865	GCCAGGAUAUUGUGAAUCA
CTNNB1	1499	NM_001904	4503130	GCUGAAACAUGCAGUUGUA
CTNNB1	1499	NM_001904	4503130	GAUAAAGGCUACUGUUGGA
CTNNB1	1499	NM_001904	4503130	CCACUAAUGUCCAGCGUUU
DNM2	1785	NM_004945	56549118	CCGAAUCAAUCGCAUCUUC
DNM2	1785	NM_004945	56549118	GACAUGAUCCUGCAGUUCA
DNM2	1785	NM_004945	56549118	CCUCCGAGCUGGCGUCUAC
DNM2	1785	NM_004945	56549118	AGUCCUACAUCAACACGAA
GOSR2	9570	NM_054022	60499002	ACGAAUCACUGCAGUUUAA
GOSR2	9570	NM_054022	60499002	GAUCCAGUCUUGCAUGGGA
GOSR2	9570	NM_054022	60499002	CGAAAUCCAAGCAAGCAUA
GOSR2	9570	NM_054022	60499002	GAUAUUCAGCCGUCUAGAA
KIF5B	3799	NM_004521	4758647	GCAGUCAGGUCAAAGAAUA
KIF5B	3799	NM_004521	4758647	GAACUGGCAUGAUAGAUGA
KIF5B	3799	NM_004521	4758647	CAACAGACAUGUAGCAGUU
SEC22B	9554	NM_004892	94429049	GAAGAAGUGUUACAACGAG
SEC22B	9554	NM_004892	94429049	CUAAGCAACUCUUUCGAAA

SEC22B	9554	NM_004892	94429049	UAACAAUGAUCGCCCGAGU
SNAP25	6616	NM_003081	18765732	GCAAUGAGAUCGAUACACA
SNAP25	6616	NM_003081	18765732	GCGAAGGGCUGACCAGUUG
SNAP25	6616	NM_003081	18765732	GGAAAGCACCCGUCGUAUG
SNX1	6642	NM_148955	71772739	GGAAAGAGCUAGCGCUGAA
SNX1	6642	NM_148955	71772739	GAAAGGGACUUCGAGAGGA
SNX1	6642	NM_148955	71772739	GAAAAGAAGUGAUACGGUU
SNX1	6642	NM_148955	71772739	AGAACCACGUGAUCAAGUA
STX1A	6804	NM_004603	95147340	GGAACACGCGGUAGACUAU
STX1A	6804	NM_004603	95147340	GGAGGAGAUUCGAGGCUUC
STX1A	6804	NM_004603	95147340	ACAUAAAGAAGACAGCAAA
STX5	6811	NM_003164	94400931	GCAAGUCCCUCUUUGAUGA
STX5	6811	NM_003164	94400931	GAGCUAACAUAUAUCAUCA
STX5	6811	NM_003164	94400931	GAGCCCAGCUGGACGUUGA
STX7	8417	NM_003569	4507294	CAAAGAAACAGAUAAGUAC
STX7	8417	NM_003569	4507294	GCGAUUAUCAGUCUCAUCA
STX7	8417	NM_003569	4507294	GUCAAGGGCAGCAGAUUAU
STX7	8417	NM_003569	4507294	GAGUUUGUUGCUCGAGUAA
STX8	9482	NM_004853	296010812	CACCAAAGCUUACCGUGAC
STX8	9482	NM_004853	296010812	UCUUGUAACUCGAGAGAGA
STX8	9482	NM_004853	296010812	GAAUGAGGGUGCCGAACCA
STX8	9482	NM_004853	296010812	UGAGAUAAUUGACGACCUU
USE1	55850	NM_018467	154354977	CGUCGAGGCUGGAGCUAAA
USE1	55850	NM_018467	154354977	CUGAGGUGAUCAAUGAAUA
USE1	55850	NM_018467	154354977	GAGAUGGACGUAAGGAAGA
USE1	55850	NM_018467	154354977	CGAAUCAUGCCUAAACUCA
VAMP1	6843	NM_014231	40549444	CUCCUAACAUGACCAGUAA
VAMP1	6843	NM_014231	40549444	CAUCACAAUUUGAGAGCAG
VAMP1	6843	NM_014231	40549444	CCAUCAUCGUGGUAGUUAU
VAMP1	6843	NM_014231	40549444	AGGCACAAGUGGAGGAGGU
VAMP3	9341	NM_004781	42544205	GGCAGGCGCUUCUCAAUUU
VAMP3	9341	NM_004781	42544205	GGAUUACUGUUCUGGUUAU
VAMP3	9341	NM_004781	42544205	GCCAAGUUGAAGAGGAAAU
VAMP7	6845	NM_005638	27545446	GGAGAAAGAUUGGAAUUAU
VAMP7	6845	NM_005638	27545446	GUACUCACAUGGCAAUUAU
VAMP7	6845	NM_005638	27545446	AAGAAGAGGUUCCAGACUA
VTI1A	143187	NM_145206	113374155	CGUCCGACUUCGAAGGUUA
VTI1A	143187	NM_145206	113374155	CGUGAAAGACUUCGGGAAA
VTI1A	143187	NM_145206	113374155	CGAGGGAUGUACAGCAACA
VTI1A	143187	NM_145206	113374155	GGUCAGGAGAUGUUGGAAA
YKT6	10652	NM_006555	34304384	GCUCAAAGCCGCAUACGAU
YKT6	10652	NM_006555	34304384	GUGAGAAGCUAGAUGACUU
YKT6	10652	NM_006555	34304384	GAAGGUACUAGAUGAAUUC

Supplementary materials and methods

Image analysis

Fig. 3: exWg

MIP of 45 (Ykt6, distance 0,5 µm) or 25 (AP2, distance 1 µm) sections covering the entire stack depicted for visualization. For quantification the average intensity projection of the corresponding stack was used. The profile of the extracellular Wg staining in the shown ROI (1142 x 300 px^2, corresponding to 80x21 μm^2), comparing exWg in the anterior (control, no GFP) with the posterior (RNAi, GFP-positive) region for this one representative example, was plotted with Fiji. For quantification of several independent samples, two ROIs (500x500 px^2, corresponding to 1245 μm^2) were placed manually in the anterior (control) and posterior (RNAi) region of the corresponding stack. The mean fluorescence of five subapical sections (distance 1 µm) is measured with Fiji and averaged per stack. This corresponds to taking the mean fluorescence of an average intensity projection of this corresponding stack. Statistical significance was determined using Student's *t*-test (two-tailed) in GraphPad Prism 6 software.

Fig. 3: Evi

MIP of 15 apical sections (distance 1 µm) depicted for visualization. For quantification the average intensity projection of the corresponding stack was used. The profile of the Evi staining in the shown ROI (1428 x 300 px^2, corresponding to 100 x 21 μm^2), comparing Evi in the anterior (control, no GFP) with the posterior (RNAi, GFP-positive) region for this one representative example, was plotted with Fiji. For quantification of several independent samples, two ROIs (500x250 px^2, corresponding to 623 μm^2) were placed manually in the anterior (control) and posterior (RNAi) region of the corresponding stack. The mean fluorescence of five subapical sections (distance 1 µm) is measured with Fiji and averaged per stack. This corresponds to taking the mean fluorescence of an average intensity projection of this corresponding stack. For quantification of Evi punctae, a maximum intensity projection of the same five subapical sections as above (distance 1 µm) was generated and thresholded using Triangle algorithm implemented in Fiji. Two manually drawn ROIs were placed in the control and the RNAi region along the entire Evi expression domain. Particles > 4 px^2 were automatically counted using Fiji Particle Analyzer within the ROIs. The number of particles was normalized to the area quantified. Statistical significance was determined using Student's *t*-test (two-tailed) in GraphPad Prism 6 software.

Fig.4: Hrs

MIP of nine sections (distance 1 µm) for visualization. For quantification of several independent samples two ROIs (500x500 px^2, corresponding to 1245 μm^2) were placed manually in the anterior (control) and posterior (RNAi) region of the corresponding stack. The mean fluorescence of five subapical sections (distance 1 µm) is measured with Fiji and averaged per stack. This corresponds to taking the mean fluorescence of an average intensity projection of this corresponding stack. The sections to be measured were chosen based on nuclear staining. The nuclei had to be apparent in the entire section. Hrs staining is also very strong in the peripodial membrane, but this signal was not included. Statistical significance was determined using Student's *t*-test (two-tailed) in GraphPad Prism 6 software.

Fig.4: Lamp1
MIP of seven sections (distance 1 µm) are depicted for visualization. Quantification was done as for Hrs.

Fig.4: Rab5
MIP of 13 sections (distance 1 µm) are depicted for visualization. Quantification was done as for Hrs.

Fig.4: Rab7

MIP of seven sections (distance 1 µm) are depicted for visualization. Quantification was done as for Hrs.

Fig. 4: FYVE

For quantification of FYVE-labelled Wg punctae, a 30px XZ section within the Wg stripe was generated. In Fiji a ROI (1500 x 250 px^2, corresponding to 105 x 17.5 μm^2) was placed at the center of the Wg expression domain. Within this ROI, particles >6 px were automatically counted and colocalization determined using the Fiji Plugin ComDet.

Fig. 5: Wg in rescue crosses with Ykt6 SNARE-mutants
MIP of six sections (distance 0,5 µm) for visualization. For quantification of several independent samples a 5 µm average intensity projection of the corresponding stack was used. Two ROIs (100x300 px^2, corresponding to 145 μm^2) were placed manually in the anterior (control) and posterior (RNAi) region of the corresponding stack. The mean fluorescence is measured with Fiji. Statistical significance was determined using Student's *t*-test (two-tailed) in GraphPad Prism 6 software.

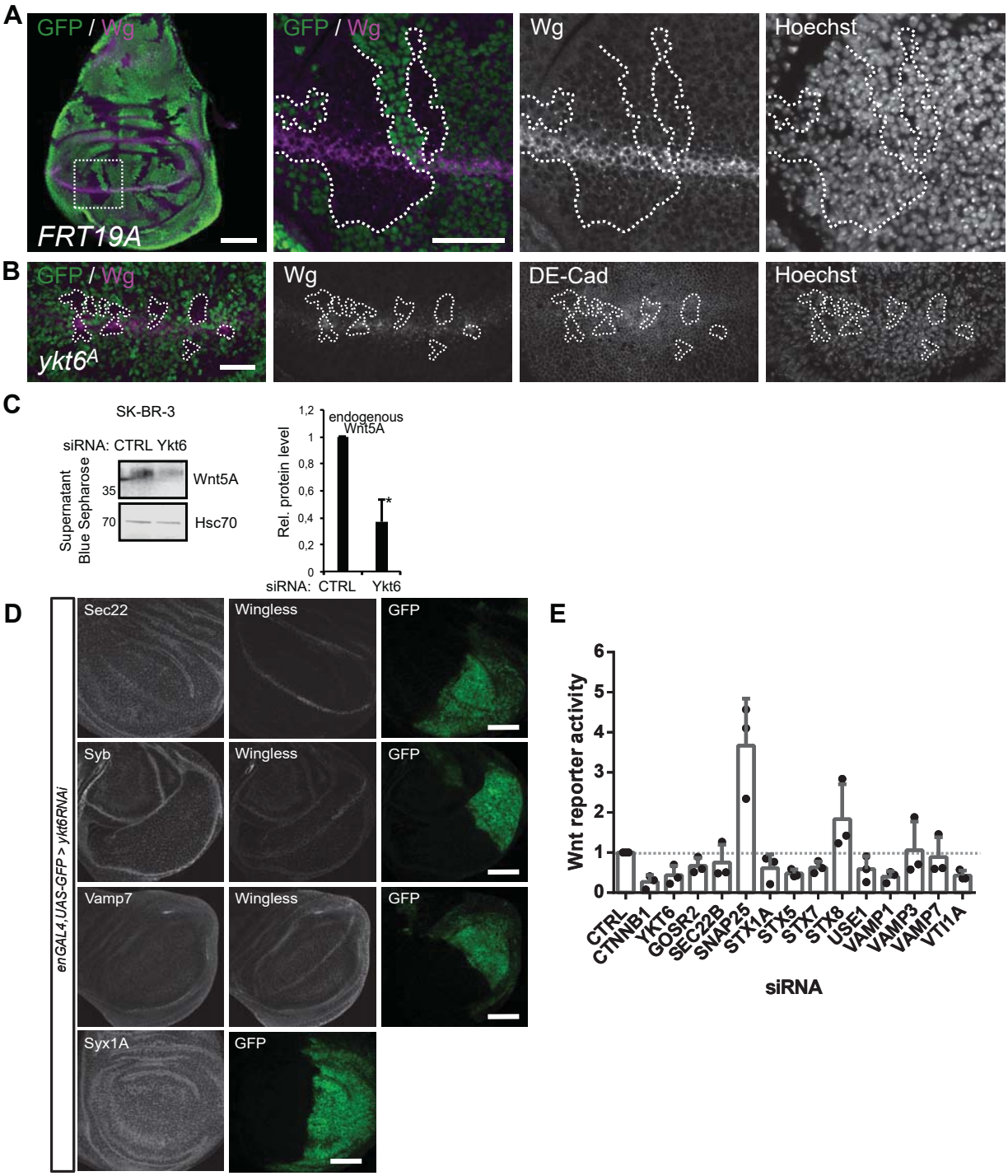

Fig. S1. Loss of Ykt6 blocks Wnt secretion.
(**A**) Induction of FRT19A control clones marked by the absence of GFP does not affect Wg secretion. The zoomed images to the right are enlarged views of the area marked with a dotted square in the overview image on the left. Maximum intensity projection of two subapical optical sections (distance 1 µm) are depicted for visualization. Scale bars, 50 µm in overview and 20 µm in other images. (**B**) Wingless protein accumulates in ykt6A clones, while DE-Cad staining is normal. Maximum intensity projection of three subapical (DE-Cad) and lateral (Wg and Hoechst) optical sections (distance 1 µm) are depicted for visualization. Scale bar 20 µm. (**C**) Wnt5A secretion from SkBr3 cells is reduced in Ykt6 knockdown cells. Quantification of three independent experiments, * p= 0,01 student t-test. (**D**) Knock-down of Ykt6 by RNAi in the posterior compartment of third instar WID marked by co-expression of GFP (engrailed-Gal4, UAS-GFP/UAS-ykt6RNAi) does not change the levels of Sec22, Syb, Vamp7 and Syx1A. Images are representative of >six WID per RNAi from two independent experiments. Scale bars represent 50 µm. (**E**) Wnt reporter assay of different SNAREs from three independent experiments. Not significant, one-way ANOVA.

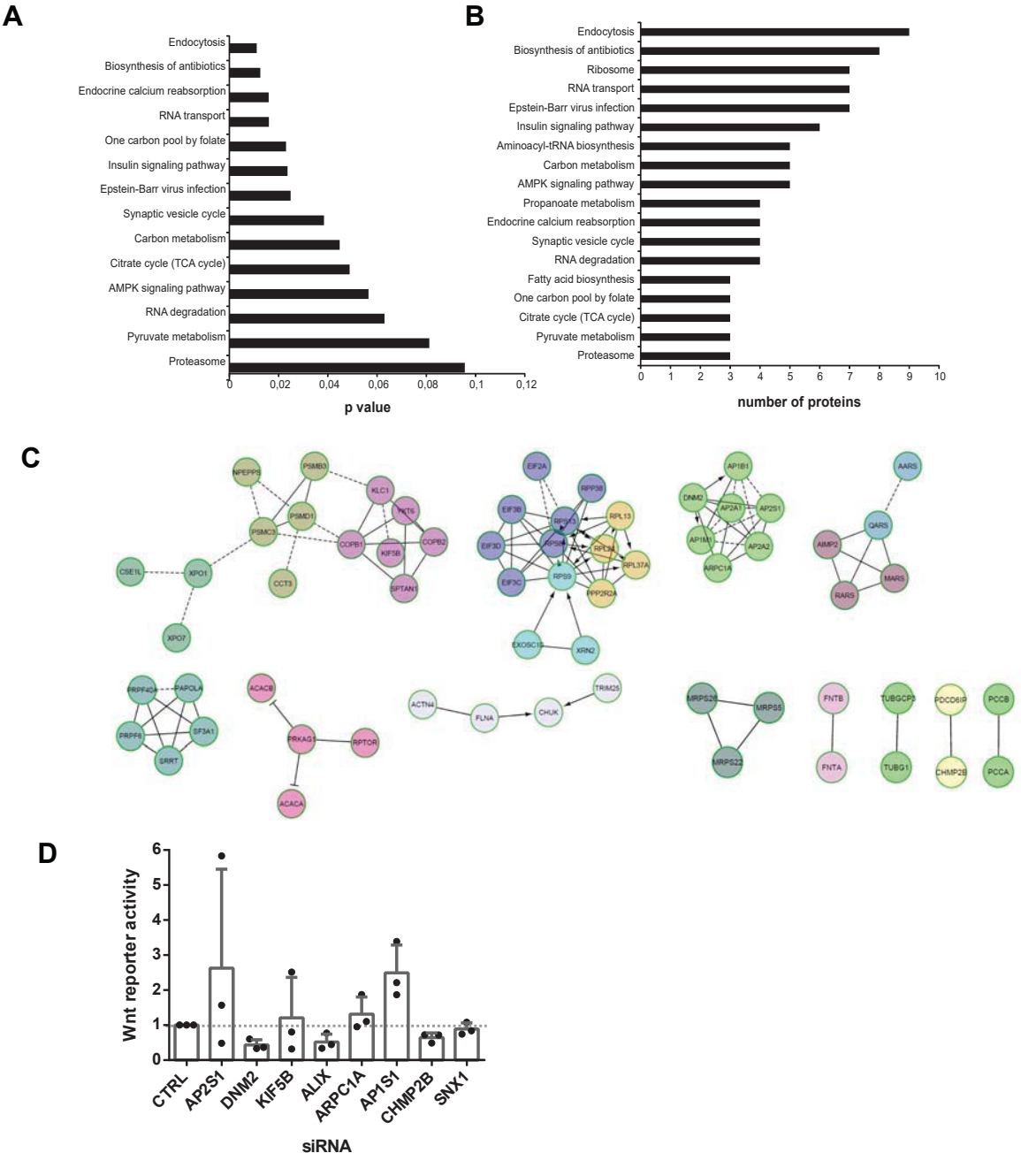

Fig. S2. Ykt6 acts on endosomal compartments after apical presentation.
(**A**) BioID-identified proteins were sorted by p-value for Kegg pathway enrichment in Ykt6-WT sample over control. (**B**) Number of proteins enriched in different Kegg pathways. (**C**) Reactome FI network analysis, networks with at least two nodes are displayed. (**D**) Wnt reporter assay of endocytosis pathway components from Fig. 3G from three independent experiments. Not significant, one-way ANOVA.

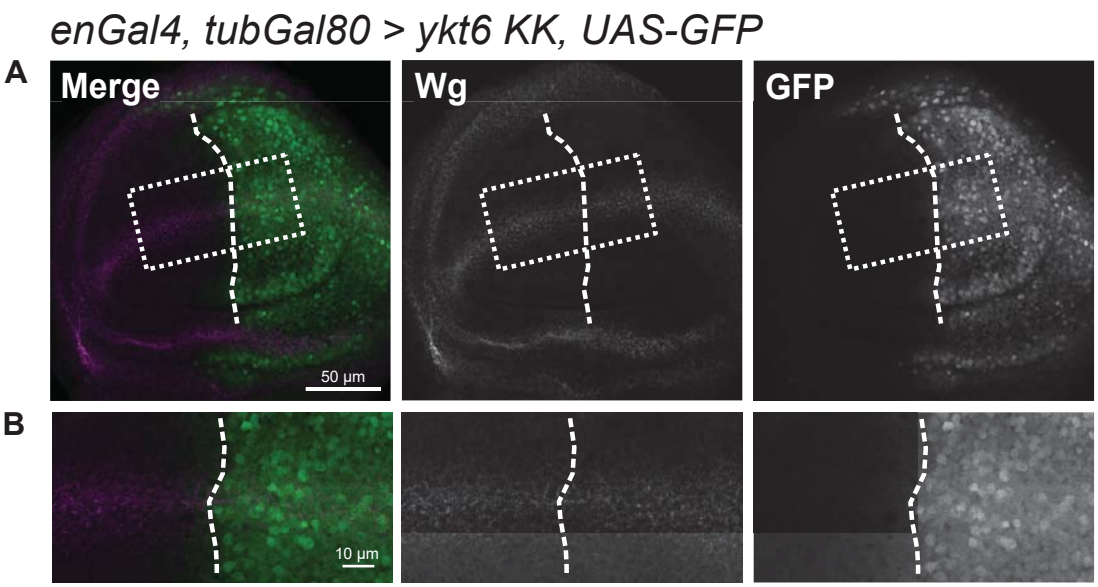

Fig. S3. Ykt6 knockdown is not sufficient to block Evi recycling.
(**A,B**) Endocytosis of anti-Wg antibody for 60min in enGal4-driven ykt6 knockdown WID. (**A**) Overview images. (**B**) Enlarged view of the area marked with a dotted square in (A). Scale bars as indicated.

A

Genotype	Viability
ykt6^{A}/Y; +/+ ; +/+	no
ykt6^{C}/Y; +/+ ; +/+	no
+/Y; hrs^{D28}/hrs^{D28} ; +/+	no
ykt6A/Y; hrs^{D28}/+ ; +/+	yes
ykt6C/Y; hrs^{D28}/+ ; +/+	yes

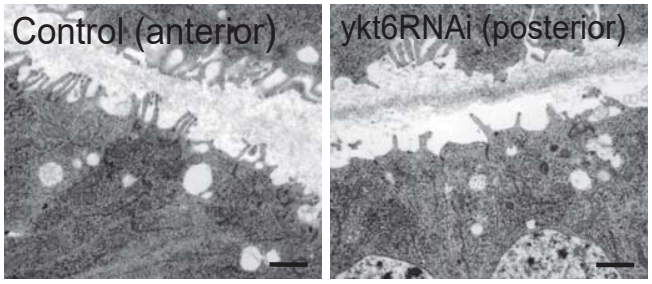

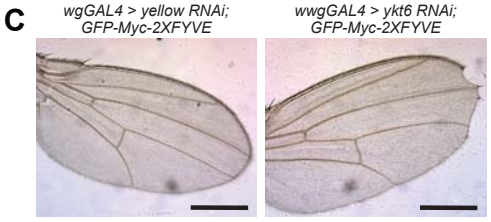

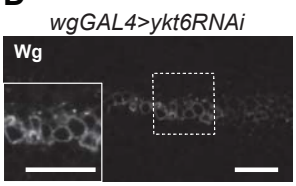

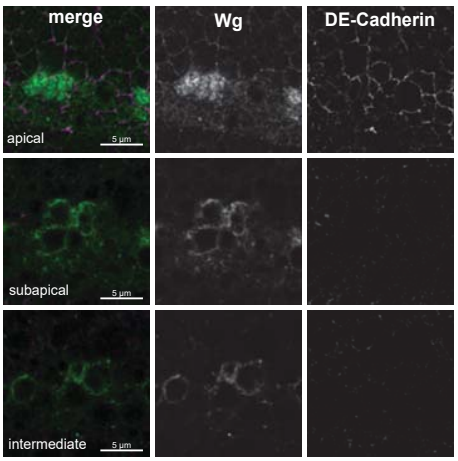

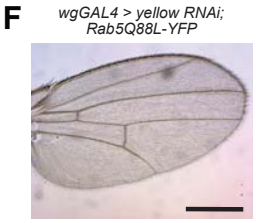

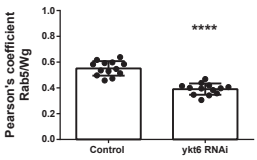

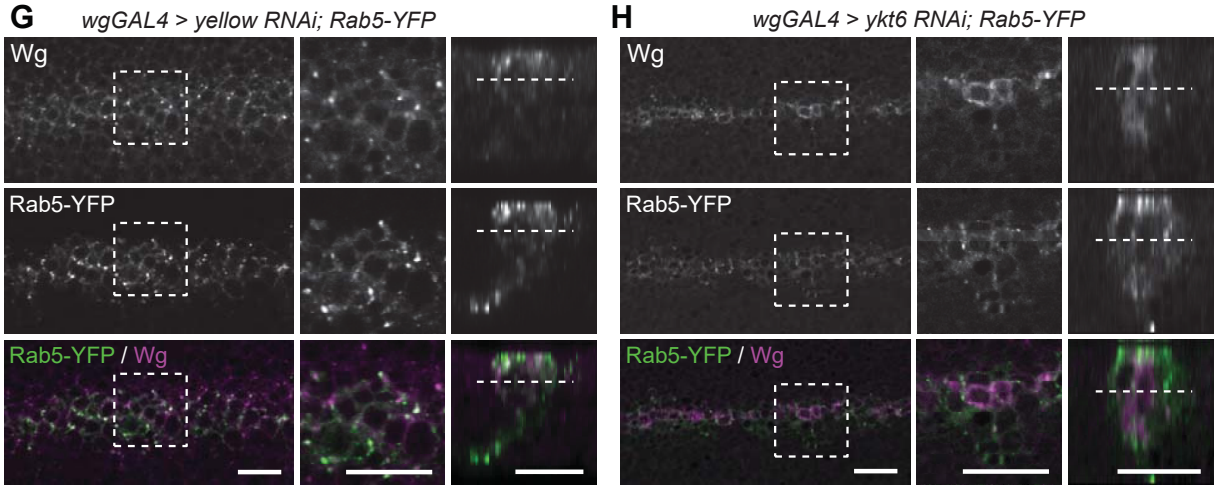

Fig. S4: Ykt6 acts on Wnt trafficking at the level of endosomes.
(**A)** Genetic interaction of *ykt6* and *hrs*. *ykt6* homozygous lethality can be rescued by removing one copy of *hrs*. (**B**) Electron microscopy images of apical membranes in WID of time-controlled RNAi of Ykt6 (engrailed-Gal4, UAS-GFP/ UAS-ykt6RNAi; tubGal80-TS/+, larvae reared for three days at days at 29°C). Scale bar is 500 nm. (**C**) UAS-GFP-Myc-2xFYVE was expressed with wgGAL4 in combination with yellow (control, left panel) or ykt6 RNAi (right panel) to analyze for adult wing notches. Scale bars 500 µm. Representative of >10 wings from three independent experiments. (**D**) wgGAL4 mediated Ykt6 RNAi leads to cortical Wg accumulation. (**E**) High resolution images of Wg and DE-Cadherin localization in wgGAL4 mediated Ykt6 RNAi by Confocal Airy Scan imaging. (**F**) UAS-Rab5Q88L-YFP was expressed with wgGAL4 in combination with yellow (control, left panel) or ykt6 RNAi (right panel) to analyze for adult wing notches. Scale bars 500 µm. Representative of >10 wings from three independent experiments. (**G, H**) UAS-Rab5-YFP was expressed with wgGAL4 in combination with yellow (control) (G) or ykt6 RNAi (H). Images represent a single confocal section. Left panel depicts a cross section, middle panel a magnification of the region boxed in the left panel. The right panel is a transverse (YZ) section of the stack. The dashed line marks the corresponding focal plane of the images shown in the left and middle. Scale bars is 10 µm in all images. (**I**) Pearson's coefficient of Rab5/Wg is decreased upon ykt6 knockdown with enGAL4,UAS-GFP;tubGAL80TS.

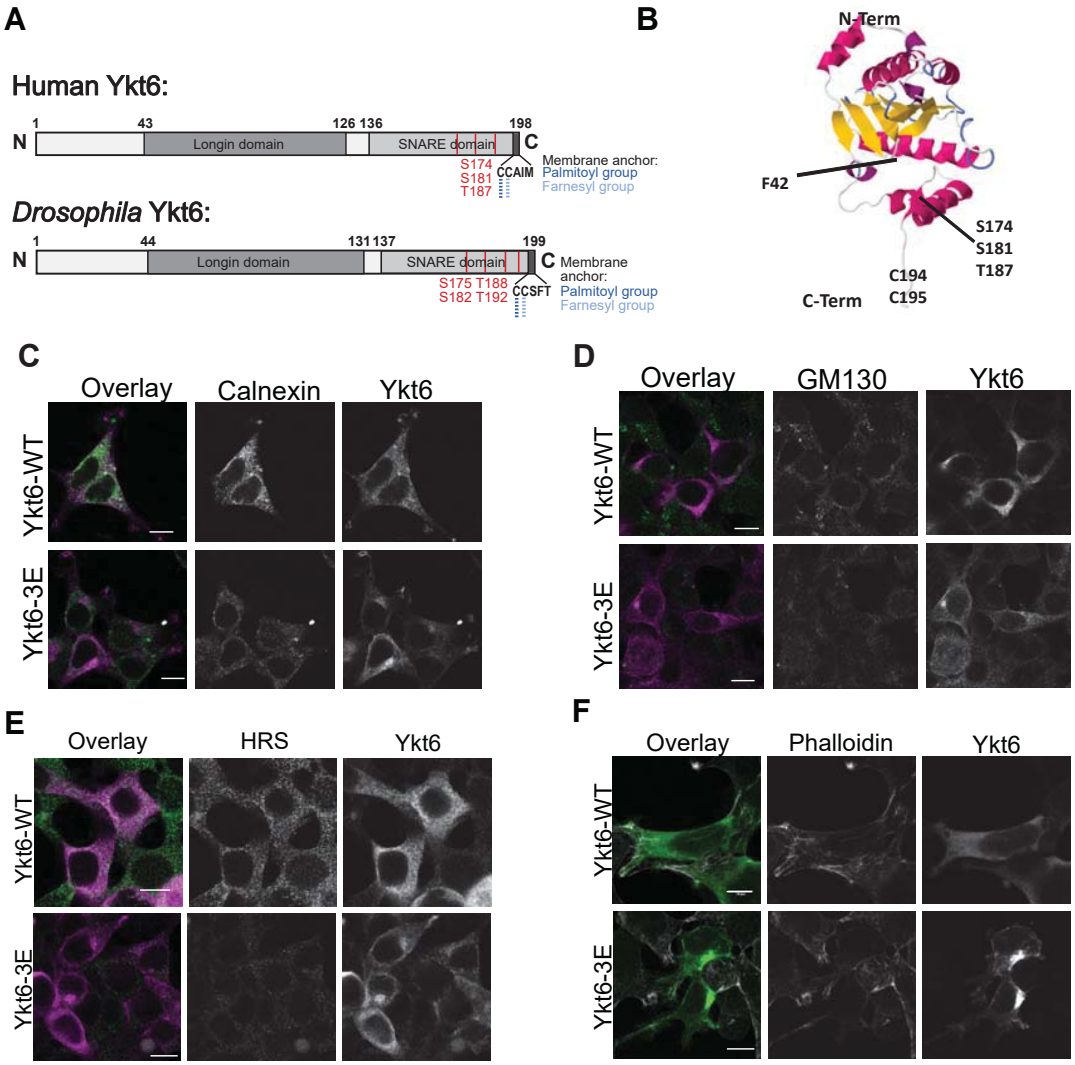

Fig. S5: Ykt6 SNARE domain is required for cycling between compartments. (**A**) Scheme of human and *Drosophila* Ykt6 with predicted phosphorylation sites in the SNARE domain. (**B**) Structural model of Ykt6 from template (3kyqA). Mutations as indicated: F42 in the Longin domain, S174, S181 and T187 in the SNARE domain and C194 and C195 in the CAAX motif for acylation. (**C-F**) Colocalization of Bio-ID-tagged Ykt6-WT and -3E in Hek293T cells with organelle markers for (**C**) ER (Calnexin), (**D**) Golgi (GM130), (**E**) endosomes (Hrs) and (**F**) F-actin (Phalloidin). Scale bars 10 µm and a representative field of view from three independent experiments is depicted.

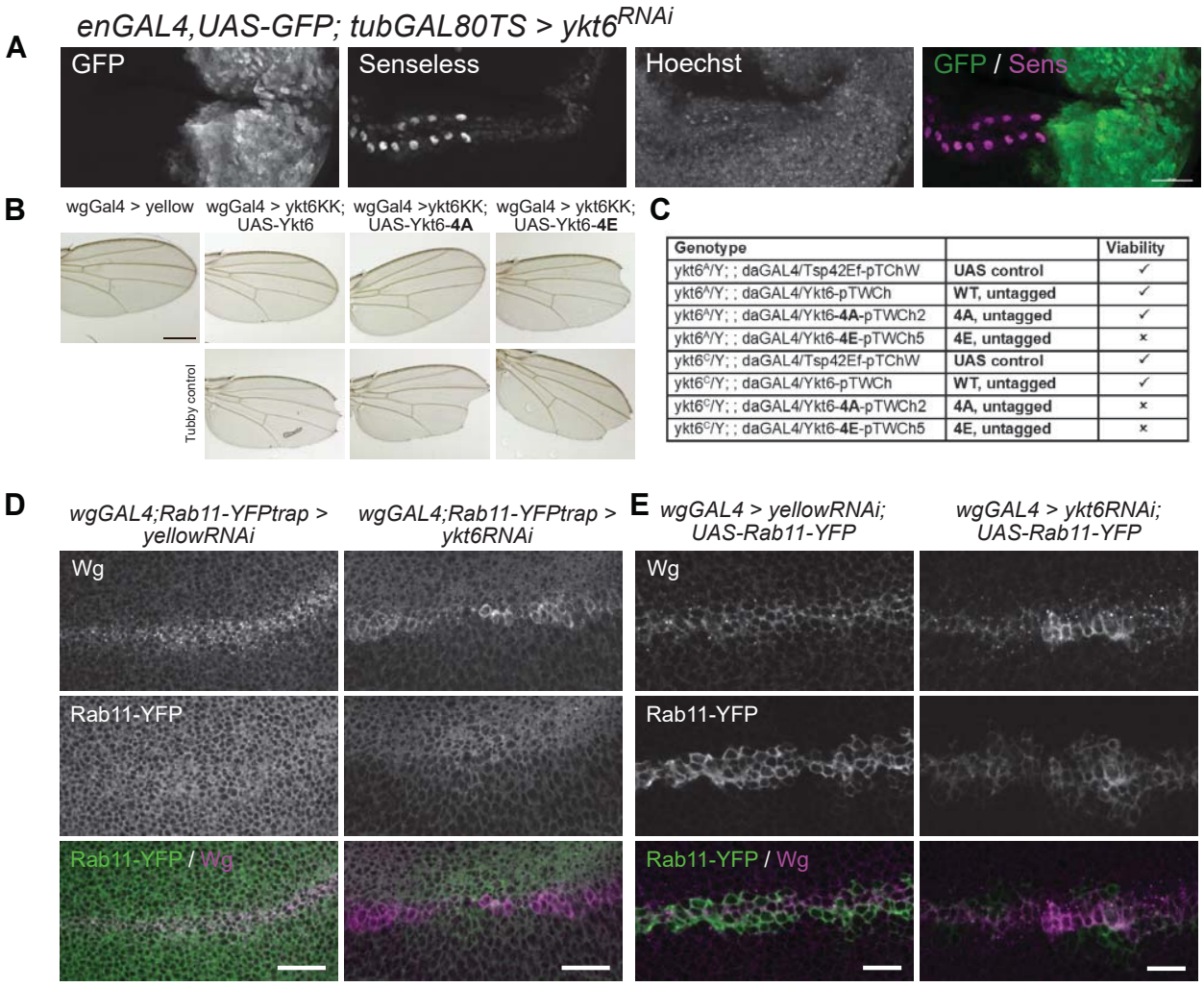

Genotype		Viability
ykt6^{A}/Y; ; daGAL4/Tsp42Ef-pTChW	UAS control	✓
ykt6^{A}/Y; ; daGAL4/Ykt6-pTWCh	WT, untagged	✓
ykt6^{A}/Y; ; daGAL4/Ykt6-**4A**-pTWCh2	4A, untagged	✓
ykt6^{A}/Y; ; daGAL4/Ykt6-**4E**-pTWCh5	4E, untagged	×
ykt6^{C}/Y; ; daGAL4/Tsp42Ef-pTChW	UAS control	✓
ykt6^{C}/Y; ; daGAL4/Ykt6-pTWCh	WT, untagged	✓
ykt6^{C}/Y; ; daGAL4/Ykt6-**4A**-pTWCh2	4A, untagged	×
ykt6^{C}/Y; ; daGAL4/Ykt6-**4E**-pTWCh5	4E, untagged	×

Fig. S6: Ykt6 SNARE domain is required in vivo. (**A**) Time-controlled depletion of Ykt6 by RNAi (engrailed-Gal4, UAS-GFP/ UAS-ykt6RNAi; tubGal80-TS/+, larvae reared for three days at days at 29°C) causes reduction of Senseless staining in the posterior WID. Images are representative of > six WIDs from three independent experiments. Scale bar: 20 µm (**B**) Depletion of ykt6 by RNAi along the dorso-ventral border using wingless-GAL4 results in adult wing notches. Wing notches can be rescued by UAS-driven co-overexpression of WT and SNARE mutant Ykt6-4A but not Ykt6-4E. All Ykt6 constructs are inserted on the third chromosome (86Fb). The images in the bottom panel show wings from the balancer flies from the same vial not co-expressing the UAS-Ykt6 constructs but only ykt6 RNAi as control. Scale bars 500 µm. These wings are representative of >10 wings from three independent experiments. (**C**) Rescue of lethality of *ykt6^{A}* and *ykt6^{C}* alleles. All Ykt6 constructs are inserted on the third chromosome (86Fb) and are expressed under the control of ubiquitous daughterless-GAL4. (**D**) yellow and ykt6 RNAi were expressed with wg-GAL4 in an endogenously tagged Rab11-YFP background. Maximum intensity projection of four sections (distance 0,5 µm) depicted for visualization. Scale bar represents 20 µm. (**E**) UAS-Rab11-YFP was expressed with wgGAL4 in combination with yellow (control, left panel) or ykt6 RNAi (right panel). Scale bars represent 20 µm.

Supplementary information

Table S1: SNARE in vivo RNAi screening results.

Click here to Download Table S1

Table S2: Proteins identified by mass spectrometry from BioID control and Ykt6-WT samples in two biological replicates

Click here to Download Table S2

Table S3: Dharmacon siRNA SMARTpools

Gene Symbol	GENE ID	Gene Accession	GI Number	Sequence
siGENOME Non-targeting Control_5#				UGGUUUACAUGUCGACUAA
AP1S1	1174	NM_057089	148536832	AAUGGUACCUGGCCACUUC
AP1S1	1174	NM_057089	148536832	GCUCGAAAGCCCAAGAUGU
AP1S1	1174	NM_057089	148536832	CAUCGAGGGCCAAGACAAU
AP2S1	1175	NM_021575	70906431	AGACGAAGGUGCUGAAACA
AP2S1	1175	NM_021575	70906431	GGUCUUAAACGAAUAUUUC
AP2S1	1175	NM_021575	70906431	AACAGAAGCUGAUCGAGGA
ARPC1A	10552	NM_006409	22907051	ACGAAGUGCACAUCUAUAA
ARPC1A	10552	NM_006409	22907051	GAAUUAAUCGCGCAGCUAC
ARPC1A	10552	NM_006409	22907051	GUGGCACGAUGGCGAGGAA
ARPC1A	10552	NM_006409	22907051	GGAAGUGGAGCACGACUCA
CHMP2B	25978	NM_014043	40254865	GAAGAUGGCUGGAGCAAUG
CHMP2B	25978	NM_014043	40254865	UAAGGAAGCUUGCAAAGUU
CHMP2B	25978	NM_014043	40254865	GCUCGAAGCUUACCAUCUG
CHMP2B	25978	NM_014043	40254865	GCCAGGAUAUUGUGAAUCA
CTNNB1	1499	NM_001904	4503130	GCUGAAACAUGCAGUUGUA
CTNNB1	1499	NM_001904	4503130	GAUAAAGGCUACUGUUGGA
CTNNB1	1499	NM_001904	4503130	CCACUAAUGUCCAGCGUUU
DNM2	1785	NM_004945	56549118	CCGAAUCAAUCGCAUCUUC
DNM2	1785	NM_004945	56549118	GACAUGAUCCUGCAGUUCA
DNM2	1785	NM_004945	56549118	CCUCCGAGCUGGCGUCUAC
DNM2	1785	NM_004945	56549118	AGUCCUACAUCAACACGAA
GOSR2	9570	NM_054022	60499002	ACGAAUCACUGCAGUUUAA
GOSR2	9570	NM_054022	60499002	GAUCCAGUCUUGCAUGGGA
GOSR2	9570	NM_054022	60499002	CGAAAUCCAAGCAAGCAUA
GOSR2	9570	NM_054022	60499002	GAUAUUCAGCCGUCUAGAA
KIF5B	3799	NM_004521	4758647	GCAGUCAGGUCAAAGAAUA
KIF5B	3799	NM_004521	4758647	GAACUGGCAUGAUAGAUGA
KIF5B	3799	NM_004521	4758647	CAACAGACAUGUAGCAGUU
SEC22B	9554	NM_004892	94429049	GAAGAAGUGUUACAACGAG
SEC22B	9554	NM_004892	94429049	CUAAGCAACUCUUUCGAAA

SEC22B	9554	NM_004892	94429049	UAACAAUGAUCGCCCGAGU
SNAP25	6616	NM_003081	18765732	GCAAUGAGAUCGAUACACA
SNAP25	6616	NM_003081	18765732	GCGAAGGGCUGACCAGUUG
SNAP25	6616	NM_003081	18765732	GGAAAGCACCCGUCGUAUG
SNX1	6642	NM_148955	71772739	GGAAAGAGCUAGCGCUGAA
SNX1	6642	NM_148955	71772739	GAAAGGGACUUCGAGAGGA
SNX1	6642	NM_148955	71772739	GAAAAGAAGUGAUACGGUU
SNX1	6642	NM_148955	71772739	AGAACCACGUGAUCAAGUA
STX1A	6804	NM_004603	95147340	GGAACACGCGGUAGACUAU
STX1A	6804	NM_004603	95147340	GGAGGAGAUUCGAGGCUUC
STX1A	6804	NM_004603	95147340	ACAUAAAGAAGACAGCAAA
STX5	6811	NM_003164	94400931	GCAAGUCCCUCUUUGAUGA
STX5	6811	NM_003164	94400931	GAGCUAACAUAUAUCAUCA
STX5	6811	NM_003164	94400931	GAGCCCAGCUGGACGUUGA
STX7	8417	NM_003569	4507294	CAAAGAAACAGAUAAGUAC
STX7	8417	NM_003569	4507294	GCGAUUAUCAGUCUCAUCA
STX7	8417	NM_003569	4507294	GUCAAGGGCAGCAGAUUAU
STX7	8417	NM_003569	4507294	GAGUUUGUUGCUCGAGUAA
STX8	9482	NM_004853	296010812	CACCAAAGCUUACCGUGAC
STX8	9482	NM_004853	296010812	UCUUGUAACUCGAGAGAGA
STX8	9482	NM_004853	296010812	GAAUGAGGGUGCCGAACCA
STX8	9482	NM_004853	296010812	UGAGAUAAUUGACGACCUU
USE1	55850	NM_018467	154354977	CGUCGAGGCUGGAGCUAAA
USE1	55850	NM_018467	154354977	CUGAGGUGAUCAAUGAAUA
USE1	55850	NM_018467	154354977	GAGAUGGACGUAAGGAAGA
USE1	55850	NM_018467	154354977	CGAAUCAUGCCUAAACUCA
VAMP1	6843	NM_014231	40549444	CUCCUAACAUGACCAGUAA
VAMP1	6843	NM_014231	40549444	CAUCACAAUUUGAGAGCAG
VAMP1	6843	NM_014231	40549444	CCAUCAUCGUGGUAGUUAU
VAMP1	6843	NM_014231	40549444	AGGCACAAGUGGAGGAGGU
VAMP3	9341	NM_004781	42544205	GGCAGGCGCUUCUCAAUUU
VAMP3	9341	NM_004781	42544205	GGAUUACUGUUCUGGUUAU
VAMP3	9341	NM_004781	42544205	GCCAAGUUGAAGAGGAAAU
VAMP7	6845	NM_005638	27545446	GGAGAAAGAUUGGAAUUAU
VAMP7	6845	NM_005638	27545446	GUACUCACAUGGCAAUUAU
VAMP7	6845	NM_005638	27545446	AAGAAGAGGUUCCAGACUA
VTI1A	143187	NM_145206	113374155	CGUCCGACUUCGAAGGUUA
VTI1A	143187	NM_145206	113374155	CGUGAAAGACUUCGGGAAA
VTI1A	143187	NM_145206	113374155	CGAGGGAUGUACAGCAACA
VTI1A	143187	NM_145206	113374155	GGUCAGGAGAUGUUGGAAA
YKT6	10652	NM_006555	34304384	GCUCAAAGCCGCAUACGAU
YKT6	10652	NM_006555	34304384	GUGAGAAGCUAGAUGACUU
YKT6	10652	NM_006555	34304384	GAAGGUACUAGAUGAAUUC

Supplementary materials and methods

Image analysis

Fig. 3: exWg

MIP of 45 (Ykt6, distance 0,5 µm) or 25 (AP2, distance 1 µm) sections covering the entire stack depicted for visualization. For quantification the average intensity projection of the corresponding stack was used. The profile of the extracellular Wg staining in the shown ROI (1142 x 300 px^2, corresponding to 80x21 μm^2), comparing exWg in the anterior (control, no GFP) with the posterior (RNAi, GFP-positive) region for this one representative example, was plotted with Fiji. For quantification of several independent samples, two ROIs (500x500 px^2, corresponding to 1245 μm^2) were placed manually in the anterior (control) and posterior (RNAi) region of the corresponding stack. The mean fluorescence of five subapical sections (distance 1 µm) is measured with Fiji and averaged per stack. This corresponds to taking the mean fluorescence of an average intensity projection of this corresponding stack. Statistical significance was determined using Student's *t*-test (two-tailed) in GraphPad Prism 6 software.

Fig. 3: Evi

MIP of 15 apical sections (distance 1 µm) depicted for visualization. For quantification the average intensity projection of the corresponding stack was used. The profile of the Evi staining in the shown ROI (1428 x 300 px^2, corresponding to 100 x 21 μm^2), comparing Evi in the anterior (control, no GFP) with the posterior (RNAi, GFP-positive) region for this one representative example, was plotted with Fiji. For quantification of several independent samples, two ROIs (500x250 px^2, corresponding to 623 μm^2) were placed manually in the anterior (control) and posterior (RNAi) region of the corresponding stack. The mean fluorescence of five subapical sections (distance 1 µm) is measured with Fiji and averaged per stack. This corresponds to taking the mean fluorescence of an average intensity projection of this corresponding stack. For quantification of Evi punctae, a maximum intensity projection of the same five subapical sections as above (distance 1 µm) was generated and thresholded using Triangle algorithm implemented in Fiji. Two manually drawn ROIs were placed in the control and the RNAi region along the entire Evi expression domain. Particles > 4 px^2 were automatically counted using Fiji Particle Analyzer within the ROIs. The number of particles was normalized to the area quantified. Statistical significance was determined using Student's *t*-test (two-tailed) in GraphPad Prism 6 software.

Fig.4: Hrs

MIP of nine sections (distance 1 µm) for visualization. For quantification of several independent samples two ROIs (500x500 px^2, corresponding to 1245 μm^2) were placed manually in the anterior (control) and posterior (RNAi) region of the corresponding stack. The mean fluorescence of five subapical sections (distance 1 µm) is measured with Fiji and averaged per stack. This corresponds to taking the mean fluorescence of an average intensity projection of this corresponding stack. The sections to be measured were chosen based on nuclear staining. The nuclei had to be apparent in the entire section. Hrs staining is also very strong in the peripodial membrane, but this signal was not included. Statistical significance was determined using Student's *t*-test (two-tailed) in GraphPad Prism 6 software.

Fig.4: Lamp1
MIP of seven sections (distance 1 µm) are depicted for visualization. Quantification was done as for Hrs.

Fig.4: Rab5
MIP of 13 sections (distance 1 µm) are depicted for visualization. Quantification was done as for Hrs.

Fig.4: Rab7

MIP of seven sections (distance 1 µm) are depicted for visualization. Quantification was done as for Hrs.

Fig. 4: FYVE

For quantification of FYVE-labelled Wg punctae, a 30px XZ section within the Wg stripe was generated. In Fiji a ROI (1500 x 250 px^2, corresponding to 105 x 17.5 μm^2) was placed at the center of the Wg expression domain. Within this ROI, particles >6 px were automatically counted and colocalization determined using the Fiji Plugin ComDet.

Fig. 5: Wg in rescue crosses with Ykt6 SNARE-mutants
MIP of six sections (distance 0,5 µm) for visualization. For quantification of several independent samples a 5 µm average intensity projection of the corresponding stack was used. Two ROIs (100x300 px^2, corresponding to 145 μm^2) were placed manually in the anterior (control) and posterior (RNAi) region of the corresponding stack. The mean fluorescence is measured with Fiji. Statistical significance was determined using Student's *t*-test (two-tailed) in GraphPad Prism 6 software.

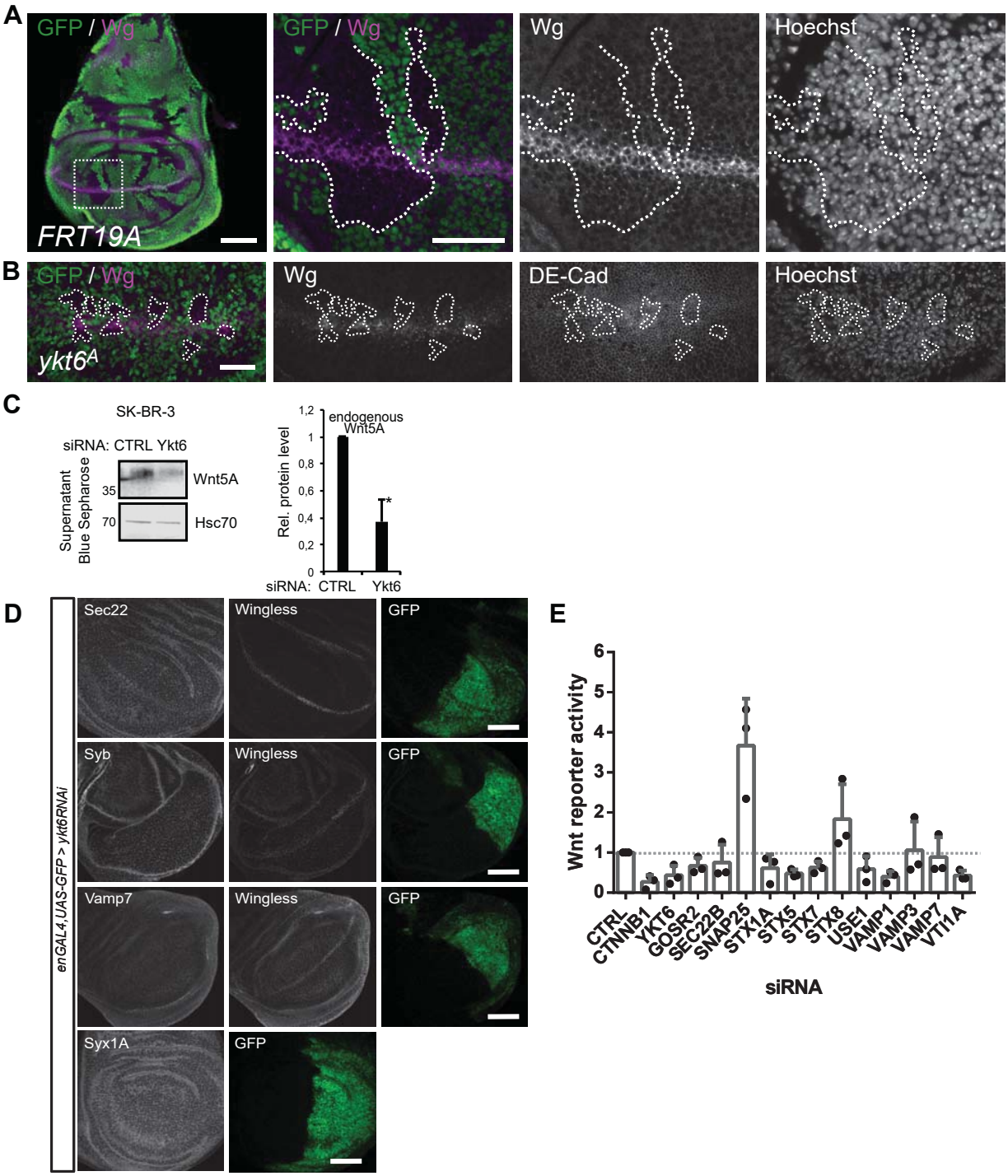

Fig. S1. Loss of Ykt6 blocks Wnt secretion.
(**A**) Induction of FRT19A control clones marked by the absence of GFP does not affect Wg secretion. The zoomed images to the right are enlarged views of the area marked with a dotted square in the overview image on the left. Maximum intensity projection of two subapical optical sections (distance 1 µm) are depicted for visualization. Scale bars, 50 µm in overview and 20 µm in other images. (**B**) Wingless protein accumulates in ykt6A clones, while DE-Cad staining is normal. Maximum intensity projection of three subapical (DE-Cad) and lateral (Wg and Hoechst) optical sections (distance 1 µm) are depicted for visualization. Scale bar 20 µm. (**C**) Wnt5A secretion from SkBr3 cells is reduced in Ykt6 knockdown cells. Quantification of three independent experiments, * p= 0,01 student t-test. (**D**) Knock-down of Ykt6 by RNAi in the posterior compartment of third instar WID marked by co-expression of GFP (engrailed-Gal4, UAS-GFP/UAS-ykt6RNAi) does not change the levels of Sec22, Syb, Vamp7 and Syx1A. Images are representative of >six WID per RNAi from two independent experiments. Scale bars represent 50 µm. (**E**) Wnt reporter assay of different SNAREs from three independent experiments. Not significant, one-way ANOVA.

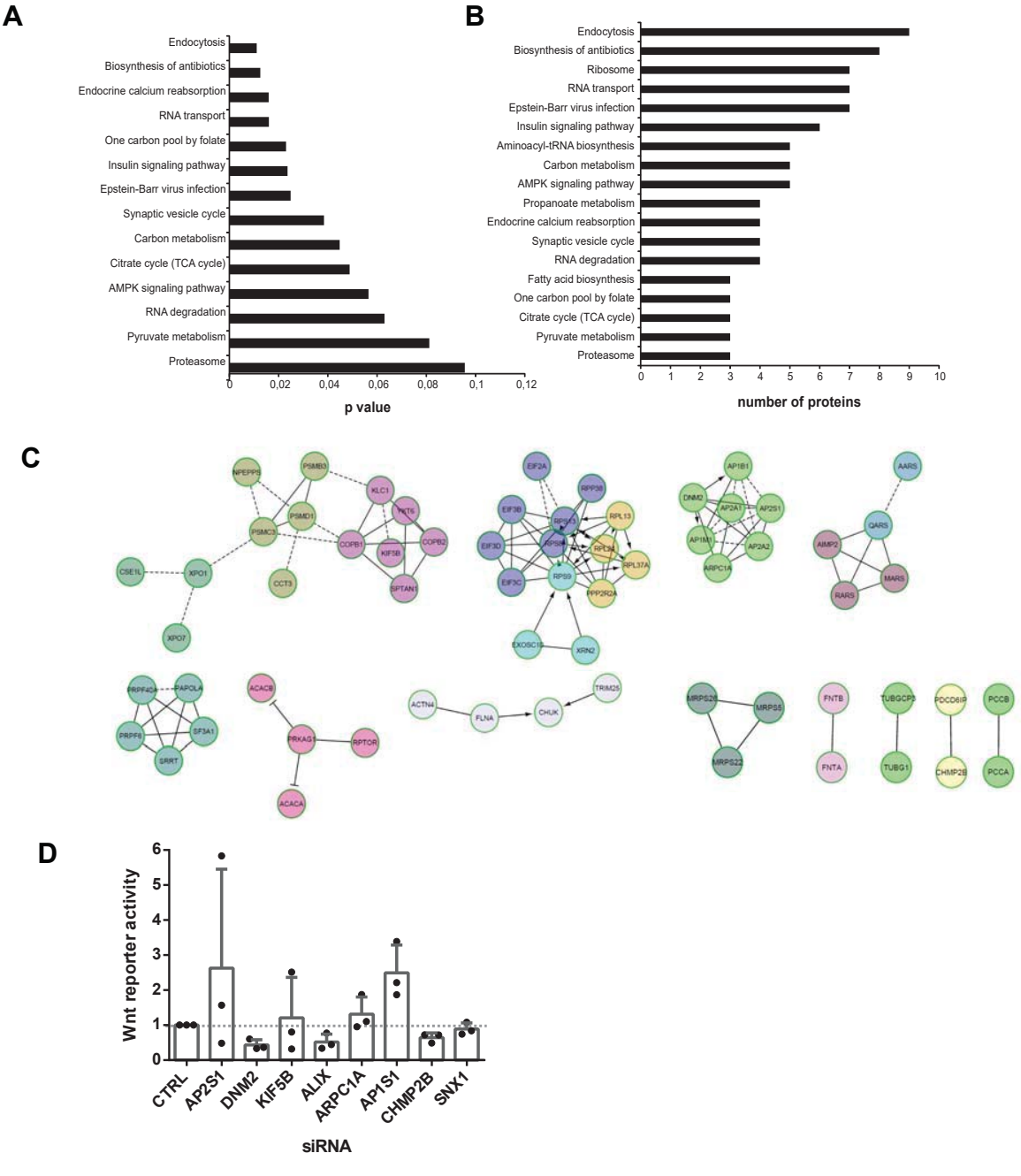

Fig. S2. Ykt6 acts on endosomal compartments after apical presentation.
(**A**) BioID-identified proteins were sorted by p-value for Kegg pathway enrichment in Ykt6-WT sample over control. (**B**) Number of proteins enriched in different Kegg pathways. (**C**) Reactome FI network analysis, networks with at least two nodes are displayed. (**D**) Wnt reporter assay of endocytosis pathway components from Fig. 3G from three independent experiments. Not significant, one-way ANOVA.

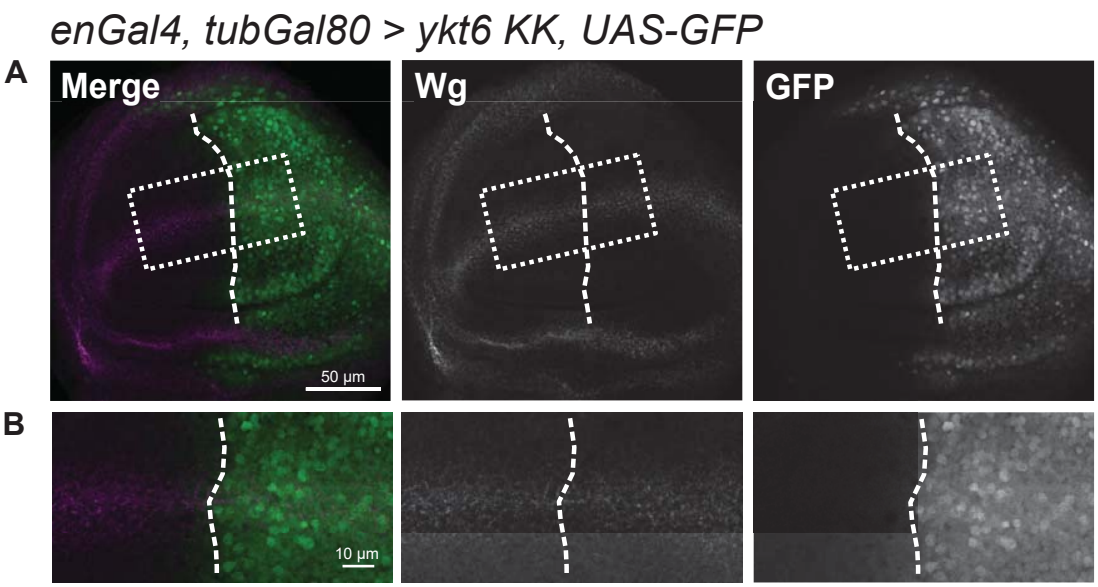

Fig. S3. Ykt6 knockdown is not sufficient to block Evi recycling.
(**A,B**) Endocytosis of anti-Wg antibody for 60min in enGal4-driven ykt6 knockdown WID. (**A**) Overview images. (**B**) Enlarged view of the area marked with a dotted square in (A). Scale bars as indicated.

A

Genotype	Viability
ykt6^{A}/Y; +/+ ; +/+	no
ykt6^{C}/Y; +/+ ; +/+	no
+/Y; hrs^{D28}/hrs^{D28} ; +/+	no
ykt6A/Y; hrs^{D28}/+ ; +/+	yes
ykt6C/Y; hrs^{D28}/+ ; +/+	yes

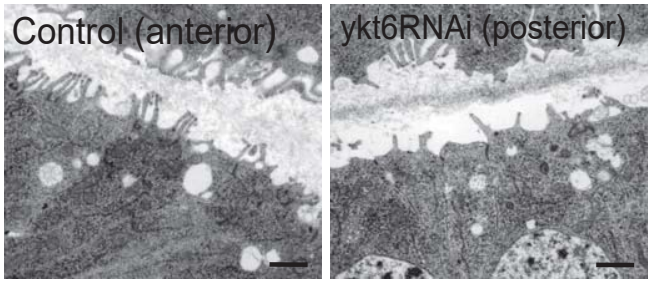

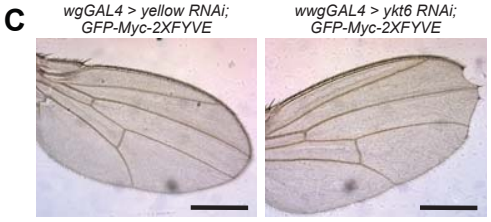

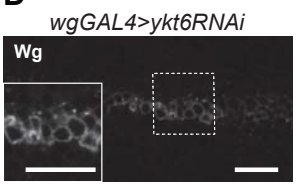

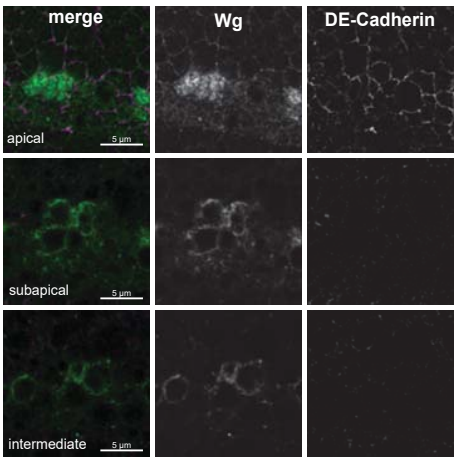

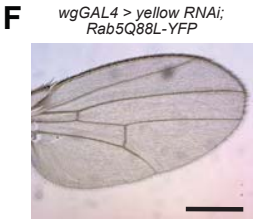

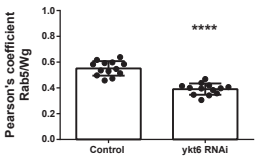

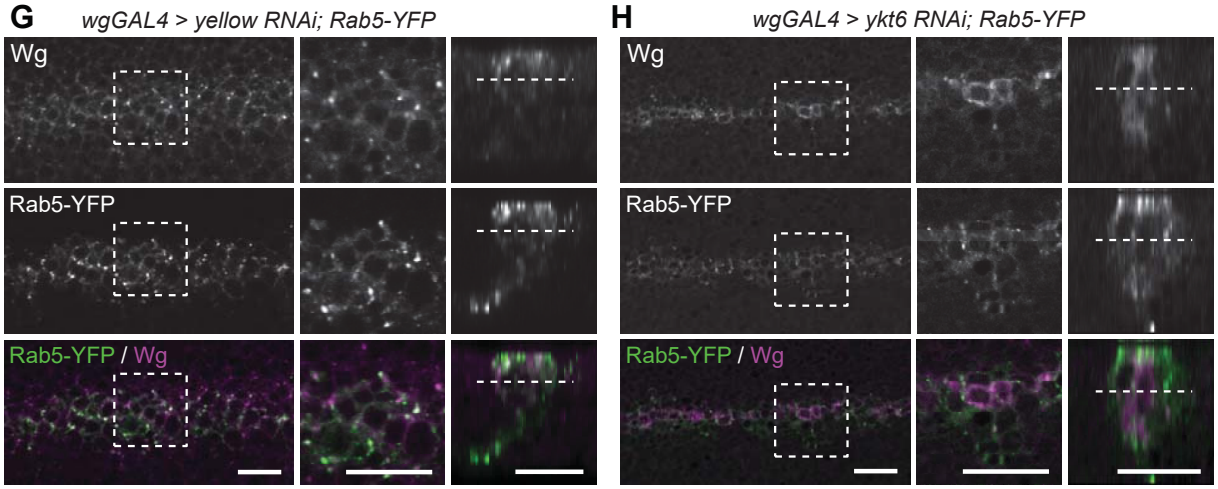

Fig. S4: Ykt6 acts on Wnt trafficking at the level of endosomes.
(**A)** Genetic interaction of *ykt6* and *hrs*. *ykt6* homozygous lethality can be rescued by removing one copy of *hrs*. (**B**) Electron microscopy images of apical membranes in WID of time-controlled RNAi of Ykt6 (engrailed-Gal4, UAS-GFP/ UAS-ykt6RNAi; tubGal80-TS/+, larvae reared for three days at days at 29°C). Scale bar is 500 nm. (**C**) UAS-GFP-Myc-2xFYVE was expressed with wgGAL4 in combination with yellow (control, left panel) or ykt6 RNAi (right panel) to analyze for adult wing notches. Scale bars 500 µm. Representative of >10 wings from three independent experiments. (**D**) wgGAL4 mediated Ykt6 RNAi leads to cortical Wg accumulation. (**E**) High resolution images of Wg and DE-Cadherin localization in wgGAL4 mediated Ykt6 RNAi by Confocal Airy Scan imaging. (**F**) UAS-Rab5Q88L-YFP was expressed with wgGAL4 in combination with yellow (control, left panel) or ykt6 RNAi (right panel) to analyze for adult wing notches. Scale bars 500 µm. Representative of >10 wings from three independent experiments. (**G, H**) UAS-Rab5-YFP was expressed with wgGAL4 in combination with yellow (control) (G) or ykt6 RNAi (H). Images represent a single confocal section. Left panel depicts a cross section, middle panel a magnification of the region boxed in the left panel. The right panel is a transverse (YZ) section of the stack. The dashed line marks the corresponding focal plane of the images shown in the left and middle. Scale bars is 10 µm in all images. (**I**) Pearson's coefficient of Rab5/Wg is decreased upon ykt6 knockdown with enGAL4,UAS-GFP;tubGAL80TS.

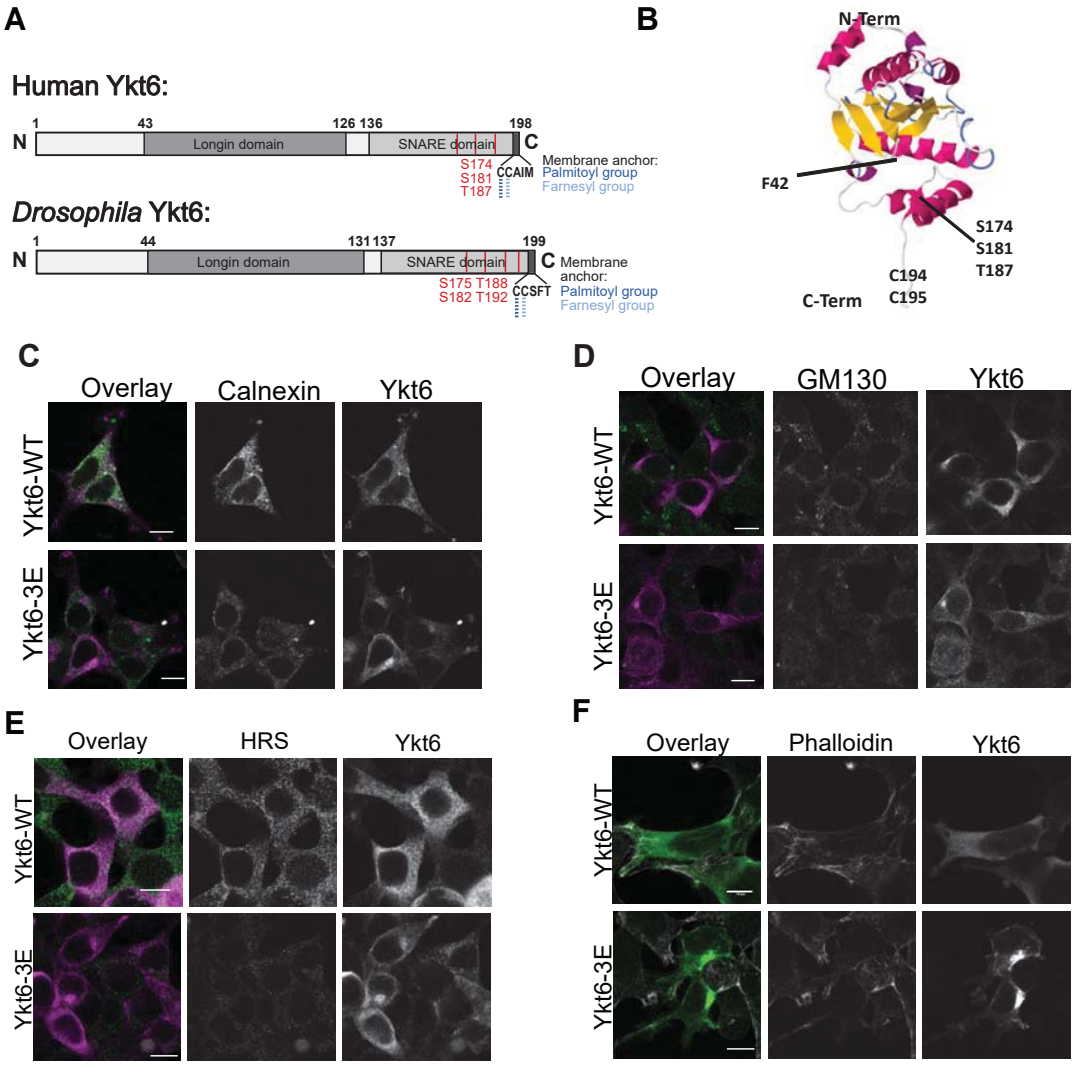

Fig. S5: Ykt6 SNARE domain is required for cycling between compartments. (**A**) Scheme of human and *Drosophila* Ykt6 with predicted phosphorylation sites in the SNARE domain. (**B**) Structural model of Ykt6 from template (3kyqA). Mutations as indicated: F42 in the Longin domain, S174, S181 and T187 in the SNARE domain and C194 and C195 in the CAAX motif for acylation. (**C-F**) Colocalization of Bio-ID-tagged Ykt6-WT and -3E in Hek293T cells with organelle markers for (**C**) ER (Calnexin), (**D**) Golgi (GM130), (**E**) endosomes (Hrs) and (**F**) F-actin (Phalloidin). Scale bars 10 µm and a representative field of view from three independent experiments is depicted.

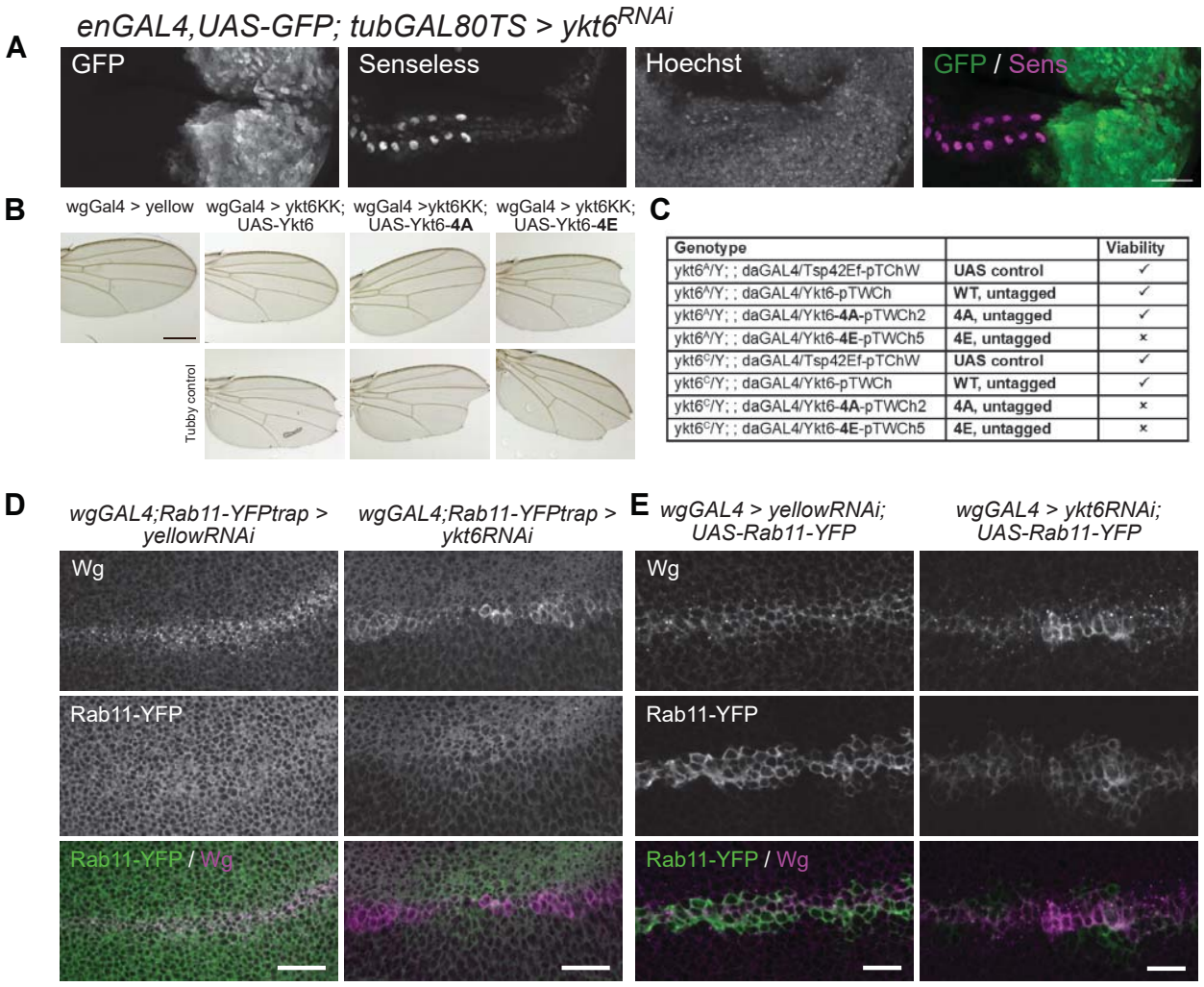

Genotype		Viability
ykt6^{A}/Y; ; daGAL4/Tsp42Ef-pTChW	UAS control	✓
ykt6^{A}/Y; ; daGAL4/Ykt6-pTWCh	WT, untagged	✓
ykt6^{A}/Y; ; daGAL4/Ykt6-**4A**-pTWCh2	4A, untagged	✓
ykt6^{A}/Y; ; daGAL4/Ykt6-**4E**-pTWCh5	4E, untagged	×
ykt6^{C}/Y; ; daGAL4/Tsp42Ef-pTChW	UAS control	✓
ykt6^{C}/Y; ; daGAL4/Ykt6-pTWCh	WT, untagged	✓
ykt6^{C}/Y; ; daGAL4/Ykt6-**4A**-pTWCh2	4A, untagged	×
ykt6^{C}/Y; ; daGAL4/Ykt6-**4E**-pTWCh5	4E, untagged	×

Fig. S6: Ykt6 SNARE domain is required in vivo. (**A**) Time-controlled depletion of Ykt6 by RNAi (engrailed-Gal4, UAS-GFP/ UAS-ykt6RNAi; tubGal80-TS/+, larvae reared for three days at days at 29°C) causes reduction of Senseless staining in the posterior WID. Images are representative of > six WIDs from three independent experiments. Scale bar: 20 µm (**B**) Depletion of ykt6 by RNAi along the dorso-ventral border using wingless-GAL4 results in adult wing notches. Wing notches can be rescued by UAS-driven co-overexpression of WT and SNARE mutant Ykt6-4A but not Ykt6-4E. All Ykt6 constructs are inserted on the third chromosome (86Fb). The images in the bottom panel show wings from the balancer flies from the same vial not co-expressing the UAS-Ykt6 constructs but only ykt6 RNAi as control. Scale bars 500 µm. These wings are representative of >10 wings from three independent experiments. (**C**) Rescue of lethality of *ykt6^{A}* and *ykt6^{C}* alleles. All Ykt6 constructs are inserted on the third chromosome (86Fb) and are expressed under the control of ubiquitous daughterless-GAL4. (**D**) yellow and ykt6 RNAi were expressed with wg-GAL4 in an endogenously tagged Rab11-YFP background. Maximum intensity projection of four sections (distance 0,5 µm) depicted for visualization. Scale bar represents 20 µm. (**E**) UAS-Rab11-YFP was expressed with wgGAL4 in combination with yellow (control, left panel) or ykt6 RNAi (right panel). Scale bars represent 20 µm.

Supplementary Table 1: SNARE *in vivo* RNAi screening results. GAL4 virgin females were crossed to RNAi males as indicated. In a primary screen using wgGAL4, adult flies were scored for wing defects. RNAi lines producing adult wing notches were further verified for Wg secretion defects in larval WID using enGAL4,UAS-GFP.

Gene name	Category		Human homologue	Lines	wgGAL4 X RNAi	enGAL4,UAS-GFP X	References
Bet1	Qc	t	Bet1	GD8421	**Notches**	**Lethal**	
Gos28	Qb	t	GOSR1 (Golgi SNAP receptor1	KK100289	No phenotype		
Membrin	Qb	t	GOSR2 (Golgi SNAP receptor2	KK109404	**Notches**	**Mild effect**	
nSyb	R	v	Vamp2, neuronal SNARE	BL31983	n.a.		
Sec20	Qb	t	BNIP1, SEC20	KK100264	**Notches**	**No effect**	
Sec22	R	v	Sec22b	BL34893	**Notches**	**Mild effect**	Li, BBRC 2015
SNAP24	Qbc	t	SNAP25	KK108209	**Notches**	**No effect**	
SNAP25	Qbc	t	no homologue	TRiP27306, 3437	No phenotype		
SNAP29	Qbc	t	SNAP29	KK107947	No phenotype		
Syb	R	v	Vamp1	KK102922	**Notches**	**Wg intracellular accu**	Yamazaki, NCB 2016
Syx1a	Qa	t	STX1A	GD33112	**Notches**	**Lethal**	
Syx4	Qa	t	no homologue	n.a.	n.a.		
Syx5	Qa	t	STX5	KK108928	**Notches**	**Lethal**	
Syx6	Qc	t	STX6	KK104795	**Notches**	**No effect**	
syx7/avl	Qa	t	STX7	KK107264	**Lethal**	**Lethal**	
Syx8	Qc	t	STX8	KK107014	**Notches**	**Mild effect**	
Syx13	Qa	t	TSNARE1	KK102432	**Notches**	**No effect**	
Syx16	Qa	t	STX16	KK109504	No phenotype		
Syx17	Qa	t	STX17	KK108825	No phenotype		
Syx18	Qa	t	STX18	KK105113	**Notches**	**Lethal**	
Use1	Qc	v	USE1	KK100019	**Notches**	**Wg intracellular accumulation**	
Vamp7	R	v	VAMP7	KK108733	No phenotype		Gao, Plos One 2017
Vti1a	Qb	t	VTI1A	KK109819,	**Notches**	**Wg reduction**	
Vti1b	Qb	t	no homologue	n.a.	n.a.		
Ykt6	R	v	YKT6	KK1515	**Notches**	**Lethal**	Gross, NCB, 2012

Supplementary Table 2:
Proteins identified by mass spectrometry from BioID control and Ykt6-WT samples in two biological replicates, replicate_1 by SWATH-MS analysis, replicate_2 by Spectral Counting analysis (for experimental details see Material and Methods section)

Linnemannstoens_mass spec replicate 1

#	Identified Proteins (4113)	Accession Number	Fisher's Exact Test (p-value): *(p < 0,00151)	Bio		Ykt6-WT		Indicative ratio
19	DNA replication licensing factor MCM4 OS=Homo sapiens GN=MCM4 PE=1 SV=5	MCM4_HUMAN	< 0,00010	3		55		18,33
2	Synaptobrevin homolog YKT6 OS=Homo sapiens GN=YKT6 PE=1 SV=1	YKT6_HUMAN	< 0,00010	10		160		16,00
27	Splicing factor 3A subunit 1 OS=Homo sapiens GN=SF3A1 PE=1 SV=1	SF3A1_HUMAN	< 0,00010	3		48		16,00
29	5'-3' exoribonuclease 2 OS=Homo sapiens GN=XRN2 PE=1 SV=1	XRN2_HUMAN	< 0,00010	3		40		13,33
26	Cluster of AP-1 complex subunit beta-1 OS=Homo sapiens GN=AP1B1 PE=1 SV=2 (AP1B1_HUMAN)	AP1B1_HUMAN	< 0,00010	4		53		13,25
43	Lon protease homolog, mitochondrial OS=Homo sapiens GN=LONP1 PE=1 SV=2	LONM_HUMAN	< 0,00010	3		33		11,00
44	AP-2 complex subunit alpha-1 OS=Homo sapiens GN=AP2A1 PE=1 SV=3	AP2A1_HUMAN	< 0,00010	3		33		11,00
46	Cluster of Hexokinase-1 OS=Homo sapiens GN=HK1 PE=1 SV=3 (HXK1_HUMAN)	HXK1_HUMAN	< 0,00010	3		32		10,67
49	Cluster of Dynamin-2 OS=Homo sapiens GN=DNM2 PE=1 SV=2 (DYN2_HUMAN)	DYN2_HUMAN	< 0,00010	3		30		10,00
50	DNA mismatch repair protein Msh2 OS=Homo sapiens GN=MSH2 PE=1 SV=1	MSH2_HUMAN	< 0,00010	3		30		10,00
52	Isoleucine--tRNA ligase, mitochondrial OS=Homo sapiens GN=IARS2 PE=1 SV=2	SYIM_HUMAN	< 0,00010	3		29		9,67
38	Ubiquitin carboxyl-terminal hydrolase 5 OS=Homo sapiens GN=USP5 PE=1 SV=2	UBP5_HUMAN	< 0,00010	4		38		9,50
55	Insulin-degrading enzyme OS=Homo sapiens GN=IDE PE=1 SV=4	IDE_HUMAN	< 0,00010	3		28		9,33
8	Neutral alpha-glucosidase AB OS=Homo sapiens GN=GANAB PE=1 SV=3	GANAB_HUMAN	< 0,00010	13		116		8,92
60	RNA-binding protein 12 OS=Homo sapiens GN=RBM12 PE=1 SV=1	RBM12_HUMAN	< 0,00010	3		26		8,67
10	Alanine--tRNA ligase, cytoplasmic OS=Homo sapiens GN=AARS PE=1 SV=2	SYAC_HUMAN	< 0,00010	12		100		8,33
64	ATP-binding cassette sub-family F member 1 OS=Homo sapiens GN=ABCF1 PE=1 SV=2	ABCF1_HUMAN	< 0,00010	3		25		8,33
65	Lymphoid-specific helicase OS=Homo sapiens GN=HELLS PE=1 SV=1	HELLS_HUMAN	< 0,00010	3		25		8,33
66	ATP-dependent RNA helicase DHX36 OS=Homo sapiens GN=DHX36 PE=1 SV=2	DHX36_HUMAN	< 0,00010	3		25		8,33
67	AP-2 complex subunit alpha-2 OS=Homo sapiens GN=AP2A2 PE=1 SV=2	AP2A2_HUMAN	< 0,00010	3		25		8,33
13	Eukaryotic translation initiation factor 3 subunit B OS=Homo sapiens GN=EIF3B PE=1 SV=3	EIF3B_HUMAN	< 0,00010	11		90		8,18
40	Double-stranded RNA-specific adenosine deaminase OS=Homo sapiens GN=ADAR PE=1 SV=4	DSRAD_HUMAN	< 0,00010	5		39		7,80
71	Monofunctional C1-tetrahydrofolate synthase, mitochondrial OS=Homo sapiens GN=MTHFD1L PE=1 SV=1	C1TM_HUMAN	< 0,00010	3		23		7,67
83	Pre-mRNA-processing factor 6 OS=Homo sapiens GN=PRPF6 PE=1 SV=1	PRP6_HUMAN	< 0,00010	3		21		7,00
90	Pre-mRNA-processing factor 40 homolog A OS=Homo sapiens GN=PRPF40A PE=1 SV=2	PR40A_HUMAN	0,00015	3		19		6,33

91	Heterogeneous nuclear ribonucleoprotein U-like protein 2 OS=Homo sapiens GN=HNRNPUL2 PE=1 SV=1	HNRL2_HUMAN	0,00015	3		19		6,33
78	HIV Tat-specific factor 1 OS=Homo sapiens GN=HTATSF1 PE=1 SV=1	HTSF1_HUMAN	< 0,00010	4		24		6,00
97	ER membrane protein complex subunit 1 OS=Homo sapiens GN=EMC1 PE=1 SV=1	EMC1_HUMAN	0,00029	3		18		6,00
98	Putative helicase MOV-10 OS=Homo sapiens GN=MOV10 PE=1 SV=2	MOV10_HUMAN	0,00029	3		18		6,00
33	Eukaryotic translation initiation factor 3 subunit C OS=Homo sapiens GN=EIF3C PE=1 SV=1	EIF3C_HUMAN	< 0,00010	9		53		5,89
23	Cluster of Kinesin-1 heavy chain OS=Homo sapiens GN=KIF5B PE=1 SV=1 (KINH_HUMAN)	KINH_HUMAN	< 0,00010	13		76		5,85
7	Heat shock 70 kDa protein 4 OS=Homo sapiens GN=HSPA4 PE=1 SV=4	HSP74_HUMAN	< 0,00010	26		150		5,77
100	RNA-binding protein 25 OS=Homo sapiens GN=RBM25 PE=1 SV=3	RBM25_HUMAN	0,00053	3		17		5,67
106	Exosome component 10 OS=Homo sapiens GN=EXOSC10 PE=1 SV=2	EXOSX_HUMAN	0,00096	3		16		5,33
107	Cluster of 2-oxoglutarate dehydrogenase, mitochondrial OS=Homo sapiens GN=OGDH PE=1 SV=3 (ODO1_HUMAN)	ODO1_HUMAN	0,00096	3		16		5,33
21	Cluster of Alpha-actinin-4 OS=Homo sapiens GN=ACTN4 PE=1 SV=2 (ACTN4_HUMAN)	ACTN4_HUMAN	< 0,00010	17		85		5,00
39	26S proteasome non-ATPase regulatory subunit 1 OS=Homo sapiens GN=PSMD1 PE=1 SV=2	PSMD1_HUMAN	< 0,00010	10		50		5,00
61	Serrate RNA effector molecule homolog OS=Homo sapiens GN=SRRT PE=1 SV=1	SRRT_HUMAN	< 0,00010	8		36		4,50
82	NAD(P) transhydrogenase, mitochondrial OS=Homo sapiens GN=NNT PE=1 SV=3	NNTM_HUMAN	< 0,00010	6		27		4,50
20	Heat shock protein 105 kDa OS=Homo sapiens GN=HSPH1 PE=1 SV=1	HS105_HUMAN	< 0,00010	22		96		4,36
36	Exportin-2 OS=Homo sapiens GN=CSE1L PE=1 SV=3	XPO2_HUMAN	< 0,00010	15		62		4,13
37	Matrin-3 OS=Homo sapiens GN=MATR3 PE=1 SV=2	MATR3_HUMAN	< 0,00010	18		66		3,67
42	Exosome complex exonuclease RRP44 OS=Homo sapiens GN=DIS3 PE=1 SV=2	RRP44_HUMAN	< 0,00010	17		62		3,65
32	Coatomer subunit beta OS=Homo sapiens GN=COPB1 PE=1 SV=3	COPB_HUMAN	< 0,00010	23		79		3,43
28	Puromycin-sensitive aminopeptidase OS=Homo sapiens GN=NPEPPS PE=1 SV=2	PSA_HUMAN	< 0,00010	26		88		3,38
17	C-1-tetrahydrofolate synthase, cytoplasmic OS=Homo sapiens GN=MTHFD1 PE=1 SV=3	C1TC_HUMAN	< 0,00010	40		131		3,28
99	Exportin-T OS=Homo sapiens GN=XPOT PE=1 SV=2	XPOT_HUMAN	0,00045	8		26		3,25
79	Cluster of N-alpha-acetyltransferase 15, NatA auxiliary subunit OS=Homo sapiens GN=NAA15 PE=1 SV=1 (NAA15_HUMAN)	NAA15_HUMAN	< 0,00010	12		38		3,17
47	Methionine--tRNA ligase, cytoplasmic OS=Homo sapiens GN=MARS PE=1 SV=2	SYMC_HUMAN	< 0,00010	24		71		2,96
73	Programmed cell death 6-interacting protein OS=Homo sapiens GN=PDCD6IP PE=1 SV=1	PDC6I_HUMAN	< 0,00010	21		53		2,52
41	Staphylococcal nuclease domain-containing protein 1 OS=Homo sapiens GN=SND1 PE=1 SV=1	SND1_HUMAN	< 0,00010	38		95		2,50
81	Importin-5 OS=Homo sapiens GN=IPO5 PE=1 SV=4	IPO5_HUMAN	< 0,00010	23		54		2,35
88	Exportin-1 OS=Homo sapiens GN=XPO1 PE=1 SV=1	XPO1_HUMAN	0,00014	34		65		1,91
101	K1C9_HUMAN-DECOY	K1C9_HUMAN	0,00061	45		74		1,64
87	Trifunctional purine biosynthetic protein adenosine-3 OS=Homo sapiens GN=GART PE=1 SV=1	PUR2_HUMAN	0,00012	68		107		1,57
105	ATP-citrate synthase OS=Homo sapiens GN=ACLY PE=1 SV=3	ACLY_HUMAN	0,00092	119		155		1,30

nemannstoens_mass spec replicate 2

#	Identified Proteins (5471)	Accession Number	ANOVA Test (P-Value): *(p <= 0.00318	Bio-1	Bio-2	Ykt6-WT-1	Ykt6-WT-2	ctrlvs WT
79	Synaptobrevin homolog YKT6 OS=Homo sapiens GN=YKT6 PE=1 SV=1	YKT6_HUMAN	< 0.00010	11	15	386	385	29,7
1890	Protein farnesyltransferase subunit beta OS=Homo sapiens GN=FNTB PE=1 SV=1	FNTB_HUMAN	0.00017	1	1	22	22	22,0
2838	Thioredoxin domain-containing protein 17 OS=Homo sapiens GN=TXNDC17 PE=1 SV=1	TXD17_HUMAN	0.0025	0	1	4	3	7,0
2324	Deubiquitinating protein VCIP135 OS=Homo sapiens GN=VCPIP1 PE=1 SV=2	VCIP1_HUMAN	< 0.00010	1	1	7	6	6,5
2289	Ubiquitin carboxyl-terminal hydrolase 15 OS=Homo sapiens GN=USP15 PE=1 SV=3	UBP15_HUMAN	0.0026	1	2	9	10	6,3
2294	Acetyl-CoA carboxylase 2 OS=Homo sapiens GN=ACACB PE=1 SV=3	ACACB_HUMAN	< 0.00010	18	17	104	105	6,0
19	Acetyl-CoA carboxylase 1 OS=Homo sapiens GN=ACACA PE=1 SV=2	ACACA_HUMAN	< 0.00010	119	121	716	649	5,7
636	Protein farnesyltransferase/geranylgeranyltransferase type-1 subunit alpha OS=Homo sapiens GN=FNTA PE=1 SV=1	FNTA_HUMAN	0.00016	8	10	54	46	5,6
2542	Gamma-tubulin complex component 3 OS=Homo sapiens GN=TUBGCP3 PE=1 SV=2	GCP3_HUMAN	0.0028	1	1	5	6	5,5
2243	Lys-63-specific deubiquitinase BRCC36 OS=Homo sapiens GN=BRCC3 PE=1 SV=2	BRCC3_HUMAN	< 0.00010	1	3	10	9	4,8
2405	Regulatory-associated protein of mTOR OS=Homo sapiens GN=RPTOR PE=1 SV=1	RPTOR_HUMAN	0.0011	2	1	7	7	4,7
3041	Perilipin-2 OS=Homo sapiens GN=PLIN2 PE=1 SV=2	PLIN2_HUMAN	0.00087	0	1	2	2	4,0
1687	Aspartyl aminopeptidase OS=Homo sapiens GN=DNPEP PE=1 SV=1	DNPEP_HUMAN	0.00039	2	2	6	8	3,5
1980	ATPase WRNIP1 OS=Homo sapiens GN=WRNIP1 PE=1 SV=2	WRIP1_HUMAN	< 0.00010	4	4	11	12	2,9
2309	Striatin OS=Homo sapiens GN=STRN PE=1 SV=4	STRN_HUMAN	0.00017	3	4	10	10	2,9
2321	Striatin-3 OS=Homo sapiens GN=STRN3 PE=1 SV=3	STRN3_HUMAN	0.0021	5	4	12	13	2,8
1307	AMP deaminase 2 OS=Homo sapiens GN=AMPD2 PE=1 SV=2	AMPD2_HUMAN	0.00054	3	4	9	10	2,7
2449	DNA-directed RNA polymerase III subunit RPC5 OS=Homo sapiens GN=POLR3E PE=1 SV=1	RPC5_HUMAN	< 0.00010	0	3	4	4	2,7
977	Serine/threonine-protein kinase Nek9 OS=Homo sapiens GN=NEK9 PE=1 SV=2	NEK9_HUMAN	0.00011	9	9	24	22	2,6
2929	Exonuclease 3'-5' domain-containing protein 2 OS=Homo sapiens GN=EXD2 PE=1 SV=2	EXD2_HUMAN	< 0.00010	1	1	3	2	2,5
2200	CDGSH iron-sulfur domain-containing protein 2 OS=Homo sapiens GN=CISD2 PE=1 SV=1	CISD2_HUMAN	0.0023	2	2	5	5	2,5
965	Tripeptidyl-peptidase 2 OS=Homo sapiens GN=TPP2 PE=1 SV=4	TPP2_HUMAN	0.0024	7	11	25	20	2,5
198	Fatty acid synthase OS=Homo sapiens GN=FASN PE=1 SV=3	FAS_HUMAN	0.0012	47	43	113	105	2,4
1826	LisH domain and HEAT repeat-containing protein KIAA1468 OS=Homo sapiens GN=KIAA1468 PE=1 SV=2	K1468_HUMAN	0.0014	4	4	10	9	2,4
893	Filamin-A OS=Homo sapiens GN=FLNA PE=1 SV=4	FLNA_HUMAN	0.0012	16	23	44	45	2,3
1003	Exportin-7 OS=Homo sapiens GN=XPO7 PE=1 SV=3	XPO7_HUMAN	0.00014	10	11	26	20	2,2
1857	TATA box-binding protein-like protein 1 OS=Homo sapiens GN=TBPL1 PE=1 SV=1	TBPL1_HUMAN	0.00087	6	7	14	14	2,2
1714	Bifunctional UDP-N-acetylglucosamine 2-epimerase/N-acetylmannosamine kinase OS=Homo sapiens GN=GNE PE=1 SV=1	GLCNE_HUMAN	0.0024	7	6	13	15	2,2
1020	Actin-related protein 2/3 complex subunit 1A OS=Homo sapiens GN=ARPC1A PE=1 SV=2	ARC1A_HUMAN	0.0013	10	9	22	18	2,1
1051	Tubulin gamma-1 chain OS=Homo sapiens GN=TUBG1 PE=1 SV=2	TBG1_HUMAN	0.0026	11	10	21	23	2,1

1086	Cluster of Poly(A) polymerase alpha OS=Homo sapiens GN=PAPOLA PE=1 SV=4 (PAPOA_HUMAN)	PAPOA_HUMAN	0.00039	13	12	23	29	2,1
1276	Microtubule-associated protein 1B OS=Homo sapiens GN=MAP1B PE=1 SV=2	MAP1B_HUMAN	0.00075	9	11	20	21	2,1
2543	N6-adenosine-methyltransferase 70 kDa subunit OS=Homo sapiens GN=METTL3 PE=1 SV=2	MTA70_HUMAN	< 0.00010	3	4	7	7	2,0
2920	AP-2 complex subunit sigma OS=Homo sapiens GN=AP2S1 PE=1 SV=2	AP2S1_HUMAN	0.00025	1	0	1	1	2,0
1139	E3 ubiquitin-protein ligase HUWE1 OS=Homo sapiens GN=HUWE1 PE=1 SV=3	HUWE1_HUMAN	0.0012	3	1	5	3	2,0
1825	Core histone macro-H2A.1 OS=Homo sapiens GN=H2AFY PE=1 SV=4	H2AY_HUMAN	0.0013	11	10	23	19	2,0
1577	Inhibitor of nuclear factor kappa-B kinase subunit alpha OS=Homo sapiens GN=CHUK PE=1 SV=2	IKKA_HUMAN	0.0019	6	6	11	13	2,0
329	Aminoacyl tRNA synthase complex-interacting multifunctional protein 2 OS=Homo sapiens GN=AIMP2 PE=1 SV=2	AIMP2_HUMAN	0.00018	28	36	64	56	1,9
904	28S ribosomal protein S5, mitochondrial OS=Homo sapiens GN=MRPS5 PE=1 SV=2	RT05_HUMAN	0.0019	10	13	22	21	1,9
781	Cluster of Coronin-1C OS=Homo sapiens GN=CORO1C PE=1 SV=1 (COR1C_HUMAN)	COR1C_HUMAN	0.0008	22	19	37	39	1,9
1315	E3 ubiquitin/ISG15 ligase TRIM25 OS=Homo sapiens GN=TRIM25 PE=1 SV=2	TRI25_HUMAN	0.00034	11	12	19	23	1,8
1296	Putative helicase MOV-10 OS=Homo sapiens GN=MOV10 PE=1 SV=2	MOV10_HUMAN	< 0.00010	10	9	18	16	1,8
669	ATP-binding cassette sub-family F member 1 OS=Homo sapiens GN=ABCF1 PE=1 SV=2	ABCF1_HUMAN	0.0018	25	24	45	42	1,8
444	60S ribosomal protein L24 OS=Homo sapiens GN=RPL24 PE=1 SV=1	RL24_HUMAN	0.00023	20	19	34	34	1,7
1829	Ribonuclease P protein subunit p38 OS=Homo sapiens GN=RPP38 PE=1 SV=2	RPP38_HUMAN	0.00011	7	8	12	12	1,6
1063	Cyclin-dependent-like kinase 5 OS=Homo sapiens GN=CDK5 PE=1 SV=3	CDK5_HUMAN	0.0027	7	5	9	10	1,6
340	Gem-associated protein 5 OS=Homo sapiens GN=GEMIN5 PE=1 SV=3	GEMI5_HUMAN	< 0.00010	40	48	73	66	1,6
1685	Charged multivesicular body protein 2b OS=Homo sapiens GN=CHMP2B PE=1 SV=1	CHM2B_HUMAN	0.0016	5	2	5	6	1,6
572	Eukaryotic translation initiation factor 3 subunit D OS=Homo sapiens GN=EIF3D PE=1 SV=1	EIF3D_HUMAN	0.00028	29	30	45	47	1,6
341	Coatomer subunit beta' OS=Homo sapiens GN=COPB2 PE=1 SV=2	COPB2_HUMAN	0.001	40	40	60	64	1,6
1531	Cluster of 5'-AMP-activated protein kinase subunit gamma-1 OS=Homo sapiens GN=PRKAG1 PE=1 SV=1 (AAKG1_HUMAN)	AAKG1_HUMAN	0.0018	12	10	17	17	1,5
1597	28S ribosomal protein S26, mitochondrial OS=Homo sapiens GN=MRPS26 PE=1 SV=1	RT26_HUMAN	0.0024	7	4	8	9	1,5
1805	Twinfilin-1 OS=Homo sapiens GN=TWF1 PE=1 SV=3	TWF1_HUMAN	0.00062	7	8	12	11	1,5
1643	Syntaxin-binding protein 3 OS=Homo sapiens GN=STXBP3 PE=1 SV=2	STXB3_HUMAN	0.0019	2	4	4	5	1,5
939	Cluster of AP-1 complex subunit mu-1 OS=Homo sapiens GN=AP1M1 PE=1 SV=3 (AP1M1_HUMAN)	AP1M1_HUMAN	0.0026	17	17	23	28	1,5
1403	Eukaryotic translation initiation factor 2A OS=Homo sapiens GN=EIF2A PE=1 SV=3	EIF2A_HUMAN	< 0.00010	11	12	15	19	1,5
221	26S protease regulatory subunit 6A OS=Homo sapiens GN=PSMC3 PE=1 SV=3	PRS6A_HUMAN	0.002	58	59	88	84	1,5
441	40S ribosomal protein S8 OS=Homo sapiens GN=RPS8 PE=1 SV=2	RS8_HUMAN	0.0017	40	40	61	55	1,5

1107	Cluster of Serine/threonine-protein phosphatase 2A 55 kDa regulatory subunit B alpha isoform OS=Homo sapiens GN=PPP2R2A PE=1 SV=1 (2ABA_HUMAN)	2ABA_HUMAN	0.0012	9	9	13	13	1,4
4	Pyruvate carboxylase, mitochondrial OS=Homo sapiens GN=PC PE=1 SV=2	PYC_HUMAN	0.00021	459	457	695	626	1,4
346	BTB/POZ domain-containing protein KCTD12 OS=Homo sapiens GN=KCTD12 PE=1 SV=1	KCD12_HUMAN	0.00011	47	59	80	72	1,4
2683	FAD-dependent oxidoreductase domain-containing protein 1 OS=Homo sapiens GN=FOXRED1 PE=1 SV=2	FXRD1_HUMAN	0.00085	3	4	6	4	1,4
803	ATP-dependent DNA helicase Q1 OS=Homo sapiens GN=RECQL PE=1 SV=3	RECQ1_HUMAN	0.0021	20	18	26	28	1,4
239	Glutamine--tRNA ligase OS=Homo sapiens GN=QARS PE=1 SV=1	SYQ_HUMAN	0.00031	61	66	92	88	1,4
1495	Cluster of 60S ribosomal protein L37a OS=Homo sapiens GN=RPL37A PE=1 SV=2 (RL37A_HUMAN)	RL37A_HUMAN	0.0028	5	5	8	6	1,4
135	Arginine--tRNA ligase, cytoplasmic OS=Homo sapiens GN=RARS PE=1 SV=2	SYRC_HUMAN	0.002	88	89	112	135	1,4
579	Elongator complex protein 1 OS=Homo sapiens GN=IKBKAP PE=1 SV=3	ELP1_HUMAN	0.0029	25	31	42	36	1,4
350	Exportin-T OS=Homo sapiens GN=XPOT PE=1 SV=2	XPOT_HUMAN	0.0005	44	43	57	63	1,4
1230	Sorting nexin-1 OS=Homo sapiens GN=SNX1 PE=1 SV=3	SNX1_HUMAN	0.0024	26	20	31	32	1,4
212	40S ribosomal protein S9 OS=Homo sapiens GN=RPS9 PE=1 SV=3	RS9_HUMAN	0.0012	26	26	34	37	1,4
277	60S ribosomal protein L13 OS=Homo sapiens GN=RPL13 PE=1 SV=4	RL13_HUMAN	0.0015	47	55	68	71	1,4
1318	Spectrin alpha chain, non-erythrocytic 1 OS=Homo sapiens GN=SPTAN1 PE=1 SV=3	SPTN1_HUMAN	0.0028	11	17	22	16	1,4
16	Propionyl-CoA carboxylase alpha chain, mitochondrial OS=Homo sapiens GN=PCCA PE=1 SV=4	PCCA_HUMAN	< 0.00010	444	455	603	614	1,4
3767	Molybdopterin synthase catalytic subunit OS=Homo sapiens GN=MOCS2 PE=1 SV=1	MOC2B_HUMAN	0.0014	2	1	2	2	1,3
1065	Kinesin light chain 1 OS=Homo sapiens GN=KLC1 PE=1 SV=2	KLC1_HUMAN	0.0029	30	27	40	36	1,3
396	Proteasome subunit beta type-3 OS=Homo sapiens GN=PSMB3 PE=1 SV=2	PSB3_HUMAN	0.0029	43	33	52	48	1,3
626	40S ribosomal protein S13 OS=Homo sapiens GN=RPS13 PE=1 SV=2	RS13_HUMAN	0.0013	20	19	26	25	1,3
709	28S ribosomal protein S22, mitochondrial OS=Homo sapiens GN=MRPS22 PE=1 SV=1	RT22_HUMAN	0.0027	24	22	31	29	1,3
18	Propionyl-CoA carboxylase beta chain, mitochondrial OS=Homo sapiens GN=PCCB PE=1 SV=3	PCCB_HUMAN	0.0029	417	436	567	545	1,3
327	Heat shock 70 kDa protein 4L OS=Homo sapiens GN=HSPA4L PE=1 SV=3	HS74L_HUMAN	0.0012	70	69	91	90	1,3
2177	Phosphomannomutase 2 OS=Homo sapiens GN=PMM2 PE=1 SV=1	PMM2_HUMAN	0.0021	5	5	6	7	1,3
45	T-complex protein 1 subunit gamma OS=Homo sapiens GN=CCT3 PE=1 SV=4	TCPG_HUMAN	< 0.00010	225	232	297	297	1,3
838	N-alpha-acetyltransferase 25, NatB auxiliary subunit OS=Homo sapiens GN=NAA25 PE=1 SV=1	NAA25_HUMAN	0.00035	16	19	24	21	1,3
141	Structural maintenance of chromosomes protein 4 OS=Homo sapiens GN=SMC4 PE=1 SV=2	SMC4_HUMAN	0.0017	67	82	100	89	1,3
705	Cluster of DNA topoisomerase 1 OS=Homo sapiens GN=TOP1 PE=1 SV=2 (TOP1_HUMAN)	TOP1_HUMAN	0.0027	14	17	18	21	1,3
2541	Peptidyl-prolyl cis-trans isomerase FKBP8 OS=Homo sapiens GN=FKBP8 PE=1 SV=2	FKBP8_HUMAN	0.00073	3	1	4	1	1,3
3059	LanC-like protein 2 OS=Homo sapiens GN=LANCL2 PE=1 SV=1	LANC2_HUMAN	0.0029	3	1	3	2	1,3

3.2 Manuscript II: Phosphorylation of Ykt6 SNARE domain regulates its membrane recruitment and activity

Citation:

Pradhipa Karuna M [1,2], Leonie Witte [1,2], Karen Linnemannstoens[1,2], Dolma Choezom[1,2], Adi Danieli-Mackay[1,2], Mona Honemann-Capito[1,2], and Julia Christina Gross [1,2,3,*]

Biomolecules 2020, *10*(11), 1560; https://doi.org/10.3390/biom10111560

https://www.mdpi.com/2218-273X/10/11/1560

Individual contributions to published article:
Applicant name: Pradhipa Karuna M (first author)

1. **Main and Supplementary Figures/Tables** (actively performed experiments and/or analyzed data)

   Main: 3C, 3D, 3E, 4A, 4B, 4C, 4D, 4E, 4F, 4G, 4H, 5J, 5K
   Supplementary: Table 2, Table 3

2. **Writing and Intellectual Contributions**

   - Contributed to writing significant parts of the manuscript such as introduction, results, discussion, materials and methods in association with Prof. Dr. Julia Gross
   - Contributed to figure arrangement and figure legends of all the figures.
   - Contributed to revision experiments, experimental design, mass spectrometry data analysis and proof-reading of the manuscript.

biomolecules

MDPI

Article

Phosphorylation of Ykt6 SNARE Domain Regulates Its Membrane Recruitment and Activity

Pradhipa Karuna M [1,2], Leonie Witte [1,2], Karen Linnemannstoens [1,2], Dolma Choezom [1,2], Adi Danieli-Mackay [1,2], Mona Honemann-Capito [1,2] and Julia Christina Gross [1,2,3,*]

1 Hematology and Oncology, University Medical Center Goettingen, 37077 Goettingen, Germany; pradhipa.karuna-m@med.uni-goettingen.de (P.K.M.); leonie.witte@med.uni-goettingen.de (L.W.); Karen.Linnemannstoens@zentr.uni-goettingen.de (K.L.); dolma.choezom@med.uni-goettingen.de (D.C.); adi.danieli@stud.uni-goettingen.de (A.D.-M.); mhonema@gwdg.de (M.H.-C.)
2 Developmental Biochemistry, University Medical Center Goettingen, 37077 Goettingen, Germany
3 HMU Health and Medical University Potsdam, 14471 Potsdam, Germany
* Correspondence: julia.gross@med.uni-goettingen.de

Received: 16 October 2020; Accepted: 11 November 2020; Published: 16 November 2020

Abstract: Sensitive factor attachment protein receptors (SNARE) proteins are important mediators of protein trafficking that regulate the membrane fusion of specific vesicle populations and their target organelles. The SNARE protein Ykt6 lacks a transmembrane domain and attaches to different organelle membranes. Mechanistically, Ykt6 activity is thought to be regulated by a conformational change from a closed cytosolic form to an open membrane-bound form, yet the mechanism that regulates this transition is unknown. We identified phosphorylation sites in the SNARE domain of Ykt6 that mediate Ykt6 membrane recruitment and are essential for cellular growth. Using proximity-dependent labeling and membrane fractionation, we found that phosphorylation regulates Ykt6 conversion from a closed to an open conformation. This conformational switch recruits Ykt6 to several organelle membranes, where it functionally regulates the trafficking of Wnt proteins and extracellular vesicle secretion in a concentration-dependent manner. We propose that phosphorylation of its SNARE domain leads to a conformational switch from a cytosolic, auto-inhibited Ykt6 to an active SNARE at different membranes.

Keywords: Ykt6 conformational switch; membrane attachment; protein trafficking; secretory pathway

1. Introduction

N-ethylmaleimide-sensitive factor attachment protein receptors (SNARE) family members drive membrane fusion by the formation of a trans-SNARE complex consisting of specific v- and t-SNAREs present at vesicle (v) and target (t) membranes. Most SNAREs have autonomously folding N-terminal domains, along with SNARE (coiled-coil) motifs and membrane anchors. The SNARE motifs are 60–70 amino acid residues long [1] and contain repeated heptad patterns of hydrophobic residues. They assemble into parallel four-helix bundles stabilized by a hydrophobic helix that faces the bundle's core. Within the hydrophobic core of the bundle X-ray crystallography [2,3] revealed an unusual central hydrophilic layer composed of three glutamines (Q) and one arginine (R) residue, which led to the classification of Q- and R-SNAREs, respectively [4].

Ykt6 is an unusual SNARE as it lacks a transmembrane domain and therefore can cycle between cytosol and membranes. Membrane localization depends on the intramolecular interaction of the N-terminal Longin and C-terminal SNARE domains and the presence of a farnesylation and reversible palmitoylation within a CCAIM/CAAX motif at the C-terminus [5]. This interaction is exemplified in yeast, where the release of Ykt6 from endosomal membranes into the cytoplasm depends on a

functional Longin domain and an intramolecular interaction with its SNARE domain to fold into a soluble, closed conformation [6]. Additionally, a recent study identified a new geranylgeranyl transferase that plays an essential role for membrane-anchored Ykt6 in proper Golgi function [7].

Albeit sometimes redundant, specific sets of SNAREs mediate distinct steps in intracellular protein trafficking [8]. Correspondingly, Ykt6 interacts with different SNARE partners in vitro [9] and is proposed to function as a membrane stress sensor within the secretory pathway of yeast [10]. In addition to its functions in the homotypic fusion of Endoplasmic Reticulum (ER) and vacuolar membranes [11,12], ER-Golgi trafficking [13] and retrograde Golgi trafficking in yeast [14–16], it was also described to function in in autophagy [16] and lysosomal stress [17]. Recent studies revealed that Ykt6 mediates several steps of autophagosome formation in human cells [18], the *Drosophila* fat body [19], and yeast [15,20]. Nevertheless, how Ykt6 is recruited to these different membranes remains unclear. Here, we investigate how the functional regulation of the SNARE domain can mechanistically regulate Ykt6 membrane recruitment and activity in mammalian cells and in *Drosophila*.

2. Material and Methods

The *Drosophila* Ykt6 coding region was amplified and the PCR product was recombined into the pDONR^{TM}221 vector using the Gateway BP Clonase II Enzyme mix (Life Technologies, Carlsbad, CA, USA). Point mutations of potential phosphorylation sites (S175, S182, T188, T192) were introduced by site-directed mutagenesis. For the generation of transgenic flies, constructs were subcloned into expression vectors pUASt-attB-rfA-mCherry and pUASt-attB-mCherry-rfA (kind gift from Sven Bogdan) by LR recombination (Life Technologies, Carlsbad, CA, USA). Human Ykt6 was amplified from hYkt6-Myc (C-Terminal myc-destination plasmids (DKFZ—Genomics and Proteomics Core Facility)) and the PCR product was inserted into pcDNA3.1MycBioID (Addgene #35700). Point mutations for Ykt6-3A (S174A, T181A, S187A), Ykt6-3E (S174E, T187E, S181E), F42A, C194A, C195A, and relevant combinations were introduced by site-directed mutagenesis. MycBioID tag was removed via Nhe1/Xho1 to obtain untagged constructs in pcDNA3.1. RUSH-EGFP-Wnt3A was constructed by amplifying the core protein sequence of Wnt3A and integrating it by Gibson cloning [21] with the Wnt3A signal peptide and the streptavidin-binding peptide sequence into the ER-hook containing the pCMV-KDEL-IVS-IRES-reporter plasmid backbone [22]. The following expression constructs were used: pCMV-Wnt3A [23], DsRed-Rab5-QL (E. De Robertis, Addgene #29688) (Table 1)

Table 1. Dharmacon siRNA SMARTpools.

Gene Symbol	GENE ID	Gene Accession	GI Number	Sequence
siGENOME Non-targeting Control_5 #				UGGUUUACAUGUCGACUAA
Ykt6	10652	NM_006555	34304384	GCUCAAAGCCGCAUACGAU GUGAGAAGCUAGAUGACUU GAAGGUACUAGAUGAAUUC
Alix	10015	NM_013374	371875333	GAAGGAUGCUUUCGAUAAA GAACAGAACCUGGAUAAUG GAGAGGGUCUGGAGAAUGA GCAGUGAGGUUGUAAAUGU

represents the non-Targeting siRNA number provided by the company.

2.1. Antibodies

Antibodies were used against Calnexin, 1:1000, (WB, rabbit), Dallas, Texas, US; CD81 1:1000 (1.3.3.22, WB, mouse (DLN-09707), Dianova, Hamburg, Germany; EEA1, 1:300 (IF, mouse (610456), BD, New Jersey, NJ, USA; GAPDH (6C5), 1:5000 [WB; mouse (AM4300)], Ambion, Austin, TX, USA; Hsc70 1:2000 (WB; mouse (sc-7298), Santa Cruz, CA, CA, USA; TSG101, 1:1000, (WB, rabbit (HPA006161), Sigma, MO, USA; Wnt3A, 1:500 (WB, rabbit), Abcam, Cambridge, UK, and Ykt6 WB and IF; mouse (sc-365732), Santa Cruz, CA, USA. Antibodies against Ykt6 were generated by immunizing

two guinea pigs with the peptides KVSADQWPNGTEATI (aa 105–119, within Longin domain) and YQNPVEADPLTKMQN (aa 131–145, covers part of the SNARE domain). Final bleeds were pooled and affinity purified against the original peptides (Eurogentec). Secondary antibodies directed against the species of interest were coupled to Alexa Fluor 488, 568, 594 and 647 IF, 1:500, Invitrogen, Carlsbad, CA, USA and 680RD and 800CW WB, 1:20,000, LiCor, Lincoln, NE, USA.

2.2. Drosophila Stocks and Genetics

The following Drosophila stocks were used in this study: *en-GAL4, UAS-GFP* (chr. II, a gift from J. Grosshans). The following stocks were obtained from the Bloomington Drosophila stock center: *UAS-Dcr; enGAL4, UAS-GFP* (#25752), *tub-GAL80TS* (#7108), and *vas-PhiC31; attP.ZH-86Fb* (#24749). The Ykt6 (KK105648) UAS-RNAi stock was obtained from the Vienna Drosophila RNAi Center. UAS-Ykt6 transgenic lines were generated according to standard protocols by φC31 integrase-mediated site-specific insertion in the attP landing site at ZH-86Fb [24]. Fly stocks were kept on standard medium containing agar, yeast, and corn flour. Crosses were performed at 25 °C or RT.

2.3. Kinase Screen

Biotinylated Ykt6-WT peptide (GEKLDDLVSKSEVLGTQSKAFYKTARKQN) was tested in one concentration against 245 Ser/Thr kinases in a radiometric, FlashPlate PlusTM-based assay. Ten out of 18 kinase hits identified among the 245 kinases were subsequently confirmed in a hit confirmation experiment. For this, three peptide concentrations in triplicate for each of the 10 tested kinase hits were used for N-terminally biotinylated peptides of Ykt6-WT and Ykt6-3E (GEKLDDLVSK**E**EVLGTQ**E**KAFYK**E**ARKQN). The Kinase screen was performed by Reaction Biology, available online: https://www.proqinase.com/products-service-biochemical-assay-services/kinasefinder, received on 15th October 2018).

2.4. Cell Culture and Transfection

Hek293T and HCT116 cells were maintained in DMEM (Gibco) supplemented with 10% fetal calf serum (Biochrom) at 37 °C in a humidified atmosphere with 5% CO_2. Cells were transiently transfected with Screenfect siRNA for siRNA and Screenfect A (Screenfect) for plasmids according to the manufacturer's instructions. Cells were identified and checked regularly for mycoplasma contamination.

2.5. Blue Sepharose Precipitation

The relative amount of Wnts secreted into cell culture supernatant was analyzed using Blue Sepharose precipitation as described [23,25]. Shortly, HEK293T cells were transiently transfected in 6-well plates with 1 µg of Wnt3A plasmids. Then, 72 h after transfection, the supernatant was collected and centrifuged at 4000× *g* rpm to remove cell debris, transferred to a fresh tube, and rotated at 4 °C for 1 h with 1% Triton X-100 and 40 µL of Blue Sepharose beads. The samples were washed and eluted from the beads using 2X SDS buffer with β-mercaptoethanol and analyzed by immunoblotting.

2.6. Extracellular Vesicle purification

Extracellular vesicles were purified by differential centrifugation as described previously [26,27]. In short, supernatants from mammalian cells were subjected to sequential centrifugation steps of 750× *g*, 1.5×10^3 g and 1.4×10^4 g, before pelleting exosomes at 1×10^5 g in a SW41Ti swinging bucket rotor for 2 h (Beckman). The supernatant was discarded, and exosomes were taken up in 1/100 of their original volume in H_2O.

2.7. Immunostainings, Microscopy, and Image Analysis

For immunofluorescence staining, cells were reverse transfected with siRNAs, seeded in 6 well dishes or 8-well microscopic coverslips, 24 h later transfected with indicated plasmids, and 48–72 h

later fixed with 4% paraformaldehyde. Cells were permeabilized with 0.1% Triton X-100 and blocked in 10% BSA/PBS. Primary antibodies in PBS were incubated for 1 h at room temperature and antibody binding was visualized by fluorochrome-conjugated secondary antibodies. Confocal images were processed with Zen lite (Zeiss, Oberkochen, Germany), Fiji/ImageJ (NIH, Rockville, Maryland, MA, USA) [28–30] and Affinity Designer (Affinity Serif, San Francisco, CA, USA).

2.8. Rab5QL Assay and Quantification

Hek293T cells were co-transfected with plasmids for Rab5Q79L-DsRed and either control, Ykt6-WT or Ykt6-3E and analyzed by immunofluorescence microscopy, and the size of enlarged Rab5Q79L-positive endosomes was measured in different biological replicates.

2.9. Membrane Fractionation

As previously described [31], HEK293T cells were seeded and transfected with Ykt6-WT plasmid. Then, 48 h post transfection, cells were lysed on ice with 1 mL of Lysis buffer A (150 mM NaCl, 50 mM HEPES, 0.1% Saponin, 1 M Glycerol, and 1% PIC) and then centrifuged at 2000× *g* for 10 min at 4 °C; then, the supernatant (cytosolic fraction) was transferred to a new tube. The pellet was lysed in 1 mL of Lysis Buffer B (150 mM NaCl, 50 mM Hepes, 1% Igepal, 1 M Glycerol and 1% PIC) and incubated rotating for 30 min at 4 °C. Then, after being centrifuged at 7000× *g* for 10 min at 4 °C, the supernatant was transferred to a new tube (membrane fraction).

2.10. BioID Pull Down and Mass Spectrometry

For large-scale BioID pull down, cells were seeded and 24 h later transfected with BioID-WT or mock constructs. Then, 36 h post transfection, 50 µM biotin was added over night. Cells were washed with PBS twice, cell fractionated, and then boiled 5 min in non-reducing SDS sample buffer (300 mM Tris-HCl pH 6.8, 12% SDS, 0.05% Bromphenolblue, 60% Glycerol, 12 mM EDTA), run a short-distance (1.5 cm) on a 4–12% NuPAGE Novex Bis-Tris Minigel (Invitrogen). Gels were stained with Coomassie Blue for visualization purposes. Full lanes were sliced into 23 equidistant slices regardless of staining, short runs cut out as a whole and diced. After washing, gel slices were reduced with dithiothreitol (DTT), alkylated with 2-iodoacetamide, and digested with trypsin overnight. Then, the resulting peptide mixtures were extracted, dried in a SpeedVac, reconstituted in 2% acetonitrile/0.1% formic acid/(*v*:*v*), and prepared for nanoLC-MS/MS as described previously [32].

For the generation of a peptide library for SWATH-MS, equal amount aliquots from each sample were pooled to a total amount of 80 µg and separated into eight fractions using a reversed phase spin column (Pierce High pH Reversed-Phase Peptide Fractionation Kit, Thermo Fisher Scientific, Waltham, Massachusetts, United States. MS analysis Protein digests were separated by nanoflow chromatography. Then, 25% of gel slices or 1 µg aliquots of digested protein were enriched on a self-packed precolumn (0.15 mm ID × 20 mm, Reprosil-Pur120 C18-AQ 5 µm, Dr. Maisch, Ammerbuch-Entringen, Germany) and separated on an analytical RP-C18 column (0.075 mm ID × 250 mm, Reprosil-Pur 120 C18-AQ, 3 µm, Dr. Maisch) using a 30 to 90 min linear gradient of 5–35% acetonitrile/0.1% formic acid (*v*:*v*) at 300 nl/ min.

SWATH-MS library generation was performed on a hybrid triple quadrupole-TOF mass spectrometer (TripleTOF 5600+) equipped with a Nanospray III ion source (Ionspray Voltage 2400 V, Interface Heater Temperature 150 °C, Sheath Gas Setting 12) and controlled by Analyst TF 1.7.1 software (SCIEX, Framingham, Massachusetts, MA, USA)build 1163 (all AB Sciex), using a Top30 data-dependent acquisition method with an MS survey scan of *m*/*z* 380–1250 accumulated for 250 ms at a resolution of 3.5×10^4 full width at half maximum (FWHM). MS/MS scans of *m*/*z* 180–1500 were accumulated for 100 ms at a resolution of 17,500 FWHM and a precursor isolation width of 0.7 FWHM, resulting in a total cycle time of 3.4 s. Precursors above a threshold MS intensity of 200 cps with charge states 2+, 3+, and 4+ were selected for MS/MS, and the dynamic exclusion time was set to 15 s. MS/MS activation was achieved by CID using nitrogen as a collision gas and the manufacturer's

default rolling collision energy settings. Two technical replicates per reversed phase fraction were analyzed to construct a spectral library.

For quantitative SWATH analysis, MS/MS data were acquired using 100 variable size windows [33] across the 400–1200 *m*/*z* range. Fragments were produced using rolling collision energy settings for charge state 2+, and fragments acquired over an *m*/*z* range of 180–1500 for 40 ms per segment. Including a 250 ms survey scan, this resulted in an overall cycle time of 4.3 s. Two replicate injections were acquired for each biological sample.

2.11. Mass Spectrometry Data Processing

For SWATH-MS analysis, protein identification was achieved using ProteinPilot Software version 5.0 (SCIEX, Framingham, Massachusetts, MA, USA) build 4769 (AB Sciex) at "thorough" settings. MS/MS spectra from the combined qualitative analyses were searched against the UniProtKB Homo sapiens reference proteome (revision February 2017. 92,928 entries) augmented with a set of 51 known common laboratory contaminants to identify 597 proteins at a False Discovery Rate (FDR) of 1%. Spectral library generation and SWATH peak extraction were achieved in PeakView Software version 2.1 (SCIEX, Framingham, Massachusetts, MA, USA) build 11041 (AB Sciex) using the SWATH quantitation microApp version 2.0 SCIEX, Framingham, Massachusetts, MA, USA) build 2003. Following retention time correction on endogenous peptides spanning the entire retention time range, peak areas were extracted using information from the MS/MS library at an FDR of 1% [34]. The 26 resulting peak areas were summed to peptide and protein area values, which were used for further statistical analysis. Reactome Functional Network analysis [35] was performed with Cytoscape [www.cytoscape.org (Accessed on 15th June 2020)] and Kegg pathway analysis was performed with David [36].

2.12. Statistics

All experiments were carried out at least in biological triplicates. Error bars indicate s.d. Statistical significance was calculated by carrying out Student's t-test where appropriate or one-way ANOVA with Dunnett's multiple comparison test to compare a control mean with the other means.

3. Results

3.1. Several Phosphorylation Sites in the Ykt6 SNARE Domain Are Evolutionarily Conserved

Specific phosphorylation sites within the SNARE domain of non-neuronal SNAREs are conserved over the plant, fungi, and animal kingdoms [37]. These sites are located within the SNARE layers and sterically block the interacting domains of the helices. Their importance was demonstrated using the example of the SNARE VAMP8, for which the phosphorylation or mutation of these sites inhibits the fusion of secretory granules [37]. To identify these conserved residues in Ykt6, we aligned its protein sequences deduced from the genomes of *S. cerevisiae*, *C. elegans*, *D. melanogaster,* and vertebrates such as *D. rerio*, *M. musculus*, and *H. sapiens* (Figure 1A). Within the largely hydrophobic SNARE alpha-helix, residues at helical layer positions are designated from 0 to +8 starting from the ionic residue (Arginine or Glutamine) toward the C-Terminus [3]. We found two conserved Serines and a Threonine (S174, S181, and T187 in the human sequence) at layers +3 and +5 and +7, respectively. Furthermore, an additional Threonine (T192) was identified in *Drosophila* at layer +8 (Figure 1A). In confirmation, position S174 was identified in different published phosphoproteomic approaches [38]. Prediction according to NetPhos 3.1 [39] suggested that the identified phosphorylation sites are potential CDK1 and PKC sites (Figure 1B). In light of the identified conserved phosphorylation sites, we decided to study the mechanistic role of possible phosphorylations in human and *Drosophila* Ykt6 in more detail (Figure 1C). To identify potential kinases that phosphorylate these sites, a biotinylated peptide of the human Ykt6 SNARE domain was subjected to a bead-based kinase screen with 245 Serine/Threonine-kinases (Figure 1D). Out of 18 kinases that phosphorylated the peptide more than two-fold over background (Supplementary Table S1), ten were selected (Figure 1E) and subjected to

a validation screen. In comparison to the human Ykt6-WT peptide, a Ykt6 peptide with three sites mutated to Glutamic acid (S174E, S181E, T187E, termed Ykt6-3E) was used to test for the specificity of these three positions. In vitro, phosphoinositide-dependent kinase-1 (PDK1) phosphorylated the Ykt6-WT SNARE domain and did not phosphorylate the Ykt6-3E peptide over the background signal (Figure 1F).

To test the physiological relevance of the identified Ykt6 phosphorylation sites, we expressed Ykt6 RNAi and overexpressed Ykt6 rescue constructs in *Drosophila* with the UAS/GAL4 system [40]. While a strong Ykt6 knockdown by enGAL4-driven UAS-Ykt6 RNAi at 25 °C was lethal at the larval stage, this phenotype was rescued by the overexpression of Ykt6-WT and a non-phosphorylatable Ykt6-4A (S175A, S1812A, T188A, T192A) mutant, but not by the overexpression of a phosphomimicking Ykt6-4E (S175E, S1812E, T188E, T192E) (Table 2, right column). Similarly, a mild enGAL4-driven Ykt6 knockdown at RT showed (1) melanotic tumors in larvae, a sign of increased cell death in combination with phagocytic clearance activity [41], and (2) wing notches in adult flies, typical cell growth, and Wnt signaling defects [42,43] In both cases, Ykt6-WT and -4A expression rescued these phenotypes, but Ykt6-4E did not (Figure 1G, middle column). Taken together, these results indicate that Ykt6 has evolutionarily conserved phosphorylation sites within the SNARE domain, which are important for Ykt6 function in cell growth.

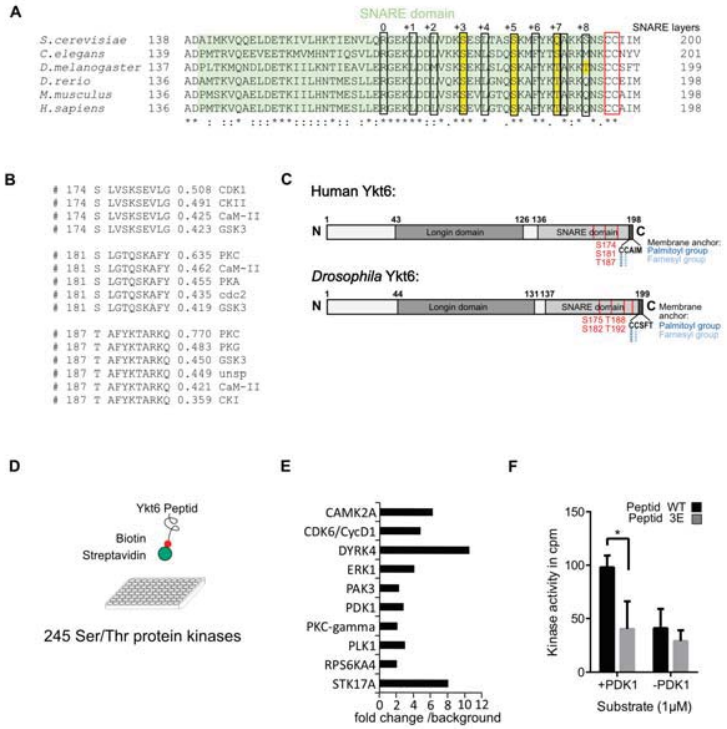

Figure 1. Several phosphorylation sites in the Ykt6 sensitive factor attachment protein receptors (SNARE) domain are evolutionarily conserved. (**A**) Sequence alignment of Ykt6 SNARE domain (Human: position 136–198) of different eukaryotes. Conserved serines and threonines at SNARE layers are marked in yellow, lipid-modified cysteines are in the red box. (**B**) PhosphoSite prediction for human Ykt6 position S174, S181, and T187 using Netphos 3.1 [39]. (**C**) Scheme of human and *Drosophila* Ykt6 with predicted phosphorylation sites that were either mutated to alanine or glutamic acid. (**D**) In vitro kinase assay of biotinylated peptide of the Ykt6-WT SNARE domain with 245 different serine/threonine kinases. (**E**) Ten out of 18 identified kinases phosphorylating Ykt6 SNARE domain >twofold over background were validated. (**F**) A validation kinase assay comparing Ykt6-WT versus Ykt6-3E found phosphoinositide-dependent kinase-1 (PDK1) as a kinase phosphorylating the SNARE domain. * = 0.05.

Table 2. Depletion of Ykt6 by RNAi (engrailed-Gal4, UAS-GFP/ UAS-ykt6 RNAi; larvae reared for three days at RT or 25 °C).

EngrailedGAL4, UAS-GFP>	**Mild Knockdown (RT)**		**Strong Knockdown (25 °C)**	
	Larvae	**Adult**	**Larvae**	**Adult**
ykt6 RNAi	Melanotic tumors	wing defects	lethal *	lethal
ykt6 RNAi; UAS-Ykt6-WT	Normal	viable	normal	viable
ykt6 RNAi; UAS Ykt6-4A	Normal	viable	normal	viable
ykt6 RNAi; UAS-Ykt6-4E	Melanotic tumors	wing defects	lethal	lethal

* Few larvae develop melanotic tumors.

3.2. Phosphomimicking Mutations Accumulate Ykt6 at Membranes in the Secretory Pathway

To investigate the mechanistic relevance of phosphorylation of the Ykt6 SNARE domain, we checked the cellular localization of Ykt6–WT or -3E by immunofluorescence microscopy. Transiently expressed constructs in HCT116 cells showed a diffuse cytoplasmic localization for Ykt6-WT, while Ykt6-3E distinctly localized to the perinuclear area and the plasma membrane (Figure 2A), suggesting a membrane association of Ykt6-3E. Co-staining with the Golgi marker GM130 revealed that Ykt6-3E strongly colocalizes with the Golgi as seen in intensity line profiles (Figure 2B), which is in line with the function of Ykt6 in the organization of Golgi apparatus [7].

Ykt6 was shown previously to be involved in Wnt secretion from *Drosophila* cells of the developing wing epithelium as well as from human cells [23,44]. To understand the dynamics of Ykt6-membrane attachment, we used Wnt3A secretion as a Ykt6-dependent process to study the role of the putative phosphorylation sites. We used "retention using selective hook" (RUSH), which is an inducible system for the release of secretory cargo [22]. This system consists of an ER-resident streptavidin-KDEL fusion protein ("hook") and a "bait"-protein fused to a streptavidin-binding peptide (SBP) to be retained in the ER in the absence of biotin (Figure 2C). We constructed a tagged Wnt3A with an integrated GFP and an SBP between the signal peptide and the core sequence of Wnt3A. In Hek293T cells, this construct was secreted into the supernatant in the presence of biotin (Figure 2D) and localizes to the ER in the absence of biotin (Figure 2E). An addition of 50 µM biotin triggered the ER-release of Wnt3A by competitive binding to the streptavidin hook, and 30 to 60 min later, Wnt3A localized to the perinuclear region, indicating transport to the Golgi (Figure 2E,F). In cells co-expressing Ykt6-WT, Wnt3A is detected both at the Golgi and in the cytoplasm at later time points (>120 min), partially co-localizing with Ykt6 (Figure 2E,G). In contrast to Ykt6-WT, the co-expression of Ykt6-3E leads to strong accumulation with Wnt3A at the plasma membrane (>120 min) (Figure 2F,H). Hence, in the presence of endogenous Ykt6, the phosphomimicking Ykt6 mutant neither has a dominant negative effect, nor blocks ER to Golgi trafficking of Wnt3A but accumulates at different post-Golgi membranes within the secretory pathway together with Wnt3A.

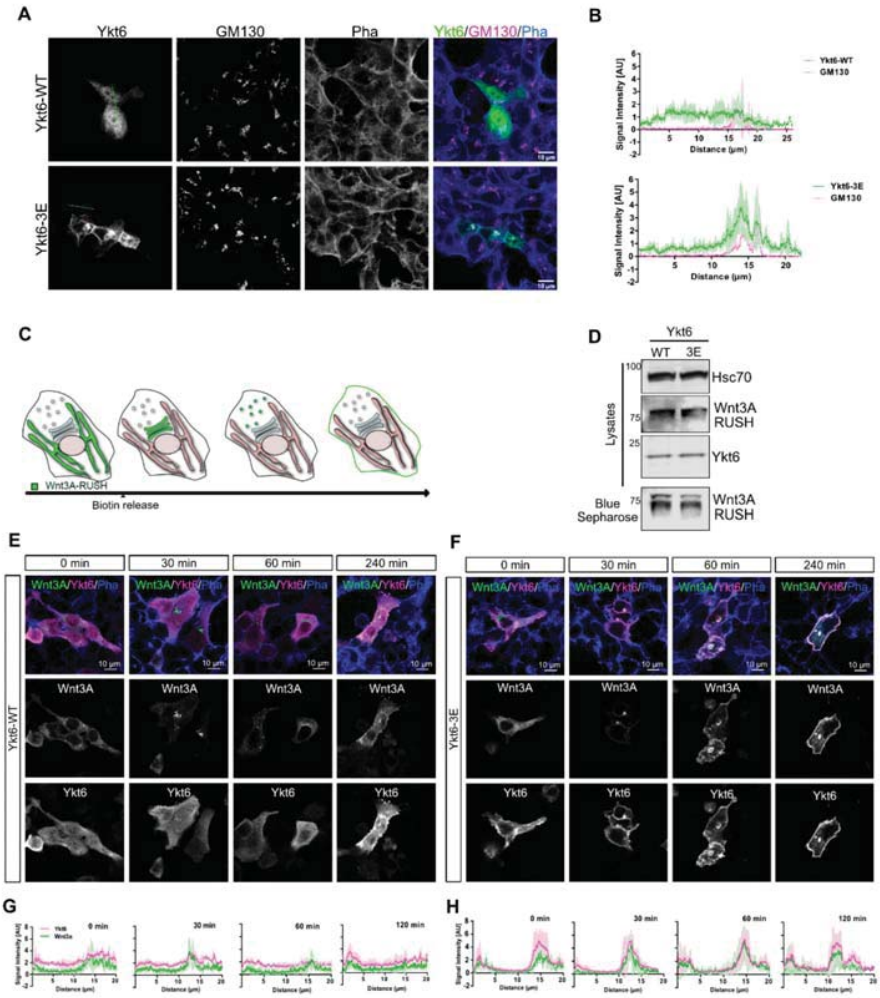

Figure 2. Phosphomimicking mutations accumulate Ykt6 at membranes in the secretory pathway. (**A**) Representative immunofluorescence and (**B**) Quantification of Ykt6-WT and -3E transfected in HCT116 cells and additionally stained for GM130, Phalloidin, and Hoechst. Scale bar 10 µm. (**C**) Scheme representation of Wnt3A-RUSH ("retention using selective hook") system. (**D**) Representative immunoblot of Wnt3A, Ykt6 WT, and -3E in Hek293T lysates and blue sepharose precipitation of Wnt3A secretion from the supernatant after 24 h of biotin treatment. (**E**) HCT116 cells transfected with RUSH-EGFP-Wnt3A in combination with Ykt6-WT and quantification in (**G**). (**F**) Ykt6-3E stained for Ykt6 and F-actin in addition to GFP and quantification in (**H**). Scale bar represents 10 µm, representative images, and quantifications of three independent experiments.

3.3. SNARE Phosphorylation Sites Determine Membrane Attachment and Autoinhibited Conformation

To further analyze the role of Ykt6 phosphorylation in membrane attachment, we used a differential detergent fractionation [31] to biochemically separate membranes from cytoplasm.

Confirming immunofluorescence results (Figure 2A), we found that Ykt6-3E partially associated with the membrane fraction, whereas Ykt6-WT was exclusively found cytoplasmically (Figure 3A, left panel, lane 5 and 7). In addition, different Ykt6 mutants previously described to impair Ykt6 conformational changes were also found only in the cytoplasmic fraction. This includes mutations of either palmitoylation (C194A) or farnesylation (C195A) sites, the palmitoyl/farnesyl (C194/195A) double mutant, and a combination of phosphomimicking and palmitoyl/farnesyl (Ykt6-3E/C194A/C195A) mutants (Figure 3A). This affirms that farnesylation and subsequent palmitoylation is required for

the stable membrane association of Ykt6 [5,17]. Mutation in the Longin domain (F42A) was shown to impair the auto-inhibited conformation by shielding the lipidation [6]. Indeed, we detected some Ykt6-F42A in the membrane fraction, while non-phosphorylatable Ykt6-3A did not show this membrane association (Figure 3A, right panel, lane 11 and 13). All constructs were expressed at levels comparable to endogenous Ykt6 in total cell lysate, excluding any effect of strong overexpression (Figure 3B). This demonstrates that phosphomimicking modifications within the SNARE domain result in a form of Ykt6 that preferentially associates with membranes, possibly through inhibition of its closed conformation.

To test whether Ykt6 expression levels might determine the level of membrane recruitment, we expressed increasing amounts of WT constructs (0.1, 0.3, and 1 μg). This leads to an expected linear increase of Ykt6 expression (Figure 3C) in the overall cell lysates. While this linear increase is also visible in the cytoplasmic fraction (Figure 3D), the level of Ykt6-3E, but not Ykt6-WT is strongly increased in the membrane fraction, (Figure 3E). This indicates that it is not the cellular level of Ykt6 determines membrane recruitment but specifically the modification of its SNARE domain.

Next, we used an unbiased BioID approach [45] to label proteins in close vicinity of Ykt6 by fusion with the prokaryotic BirA* domain (Figure 3F). N-terminally tagged Ykt6-WT and mutant constructs were expressed at comparable levels (Figure 3G) in the presence of 50 μM biotin. Biotinylated proteins were purified by streptavidin pulldown and subjected to mass spectrometry to define the "proxisome" of the functional Ykt6 SNARE domain (Figure 3F). We found Ykt6 highly enriched among the biotinylated proteins compared to background proteins labeled by the BioID alone, indicating an ability of the N-terminal BioID domain to intra- or intermolecularly label Ykt6. We hypothesized that the closed conformation of Ykt6 could interfere with self-labeling and compared the biotin-labeling ability of Ykt6-3E with different Ykt6 point mutations known to interfere with the closed conformation (Figure 3H). Both cytosolic and membrane fractions were analyzed by immuno-blotting for streptavidin-labeled Ykt6-BioID. Compared to Ykt6-WT, the phosphomimicking (3E) and the palmitoyl/farnesyl (C194/195A) double mutant BioID constructs were strongly labeled by the N-terminal BioID domain in the cytoplasmic fraction (Figure 3H, left panel, lane 6, and 12 and quantification in (I). Minor self-labeling of Ykt6-WT, due to binding of the functional Longin domain to the farnesyl group, suggests that a large portion acquires a closed conformation, which is in agreement with the lower Ykt6-WT levels in the membrane fraction (Figure 3A, lane 5). In contrast, combined mutations of palmitoylation/farnesylation sites and the phosphomimicking mutations (Ykt6-3E/C194A/C195A) lead to a more unstable and open conformation, allowing stronger self-labeling by the N-terminal BioID (Figure 3H,I). Taken together, these complementary approaches suggest that modification of the Ykt6 SNARE domain can prevent Ykt6 from assuming a closed auto-inhibited conformation and thereby promote Ykt6 membrane recruitment.

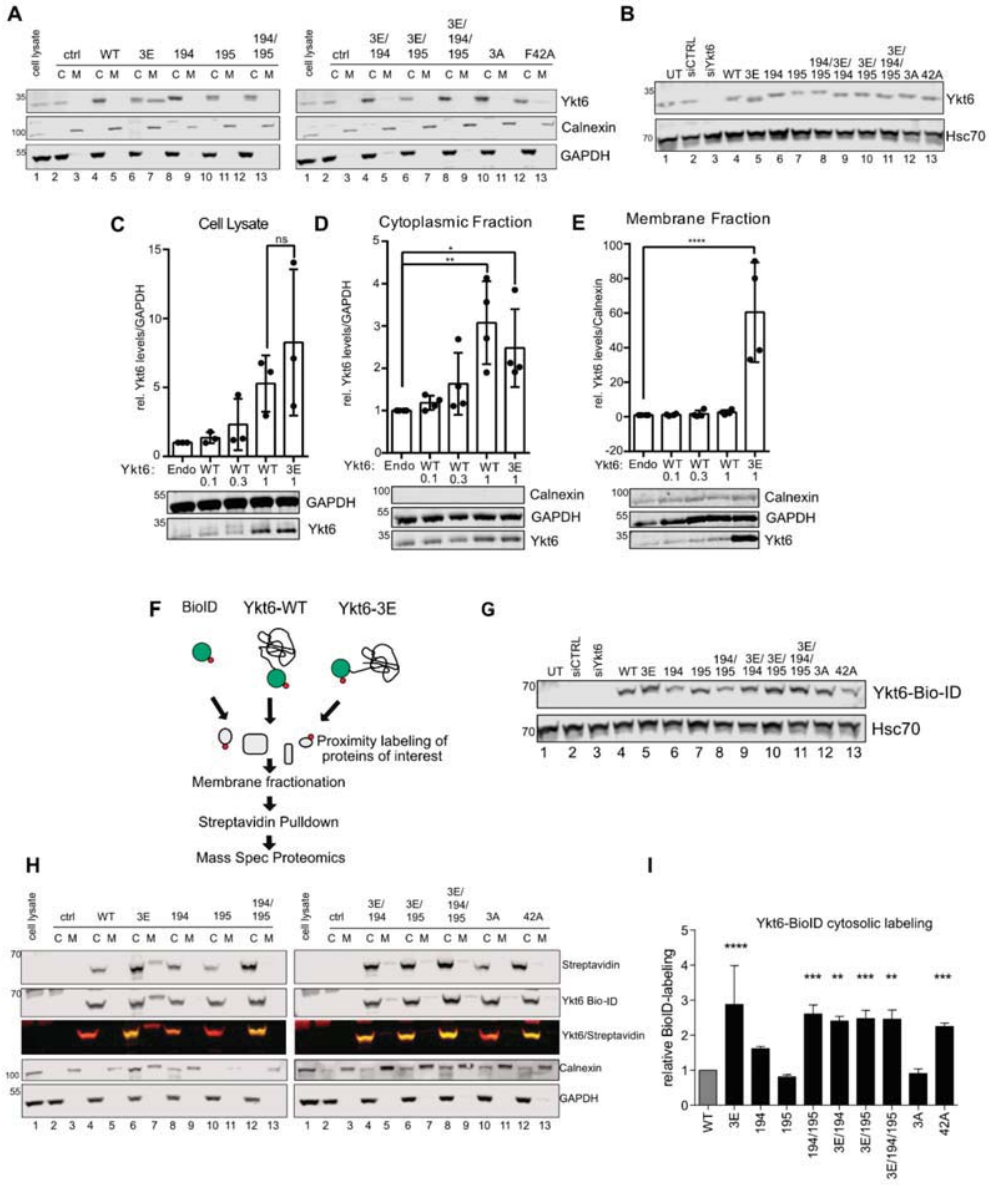

Figure 3. SNARE phosphorylation sites determine membrane attachment and auto-inhibited conformation. (**A**) Representative immunoblot of cell fractionation of different Ykt6 mutant constructs transfected in Hek293T cells and stained with Ykt6 and fraction markers GADPH for cytoplasmic (C) and Calnexin for membrane (M) fraction ($n = 4$). (**B**) Representative immunoblot of Ykt6 knockdown and overexpression of different Ykt6 mutant constructs with Hsc70 as a loading control. (**C**) Representative immunoblot and quantification of overexpressed Ykt6-WT construct in three different concentrations (0.1 µg, 0.3 µg, and 1 µg), along with overexpressed Ykt6-3E construct and endogenous Ykt6 from three biological replicates. (**D**) Representative blot and quantification of endogenous and overexpressed Ykt6-WT (0.1 µg, 0.3 µg, and 1 µg), 3E (1 µg) in the cytoplasmic fraction, n = 4 (**E**) Representative blot

and quantification of endogenous and overexpressed Ykt6-WT (0.1 µg, 0.3 µg, and 1 µg) or 3E (1 µg) in the membrane fraction, $n = 4$. (**F**) Scheme of biotin-labeling assay. Biotin–ligase BioID was expressed alone or as Ykt6-WT or -3E fusion constructs in Hek293T cells in the presence of 50 µM biotin. After membrane fractionation, proteins were streptavidin-purified and subjected to mass spectrometry or immunoblotting. (**G**) Representative immunoblot of Ykt6 knockdown and overexpression of different Bio-ID-tagged Ykt6 mutant constructs with Hsc70 as a loading control (**H**) Representative immunoblot of cell fractionation of different Ykt6-BioID constructs transfected in Hek293 cells, stained with Streptavidin, Ykt6 and fraction markers as in (**B**) ($n = 3$). (**I**) Quantification of biotin labeling in the cytosolic fraction of (**H**). * = 0.05, ** = 0.01, *** = 0.001, **** = 0.0001.

3.4. Ykt6 SNARE Domain-Dependent Proximity Proteome

Ykt6 is involved in the homotypic fusion of ER and vacuolar membranes, retrograde Golgi trafficking in yeast, and autophagosome formation [12,15,19,46]. However, the mechanism of how Ykt6 is recruited to those different organelles is not well understood. As the phosphomimicking Ykt6-3E construct was present in the membrane fraction and was labeled strongly by the N-terminal BioID domain compared to Ykt6-WT, we next subjected the pull-down of membrane and cytoplasmic fractions to mass spectrometry in order to identify biotinylated proteins in both fractions. We reasoned that although Ykt6-WT steady-state membrane levels were low, BioID labeling might label transient Ykt6-WT interaction partners at membranes during its cycling. Ykt6-WT and -3E were detected at similar levels among biotinylated proteins of the cytoplasmic fraction, but Ykt6-3E was approximately six-fold enriched over Ykt6-WT in the membrane fraction (Supplementary Table S2). We identified a total of 241 enriched proteins in Ykt6-WT and 235 enriched proteins in -3E, indicating that labeling by both constructs was similarly successful. Then, we performed an enrichment analysis based on PANTHER classification of the identified proteins [47]. At first, we compared the enriched biological processes of Ykt6-WT between the cytoplasmic and the membrane fraction (Figure 4A–C). Among the biological processes exclusive to the membrane fractionated Ykt6-WT proxisome were vesicle trafficking, regulated exocytosis, organelle organization, and various biosynthetic processes (Figure 4C). This further infers that the membrane-bound Ykt6 acts as an active SNARE proximal to very different cellular processes.

Next, we compared the processes differentially identified in the proxisomes of theYkt6-WT and -3E of membrane fractions (Figure 4D–H). GO term enrichment and Reactome pathway analysis showed Ykt6-WT to be proximal to processes such as Golgi-ER traffic and autophagy, among others. In contrast, Ykt6-3E was proximal to Akt and Wnt Signaling, protein folding, and protein ubiquitination (Figure 4F,H). This suggests that modification of the Ykt6 SNARE domain plays a role in the functional membrane attachment of Ykt6 in specific cellular pathways.

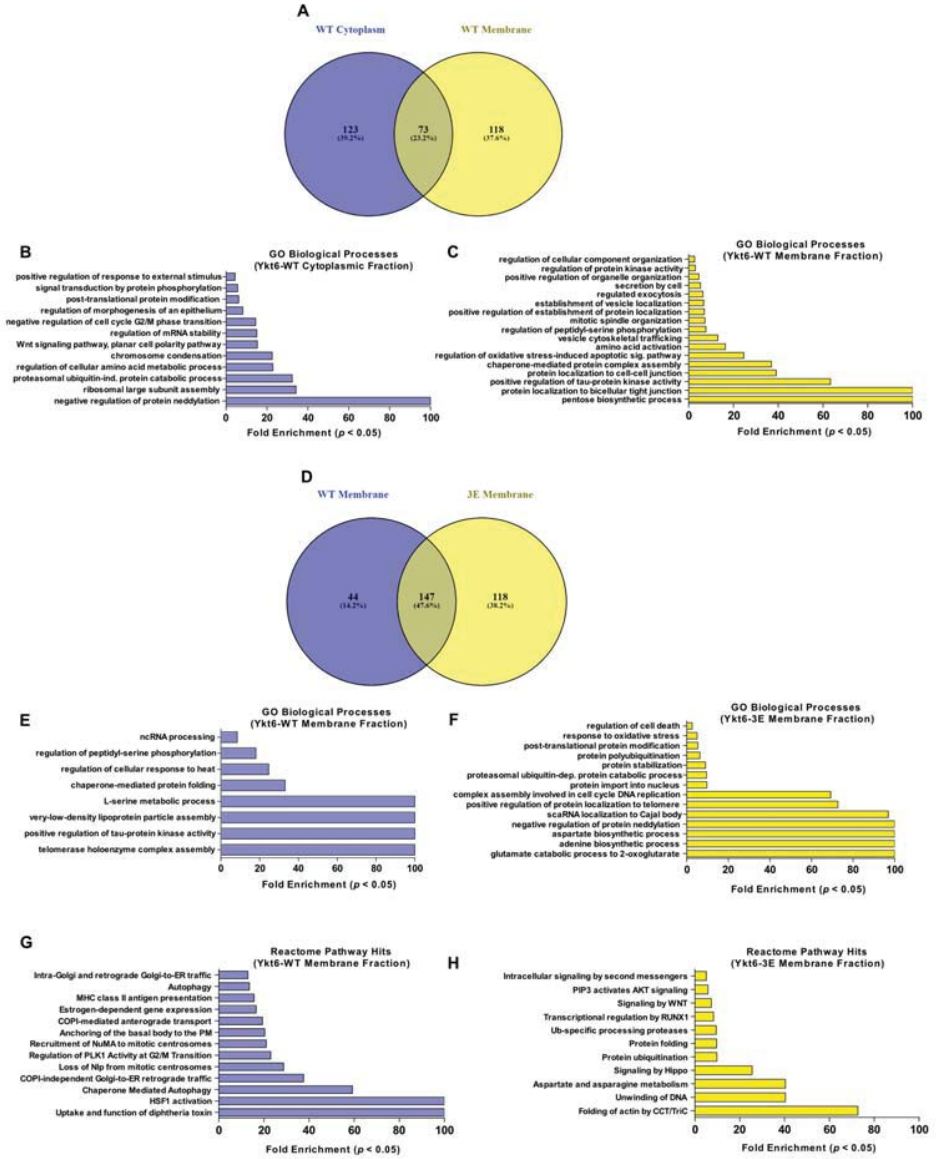

Figure 4. Ykt6 SNARE-dependent proximity proteome. (**A**) Proteins enriched in Ykt6-WT cytoplasmic fraction versus membrane fraction. (**B**,**C**) Enriched GO biological processes of Ykt6-WT in cytoplasmic versus membrane fraction. (**D**) Proteins up-regulated between Ykt6-WT versus Ykt6-3E in the membrane fraction. (**E**,**F**) Enriched GO biological processes of Ykt6-WT and -3E with a (p-value < 0.05) as determined by Fisher Exact Test with the Benjamini–Hochberg False Discovery Rate < 0.05. (**G**,**H**) Enriched Reactome Pathway hits of Ykt6-WT and -3E in the membrane fraction based on FDR < 0.05.

3.5. Ykt6 Regulates EV Secretion in a Concentration-Dependent Manner

Due to the role of Ykt6 in autophagosome formation [15,18,19] and extracellular vesicle (EV) secretion [23] we next wanted to address how Ykt6 conformational changes via the phosphorylation sites in the SNARE domain affect endosomal sorting and EV secretion. Exosomes are a population of small extracellular vesicles. They are generated as intraluminal vesicles (ILVs) by inward budding of the limiting membrane of multivesicular bodies (MVBs) and can be secreted in an ESCRT- as well as an Alix-Syntenin-dependent manner [48]. Microautophagy, which is involved in the degradation of soluble cytosol, occurs during MVB formation and shares the ESCRT components for vesicle formation and cargo internalization [49]. To understand whether Ykt6 membrane recruitment plays a role at the level of cargo sorting into ILVs, we used constitutively active Rab5 (Rab5Q79L) to enlarge endosomes and thereby visualize whether cargo is present at the limiting membrane or within MVBs [50]. In Rab5Q79L-expressing Hek293T cells, overexpressed Ykt6-WT as well as -3E localized inside enlarged endosomes (Figure 5A). However, in Ykt6-3E overexpressing cells, those endosomes were significantly smaller than in Ykt6-WT (Figure 5B), indicating that the mutated SNARE domain might hinder endosomal fusion events activated by Rab5Q79L. Interestingly, under serum-fed conditions, Ykt6 had no effect on the levels of p62, as a readout of autophagy induction (Figure 5C), suggesting that the non-canonical role of Ykt6 in autophagy could be starvation-dependent [51,52].

A portion of ILVs is secreted as exosomes by the fusion of MVBs with the plasma membrane. Thus, we next compared the effect of Ykt6 on EV secretion into the supernatant of Hek293T cells. Knockdown of Ykt6 as well as Alix reduced the level of EVs as measured by nanoparticle tracking analysis (NTA) after differential ultracentrifugation for EV isolation (Figure 5D,F,G). Surprisingly, similar to Ykt6 knockdown, the overexpression of tagged Ykt6-WT significantly reduced secretion of EVs, but Ykt6-3E did not (Figure 5E,H,I). This suggests that the amount of Ykt6 regulates its function in secretory processes and further highlights that in line with the effect observed on Rab5Q79L endosomes, Ykt6 function can be impaired by modification of the Ykt6 SNARE domain. Ykt6 knockdown was previously shown to reduce Wnt as well as exosome secretion [23]; thus, we next checked Wnt levels on exosomes (P100) purified from the supernatant of Hek293T cells. Here, the overexpression of Ykt6-WT as well as Ykt6-3E reduced the level of Wnt3A (Figure 5J). Membrane recruitment of Ykt6 was not increased with higher levels of Ykt6-WT (Figure 3E). However, looking at the secretion of Wnt3A, we found that increasing amounts of Ykt6-WT decreased the level of Wnt3A on exosomes to a level similar to Ykt6 knockdown (Figure 5K). This could imply that the phosphorylation and fusion competence of Ykt6 present at endosomal membranes is a concentration-dependent process in exosome secretion.

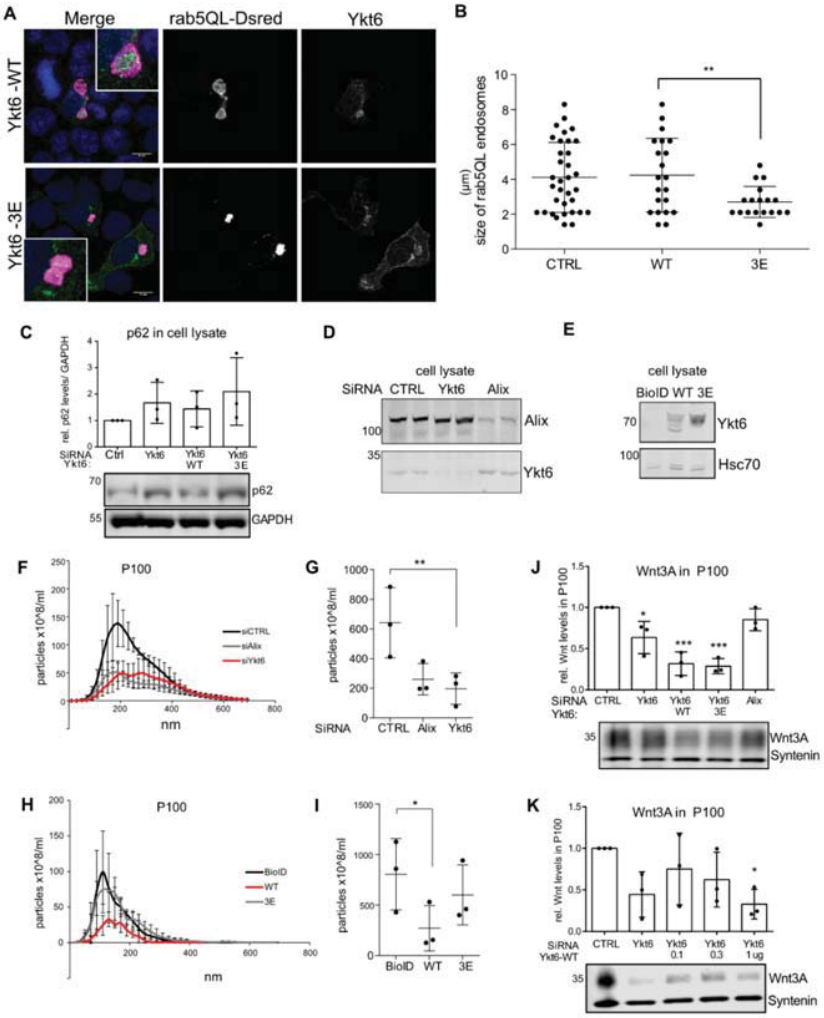

Figure 5. Ykt6 regulates extracellular vesicle (EV) secretion in a concentration-dependent manner. (**A**) Hek293T cells were co-transfected with plasmids for Rab5Q79L-DsRed and either control, Ykt6-WT, or Ykt6-3E and analyzed by immunofluorescence microscopy. Scale bar represents 10 µm. (**B**) Quantification of (**A**), number of endosomes: control (n = 34), Ykt6-WT (n = 21), or Ykt6-3E (n = 18) from two independent biological replicates. (**C**) Representative blot and quantifications of p62 levels in HCT116 cells transfected with siRNA against control or Ykt6 and Ykt6-WT or 3E. (**D**) Immunoblot of Hek293T cells transfected with siRNA against control, Ykt6, or Alix. (**E**) Immunoblot of Hek293T cells transfected with Ykt6-WT, -3E, and BioID mock plasmid. (**F**) Extracellular vesicles (EV) were purified from the supernatant. EVs in P100 are centrifuged 1 h at 100,000× g. Size profile of P100-EV was analyzed by nanoparticle tracking analysis (NTA). (**G**) Quantification of 100–200 nm EV size profile in (**D**) from three biological replicates. Significance level ** = 0.01. (**H**) NTA EV size profile of P100 from (**F**,**I**) Quantification of 100–200 nm sized EVs from (G) from three biological replicates. * = 0.05. (**J**,**K**) Immunoblot and quantification of Wnt3A in P100 purified from Hek293T cells transfected with siRNA against control, Ykt6 or Alix and (J) Ykt6-WT or 3E, *** = 0.001 and (**K**) Ykt6-WT in three different concentrations (0.1, 0.3, and 1 µg DNA) * = 0.05.

4. Discussion

The fusion of eukaryotic transport vesicles with target organelles requires membrane-bridging complexes of membrane anchored SNAREs. Ykt6 is lacking a transmembrane domain, and thus, its site of action is determined by changing from a soluble to a membrane-bound conformation. How Ykt6

is recruited to membranes remains unclear. Here, we investigate how the functional regulation of its SNARE domain can mechanistically regulate Ykt6 membrane attachment and its activity in mammalian cells and in *Drosophila*. We found that Ykt6 membrane attachment is regulated by modifications in its SNARE domain, and that this regulation affects cell survival in vivo. Ykt6 phosphorylation and attachment further affect the Ykt6 proximity profile and the cellular processes in which it takes part. Specific secretory processes, such as Wnt and EV secretion, furthermore depend on a functional Ykt6 SNARE domain and could thus be regulated by Ykt6 phosphorylation. Under normal growth conditions, these processes seem to be more important for cellular function, than its role in autophagosome formation. As it has also been reported that Ykt6 is involved in autophagosome–lysosome fusion in human cells and *Drosophila* fat body under starvation-induced conditions [15,19], it is possible that Ykt6 is allocated to alternate compartments, especially under nutrient stress condition [51,52].

Non-neuronal SNAREs possess evolutionarily conserved phosphorylation sites [37], which seem to prevent membrane fusion when SNAREs are phosphorylated. Based on our data, Ykt6 functions in a similar manner, as Ykt6-3E seems to prevent fusion as well. Yet, dynamic membrane recruitment is specific to SNAREs lacking a transmembrane domain such as Ykt6. Indeed, self-labeling and membrane attachment of different Ykt6 mutants varies and in agreement with previous work [53] hints toward a two-step process of activation that is specific to Ykt6 and involves (1) a change from closed to open confirmation and (2) membrane recruitment. Post-membrane recruitment, true for all SNAREs with phosphorylation sites in the SNARE domain [37], phosphorylation would prevent the fusion of different SNAREs to mediate membrane fusion.

Protein acylation is a regulatory post-translational modification regulating membrane association and the dissociation of its target proteins. The F42 position has been previously shown to participate in intramolecular interactions between the Ykt6 Longin domain and the SNARE motif. The hydrophobic face at position F42 within the Longin domain seems to accommodate the farnesyl anchor, as seen in a crystal structure with dodecylphosphocholine (DPC) [7]. This intramolecular binding explains the membrane association of Ykt6 when F42 is mutated (Figure 3A, right panel, lane13). Similarly, the phosphorylation sites we identified (S174/S181/T187) are directly facing this interface and therefore likely impact the tight folding of Ykt6 into a closed conformation and thus membrane attachment (Figure 3E). Interestingly, the non-phosphorylatable mutant Ykt6-3A does not attach to membranes by itself, yet it is able to rescue the growth defects in vivo (Figure 1G). Taken together, this suggests that the phosphorylation of Ykt6 prevents the conformational switch to the inactive state, which leads to membrane stabilization. Likely, an additional step is required to render Ykt6 fusion-competent, as Ykt6-3E did not rescue Ykt6 KD in vivo, but it had no dominant-negative effects in the presence of endogenous Ykt6. This last step toward fusion-competent Ykt6 could be achieved by dephosphorylation [52], for example by calcineurin, as suggested by a recent study [54].

Which signaling pathways could stimulate the phosphorylation of Ykt6 and therefore its membrane recruitment? As PKC gets activated in the context of endocytosis to recruit adaptor complexes to endosomes [55,56] local PKC-dependent conformation changes and subsequent palmitoylation could stimulate Ykt6 association with endosomes. Similarly, PDK1 is a growth factor-dependent kinase that could phosphorylate Ykt6 in the presence of mitogenic signals that require Wnt secretion and/or autophagy. Moreover, the Netphos prediction of Ykt6 S174 to be a CDK1 target and the fact that proteins proximal of Ykt6 are involved in cell cycle regulation opens interesting questions of whether Ykt6 is involved in cell growth-dependent regulations of organelle fusion. Furthermore, the identification of three phosphorylation sites bears the possibility that the three sites are individually targeted by different signaling pathways and differ in their role in recruiting and stabilizing Ykt6 to and at membranes under permissive circumstances. Yet, the physiological relevance of Ykt6 phosphorylation remains to be demonstrated, and more detailed analysis is necessary to understand the interconnection and hierarchy of different signaling pathways targeting Ykt6.

Interestingly, other SNAREs such as Syntaxin-5 are modified by monoubiquitination that regulates Golgi integrity during cell cycle progression [57]. In addition to position S174 in Ykt6 being identified

in Phosphoproteomic studies, its Lysine 182 and 186 (K182,K186) were found to be ubiquitinated in different human cell lines and the mouse liver [58–60]. These positions lie close by the analyzed phosphorylation sites (S181, T187). Thus, Ykt6 function and its membrane recruitment could be the target of different posttranscriptional modifications at the crossroad of cellular trafficking events in cellular growth.

Supplementary Materials: The following are available online at http://www.mdpi.com/2218-273X/10/11/1560/s1, Table S1: Ykt6 SNARE in vitro kinase screening results. Kinase finder and validation screen. Supplementary Table S2: Proteins identified by mass spectrometry from BioID control, Ykt6-WT and Ykt6-3E samples in two technical replicates by SWATH (for experimental details see Material and Methods section). Supplementary Table S3: List of abbreviations.

Author Contributions: P.K.M. and A.D.-M. designed and carried out cell culture experiments and data analysis. L.W. and D.C. performed immunofluorescence analysis, K.L. carried out *Drosophila* experiments and data analysis. M.H.-C. generated fly lines and constructs. All the authors have read and agreed to the published version of the manuscript. J.C.G. conceived and supervised the study and wrote the paper with the help and comments of all authors. All authors have read and agreed to the published version of the manuscript.

Funding: This research and the APC was funded by the DFG-funded Research Center SFB1324/1—project number 331351713.

Acknowledgments: The authors thank the Core Facility Proteomics at the Institute of Clinical Chemistry, UMG. Research in the lab of JCG is supported by the DFG-funded Research Center SFB1324/1—project number 331351713 and GR4810/2-1, the Research program of the University Medical Center, University of Göttingen and a postdoctoral fellowship to K.L. by the Dorothea Schlözer Program, University of Göttingen.

Conflicts of Interest: The authors declare no conflict of interest.

References

1. Weimbs, T.; Low, S.H.; Chapin, S.J.; Mostov, K.E.; Bucher, P.; Hofmann, K. A conserved domain is present in different families of vesicular fusion proteins: A new superfamily. *Proc. Natl. Acad. Sci. USA* **1997**, *94*, 3046–3051. [CrossRef] [PubMed]
2. Antonin, W.; Fasshauer, D.; Becker, S.; Jahn, R.; Schneider, T.R. Crystal structure of the endosomal SNARE complex reveals common structural principles of all SNAREs. *Nat. Genet.* **2002**, *9*, 107–111. [CrossRef] [PubMed]
3. Sutton, R.B.; Fasshauer, D.; Jahn, R.; Brunger, A.T. Crystal structure of a SNARE complex involved in synaptic exocytosis at 2.4 Å resolution. *Nature* **1998**, *395*, 347–353. [CrossRef] [PubMed]
4. Ungar, D.; Hughson, F.M. SNARE Protein Structure and Function. *Annu. Rev. Cell Dev. Biol.* **2003**, *19*, 493–517. [CrossRef] [PubMed]
5. Fukasawa, M.; Varlamov, O.; Eng, W.S.; Söllner, T.H.; Rothman, J.E. Localization and activity of the SNARE Ykt6 determined by its regulatory domain and palmitoylation. *Proc. Natl. Acad. Sci. USA* **2004**, *101*, 4815–4820. [CrossRef]
6. Tochio, H. An Autoinhibitory Mechanism for Nonsyntaxin SNARE Proteins Revealed by the Structure of Ykt6p. *Science* **2001**, *293*, 698–702. [CrossRef]
7. Shirakawa, R.; Goto-Ito, S.; Goto, K.; Wakayama, S.; Kubo, H.; Sakata, N.; Trinh, D.A.; Yamagata, A.; Sato, Y.; Masumoto, H.; et al. A SNARE geranylgeranyltransferase essential for the organization of the Golgi apparatus. *EMBO J.* **2020**, *39*, e104120. [CrossRef]
8. Dingjan, I.; Linders, P.T.A.; Verboogen, D.R.J.; Revelo, N.H.; Ter Beest, M.; Bogaart, G.V.D. Endosomal and Phagosomal SNAREs. *Physiol. Rev.* **2018**, *98*, 1465–1492. [CrossRef]
9. Tsui, M.M.; Banfield, D.K. Yeast Golgi SNARE interactions are promiscuous. *J. Cell Sci.* **2000**, *113*, 145–152.
10. Dietrich, L.E.P.; Gurezka, R.; Veit, M.; Ungermann, C. The SNARE Ykt6 mediates protein palmitoylation during an early stage of homotypic vacuole fusion. *EMBO J.* **2003**, *23*, 45–53. [CrossRef]
11. Ungermann, C.; Nichols, B.J.; Pelham, H.R.B.; Wickner, W. A Vacuolar v–t-SNARE Complex, the Predominant Form In Vivo and on Isolated Vacuoles, Is Disassembled and Activated for Docking and Fusion. *J. Cell Biol.* **1998**, *140*, 61–69. [CrossRef] [PubMed]
12. Ungermann, C.; Von Mollard, G.F.; Jensen, O.N.; Margolis, N.; Stevens, T.H.; Wickner, W. Three v-SNAREs and Two t-SNAREs, Present in a Pentameric cis-SNARE Complex on Isolated Vacuoles, Are Essential for Homotypic Fusion. *J. Cell Biol.* **1999**, *145*, 1435–1442. [CrossRef] [PubMed]

13. McNew, J.A.; Søgaard, M.; Lampen, N.M.; Machida, S.; Ye, R.R.; Lacomis, L.; Tempst, P.; Rothman, J.E.; Söllner, T.H. Ykt6p, a Prenylated SNARE Essential for Endoplasmic Reticulum-Golgi Transport. *J. Biol. Chem.* **1997**, *272*, 17776–17783. [CrossRef] [PubMed]
14. Kweon, Y.; Rothe, A.; Conibear, E.; Stevens, T.H. Ykt6p is a multifunctional yeast R-SNARE that is required for multiple membrane transport pathways to the vacuole. *Mol. Biol. Cell* **2003**, *14*, 1868–1881. [CrossRef] [PubMed]
15. Bas, L.; Papinski, D.; Licheva, M.; Torggler, R.; Rohringer, S.; Schuschnig, M.; Kraft, C. Reconstitution reveals Ykt6 as the autophagosomal SNARE in autophagosome–vacuole fusion. *J. Cell Biol.* **2018**, *217*, 3656–3669. [CrossRef]
16. Nair, U.; Klionsky, D.J. Autophagosome biogenesis requires SNAREs. *Autophagy* **2011**, *7*, 1570–1572. [CrossRef]
17. Cuddy, L.K.; Wani, W.Y.; Morella, M.L.; Pitcairn, C.; Tsutsumi, K.; Fredriksen, K.; Justman, C.J.; Grammatopoulos, T.N.; Belur, N.R.; Zunke, F.; et al. Stress-Induced Cellular Clearance Is Mediated by the SNARE Protein ykt6 and Disrupted by α-Synuclein. *Neuron* **2019**, *104*, 869–884. [CrossRef]
18. Matsui, T.; Jiang, P.; Nakano, S.; Sakamaki, Y.; Yamamoto, H.; Mizushima, N. Autophagosomal YKT6 is required for fusion with lysosomes independently of syntaxin 17. *J. Cell Biol.* **2018**, *217*, 2633–2645. [CrossRef]
19. Takáts, S.; Glatz, G.; Szenci, G.; Boda, A.; Horváth, G.V.; Hegedűs, K.; Kovács, A.L.; Juhász, G. Non-canonical role of the SNARE protein Ykt6 in autophagosome-lysosome fusion. *PLoS Genet.* **2018**, *14*, e1007359. [CrossRef]
20. Gao, J.; Reggiori, F.; Ungermann, C. A novel in vitro assay reveals SNARE topology and the role of Ykt6 in autophagosome fusion with vacuoles. *J. Cell Biol.* **2018**, *217*, 3670–3682. [CrossRef]
21. Gibson, D.G.; Young, L.; Chuang, R.-Y.; Venter, J.C.; Hutchison, C.A.; Smith, H.O. Enzymatic assembly of DNA molecules up to several hundred kilobases. *Nat. Methods* **2009**, *6*, 343–345. [CrossRef] [PubMed]
22. Boncompain, G.; Divoux, S.; Gareil, N.; De Forges, H.; Lescure, A.; Latreche, L.; Mercanti, V.; Jollivet, F.; Raposo, G.; Perez, F. Synchronization of secretory protein traffic in populations of cells. *Nat. Methods* **2012**, *9*, 493–498. [CrossRef] [PubMed]
23. Gross, J.C.; Chaudhary, V.; Bartscherer, K.; Boutros, M. Active Wnt proteins are secreted on exosomes. *Nat. Cell Biol.* **2012**, *14*, 1036–1045. [CrossRef] [PubMed]
24. Bischof, J.; Maeda, R.K.; Hediger, M.; Karch, F.; Basler, K. An optimized transgenesis system for Drosophila using germ-line-specific phiC31 integrases. *Proc. Natl. Acad. Sci. USA* **2007**, *104*, 3312–3317. [CrossRef] [PubMed]
25. Glaeser, K.; Boutros, M.; Gross, J.C. Biochemical Methods to Analyze Wnt Protein Secretion. *Breast Cancer* **2016**, *1481*, 17–28. [CrossRef]
26. Théry, C.; Amigorena, S.; Raposo, G.; Clayton, A. Isolation and Characterization of Exosomes from Cell Culture Supernatants and Biological Fluids. *Curr. Protoc. Cell Biol.* **2006**, *30*, 3.22.1–3.22.29. [CrossRef]
27. Menck, K.; Sönmezer, C.; Worst, T.S.; Schulz, M.; Dihazi, G.H.; Streit, F.; Erdmann, G.; Kling, S.; Boutros, M.; Binder, C.; et al. Neutral sphingomyelinases control extracellular vesicles budding from the plasma membrane. *J. Extracell. Vesicles* **2017**, *6*, 1378056. [CrossRef] [PubMed]
28. Schindelin, J.; Arganda-Carreras, I.; Frise, E.; Kaynig, V.; Longair, M.; Pietzsch, T.; Preibisch, S.; Rueden, C.; Saalfeld, S.; Schmid, B.; et al. Fiji: An open-source platform for biological-image analysis. *Nat. Methods* **2012**, *9*, 676–682. [CrossRef] [PubMed]
29. Schneider, C.A.; Rasband, W.S.; Eliceiri, K.W. NIH Image to ImageJ: 25 years of image analysis. *Nat. Methods* **2012**, *9*, 671–675. [CrossRef]
30. Rueden, C.T.; Schindelin, J.E.; Hiner, M.C.; Dezonia, B.E.; Walter, A.E.; Arena, E.T.; Eliceiri, K.W. ImageJ2: ImageJ for the next generation of scientific image data. *BMC Bioinform.* **2017**, *18*, 1–26. [CrossRef]
31. Baghirova, S.; Hughes, B.G.; Hendzel, M.J.; Schulz, R. Sequential fractionation and isolation of subcellular proteins from tissue or cultured cells. *MethodsX* **2015**, *2*, 440–445. [CrossRef] [PubMed]
32. Atanassov, I.; Urlaub, H. Increased proteome coverage by combining PAGE and peptide isoelectric focusing: Comparative study of gel-based separation approaches. *Proteomics* **2013**, *13*, 2947–2955. [CrossRef] [PubMed]
33. Zhang, Y.; Bilbao, A.; Bruderer, T.; Luban, J.; Strambio-De-Castillia, C.; Lisacek, F.; Hopfgartner, G.; Varesio, E. The Use of Variable Q1 Isolation Windows Improves Selectivity in LC–SWATH–MS Acquisition. *J. Proteome Res.* **2015**, *14*, 4359–4371. [CrossRef] [PubMed]

34. Lambert, J.-P.; Ivosev, G.; Couzens, A.L.; Larsen, B.; Taipale, M.; Lin, Z.-Y.; Zhong, Q.; Lindquist, S.; Vidal, M.; Aebersold, R.; et al. Mapping differential interactomes by affinity purification coupled with data-independent mass spectrometry acquisition. *Nat. Methods* **2013**, *10*, 1239–1245. [CrossRef]
35. Gobert, C.; Bracco, L.; Rossi, F.; Olivier, M.; Tazi, J.; Lavelle, F.; Larsen, A.K.; Riou, J.-F. Modulation of DNA Topoisomerase I Activity byp53. *Biochemistry* **1996**, *35*, 5778–5786. [CrossRef]
36. Sherman, B.T.; Lempicki, R.A. Systematic and integrative analysis of large gene lists using DAVID bioinformatics resources. *Nat. Protoc.* **2009**, *4*, 44–57.
37. Malmersjö, S.; Di Palma, S.; Diao, J.; Lai, Y.; A Pfuetzner, R.; Wang, A.L.; A McMahon, M.; Hayer, A.; Porteus, M.; Bodenmiller, B.; et al. Phosphorylation of residues inside the SNARE complex suppresses secretory vesicle fusion. *EMBO J.* **2016**, *35*, 1810–1821. [CrossRef]
38. Stuart, S.A.; Houel, S.; Lee, T.; Wang, N.; Old, W.M.; Ahn, N.G. A phosphoproteomic comparison of B-RAFV600E and MKK1/2 inhibitors in melanoma cells. *Mol. Cell. Proteom.* **2015**, *14*, 1599–1615. [CrossRef]
39. Blom, N.; Sicheritz-Pontén, T.; Gupta, R.; Gammeltoft, S.; Brunak, S. Prediction of post-translational glycosylation and phosphorylation of proteins from the amino acid sequence. *Proteomics* **2004**, *4*, 1633–1649. [CrossRef]
40. Brand, A.H.; Perrimon, N. Targeted gene expression as a means of altering cell fates and generating dominant phenotypes. *Development* **1993**, *118*, 401–415.
41. Minakhina, S.; Steward, R. Melanotic Mutants in Drosophila: Pathways and Phenotypes. *Genet* **2006**, *174*, 253–263. [CrossRef] [PubMed]
42. Parchure, A.; Vyas, N.; Mayor, S. Wnt and Hedgehog: Secretion of Lipid-Modified Morphogens. *Trends Cell Biol.* **2017**, *28*, 157–170. [CrossRef]
43. Swarup, S.; Verheyen, E.M. Wnt/wingless signaling in Drosophila. *Cold Spring Harb. Perspect. Biol.* **2012**, *4*, 1–16. [CrossRef] [PubMed]
44. Linnemannstöns, K.; Witte, L.; Pradhipa, K.M.; Kittel, J.C.; Danieli, A.; Müller, D.; Nitsch, L.; Honemann-Capito, M.; Grawe, F.; Wodarz, A.; et al. Ykt6-dependent endosomal recycling is required for Wnt secretion in the Drosophila wing epithelium. *Development* **2020**, *147*, dev185421. [CrossRef] [PubMed]
45. Roux, K.J.; Kim, D.I.; Burke, B. BioID: A Screen for Protein-Protein Interactions. *Curr. Protoc. Protein Sci.* **2013**, *74*, 19.23.1–19.23.14. [CrossRef] [PubMed]
46. Dietrich, L.E.; Peplowska, K.; LaGrassa, T.J.; Hou, H.; Rohde, J.; Ungermann, C. The SNARE Ykt6 is released from yeast vacuoles during an early stage of fusion. *EMBO Rep.* **2005**, *6*, 245–250. [CrossRef] [PubMed]
47. Mi, H.; Muruganujan, A.; Casagrande, J.T.; Thomas, P.D. Large-scale gene function analysis with the PANTHER classification system. *Nat. Protoc.* **2013**, *8*, 1551–1566. [CrossRef] [PubMed]
48. Baietti, M.F.; Zhang, Z.; Mortier, E.; Melchior, A.; DeGeest, G.; Geeraerts, A.; Ivarsson, Y.; Depoortere, F.; Coomans, C.; Vermeiren, E.; et al. Syndecan–syntenin–ALIX regulates the biogenesis of exosomes. *Nat. Cell Biol.* **2012**, *14*, 677–685. [CrossRef]
49. Sahu, R.; Kaushik, S.; Clement, C.C.; Cannizzo, E.S.; Scharf, B.; Follenzi, A.; Potolicchio, I.; Nieves, E.; Cuervo, A.M.; Santambrogio, L. Microautophagy of cytosolic proteins by late endosomes. *Dev. Cell* **2011**, *20*, 131–139. [CrossRef]
50. Stenmark, H.; Parton, R.; Steele-Mortimer, O.; Lütcke, A.; Gruenberg, J.; Zerial, M. Inhibition of rab5 GTPase activity stimulates membrane fusion in endocytosis. *EMBO J.* **1994**, *13*, 1287–1296. [CrossRef]
51. Saito, Y.; Li, L.; Coyaud, E.; Luna, A.; Sander, C.; Raught, B.; Asara, J.M.; Brown, M.; Muthuswamy, S.K. LLGL2 rescues nutrient stress by promoting leucine uptake in ER+ breast cancer. *Nat. Cell Biol.* **2019**, *569*, 275–279. [CrossRef] [PubMed]
52. Gao, J.; Kurre, R.; Rose, J.; Walter, S.; Fröhlich, F.; Piehler, J.; Reggiori, F.; Ungermann, C. Function of the SNARE Ykt6 on autophagosomes requires the Dsl1 complex and the Atg1 kinase complex. *EMBO Rep.* **2020**, 1–18. [CrossRef] [PubMed]
53. Wen, W.; Yu, J.; Pan, L.; Wei, Z.; Weng, J.; Wang, W.; Ong, Y.S.; Tran, T.H.T.; Hong, W.; Zhang, M. Lipid-Induced Conformational Switch Controls Fusion Activity of Longin Domain SNARE Ykt6. *Mol. Cell* **2010**, *37*, 383–395. [CrossRef] [PubMed]
54. McGrath, K.; Dergai, M.; Agarwal, S.; Chung, D.; Van Rossum, D.B.; Shevade, A.; Kuchin, S.; Zaichick, S.; Savas, J.N.; Fasshauer, D.; et al. A conformational switch driven by phosphorylation regulates Ykt6 activity in macroautophagy. *BioRxiv* **2020**. Available Online: https://www.biorxiv.org/content/10.1101/2020.03.15.992727v1 (accessed on 16 November 2020). [CrossRef]

55. Lau, C.G.; Takayasu, Y.; Rodenas-Ruano, A.; Paternain, A.V.; Lerma, J.; Bennett, M.V.L.; Zukin, R.S. SNAP-25 Is a Target of Protein Kinase C Phosphorylation Critical to NMDA Receptor Trafficking. *J. Neurosci.* **2010**, *30*, 242–254. [CrossRef]
56. Nazarewicz, R.R.; Salazar, G.; Patrushev, N.; Martin, A.S.; Hilenski, L.; Xiong, S.; Alexander, R.W. Early Endosomal Antigen 1 (EEA1) Is an Obligate Scaffold for Angiotensin II-induced, PKC-α-dependent Akt Activation in Endosomes. *J. Biol. Chem.* **2011**, *286*, 2886–2895. [CrossRef]
57. Huang, S.; Tang, D.; Wang, Y. Monoubiquitination of Syntaxin 5 Regulates Golgi Membrane Dynamics during the Cell Cycle. *Dev. Cell* **2016**, *38*, 73–85. [CrossRef]
58. Wagner, S.A.; Beli, P.; Weinert, B.T.; Nielsen, M.L.; Cox, J.; Mann, M.; Choudhary, C. A Proteome-wide, Quantitative Survey of In Vivo Ubiquitylation Sites Reveals Widespread Regulatory Roles. *Mol. Cell. Proteom.* **2011**, *10*, M111.013284. [CrossRef]
59. Povlsen, L.K.; Beli, P.; Wagner, S.A.; Poulsen, S.L.; Sylvestersen, K.B.; Poulsen, J.W.; Nielsen, M.L.; Bekker-Jensen, S.; Mailand, N.; Choudhary, C. Systems-wide analysis of ubiquitylation dynamics reveals a key role for PAF15 ubiquitylation in DNA-damage bypass. *Nat. Cell Biol.* **2012**, *14*, 1089–1098. [CrossRef]
60. Akimov, V.; Barrio-Hernandez, I.; Hansen, S.V.F.; Hallenborg, P.; Pedersen, A.-K.; Bekker-Jensen, D.B.; Puglia, M.; Christensen, S.D.K.; Vanselow, J.T.; Nielsen, M.M.; et al. UbiSite approach for comprehensive mapping of lysine and N-terminal ubiquitination sites. *Nat. Struct. Mol. Biol.* **2018**, *25*, 631–640. [CrossRef]

Supplementary Table 1

Phosphorylation profile of peptide "Ykt6-WT" in 245 Ser/Thr kinase assays; singlicate measurements
Sample peptide concentration: 1 µM
All values in cpm

				A	B	C	D	
#	Kinase (ProQinase Lot #)	External Vendor Lot #	Enzyme, ng/well	Kinase activity with peptide	Kinase activity w/o peptide	Peptide background, median n=3	Kinase activity with peptide, corrected (A-C)	Activity Ratio (D/B)
Serine/ Threonine Kinases								
1	ACV-R1 (Lot001)		20	421	271	162	259	0.96
2	ACV-R1B (Lot001)	INV_35826	10	138	105	162	-24	-0.23
3	ACV-R2A (Lot001)	INV_862446	40	255	201	162	93	0.46
4	ACV-R2B (Lot001)	INV_745099	25	231	120	162	69	0.58
5	ACV-RL1 (Lot002)	INV_511550	20	243	253	162	81	0.32
6	AKT1 (Lot007)		25	337	322	162	175	0.54
7	AKT2 (Lot003)		200	406	514	162	244	0.47
8	AKT3 (Lot004)		10	279	92	162	117	1.27
9	AMPK-alpha1 (Lot001)		200	1012	822	162	850	1.03
10	ARK5 (Lot002)		100	557	534	162	395	0.74
11	ASK1 (Lot001)	INV_666419	2	553	298	162	391	1.31
12	Aurora-A (Lot004)		50	771	725	162	609	0.84
13	Aurora-B (Lot008)		100	484	430	162	322	0.75
14	Aurora-C (Lot009)		100	397	253	162	235	0.93
15	BMPR1A (Lot002)	INV_834034	50	234	286	162	72	0.25
16	B-RAF VE (Lot002)		25	135	126	162	-27	-0.21
17	B-RAF wt (Lot001)		25	168	123	162	6	0.05
18	BRSK1 (Lot001)	INV_36097	3	102	183	162	-60	-0.33
19	BRSK2 (Lot002)	CAR_08CBS-0302	25	157	106	162	-5	-0.05
20	BUB1B (Lot002)	CAR_08CBS-1281	35	79	113	162	-83	-0.73
21	CAMK1D (Lot001)	INV_33214	100	397	421	162	235	0.56
22	CAMK2A (Lot001)	INV_28192	2	1656	240	162	1494	6.23
23	CAMK2B (Lot001)	INV_35330	100	174	164	162	12	0.07
24	CAMK2D (Lot001)	INV_31647	1	570	629	162	408	0.65
25	CAMK2G (Lot001)	MIL_D8NN026U	5	123	126	162	-39	-0.31
26	CAMK4 (Lot001)	INV_35391	75	316	577	162	154	0.27
27	CAMKK1 (Lot001)	INV_406782	30	95	101	162	-67	-0.66
28	CAMKK2 (Lot001)	INV_35319	10	735	190	162	573	3.02
29	CDC42BPA (Lot001)	INV_36844	10	565	352	162	403	1.14
30	CDC42BPB (Lot001)		25	200	22	162	38	1.73
31	CDC7/ASK (Lot001)	CAR_10CBS-0119	10	126	94	162	-36	-0.38
32	CDK1/CycA (Lot005)		15	210	78	162	48	0.62
33	CDK1/CycE (Lot001)		50	118	55	162	-44	-0.80
34	CDK16/CycY (Lot001)		20	84	181	162	-78	-0.43
35	CDK1CycB1 (Lot025)		25	312	131	162	150	1.15
36	CDK2/CycA (Lot005)		50	556	256	162	394	1.54
37	CDK2/CycE (Lot009)		10	322	117	162	160	1.37
38	CDK3/CycE (Lot001)		10	246	123	162	84	0.68
39	CDK4/CycD1 (Lot007)		25	27	69	162	-135	-1.96
40	CDK4/CycD3 (Lot001)		10	72	25	162	-90	-3.60
41	CDK5/p25NCK (Lot001)		15	147	128	162	-15	-0.12
42	CDK5/p35NCK (Lot001)		15	42	29	162	-120	-4.14
43	CDK6/CycD1 (Lot004)		200	458	62	162	296	4.77
44	CDK6/CycD3 (Lot003)	CAR_09CBS-0622	20	81	58	162	-81	-1.40
45	CDK7CycH (Lot002)		50	502	190	162	340	1.79
46	CDK8/CycC (Lot002)		50	391	232	162	229	0.99
47	CDK9/CycK (Lot001)	INV_35774	40	111	349	162	-51	-0.15
48	CDK9/CycT (Lot004)		15	337	174	162	175	1.01
49	CHK1 (Lot002)		50	733	490	162	571	1.17
50	CHK2 (Lot002)	INV_31541	10	316	409	162	154	0.38
51	CK1-alpha1 (Lot001)		100	636	276	162	474	1.72
52	CK1-delta (Lot001)	INV_33225	5	352	267	162	190	0.71
53	CK1-epsilon (Lot001)	INV_31778	2.5	391	346	162	229	0.66
54	CK1-gamma1 (Lot001)	INV_34360	5	194	171	162	32	0.19
55	CK1-gamma2 (Lot001)	INV_31770	10	322	207	162	160	0.77
56	CK1-gamma3 (Lot001)	INV_34380	5	131	177	162	-31	-0.18
57	CK2-alpha1 (Lot003)		20	286	171	162	124	0.73
58	CK2-alpha2 (Lot001)		50	184	62	162	22	0.35
59	CLK1 (Lot001)		400	481	332	162	319	0.96
60	CLK2 (Lot001)	INV_271879	2	289	157	162	127	0.81
61	CLK3 (Lot002)		10	1144	513	162	982	1.91
62	CLK4 (Lot001)	INV_34379	100	289	88	162	127	1.44
63	COT (Lot018)		300	1418	1460	162	1256	0.86

				A	B	C	D	
#	Kinase (ProQinase Lot #)	External Vendor Lot #	Enzyme, ng/well	Kinase activity with peptide	Kinase activity w/o peptide	Peptide background, median n=3	Kinase activity with peptide, corrected (A-C)	Activity Ratio (D/B)
64	DAPK1 (Lot002)		40	603	238	162	441	1.85
65	DAPK2 (Lot001)	INV_32159	10	620	769	162	458	0.60
66	DAPK3 (Lot001)	INV_33763	10	76	99	162	-86	-0.87
67	DCAMKL2 (Lot001)	INV_35320	20	113	231	162	-49	-0.21
68	DMPK (Lot001)	INV_34024	80	262	380	162	100	0.26
69	DNA-PK (Lot001)	INV_727478	10	586	425	162	424	1.00
70	DYRK1A (Lot002)	INV_38993	10	266	279	162	104	0.37
71	DYRK1B (Lot001)	INV_450178	2	327	130	162	165	1.27
72	DYRK2 (Lot001)	CAR_09CBS-1249E	4	162	183	162	0	0.00
73	DYRK3 (Lot001)	INV_290370	3	211	301	162	49	0.16
74	DYRK4 (Lot002)	INV_37361	50	1548	132	162	1386	10.50
75	EEF2K (Lot001)	INV_38185	8	111	60	162	-51	-0.85
76	EIF2AK2 (Lot001)	INV_374655	10	224	156	162	62	0.40
77	EIF2AK3 (Lot001)	INV_390343Z2C	20	309	180	162	147	0.82
78	ERK1 (Lot002)		20	305	35	162	143	4.09
79	ERK2 (Lot004)		10	360	227	162	198	0.87
80	ERK7 (Lot002)		50	322	292	162	160	0.55
81	GRK2 (Lot001)	INV_31090	50	150	126	162	-12	-0.10
82	GRK3 (Lot001)	INV_34008	10	72	326	162	-90	-0.28
83	GRK4 (Lot002)	INV_401163	5	109	221	162	-53	-0.24
84	GRK5 (Lot001)	INV_38284	5	156	130	162	-6	-0.05
85	GRK6 (Lot002)	INV_37437	15	178	204	162	16	0.08
86	GRK7 (Lot001)	INV_34013	5	285	528	162	123	0.23
87	GSG2 (Lot002)	INV_869949	7	312	263	162	150	0.57
88	GSK3-alpha (Lot001)	INV_29135	50	389	376	162	227	0.60
89	GSK3-beta (Lot003)		50	428	237	162	266	1.12
90	HIPK1 (Lot001)	INV_37497	20	211	62	162	49	0.79
91	HIPK2 (Lot001)	INV_452552	20	233	144	162	71	0.49
92	HIPK3 (Lot001)	INV_35332	20	76	103	162	-86	-0.83
93	HIPK4 (Lot001)	INV_719847	20	108	95	162	-54	-0.57
94	HRI (Lot001)		80	415	201	162	253	1.26
95	IKK-alpha (Lot003)	INV_447027	50	204	140	162	42	0.30
96	IKK-beta (Lot005)		100	256	152	162	94	0.62
97	IKK-epsilon (Lot007)		20	204	323	162	42	0.13
98	IRAK1 (Lot002)	INV_472069	20	292	319	162	130	0.41
99	IRAK4 (Lot006)		10	76	123	162	-86	-0.70
100	JNK1 (Lot005)		5	38	35	162	-124	-3.54
101	JNK2 (Lot003)		5	481	241	162	319	1.32
102	JNK3 (Lot001)		5	55	120	162	-107	-0.89
103	LIMK1 (Lot001)	INV_367810	50	162	253	162	0	0.00
104	LIMK2 (Lot001)	INV_355434	150	735	920	162	573	0.62
105	LRRK G2019S (Lot001)	INV_513572	5	227	178	162	65	0.37
106	LRRK2 I2020T (Lot001)	INV_586693	50	367	57	162	205	3.60
107	LRRK2 R1441C (Lot001)	INV_612366	50	135	87	162	-27	-0.31
108	LRRK2 wt (Lot002)	INV_698199	75	138	141	162	-24	-0.17
109	MAP3K1 (Lot001)		10	532	102	162	370	3.63
110	MAP3K10 (Lot001)	INV_34554	25	141	144	162	-21	-0.15
111	MAP3K11 (Lot001)	INV_34029	25	190	108	162	28	0.26
112	MAP3K7/MAP3K7IP1 (Lot001)	INV_452618	10	157	111	162	-5	-0.05
113	MAP3K9 (Lot002)	INV_762486	15	322	293	162	160	0.55
114	MAP4K2 (Lot001)	INV_35217	4	201	386	162	39	0.10
115	MAP4K4 (Lot001)	INV_33761	5	447	178	162	285	1.60
116	MAP4K5 (Lot001)	INV_33456	3	302	150	162	140	0.93
117	MAPKAPK2 (Lot004)		10	114	343	162	-48	-0.14
118	MAPKAPK3 (Lot001)		10	58	45	162	-104	-2.31
119	MAPKAPK5 (Lot005)		20	282	175	162	120	0.69
120	MARK1 (Lot001)		100	1157	658	162	995	1.51
121	MARK2 (Lot002)	INV_503177	5	130	251	162	-32	-0.13
122	MARK3 (Lot001)		100	894	712	162	732	1.03
123	MARK4 (Lot001)	INV_304213	5	258	307	162	96	0.31
124	MEK1 wt (Lot002)		50	404	140	162	242	1.73
125	MEK2 (Lot001)	INV_32519	100	180	183	162	18	0.10
126	MEK5 (Lot005)		100	240	340	162	78	0.23
127	MEKK2 (Lot003)	INV_34361	15	490	246	162	328	1.33
128	MEKK3 (Lot001)	INV_34560	15	197	157	162	35	0.22
129	MELK (Lot001)		100	136	42	162	-26	-0.62
130	MINK1 (Lot002)		10	234	45	162	72	1.60
131	MKK4 (Lot004)		50	227	133	162	65	0.49
132	MKK6SDTD (Lot001)		50	509	130	162	347	2.67
133	MKK7 (Lot002)		150	295	289	162	133	0.46
134	MKNK1 (Lot001)	INV_652363	15	217	65	162	55	0.85
135	MKNK2 (Lot001)	INV_504229	10	418	283	162	256	0.90
136	MLK4 (Lot002)		50	89	89	162	-73	-0.82

				A	B	C	D	
#	Kinase (ProQinase Lot #)	External Vendor Lot #	Enzyme, ng/well	Kinase activity with peptide	Kinase activity w/o peptide	Peptide background, median n=3	Kinase activity with peptide, corrected (A-C)	Activity Ratio (D/B)
137	MST1 (Lot002)		5	761	315	162	599	1.90
138	MST2 (Lot003)		10	165	350	162	3	0.01
139	MST3 (Lot001)	INV_32932	20	228	187	162	66	0.35
140	MST4 (Lot001)		100	311	149	162	149	1.00
141	mTOR (Lot001)	INV_533404	20	103	228	162	-59	-0.26
142	MYLK (Lot001)	INV_36152	25	507	468	162	345	0.74
143	MYLK2 (Lot001)		2.5	147	76	162	-15	-0.20
144	MYLK3 (Lot001)	INV_34028	50	89	556	162	-73	-0.13
145	NEK1 (Lot001)	INV_35267	5	1030	732	162	868	1.19
146	NEK11 (Lot001)	INV_38163	25	405	642	162	243	0.38
147	NEK2 (Lot002)		50	2697	1429	162	2535	1.77
148	NEK3 (Lot001)	INV_34362	10	152	165	162	-10	-0.06
149	NEK4 (Lot002)	INV_35817	4	713	363	162	551	1.52
150	NEK6 (Lot001)		20	133	59	162	-29	-0.49
151	NEK7 (Lot002)		25	42	103	162	-120	-1.17
152	NEK9 (Lot001)	INV_38162	2	857	741	162	695	0.94
153	NIK (Lot003)		350	3591	2874	162	3429	1.19
154	NLK (Lot002)		10	321	208	162	159	0.76
155	p38-alpha (Lot005)		10	211	91	162	49	0.54
156	p38-beta (Lot004)		3	256	29	162	94	3.24
157	p38-delta (Lot001)		2	171	77	162	9	0.12
158	p38-gamma (Lot001)	INV_32881	5	55	110	162	-107	-0.97
159	PAK1 (Lot002)		15	248	113	162	86	0.76
160	PAK2 (Lot001)		25	110	164	162	-52	-0.32
161	PAK3 (Lot001)		20	235	32	162	73	2.28
162	PAK4 (Lot004)		50	250	418	162	88	0.21
163	PAK6 (Lot001)		25	239	113	162	77	0.68
164	PAK7 (Lot001)		15	116	277	162	-46	-0.17
165	PASK (Lot001)	INV_34883	50	216	177	162	54	0.31
166	PBK (Lot003)		200	181	106	162	19	0.18
167	PDK1 (Lot002)		20	470	110	162	308	2.80
168	PHKG1 (Lot001)	INV_34488	5	151	155	162	-11	-0.07
169	PHKG2 (Lot001)	INV_37321	10	296	145	162	134	0.92
170	PIM1 (Lot003)		2	84	42	162	-78	-1.86
171	PIM2 (Lot002)		50	161	84	162	-1	-0.01
172	PIM3 (Lot007)		25	181	140	162	19	0.14
173	PKA (Lot002)	INV_37377	5	147	120	162	-15	-0.13
174	PKC-alpha (Lot005)		2.5	191	192	162	29	0.15
175	PKC-beta1 (Lot004)		2.5	140	205	162	-22	-0.11
176	PKC-beta2 (Lot003)		5	103	72	162	-59	-0.82
177	PKC-delta (Lot004)		25	390	294	162	228	0.78
178	PKC-epsilon (Lot006)		10	992	616	162	830	1.35
179	PKC-eta (Lot005)		10	293	429	162	131	0.31
180	PKC-gamma (Lot007)		10	367	97	162	205	2.11
181	PKC-iota (Lot006)		50	367	193	162	205	1.06
182	PKC-mu (Lot004)		20	250	168	162	88	0.52
183	PKC-nu (Lot002)		50	451	150	162	289	1.93
184	PKC-theta (Lot008)		2.5	219	130	162	57	0.44
185	PKC-zeta (Lot005)		50	1918	1115	162	1756	1.57
186	PKC-zeta wt aa184-592 (Lot001)		10	55	96	162	-107	-1.11
187	PKMYT1 (Lot002)	CAR_09CBS-0180	35	79	96	162	-83	-0.86
188	PKN3 (Lot002)	CAR_09CBS-1290	20	136	45	162	-26	-0.58
189	PLK1 (Lot013)		50	757	200	162	595	2.98
190	PLK3 (Lot001)		30	496	248	162	334	1.35
191	PRK1 (Lot004)		25	254	274	162	92	0.34
192	PRK2 (Lot001)	INV_34557	20	133	109	162	-29	-0.27
193	PRKD2 (Lot001)	INV_34015	5	157	219	162	-5	-0.02
194	PRKG1 (Lot001)	INV_36099	12.5	61	29	162	-101	-3.48
195	PRKG2 (Lot002)	INV_273926	1	229	145	162	67	0.46
196	PRKX (Lot001)	INV_34283	10	93	48	162	-69	-1.44
197	RAF1 YDYD (Lot001)		10	68	126	162	-94	-0.75
198	RIPK2 (Lot003)		50	79	89	162	-83	-0.93
199	RIPK5 (Lot001)	INV_38724	10	495	366	162	333	0.91
200	ROCK1 (Lot001)	INV_37178	4	130	137	162	-32	-0.23
201	ROCK2 (Lot002)		2.5	202	79	162	40	0.51
202	RPS6KA1 (Lot002)	INV_386267	10	120	103	162	-42	-0.41
203	RPS6KA2 (Lot001)	INV_34468	10	400	485	162	238	0.49
204	RPS6KA3 (Lot002)	INV_37397	5	190	219	162	28	0.13
205	RPS6KA4 (Lot001)	INV_34070	50	1189	509	162	1027	2.02
206	RPS6KA5 (Lot001)	INV_33702	25	116	238	162	-46	-0.19
207	RPS6KA6 (Lot001)	INV_37496	2	209	271	162	47	0.17
208	S6K (Lot006)		50	157	140	162	-5	-0.04
209	S6K-beta (Lot002)	INV_34389	100	263	345	162	101	0.29

				A	B	C	D	
#	Kinase (ProQinase Lot #)	External Vendor Lot #	Enzyme, ng/well	Kinase activity with peptide	Kinase activity w/o peptide	Peptide background, median n=3	Kinase activity with peptide, corrected (A-C)	Activity Ratio (D/B)
210	**SAK (Lot003)**		100	2694	2346	162	**2532**	**1.08**
211	**SGK1 (Lot005)**		50	463	195	162	**301**	**1.54**
212	**SGK2 (Lot001)**	INV_34433	20	123	157	162	**-39**	**-0.25**
213	**SGK3 (Lot004)**		50	285	280	162	**123**	**0.44**
214	**SIK1 aa1-350 (Lot003)**		50	165	126	162	**3**	**0.02**
215	**SIK2 (Lot001)**		10	116	230	162	**-46**	**-0.20**
216	**SLK (Lot001)**	INV_34390	25	35	45	162	**-127**	**-2.82**
217	**SNARK (Lot001)**		200	989	1088	162	**827**	**0.76**
218	**SNK (Lot007)**		50	669	253	162	**507**	**2.00**
219	**SRPK1 (Lot001)**		25	431	240	162	**269**	**1.12**
220	**SRPK2 (Lot001)**		20	395	362	162	**233**	**0.64**
221	**STK17A (Lot001)**	INV_33789	25	1761	198	162	**1599**	**8.08**
222	**STK23 (Lot002)**	INV_285180	25	683	457	162	**521**	**1.14**
223	**STK25 (Lot001)**	INV_33163	20	160	123	162	**-2**	**-0.02**
224	**STK33 (Lot001)**	INV_36048	50	486	364	162	**324**	**0.89**
225	**STK39 (Lot001)**	CAR_08CBS-0864	50	726	992	162	**564**	**0.57**
226	**TAOK2 (Lot001)**	INV_622141	20	213	229	162	**51**	**0.22**
227	**TAOK3 (Lot005)**		50	537	180	162	**375**	**2.08**
228	**TBK1 (Lot004)**		5	141	271	162	**-21**	**-0.08**
229	**TGFB-R1 (Lot003)**		10	138	105	162	**-24**	**-0.23**
230	**TGFB-R2 (Lot001)**	CAR_09CBS-0960	10	42	71	162	**-120**	**-1.69**
231	**TLK1 (Lot002)**		15	363	369	162	**201**	**0.54**
232	**TLK2 (Lot002)**		10	369	175	162	**207**	**1.18**
233	**TSF1 (Lot002)**		25	114	90	162	**-48**	**-0.53**
234	**TSK2 (Lot002)**		25	439	346	162	**277**	**0.80**
235	**TSSK1 (Lot001)**	INV_31989	5	113	123	162	**-49**	**-0.40**
236	**TTBK1 (Lot004)**		10	109	113	162	**-53**	**-0.47**
237	**TTBK2 (Lot002)**	CAR_08CBS-1131	5	399	78	162	**237**	**3.04**
238	**TTK (Lot003)**		100	2092	1636	162	**1930**	**1.18**
239	**VRK1 (Lot001)**		50	2590	1947	162	**2428**	**1.25**
240	**VRK2 (Lot001)**	CAR_08CBS-0814	20	431	191	162	**269**	**1.41**
241	**WEE1 (Lot005)**		200	178	185	162	**16**	**0.09**
242	**WNK1 (Lot001)**		50	82	103	162	**-80**	**-0.78**
243	**WNK2 (Lot001)**	INV_35976	40	243	154	162	**81**	**0.53**
244	**WNK3 (Lot001)**	INV_36047	10	195	191	162	**33**	**0.17**
245	**ZAK (Lot001)**	INV_34603	4	332	308	162	**170**	**0.55**

all hits >2fold over background

Name	gene symbol	fold	follow up
DYRK4	DYRK4	10.50	Yes
STK17A	STK17A	8.08	Yes
CAMK2A	CAMK2A	6.23	Yes
CDK6/CycD1	CDK6	4.77	Yes
ERK1	MAPK3	4.09	Yes
MAP3K1	MAP3K1	3.63	No
LRRK2	LRRK2	3.60	No
p38-beta	MAPK11	3.24	No
TTBK2	TTBK2	3.04	No
CAMKK2	CAMKK2	3.02	No
PLK1	PLK1	2.98	Yes
PDK1	PDK1	2.80	Yes
MKK6SDTD	MAP2K6	2.67	No
PAK3	PAK3	2.28	Yes
PKC-gamma	prkcg	2.11	Yes
TAOK3	TAOK3	2.08	No
RPS6KA4	RPS6KA4	2.02	Yes
SNK	PLK2	2.00	No

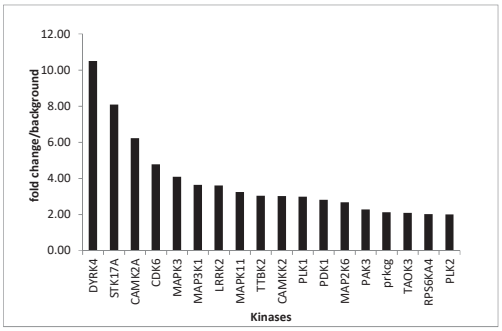

Name	gene symbol	fold	follow up
MAP3K1	MAP3K1	3.63	No
LRRK2	LRRK2	3.60	No
p38-beta	MAPK11	3.24	No
TTBK2	TTBK2	3.04	No
CAMKK2	CAMKK2	3.02	No
MKK6SDTD	MAP2K6	2.67	No
TAOK3	TAOK3	2.08	No
SNK	PLK2	2.00	No
DYRK4	DYRK4	10.50	Yes
STK17A	STK17A	8.08	Yes
CAMK2A	CAMK2A	6.23	Yes
CDK6/CycD1	CDK6	4.77	Yes
ERK1	MAPK3	4.09	Yes
PLK1	PLK1	2.98	Yes
PDK1	PDK1	2.80	Yes
PAK3	PAK3	2.28	Yes
PKC-gamma	prkcg	2.11	Yes
RPS6KA4	RPS6KA4	2.02	Yes

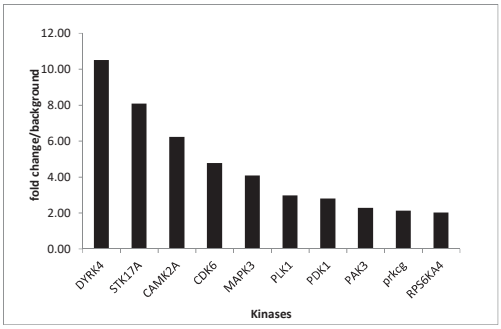

Peptide "Ykt6_WT"
Kinase activity in cpm; mean values, triplicate measurement

Enzyme	+		-		+		-		+		-		+		-	
Substrate (µM)	0.00		0.00		0.25		0.25		0.50		0.50		1.00		1.00	
Enzyme (ng/well)	Mean	SD	Mean	SD	Mean	SD	Mean	SD	Mean	SD	Mean	SD	Mean	SD	Mean	SD
CAMK2A	2	28	8	13	12	30	25	21	21	15	2	26	23	25	13	52	45
CDK6/CycD1	200	26	23	29	17	26	16	22	9	33	14	44	19	44	18	41	11
DYRK4	50	44	20	29	17	42	24	22	9	20	24	44	19	39	23	41	11
ERK1	20	36	31	29	17	18	15	22	9	34	10	44	19	33	10	41	11
PAK3	20	103	35	29	17	43	18	22	9	46	10	44	19	59	6	41	11
PDK1	20	54	19	29	17	69	32	22	9	55	20	44	19	98	18	41	11
PKC-gamma	10	30	26	29	17	29	20	22	9	51	29	44	19	28	11	41	11
PLK1	50	94	28	29	17	95	15	22	9	112	31	44	19	102	30	41	11
RPS6KA4	50	30	31	24	15	18	2	23	8	64	47	30	19	35	21	44	7
STK17A	25	52	18	24	15	44	8	23	8	50	11	30	19	41	12	44	7

Peptide "Ykt6 3E"
Kinase activity in cpm; mean values, triplicate measurement

Enzyme	+		-		+		-		+		-		+		-	
Substrate (µM)	0.00		0.00		0.25		0.25		0.50		0.50		1.00		1.00	
Enzyme (ng/well)	Mean	SD	Mean	SD	Mean	SD	Mean	SD	Mean	SD	Mean	SD	Mean	SD	Mean	SD
CAMK2A	2	46	13	21	20	41	18	22	22	58	41	28	28	27	6	22	23
CDK6/CycD1	200	23	20	51	5	40	7	31	14	16	7	27	6	19	5	29	10
DYRK4	50	30	16	51	5	31	17	31	14	40	32	27	6	24	22	29	10
ERK1	20	2	3	51	5	20	10	31	14	26	33	27	6	7	10	29	10
PAK3	20	62	41	51	5	74	21	31	14	45	5	27	6	41	5	29	10
PDK1	20	22	8	51	5	51	9	31	14	42	9	27	6	40	26	29	10
PKC-gamma	10	33	19	51	5	26	17	31	14	30	13	27	6	25	33	29	10
PLK1	50	92	27	51	5	90	14	31	14	68	17	27	6	109	28	29	10
RPS6KA4	50	61	24	49	2	26	7	24	17	47	26	20	6	42	7	26	14
STK17A	25	22	15	49	2	2	3	24	17	23	16	20	6	3	5	26	14

Supplementary Table 2

ID	Cyto	Cyto	Memb	Memb
	WT	3E	WT	3E
PSB5_HUMAN	3.643392235	2.413877657	0.690135106	0.941776798
YKT6_HUMAN	2.915966619	3.421979586	0.033567302	2.530190486
PYC_HUMAN	2.839072702	0.618967756	-0.398050854	-0.825614601
UBP5_HUMAN	2.304822063	0.408099197	-0.645703007	0.777058683
ACHB4_HUMAN	2.179009555	2.058720784	-7.791270493	0.426658983
E5RJ48_HUMAN	1.933526663	1.428893799	-0.128402523	1.030475893
H12_HUMAN	1.905356294	1.666114398	-0.119204177	-0.356461876
F6WQW2_HUMAN	1.864713183	2.586435028	-0.201419537	-0.58531555
ACACA_HUMAN	1.855418553	-0.001974453	-0.682772605	-0.354724418
F8WCF6_HUMAN	1.836899238	2.146713215	-0.284686785	0.819942203
RL21_HUMAN	1.630976194	2.192906551	2.433770913	2.771636233
IF4H_HUMAN	1.623205846	0.866814639	-1.590668437	-0.351369614
BZW1_HUMAN	1.604607022	1.874391104	0.136716125	1.156769266
H2AV_HUMAN	1.545391093	0.83793214	-0.368691475	-3.700958758
G3BP2_HUMAN	1.524303353	1.870416138	-0.301913378	-0.508181432
K7EK07_HUMAN	1.439987671	-1.031073858	0.167969706	0.310146178
M0R2B0_HUMAN	1.41994989	1.298136022	0.091872618	-0.708845678
K1C10_HUMAN	1.332185871	0.064699166	1.24459466	0.684197831
NACAM_HUMAN	1.271479132	2.081191833	-2.210557298	0.266322198
HNRPM_HUMAN	1.177926065	1.365902741	-0.175798292	0.189243485
K22E_HUMAN	1.163863794	0.402657212	0.833642165	0.472415218
E7ETK0_HUMAN	1.133054954	0.958654108	-0.578553273	-0.816597424
E7EQ69_HUMAN	1.086161742	1.790047828	-0.75951904	0.491249211
SSRP1_HUMAN	1.064422143	0.542109678	-0.626781219	-0.504474727
RL7A_HUMAN	1.013619146	1.064043625	0.85363251	0.742622953
K2C1_HUMAN	0.987825572	0.295264928	1.183045784	0.365720194
F8W727_HUMAN	0.984609388	0.914281152	0.040902936	1.233116246
K1C14_HUMAN	0.938078908	-0.475929042	1.590900082	0.536689027
J3KPX7_HUMAN	0.898397824	-0.654162352	-0.975450903	1.287666746
ELAV1_HUMAN	0.891409944	0.643370223	-0.121218834	1.129027212
M0QYS1_HUMAN	0.836966664	0.987333167	-0.328699368	-1.509521106
H2BFS_HUMAN	0.811755929	0.168784666	-0.35802173	-0.320829662
A0A087WY10_HUMAN	0.775683395	-1.217530663	-0.131980452	0.124392973
RL23A_HUMAN	0.767456196	0.328086772	0.75589067	0.186714299
FBRL_HUMAN	0.754961672	0.182198301	-0.015765097	-0.069038166
MARE1_HUMAN	0.741616403	0.583635759	-0.290245104	-0.132828957
H4_HUMAN	0.728516416	-0.000375575	-0.347696039	-0.414511901
ADT2_HUMAN	0.728233864	0.807324293	-0.493857283	0.002817047
A0A0A0MQR7_HUMAN	0.718456959	0.59887308	0.108224485	-0.356358107
H2B2D_HUMAN	0.717822622	-0.047460442	-0.416170293	-0.387909173
RS10_HUMAN	0.716498719	0.763742326	-1.421621727	0.04031001
E9PF18_HUMAN	0.713399677	0.160388979	-0.259293173	-0.140513201
H0YKD8_HUMAN	0.707636469	0.901128305	-0.181901328	-1.361477277
RDH14_HUMAN	0.646734482	0.056863274	-0.244949542	-0.067161675
C1K3N0_HUMAN	0.639636563	-0.377435032	-1.02525825	0.374004212
PRS4_HUMAN	0.632628487	-0.161227651	-1.397185159	0.350499022
ANM5_HUMAN	0.631575266	1.008234341	0.259027801	0.411854276
AHSA1_HUMAN	0.630822513	0.28135626	-0.343781042	-0.049886747
AIFM1_HUMAN	0.621954179	-0.697459779	-0.093814826	-0.787440741
E7EPB3_HUMAN	0.617746822	0.558441742	-0.847730248	-0.256998649
PSB2_HUMAN	0.604348441	0.225906012	-1.003821521	-0.970710091
PSMD2_HUMAN	0.598396624	0.497369764	-0.513818011	0.464798514
SYK_HUMAN	0.582944924	0.163134092	-1.17005648	-0.289275317
F6TLX2_HUMAN	0.57328199	0.725177418	-1.799480025	-0.167077045
H7C0C1_HUMAN	0.567248547	0.338591681	0.37302985	0.243822694
F8VPD4_HUMAN	0.559612704	-0.004104435	-0.883755262	0.587416522

J3KQ32_HUMAN	0.533662308	0.685505216	0.220961479	0.098905356
Q5JXI8_HUMAN	0.52933448	0.049809361	0.096691699	0.330815434
TBR1_HUMAN	0.493349467	0.445085652	0.221644888	0.549556022
UBC12_HUMAN	0.492369256	0.323893818	-0.529077904	1.366396327
E9PES6_HUMAN	0.481468471	0.408907301	-0.409461424	-0.245716713
ILF3_HUMAN	0.47815852	0.295423535	0.515897901	0.717899201
K7ERI7_HUMAN	0.465736903	-1.634174484	-0.062989957	0.662599568
Q5T9B7_HUMAN	0.452747206	0.889824722	0.161442994	0.240681062
B1AK88_HUMAN	0.434458432	0.210632828	-0.395244377	0.736742747
Q5HY81_HUMAN	0.420092315	0.556542646	0.343194382	1.131754322
PDIA6_HUMAN	0.413189728	-0.001900356	-0.485801035	-0.068936417
G8JLB6_HUMAN	0.409824334	0.33558438	0.079274695	0.652227618
SYVC_HUMAN	0.409195679	0.046029076	-0.467561957	-0.193791804
RS14_HUMAN	0.408912501	0.295308871	-1.030170825	-0.978365641
DNJC8_HUMAN	0.406992081	0.384801597	-0.456639068	0.509194487
A0A0U1RRM4_HUMAN	0.406613007	0.45431615	0.001340944	0.55447042
SYYC_HUMAN	0.384242702	-0.396032569	-2.520191415	1.027403655
GCN1_HUMAN	0.381883814	-0.460660326	0.768334966	0.544553518
UBAP2_HUMAN	0.381441924	1.176308259	-0.320530013	-0.683949127
AATM_HUMAN	0.372487744	0.705816044	-0.634876787	0.528424431
OAT_HUMAN	0.364179417	-0.669083935	0.317645309	0.755629675
FEN1_HUMAN	0.350450385	-0.035312598	-0.654645746	-0.319530868
E7EX53_HUMAN	0.3461319	0.368948591	1.10666813	-0.389729962
B4DJV2_HUMAN	0.338837564	0.632056088	-1.222718263	-0.289142443
PA1B2_HUMAN	0.338580745	0.194655853	0.747872085	-0.018819209
E9PHF7_HUMAN	0.32074068	-0.044269198	-0.497900578	-0.19772573
A0A087WW66_HUMAN	0.317148821	0.213203361	-1.002745342	-0.390952455
CAND1_HUMAN	0.317047687	0.435351607	0.229753106	0.444193661
F8W6I7_HUMAN	0.310846656	0.447082108	0.393848396	0.537588269
TBA1B_HUMAN	0.300149498	0.128627007	-0.254481245	0.194769421
J3KTA4_HUMAN	0.299417863	0.374458067	0.942723184	-0.310535095
I3L504_HUMAN	0.295282554	0.159902992	-1.47772244	0.065274046
RS21_HUMAN	0.294235611	-0.221192949	-0.480583753	0.035928317
PRS7_HUMAN	0.284830443	-0.119979462	-1.51209086	-2.159315522
COPG1_HUMAN	0.284782446	0.069589438	-0.728383909	-0.730872434
RL5_HUMAN	0.281625085	0.421758149	-0.270840562	1.583836495
J3QRI7_HUMAN	0.281214339	0.278974642	-0.415246795	-0.256625487
CGL_HUMAN	0.279983422	0.583246552	0.167969062	0.395698148
RL7_HUMAN	0.279399888	0.243596663	-0.31465013	0.037214954
PPIB_HUMAN	0.274673964	0.436190891	0.623828976	0.20093175
H0YA96_HUMAN	0.274605604	0.38360505	0.737579765	0.856733518
E9PLL6_HUMAN	0.269642002	-0.094604378	-0.136526454	-0.278796641
M0R261_HUMAN	0.25228787	0.085825863	-2.589688108	-2.941490526
RL4_HUMAN	0.250274848	0.47812315	-0.309472996	0.312679088
PEBP1_HUMAN	0.246963705	0.252824328	0.861655338	0.511370299
E9PD53_HUMAN	0.243259007	-0.00873305	-0.423896072	-0.166179809
PRS6B_HUMAN	0.239562842	0.052628366	0.121037694	1.005008708
RS2_HUMAN	0.224895367	0.149970188	0.187845503	1.027591888
SF3B1_HUMAN	0.21915884	-1.54158216	-0.669214558	-1.601889622
RS23_HUMAN	0.218765948	0.234801413	0.068968088	-0.0495927
UBE2K_HUMAN	0.206896239	-0.698586198	-0.244189995	0.210653343
SYQ_HUMAN	0.206146937	0.089626848	0.465038987	0.783459089
RL13_HUMAN	0.206120708	0.218850699	-0.404528883	-0.280319757
AL9A1_HUMAN	0.202913655	0.604124809	-0.166865623	0.168428758
RL11_HUMAN	0.191961001	0.154702992	-0.104570785	0.081572168
PSA7_HUMAN	0.191799508	0.198774496	1.415895372	0.961301697
DDB1_HUMAN	0.190745786	-0.016441561	-0.339232042	-0.246083276
CAP1_HUMAN	0.187150795	-0.069717356	0.12846062	0.912901189
XRCC6_HUMAN	0.185414387	0.32661336	0.580910737	0.624682966
A0A087WVQ6_HUMAN	0.180367923	0.031827663	-0.043369178	-0.557552654
MCM5_HUMAN	0.177936502	-0.527861813	0.167759598	0.420925344

MDHM_HUMAN	0.177388478	0.208625864	0.483366682	0.241203234
M0R3D6_HUMAN	0.177203505	0.032288809	-0.193804403	0.51815413
RS13_HUMAN	0.174728966	-0.078556988	-0.784124527	0.150028199
RAGP1_HUMAN	0.172025709	0.354016346	-0.155891154	-0.098205877
PYRG1_HUMAN	0.170994756	-0.982556645	-0.665119331	-0.705944827
TALDO_HUMAN	0.166349859	0.138794085	-0.441695247	0.389290593
J3QQ67_HUMAN	0.162958209	-0.119045319	-0.372456692	-0.304645765
EIF3F_HUMAN	0.150215048	-0.122878816	-0.19277577	-0.137609661
AIMP2_HUMAN	0.15016443	0.199964116	-0.32389609	0.300780599
G3V576_HUMAN	0.149765759	0.049311069	0.300849194	0.36595202
RL24_HUMAN	0.14383056	0.19162009	-1.494094449	-1.306750561
RL35_HUMAN	0.143726964	0.215621411	0.566889045	-1.518633421
MOB1A_HUMAN	0.142133155	0.081493537	-0.749154662	0.133957732
MCM6_HUMAN	0.141486442	-0.036728139	-0.364212955	0.758848859
Q1JUQ3_HUMAN	0.138885746	0.154850726	-0.60169372	-0.542799516
GDIB_HUMAN	0.135713889	-0.431168615	0.2209942	0.570787527
BAF_HUMAN	0.135588932	0.460287042	-0.805405436	-0.136325861
RS18_HUMAN	0.129507323	0.056873499	0.512383231	-0.222670322
A0A0B4J1R6_HUMAN	0.127185168	0.057926611	-1.711461852	-1.274330053
UCHL1_HUMAN	0.124208587	0.07209254	0.290276538	0.324852939
SYRC_HUMAN	0.120079854	-0.167601499	-0.559202366	0.060110846
RL8_HUMAN	0.119620511	0.034073937	-0.167077289	-0.783902436
RS6_HUMAN	0.118849935	0.154785152	0.420161493	-0.240050977
RL12_HUMAN	0.113096026	0.118232258	-0.230538342	-0.151268093
LDHA_HUMAN	0.111596645	0.003318675	-0.089538342	-0.706540012
J3QSB5_HUMAN	0.111064483	0.244120692	0.033247091	-0.275901938
RS26_HUMAN	0.110928173	0.239715671	-1.144564849	-0.258323877
PDIA3_HUMAN	0.107647212	0.51223267	-3.059391506	-2.739529654
Q96C32_HUMAN	0.105023302	-0.140836309	-0.300838479	-0.287015838
SND1_HUMAN	0.10466287	0.210444692	0.276396093	0.151596645
J3QQT2_HUMAN	0.103801068	-0.045622206	-0.429578984	-2.036203634
BIEA_HUMAN	0.100143668	0.170837734	-1.60717252	-0.953603017
E9PK47_HUMAN	0.09660361	0.494415166	0.413135057	0.34107746
Q5W0H4_HUMAN	0.0940736	-0.007585332	-0.695296965	-0.677406978
SYMC_HUMAN	0.093232668	0.068599119	-0.750524004	0.266531296
A0A087X020_HUMAN	0.09224963	0.011669885	-0.221587116	1.443769165
PSB6_HUMAN	0.089324205	-0.016859767	-0.491525746	-0.147164376
1433B_HUMAN	0.089298005	0.173400376	-0.440424502	0.158562787
A8MUA9_HUMAN	0.086710594	-0.111700572	0.161232655	0.253631298
RL23_HUMAN	0.08292879	0.202322689	0.127977359	0.174480356
RS25_HUMAN	0.078589814	0.068105711	-0.276107982	0.080286773
H0YAG8_HUMAN	0.076600573	-0.394658339	1.003634	2.797469992
LA_HUMAN	0.075440093	0.489789551	0.461541852	-0.144396954
APEX1_HUMAN	0.068805293	0.024993279	-1.787031376	-0.369650513
E9PK25_HUMAN	0.067002018	0.087441534	0.349240813	-0.00100417
GSTO1_HUMAN	0.062475728	0.065832628	-0.440242499	0.317376388
SAHH_HUMAN	0.061753923	0.184262508	0.314668407	0.775136846
RS27_HUMAN	0.06130115	0.058520971	0.032026952	0.348822034
1433E_HUMAN	0.058354018	0.059688366	-1.809755837	-0.108916643
K7EJB9_HUMAN	0.056915609	1.127688306	0.808980758	0.565133314
FNTA_HUMAN	0.055178518	2.579198342	-0.249145739	0.458684829
H7C2W9_HUMAN	0.05437847	0.436141475	0.886036686	1.283351735
RL6_HUMAN	0.04981943	0.134318567	0.019444028	0.086657437
IF4A1_HUMAN	0.044976562	-0.003542	0.04772537	0.296120758
C9J592_HUMAN	0.043601373	-0.165695169	-0.283954114	0.309659679
A0A024RA52_HUMAN	0.041149587	0.035168191	-1.076232237	-0.670799301
E5RI99_HUMAN	0.041009673	-0.297823568	0.415077949	1.442996205
HINT1_HUMAN	0.033004507	0.059001487	-0.315365673	2.74535611
PRPS1_HUMAN	0.032523406	-0.025922461	0.471464401	0.520236642
UBA1_HUMAN	0.030428349	-0.002071005	0.028851208	0.104146314
TPIS_HUMAN	0.028859595	0.080255725	0.345953333	0.291441303

H0Y5B4_HUMAN	0.025724297	0.52239229	-0.344452207	-0.120987862
CND1_HUMAN	0.024786273	-0.259002011	-0.234178776	0.924613043
Q32Q12_HUMAN	0.024666913	-0.199392419	0.022051398	0.074287735
KCRB_HUMAN	0.024371734	0.015735716	-0.859885508	0.159772327
RD23B_HUMAN	0.022191288	-0.220512155	-0.173763445	0.317960416
M0QZC5_HUMAN	0.022120672	0.307551073	0.931188172	0.770520537
RL34_HUMAN	0.020802509	0.338122881	-0.541090285	-0.006340203
B4DY09_HUMAN	0.019946772	0.371324466	-0.129492685	0.039783805
E9PFT6_HUMAN	0.01900142	-0.060856971	-0.657019022	-0.262848699
A0A0D9SG12_HUMAN	0.014501322	-0.143904134	1.438553454	-0.224341528
RS3_HUMAN	0.01240675	0.132543483	-0.416692679	0.683123215
HNRPU_HUMAN	0.01098035	0.181267176	-0.573849773	-0.302759789
J3QR09_HUMAN	0.008057671	0.182600088	0.54248746	0.92003216
PA2G4_HUMAN	0.006956902	-0.182517004	-0.564908585	-0.164473043
PSA5_HUMAN	0.005985042	-0.000192349	-0.678014954	-0.488139467
IF4A3_HUMAN	0.003740331	0.035904043	0.575267967	0.531149163
C1QBP_HUMAN	0.002755925	0.548320979	-0.131891892	-0.275130458
ATPA_HUMAN	0.000696417	0.420344855	-0.199494949	0.031934049
RAP1A_HUMAN	-0.009437441	0.10636284	-0.542957706	-0.787076425
PUR2_HUMAN	-0.01008044	-0.287592066	-0.170523132	0.742177117
RL27_HUMAN	-0.015586649	0.754710557	0.545080016	0.711266472
RS19_HUMAN	-0.019300565	0.133722812	-0.23870432	-0.022352729
ATPB_HUMAN	-0.023527233	-0.530650026	-0.197423535	-0.141930267
LDHB_HUMAN	-0.024186026	-0.010253867	0.56487805	0.549052354
PCNA_HUMAN	-0.028319559	0.132537596	-0.753903885	-0.571873659
HPRT_HUMAN	-0.031455074	0.205107734	1.06324704	0.745979061
MDHC_HUMAN	-0.032067705	0.072806858	0.019295585	0.471208697
PARK7_HUMAN	-0.034175138	0.256586915	-0.033033639	0.013800483
TBA1A_HUMAN	-0.035022115	0.004700343	-0.698134843	-0.305324268
CAH2_HUMAN	-0.036679421	-0.020110313	0.380434102	0.014523351
RS4X_HUMAN	-0.038269578	0.095718239	0.531144865	-0.001711891
SSBP_HUMAN	-0.042311249	-0.137365567	0.046902498	0.538445772
J3KR24_HUMAN	-0.049505238	-0.051943982	-0.140633272	-0.084164295
J3KQ18_HUMAN	-0.050192289	-0.039348515	0.017048181	0.378387737
SPG20_HUMAN	-0.050585044	-0.306343996	-0.981226834	-0.096457035
F5GX11_HUMAN	-0.05082505	-0.101466006	-0.033064367	0.091219095
APT_HUMAN	-0.055526516	-0.10857529	-1.541853038	0.04948489
HMGB1_HUMAN	-0.055640893	-0.074938541	0.036607264	0.552811278
LGUL_HUMAN	-0.05931378	-0.160942861	0.099248826	-0.747602652
Q5JR95_HUMAN	-0.059392325	-0.221344424	0.07519873	0.522389966
ENOA_HUMAN	-0.060245038	-0.010447207	1.830100132	0.617767342
MYH9_HUMAN	-0.063842059	-0.121594087	-0.874428833	-0.105847144
RINI_HUMAN	-0.064123582	0.633841068	0.12515209	0.019812276
J3KPS3_HUMAN	-0.064873164	0.129417695	0.525412876	0.385946803
RHOA_HUMAN	-0.065083049	-0.138362754	-0.072273926	-0.393707554
RTCB_HUMAN	-0.066588636	-0.251853943	-0.512980491	-0.590478429
A0A0C4DFV9_HUMAN	-0.069726282	0.077278155	0.130006553	0.402878942
RL10A_HUMAN	-0.071521219	0.058987185	0.289567212	-0.598381209
PROF1_HUMAN	-0.072746589	0.130813187	-0.335569704	0.62076848
GLYM_HUMAN	-0.073682598	-0.11720892	0.32779799	0.676700054
PPIA_HUMAN	-0.076611693	0.098810855	0.554360262	0.769430215
E9PRY8_HUMAN	-0.076737283	-0.138227595	1.351541365	0.222606383
SERC_HUMAN	-0.081057805	0.04199665	0.344909089	-0.140382377
H3BRU6_HUMAN	-0.085536177	-0.012343377	-0.358129465	0.283097997
RAB5C_HUMAN	-0.089445798	-0.082884793	-0.242387182	0.146947957
RS7_HUMAN	-0.091355311	0.101576047	-1.11746596	-0.137148457
PGK1_HUMAN	-0.092142741	-0.161529254	-0.053520417	-0.062383914
RS12_HUMAN	-0.092945545	-0.098257123	-0.038665923	-0.271752335
H0Y711_HUMAN	-0.096235136	0.112291434	-0.879134282	0.490825379
G3V5Z7_HUMAN	-0.099691984	-0.574156745	0.096908056	0.329374141
ACTG_HUMAN	-0.10016194	0.012634925	0.066745784	0.021029372

J3KQE5_HUMAN	-0.100370094	0.013913562	2.000477429	1.963974424
K2C5_HUMAN	-0.100378991	0.740577481	-0.480903561	0.045510925
MIF_HUMAN	-0.102243733	-0.202750873	0.201793117	-0.262449871
PFKAP_HUMAN	-0.104743338	-0.726620259	-0.175653801	0.561499405
SP16H_HUMAN	-0.105686561	0.321471654	0.011814356	0.564076432
1433G_HUMAN	-0.10619583	-0.185018395	-1.195911704	-0.758799859
AATC_HUMAN	-0.107254298	0.323959567	-0.257704136	0.522115938
F8W1A4_HUMAN	-0.11128203	-0.057711766	0.434965359	-0.01444661
TPM3_HUMAN	-0.112177805	0.020149702	0.975829706	0.477891177
K7ES02_HUMAN	-0.112403449	-1.350458098	-0.363803332	-0.205484219
PZP_HUMAN	-0.11278292	0.092676813	0.843287449	0.676630721
SYAC_HUMAN	-0.113562575	-0.357199325	-0.221646936	0.359965611
ENPL_HUMAN	-0.115530202	0.023944577	-0.04972998	-0.200015117
B0YJC4_HUMAN	-0.117529129	-0.291908047	-0.190726784	-0.103430777
EIF3A_HUMAN	-0.121247339	-0.163343307	0.330607339	0.265838399
HNRPK_HUMAN	-0.121358827	0.034664598	0.450019208	0.276356852
UB2L3_HUMAN	-0.121759282	0.0080751	1.027878962	0.207922926
NUCL_HUMAN	-0.126930053	-0.257192164	0.354802754	-0.1213661
ACTN4_HUMAN	-0.12774588	0.459122532	0.065278226	-0.035295061
XPO5_HUMAN	-0.129753535	-0.228111289	-0.969408095	-0.207922811
PRDX2_HUMAN	-0.130186208	-0.184505486	0.815992741	0.767119439
SYDC_HUMAN	-0.132683387	-0.345557591	0.783541089	0.530980065
DX39B_HUMAN	-0.13446151	0.105453654	0.460108684	0.988461582
MCCB_HUMAN	-0.137343904	-0.141184021	-0.365756419	-0.164280845
SYNC_HUMAN	-0.138547001	0.116480054	-1.357090631	0.265936335
CDC37_HUMAN	-0.138566552	-0.131730366	1.147933893	0.642099461
ACLY_HUMAN	-0.144323214	-0.068586717	-0.798674159	-0.715578613
M0R210_HUMAN	-0.144829229	0.115297808	-0.643506266	-0.787160116
H0Y4R1_HUMAN	-0.149841716	-0.009588031	-1.03264988	-0.264525784
E5RGA2_HUMAN	-0.151364215	0.012828121	0.36577162	0.511613948
HS90B_HUMAN	-0.153075387	-0.058485211	0.284537448	-0.397488472
IF2A_HUMAN	-0.162877193	0.638522397	-0.052749497	0.629636713
H7BY58_HUMAN	-0.162947561	-0.126429164	-0.131308333	0.137432808
TCP4_HUMAN	-0.165467685	-0.399336051	-0.144920314	0.626865518
RS28_HUMAN	-0.168853544	-1.65108153	0.082206181	-0.191244607
PRKDC_HUMAN	-0.169805615	0.205736072	-0.170569257	0.323659438
RL3_HUMAN	-0.170818118	-0.184063555	-0.104380126	-0.536194459
R4GNH3_HUMAN	-0.171010038	-0.373629137	-0.200927536	-0.237922197
G3P_HUMAN	-0.175568242	0.102173635	0.272679952	-0.064806051
C9JPM4_HUMAN	-0.177562057	0.512819476	-0.455767175	0.161858394
IPO4_HUMAN	-0.178678411	-0.392742914	-0.584631073	0.261133623
RFA1_HUMAN	-0.179752064	0.241797292	-0.300718491	-0.695715637
EF1G_HUMAN	-0.180789158	-0.147914332	-0.468243194	-0.005493582
ANT3_HUMAN	-0.182823041	-0.04707288	-0.220486432	0.419566232
MAT2B_HUMAN	-0.183503671	-0.66435283	0.629532612	-0.037770243
B0QY89_HUMAN	-0.195136511	-0.524964274	-0.485929122	0.220987908
RL35A_HUMAN	-0.196234351	-0.663770729	-1.252714038	2.44885408
HS90A_HUMAN	-0.198574041	-0.178140994	0.071732946	-0.033267967
TXND5_HUMAN	-0.200183572	-0.009783613	-1.211813324	-0.499819565
E7EX29_HUMAN	-0.201897736	-0.316200619	0.015589242	-0.40417548
CH10_HUMAN	-0.205078723	-0.05196243	0.30369671	-0.489298407
PSB1_HUMAN	-0.205174355	-0.137974628	-0.672741568	-0.787833237
EF1A3_HUMAN	-0.2053308	-0.139208453	0.240151329	0.036924071
HSP7C_HUMAN	-0.211945293	-0.196691961	-0.221402305	-0.228864881
SODC_HUMAN	-0.212243054	0.440408961	-0.333019061	-0.007499153
A0A024R4M0_HUMAN	-0.21320292	-0.305532395	0.361897953	-0.10719992
E7ER44_HUMAN	-0.213738605	-0.881767101	-0.733033355	-0.67575632
RACK1_HUMAN	-0.215084264	-0.07689946	0.717134147	-0.354352261
IMB1_HUMAN	-0.215326242	-0.279472728	-0.608067922	-0.042656125
GRP78_HUMAN	-0.219942946	-0.161503974	-0.392705581	0.583343526
RS20_HUMAN	-0.225274194	0.024806745	-0.650108838	-1.559194266

CALX_HUMAN	-0.227352162	-0.013600672	0.578606676	1.106166303
TIF1B_HUMAN	-0.231467924	0.116560253	-0.061513416	-0.469953534
PRDX6_HUMAN	-0.231859519	-0.188995154	-0.391614107	0.063392247
STMN1_HUMAN	-0.233276236	-0.328542356	-0.207608808	0.593447164
CNBP_HUMAN	-0.235722001	-0.292717487	-0.086241681	-0.089018752
PSD11_HUMAN	-0.236642906	-0.531236481	-0.365169475	0.002531479
PRS8_HUMAN	-0.239348651	0.108424899	-0.068588818	-0.930746799
C9J9K3_HUMAN	-0.239380792	0.00980547	0.443756303	1.403780404
IPYR_HUMAN	-0.239540561	-0.580621854	0.538607649	0.078227719
MCM3_HUMAN	-0.239998464	-0.231909553	-0.357391485	0.215754209
SYWC_HUMAN	-0.241149885	-0.160459922	3.785741054	3.95996639
XRCC5_HUMAN	-0.241701255	-0.318198569	0.240403491	0.676383184
THIO_HUMAN	-0.244034239	-0.088170782	0.334296731	0.567197556
A0A024QZP7_HUMAN	-0.246321707	-0.105693367	-0.650580063	-0.020181286
PRDX1_HUMAN	-0.247047662	-0.164532751	-0.219924821	-0.241391391
PCBP1_HUMAN	-0.248241467	0.05447084	-0.431947265	-0.233027596
DCTP1_HUMAN	-0.259537915	0.118038012	0	-1.601001755
H0YN26_HUMAN	-0.262677678	-0.025178547	-0.103509131	0.989051497
PSMD3_HUMAN	-0.263515399	-0.547966034	-0.509505559	0.289506914
A2MG_HUMAN	-0.265407807	-0.130773493	0.111218681	0.775175418
PSA4_HUMAN	-0.270301006	0.197040493	1.582831196	1.542776195
DYHC1_HUMAN	-0.272484283	-0.191386648	0.392642693	0.228876401
MYH10_HUMAN	-0.273327754	-1.059545336	1.464921139	0.90340336
H0Y8C6_HUMAN	-0.274433786	0.087650802	-0.149774379	-0.051098589
CH60_HUMAN	-0.277822851	-0.262686601	-0.102807752	-0.160710224
ROA2_HUMAN	-0.278360125	-0.275357932	1.03134618	0.669568741
A0A0B4J1W3_HUMAN	-0.280176223	-0.298002093	-1.111226872	-0.590441634
EF1B_HUMAN	-0.283171019	-0.053255429	0.074515139	0.463279086
H7C2I1_HUMAN	-0.290610039	-0.289137075	0.795739815	0.38992662
XPO2_HUMAN	-0.292040275	-0.101410953	-0.511900763	1.289729266
PSDE_HUMAN	-0.292085268	-0.121165421	0.510987122	1.311409764
E9PDR0_HUMAN	-0.292695268	-0.036950348	-0.211002602	-0.138762228
SYEP_HUMAN	-0.297617847	-0.124428567	-0.303165906	-0.7686935
NDKA_HUMAN	-0.298057362	-0.279560247	-0.006328208	0.780050775
PEPD_HUMAN	-0.298542171	-0.417865822	-0.508357124	0.363521884
EFTU_HUMAN	-0.302608914	0.022390873	-0.199720137	0.469186048
RS15A_HUMAN	-0.303516334	-0.311658106	0.064673839	0.445362159
E9PKT8_HUMAN	-0.308497998	-0.115191756	0.015260711	0.96535939
TCPQ_HUMAN	-0.308902719	-0.421847326	0.330429457	0.822687977
J3KR44_HUMAN	-0.310516466	-0.308123445	-0.051710562	2.18233026
PARP1_HUMAN	-0.316341062	0.181473406	0.357900234	0.686104073
SYG_HUMAN	-0.317948425	-0.297007162	1.13595924	0.302215846
A0A087WTP3_HUMAN	-0.319503555	-0.04628251	-0.012478557	-0.189286509
ACTZ_HUMAN	-0.321869276	-1.352450236	-0.349741173	-1.056537198
A0A0G2JIW1_HUMAN	-0.322980571	-0.173497762	-0.377861982	-0.642591368
RAB1A_HUMAN	-0.325183057	-0.165789197	0.468910285	0.560530443
FLNB_HUMAN	-0.327512866	-0.423401956	-0.165665457	0.721000041
EF2_HUMAN	-0.328606832	-0.058246558	-0.014740223	0.196084818
A0A087X0K1_HUMAN	-0.330135278	-1.033047814	0.100616451	-0.601145971
EIF3D_HUMAN	-0.332352297	-0.39416145	-0.657214225	-0.224022456
TEX36_HUMAN	-0.337609451	-0.104707933	-0.774050213	-0.078022938
RS3A_HUMAN	-0.342281175	0.299503377	-0.223017774	-0.552906506
ARL3_HUMAN	-0.343304598	-1.15652783	0.361248105	0.266293363
H2AX_HUMAN	-0.352280482	0.266965639	-1.055610454	0.113200458
FABP5_HUMAN	-0.354301625	0.331649032	0.448258479	0.275427798
NPM_HUMAN	-0.355222178	-0.11289767	-0.224118341	0.109633228
HSP74_HUMAN	-0.358790399	-0.085432973	0.238286503	0.744705471
PDIA1_HUMAN	-0.362184396	0.017271665	0.356066236	-0.038485714
RLA0_HUMAN	-0.365766402	-0.002147263	0.105541898	0.183330772
ETFB_HUMAN	-0.373835086	-0.097440806	0.105601354	-0.344560921
ESTD_HUMAN	-0.377467673	0.081531956	-0.139470047	-0.027319799

FETUA_HUMAN	-0.384614261	-0.088691173	-3.858509117	-3.766034325
ARF1_HUMAN	-0.388894388	-0.035068282	0.77173747	-0.153724834
E9PR30_HUMAN	-0.390100695	-0.436695336	-1.499579531	-0.333183911
1433T_HUMAN	-0.39597342	-0.163838631	0.453108268	0.829567922
SERA_HUMAN	-0.396682844	-0.039878164	0.388047044	0.527216158
PGAM1_HUMAN	-0.40641867	-0.186123732	0.309450356	0.076249572
TAGL2_HUMAN	-0.411149953	0.543150873	-0.179166298	-0.111593205
EIF3B_HUMAN	-0.416764229	0.026075637	-0.376599942	-0.212468829
H0Y9V9_HUMAN	-0.422676171	-0.052301312	-0.904384088	-2.796377393
H0Y8E6_HUMAN	-0.429379685	0.709915513	-1.56837755	-0.489813358
SYLC_HUMAN	-0.430193016	0.262496997	-0.182959414	-0.520769051
XPO1_HUMAN	-0.437687318	-0.171509562	0.894029418	1.03950637
PSA3_HUMAN	-0.443811576	-0.27852823	-0.708400372	1.641688007
RUVB1_HUMAN	-0.444561275	-0.390412384	-0.013510704	0.433703695
AN32B_HUMAN	-0.4490547	-0.979966146	-0.158506075	-0.104276199
NADC_HUMAN	-0.45917854	-0.715644973	-0.258838062	-0.072084447
PSD12_HUMAN	-0.459278891	-2.779304277	-1.140811674	-0.481700053
PRP19_HUMAN	-0.460303777	0.15267894	-0.89000042	0.076444069
UBE2N_HUMAN	-0.462067487	-0.528248817	-0.365590155	-0.332098582
A6NFX8_HUMAN	-0.462444561	-0.042028017	0.958638786	0.351830262
Q5SQT8_HUMAN	-0.465700643	-0.460234628	0.804443237	0.057932827
6PGD_HUMAN	-0.48063745	-0.005409912	0.107596997	0.418492322
ADT3_HUMAN	-0.481546982	-0.396862626	-0.464623395	-0.106100786
NASP_HUMAN	-0.489357121	-0.108686247	-0.404104021	-0.281773107
H0YLA2_HUMAN	-0.497475879	-0.958826463	0.435187027	0.996104993
M0R0R2_HUMAN	-0.497622655	-0.256813013	-0.654147319	-0.811792865
PGM1_HUMAN	-0.501567176	-0.101803387	1.38417385	0.713169229
A0A0A0MSQ0_HUMAN	-0.503063584	-0.339021833	0.26548475	0.179780987
G6PD_HUMAN	-0.505835962	-0.23959011	0.783781555	0.97994386
E9PLT0_HUMAN	-0.508137741	-0.71021251	-1.241174846	-1.045797574
DC1I2_HUMAN	-0.512670853	-1.156354627	0.863368025	-1.42349706
SMD1_HUMAN	-0.51525138	-0.33623488	0.08171379	-0.147428213
KPYM_HUMAN	-0.520604485	-0.091335982	0.112860499	0.089036377
F5H796_HUMAN	-0.521934642	-0.12676176	0.109583197	-0.14225692
GUAA_HUMAN	-0.522071616	-2.353383232	0.538440035	0.803531642
PSME3_HUMAN	-0.523202251	-0.691342662	-0.757821001	-0.63721664
COR1C_HUMAN	-0.529380517	-0.235553396	0.010167044	0.586837124
C1TC_HUMAN	-0.542115234	-0.327977296	-0.47672455	0.386954436
DDX1_HUMAN	-0.551027914	-0.924272824	-1.186671206	-0.93144281
E7EQR4_HUMAN	-0.562182712	-0.273712082	-0.312561181	-0.606896773
H0YLU7_HUMAN	-0.56550106	0.066437791	0.037252352	0.010911819
K7EL40_HUMAN	-0.583367877	-2.414073427	0.67872493	0.321449304
A0A087WYT3_HUMAN	-0.587427562	-0.538486904	-0.38748771	0.325177281
LMNB1_HUMAN	-0.592782065	0.757845068	-0.323111938	-0.662405909
AIMP1_HUMAN	-0.600087063	-0.576624733	-0.506726978	1.043806734
ANXA5_HUMAN	-0.604665143	-0.044283578	0.68207336	1.049315331
PUR6_HUMAN	-0.607863937	-0.404098963	-0.739832191	-0.281270013
FKBP4_HUMAN	-0.611314873	-0.032942716	0.271303162	-0.346979651
CYBP_HUMAN	-0.611688833	0.020501306	-0.78320485	0.593252871
H0YA22_HUMAN	-0.613220493	0.438929779	-0.014702357	-1.265392076
Q5TEJ7_HUMAN	-0.639348685	0.019297379	-0.499946247	0.459274598
RB11B_HUMAN	-0.643824798	-0.691250859	-0.619719126	-0.827895587
TBB5_HUMAN	-0.644231389	-0.356617715	-0.340315996	-0.260970186
GRP75_HUMAN	-0.652161383	-0.213944813	-0.320100942	0.415291591
STRAP_HUMAN	-0.658802994	-1.105463913	0.213188951	1.045649854
STIP1_HUMAN	-0.660688811	-0.320473753	-0.492622226	0.260704584
E9PMD7_HUMAN	-0.663939348	-0.646382868	-0.566331485	-0.4798469
J3QQX2_HUMAN	-0.66501629	-1.168692344	-0.41135858	0.514824651
KINH_HUMAN	-0.669369587	-0.79084778	0.036313493	0.356519201
FLNA_HUMAN	-0.671797672	-0.623504489	0.346446359	0.337401368
TBB4B_HUMAN	-0.67718558	-0.368613207	-1.801356413	-0.114249236

A0A087X2I1_HUMAN	-0.685696227	-0.694581712	-1.368432236	0.063374072
SMC2_HUMAN	-0.688451116	-0.557456554	0.079063068	0.17252243
ALDR_HUMAN	-0.690298595	0.231861061	0.744186199	0.5348833
GANAB_HUMAN	-0.6953509	-0.655009995	0.21596124	1.489742049
H0YNW5_HUMAN	-0.697825788	-0.596615203	-0.934202082	-0.335373595
E9PC52_HUMAN	-0.708854075	-0.626423062	-3.539930819	0.10673851
TLN1_HUMAN	-0.71125011	-0.334577035	0.831912184	0.836748751
IPO7_HUMAN	-0.713569543	-0.249709616	-0.587428462	-0.425815936
RUVB2_HUMAN	-0.729246324	-0.664948164	-0.181615655	-0.528751124
PPAC_HUMAN	-0.73207135	-0.843807114	0.233411291	-0.084148878
DHX9_HUMAN	-0.742836279	-0.17609205	-0.800036513	-0.590335166
TCPB_HUMAN	-0.745740528	-0.642175393	-0.487998208	-0.427572059
HS105_HUMAN	-0.751023946	-0.363694302	0.812235624	0.933557377
A0A0A0MTS2_HUMAN	-0.764721248	-0.197304427	-0.311835453	0.723889609
E9PGM1_HUMAN	-0.766572314	-0.553894928	-0.184895704	-0.354193918
K7EN20_HUMAN	-0.769345515	-0.54935636	-0.498546222	0.467680822
COR1B_HUMAN	-0.770630299	-0.562054102	-0.591645818	-0.77903205
TCPG_HUMAN	-0.786917962	-0.727083187	-1.255626472	-0.644152204
PDLI1_HUMAN	-0.792193235	0.240744886	-0.716130566	0.753029386
FAS_HUMAN	-0.802356836	-0.621686081	-1.070616857	-0.511831207
SFPQ_HUMAN	-0.816440645	0.018612056	0.467126111	0.556616026
SF3B3_HUMAN	-0.818756905	0.009139743	-0.721603387	-0.806580602
VINC_HUMAN	-0.836976625	-0.353624908	-1.089599419	0.343100837
TCPH_HUMAN	-0.840329719	-0.863717945	-0.099012969	0.306614207
TCPZ_HUMAN	-0.841024878	-0.781405395	-0.24896335	-0.324721845
TCPD_HUMAN	-0.850542675	-0.662836703	-0.235248842	0.275676578
TCPE_HUMAN	-0.851795853	-0.62023881	-0.223258691	-0.163183287
FNTB_HUMAN	-0.852104534	1.688824469	-0.26967378	-0.415204312
IMA1_HUMAN	-0.926998371	0.172193403	-0.639281681	-0.040688928
HSPB1_HUMAN	-0.930454465	0.188708185	-0.0367759	0.281738326
GLRX3_HUMAN	-0.943046368	-0.023881881	-0.033367152	-0.222941645
DCTN2_HUMAN	-0.959693108	-0.940436747	0.192596217	-0.318661937
CAZA1_HUMAN	-0.965371887	-0.299200109	-0.960084123	-0.882991729
PSD13_HUMAN	-1.00715283	-0.147859546	-0.318924027	1.447843347
GSTP1_HUMAN	-1.013416488	-0.393753321	0.271368563	1.373405192
AT5F1_HUMAN	-1.070899059	-0.553558192	-0.036135914	-0.101609221
TERA_HUMAN	-1.071114557	-0.695199501	-0.284509177	-0.32592746
TCPA_HUMAN	-1.071786698	-0.817794095	-0.298613996	0.025232471
SMD3_HUMAN	-1.096473068	-0.142218958	0.435458333	0.410252709
NUDC_HUMAN	-1.124800519	-0.672438332	-0.22148855	-0.388326704
1433F_HUMAN	-1.132611279	0.316749664	0.410346005	0.611160673
ARP3B_HUMAN	-1.156989453	-1.074762074	-0.171674137	0.288411191
F8VVL1_HUMAN	-1.171515406	-0.092875966	0.422256434	0.11259603
IMA3_HUMAN	-1.205009821	-0.245976296	-0.836297464	0.323483233
Q5T4U5_HUMAN	-1.217657541	-1.318180748	-0.108490606	0.163468183
SYHC_HUMAN	-1.25342523	-0.698311759	0.133515691	-0.091544686
PDIA4_HUMAN	-1.324377524	-0.849164302	0.41407411	-0.347944697
PAIRB_HUMAN	-1.433967418	-2.566205612	-2.458242386	-1.865739184
D6RGI3_HUMAN	-1.542140827	-0.648961205	-0.1271926	-0.692177152
HUWE1_HUMAN	-1.672188851	-0.898304697	0.366684741	0.218047535
CBS_HUMAN	-1.839800773	-0.614840379	0.082136538	-0.15166685
G3V1Q4_HUMAN	-1.925667415	-0.386422127	-0.396608162	-0.925999024
E9PPJ0_HUMAN	-1.971331922	-1.09104588	-0.357410572	-0.579317731
D6RF35_HUMAN	-2.323488327	-2.927153792	-0.771420032	0.605069605
IF2GL_HUMAN	-2.499611894	-0.407011914	1.483082512	-0.112335445
SIAS_HUMAN	-2.875655937	-0.876590287	-0.391022603	2.337408799
DDX21_HUMAN	-2.901722899	-2.864221537	-1.196062306	-1.020188266
SRP68_HUMAN	-3.48789117	-0.072987203	-0.373512495	1.594721881
ECHM_HUMAN	-3.841667817	-3.993557317	4.145855135	0.852436703
2AAA_HUMAN	-4.061098586	-0.259084127	-0.547765802	-0.63668686

Ykt6-WT (Cytoplasmic Fraction)	Ykt6-WT (Membrane Fraction)	Common Proteins
PYC_HUMAN	ECHM_HUMAN	PSB5_HUMAN
UBP5_HUMAN	SYWC_HUMAN	YKT6_HUMAN
ACHB4_HUMAN	J3KQE5_HUMAN	RL21_HUMAN
E5RJ48_HUMAN	ENOA_HUMAN	BZW1_HUMAN
H12_HUMAN	PSA4_HUMAN	K7EK07_HUMAN
F6WQW2_HUMAN	IF2GL_HUMAN	M0R2B0_HUMAN
ACACA_HUMAN	MYH10_HUMAN	K1C10_HUMAN
F8WCF6_HUMAN	PGM1_HUMAN	K22E_HUMAN
IF4H_HUMAN	E9PRY8_HUMAN	RL7A_HUMAN
H2AV_HUMAN	CDC37_HUMAN	K2C1_HUMAN
G3BP2_HUMAN	SYG_HUMAN	F8W727_HUMAN
NACAM_HUMAN	HPRT_HUMAN	K1C14_HUMAN
HNRPM_HUMAN	ROA2_HUMAN	RL23A_HUMAN
E7ETK0_HUMAN	UB2L3_HUMAN	A0A0A0MQR7_HUMAN
E7EQ69_HUMAN	TPM3_HUMAN	ANM5_HUMAN
SSRP1_HUMAN	A6NFX8_HUMAN	H7C0C1_HUMAN
J3KPX7_HUMAN	XPO1_HUMAN	J3KQ32_HUMAN
ELAV1_HUMAN	DC1I2_HUMAN	Q5JXI8_HUMAN
M0QYS1_HUMAN	PZP_HUMAN	TBR1_HUMAN
H2BFS_HUMAN	TLN1_HUMAN	ILF3_HUMAN
A0A087WY10_HUMAN	PRDX2_HUMAN	Q5T9B7_HUMAN
FBRL_HUMAN	HS105_HUMAN	Q5HY81_HUMAN
MARE1_HUMAN	Q5SQT8_HUMAN	G8JLB6_HUMAN
H4_HUMAN	H7C2I1_HUMAN	A0A0U1RRM4_HUMAN
ADT2_HUMAN	G6PD_HUMAN	GCN1_HUMAN
H2B2D_HUMAN	SYDC_HUMAN	OAT_HUMAN
RS10_HUMAN	ARF1_HUMAN	E7EX53_HUMAN
E9PF18_HUMAN	ALDR_HUMAN	PA1B2_HUMAN
H0YKD8_HUMAN	RACK1_HUMAN	CAND1_HUMAN
RDH14_HUMAN	ANXA5_HUMAN	F8W6I7_HUMAN
C1K3N0_HUMAN	K7EL40_HUMAN	J3KTA4_HUMAN
PRS4_HUMAN	MAT2B_HUMAN	CGL_HUMAN
AHSA1_HUMAN	CALX_HUMAN	PPIB_HUMAN
AIFM1_HUMAN	LDHB_HUMAN	H0YA96_HUMAN
E7EPB3_HUMAN	PPIA_HUMAN	PEBP1_HUMAN
PSB2_HUMAN	RL27_HUMAN	PRS6B_HUMAN
PSMD2_HUMAN	IPYR_HUMAN	RS2_HUMAN
SYK_HUMAN	GUAA_HUMAN	RS23_HUMAN
F6TLX2_HUMAN	RS4X_HUMAN	SYQ_HUMAN
F8VPD4_HUMAN	J3KPS3_HUMAN	PSA7_HUMAN
UBC12_HUMAN	PSDE_HUMAN	CAP1_HUMAN
E9PES6_HUMAN	RAB1A_HUMAN	XRCC6_HUMAN
K7ERI7_HUMAN	SFPQ_HUMAN	MCM5_HUMAN

B1AK88_HUMAN	DX39B_HUMAN	MDHM_HUMAN
PDIA6_HUMAN	1433T_HUMAN	G3V576_HUMAN
SYVC_HUMAN	HNRPK_HUMAN	RL35_HUMAN
RS14_HUMAN	FABP5_HUMAN	GDIB_HUMAN
DNJC8_HUMAN	C9J9K3_HUMAN	RS18_HUMAN
SYYC_HUMAN	SMD3_HUMAN	UCHL1_HUMAN
UBAP2_HUMAN	H0YLA2_HUMAN	RS6_HUMAN
AATM_HUMAN	F8W1A4_HUMAN	J3QSB5_HUMAN
FEN1_HUMAN	F8VVL1_HUMAN	SND1_HUMAN
B4DJV2_HUMAN	PDIA4_HUMAN	E9PK47_HUMAN
E9PHF7_HUMAN	1433F_HUMAN	A8MUA9_HUMAN
A0A087WW66_HUMAN	DYHC1_HUMAN	RL23_HUMAN
TBA1B_HUMAN	SERA_HUMAN	H0YAG8_HUMAN
I3L504_HUMAN	CAH2_HUMAN	LA_HUMAN
RS21_HUMAN	HUWE1_HUMAN	E9PK25_HUMAN
PRS7_HUMAN	E5RGA2_HUMAN	SAHH_HUMAN
COPG1_HUMAN	A0A024R4M0_HUMAN	RS27_HUMAN
RL5_HUMAN	ARL3_HUMAN	K7EJB9_HUMAN
J3QRI7_HUMAN	PARP1_HUMAN	H7C2W9_HUMAN
RL7_HUMAN	PDIA1_HUMAN	RL6_HUMAN
E9PLL6_HUMAN	NUCL_HUMAN	IF4A1_HUMAN
M0R261_HUMAN	FLNA_HUMAN	E5RI99_HUMAN
RL4_HUMAN	SERC_HUMAN	PRPS1_HUMAN
E9PD53_HUMAN	THIO_HUMAN	UBA1_HUMAN
SF3B1_HUMAN	EIF3A_HUMAN	TPIS_HUMAN
UBE2K_HUMAN	TCPQ_HUMAN	Q32Q12_HUMAN
RL13_HUMAN	GLYM_HUMAN	M0QZC5_HUMAN
AL9A1_HUMAN	PGAM1_HUMAN	A0A0D9SG12_HUMAN
RL11_HUMAN	CH10_HUMAN	J3QR09_HUMAN
DDB1_HUMAN	RL10A_HUMAN	IF4A3_HUMAN
A0A087WVQ6_HUMAN	HS90B_HUMAN	
M0R3D6_HUMAN	G3P_HUMAN	
RS13_HUMAN	GSTP1_HUMAN	
RAGP1_HUMAN	FKBP4_HUMAN	
PYRG1_HUMAN	A0A0A0MSQ0_HUMAN	
TALDO_HUMAN	XRCC5_HUMAN	
J3QQ67_HUMAN	EF1A3_HUMAN	
EIF3F_HUMAN	HSP74_HUMAN	
AIMP2_HUMAN	PPAC_HUMAN	
RL24_HUMAN	GANAB_HUMAN	
MOB1A_HUMAN	STRAP_HUMAN	
MCM6_HUMAN	MIF_HUMAN	
Q1JUQ3_HUMAN	DCTN2_HUMAN	
BAF_HUMAN	SYHC_HUMAN	
A0A0B4J1R6_HUMAN	A0A0C4DFV9_HUMAN	
SYRC_HUMAN	RINI_HUMAN	
RL8_HUMAN	KPYM_HUMAN	

RL12_HUMAN	A2MG_HUMAN	
LDHA_HUMAN	F5H796_HUMAN	
RS26_HUMAN	6PGD_HUMAN	
PDIA3_HUMAN	ETFB_HUMAN	
Q96C32_HUMAN	RLA0_HUMAN	
J3QQT2_HUMAN	A0A087X0K1_HUMAN	
BIEA_HUMAN	LGUL_HUMAN	
Q5W0H4_HUMAN	G3V5Z7_HUMAN	
SYMC_HUMAN	RS28_HUMAN	
A0A087X020_HUMAN	CBS_HUMAN	
PSB6_HUMAN	SMD1_HUMAN	
1433B_HUMAN	SMC2_HUMAN	
RS25_HUMAN	Q5JR95_HUMAN	
APEX1_HUMAN	EF1B_HUMAN	
GSTO1_HUMAN	HS90A_HUMAN	
1433E_HUMAN	ACTG_HUMAN	
FNTA_HUMAN	ACTN4_HUMAN	
C9J592_HUMAN	RS15A_HUMAN	
A0A024RA52_HUMAN	SSBP_HUMAN	
HINT1_HUMAN	H0YLU7_HUMAN	
H0Y5B4_HUMAN	HMGB1_HUMAN	
CND1_HUMAN	KINH_HUMAN	
KCRB_HUMAN	MDHC_HUMAN	
RD23B_HUMAN	J3KQ18_HUMAN	
RL34_HUMAN	E7EX29_HUMAN	
B4DY09_HUMAN	E9PKT8_HUMAN	
E9PFT6_HUMAN	SP16H_HUMAN	
RS3_HUMAN	COR1C_HUMAN	
HNRPU_HUMAN		
PA2G4_HUMAN		
PSA5_HUMAN		
C1QBP_HUMAN		
ATPA_HUMAN		

Ykt6-WT (Membrane Fraction)	Ykt6-3E (Membrane Fraction)	Common Proteins
IF2GL_HUMAN	HINT1_HUMAN	ECHM_HUMAN
A0A0D9SG12_HUMAN	RL35A_HUMAN	SYWC_HUMAN
E7EX53_HUMAN	SIAS_HUMAN	RL21_HUMAN
J3KTA4_HUMAN	J3KR44_HUMAN	J3KQE5_HUMAN
DC1I2_HUMAN	PSA3_HUMAN	ENOA_HUMAN
ARF1_HUMAN	SRP68_HUMAN	K1C14_HUMAN
PA1B2_HUMAN	RL5_HUMAN	PSA4_HUMAN
RACK1_HUMAN	PSD13_HUMAN	MYH10_HUMAN
MAT2B_HUMAN	A0A087X020_HUMAN	PSA7_HUMAN
RL35_HUMAN	UBC12_HUMAN	PGM1_HUMAN
RS4X_HUMAN	XPO2_HUMAN	E9PRY8_HUMAN
RS18_HUMAN	J3KPX7_HUMAN	K1C10_HUMAN
LA_HUMAN	ELAV1_HUMAN	K2C1_HUMAN
F8W1A4_HUMAN	AIMP1_HUMAN	CDC37_HUMAN
RS6_HUMAN	E5RJ48_HUMAN	SYG_HUMAN
PDIA4_HUMAN	SYYC_HUMAN	HPRT_HUMAN
A0A024R4M0_HUMAN	H0YN26_HUMAN	ROA2_HUMAN
PDIA1_HUMAN	CND1_HUMAN	UB2L3_HUMAN
NUCL_HUMAN	F8WCF6_HUMAN	H0YAG8_HUMAN
E9PK25_HUMAN	NDKA_HUMAN	TPM3_HUMAN
SERC_HUMAN	UBP5_HUMAN	A6NFX8_HUMAN
CH10_HUMAN	MCM6_HUMAN	M0QZC5_HUMAN
RL10A_HUMAN	PDLI1_HUMAN	XPO1_HUMAN
HS90B_HUMAN	PUR2_HUMAN	H7C2W9_HUMAN
G3P_HUMAN	B1AK88_HUMAN	PEBP1_HUMAN
FKBP4_HUMAN	A0A0A0MTS2_HUMAN	RL7A_HUMAN
PPAC_HUMAN	FLNB_HUMAN	PZP_HUMAN
MIF_HUMAN	RS3_HUMAN	K22E_HUMAN
DCTN2_HUMAN	K7ERI7_HUMAN	TLN1_HUMAN
SYHC_HUMAN	IF2A_HUMAN	PRDX2_HUMAN
F5H796_HUMAN	TCP4_HUMAN	HS105_HUMAN
A0A0A0MQR7_HUMAN	PROF1_HUMAN	K7EJB9_HUMAN
ETFB_HUMAN	D6RF35_HUMAN	Q5SQT8_HUMAN
A0A087X0K1_HUMAN	STMN1_HUMAN	H7C2I1_HUMAN
LGUL_HUMAN	CYBP_HUMAN	G6PD_HUMAN
M0R2B0_HUMAN	F8VPD4_HUMAN	SYDC_HUMAN
RS28_HUMAN	GRP78_HUMAN	GCN1_HUMAN
CBS_HUMAN	PFKAP_HUMAN	RL23A_HUMAN
SMD1_HUMAN	AATM_HUMAN	ALDR_HUMAN
HS90A_HUMAN	AATC_HUMAN	H0YA96_HUMAN
RS23_HUMAN	M0R3D6_HUMAN	PSB5_HUMAN
ACTN4_HUMAN	J3QQX2_HUMAN	ANXA5_HUMAN
J3QSB5_HUMAN	DNJC8_HUMAN	K7EL40_HUMAN
E7EX29_HUMAN	E7EQ69_HUMAN	PPIB_HUMAN
	H0Y711_HUMAN	XRCC6_HUMAN

	EFTU_HUMAN	CALX_HUMAN
	K7EN20_HUMAN	IF4A3_HUMAN
	PSMD2_HUMAN	LDHB_HUMAN
	Q5TEJ7_HUMAN	PPIA_HUMAN
	FNTA_HUMAN	RL27_HUMAN
	RUVB1_HUMAN	J3QR09_HUMAN
	ACHB4_HUMAN	IPYR_HUMAN
	ANT3_HUMAN	GUAA_HUMAN
	GRP75_HUMAN	J3KPS3_HUMAN
	TALDO_HUMAN	ILF3_HUMAN
	C1TC_HUMAN	PSDE_HUMAN
	C1K3N0_HUMAN	MDHM_HUMAN
	PEPD_HUMAN	PRPS1_HUMAN
	SYAC_HUMAN	RAB1A_HUMAN
	PRS4_HUMAN	SFPQ_HUMAN
	VINC_HUMAN	SYQ_HUMAN
	A0A087WYT3_HUMAN	DX39B_HUMAN
	PRKDC_HUMAN	1433T_HUMAN
	IMA3_HUMAN	HNRPK_HUMAN
	RD23B_HUMAN	FABP5_HUMAN
	GSTO1_HUMAN	C9J9K3_HUMAN
	RL4_HUMAN	SMD3_HUMAN
	C9J592_HUMAN	H0YLA2_HUMAN
	TCPH_HUMAN	F8VVL1_HUMAN
	AIMP2_HUMAN	E5RI99_HUMAN
	PSMD3_HUMAN	E9PK47_HUMAN
	ARP3B_HUMAN	1433F_HUMAN
	H3BRU6_HUMAN	F8W6I7_HUMAN
	HSPB1_HUMAN	DYHC1_HUMAN
	TCPD_HUMAN	SERA_HUMAN
	SYMC_HUMAN	CAH2_HUMAN
	NACAM_HUMAN	H7C0C1_HUMAN
	SYNC_HUMAN	HUWE1_HUMAN
	IPO4_HUMAN	E5RGA2_HUMAN
	STIP1_HUMAN	ARL3_HUMAN
	B0QY89_HUMAN	PARP1_HUMAN
	MCM3_HUMAN	FLNA_HUMAN
	UBE2K_HUMAN	TPIS_HUMAN
	EF2_HUMAN	Q5HY81_HUMAN
	TBA1B_HUMAN	THIO_HUMAN
	HNRPM_HUMAN	EIF3A_HUMAN
	AL9A1_HUMAN	TCPQ_HUMAN
	Q5T4U5_HUMAN	GLYM_HUMAN
	C9JPM4_HUMAN	OAT_HUMAN
	KCRB_HUMAN	SAHH_HUMAN
	1433B_HUMAN	PGAM1_HUMAN
	RS13_HUMAN	G3V576_HUMAN

	RAB5C_HUMAN	UCHL1_HUMAN
	H7BY58_HUMAN	SND1_HUMAN
	MOB1A_HUMAN	GSTP1_HUMAN
	A0A087WY10_HUMAN	A0A0A0MSQ0_HUMAN
	H2AX_HUMAN	ANM5_HUMAN
	NPM_HUMAN	XRCC5_HUMAN
	E9PC52_HUMAN	EF1A3_HUMAN
	F5GX11_HUMAN	HSP74_HUMAN
	RL11_HUMAN	CAND1_HUMAN
	RS25_HUMAN	TBR1_HUMAN
	PRP19_HUMAN	GDIB_HUMAN
	I3L504_HUMAN	J3KQ32_HUMAN
	PRDX6_HUMAN	GANAB_HUMAN
	A0A087X2I1_HUMAN	STRAP_HUMAN
	SYRC_HUMAN	RS2_HUMAN
	APT_HUMAN	K7EK07_HUMAN
	K2C5_HUMAN	CGL_HUMAN
	RS10_HUMAN	MCM5_HUMAN
	B4DY09_HUMAN	Q5T9B7_HUMAN
	RL7_HUMAN	A8MUA9_HUMAN
	RS21_HUMAN	BZW1_HUMAN
	ATPA_HUMAN	A0A0C4DFV9_HUMAN
	TCPA_HUMAN	CAP1_HUMAN
	PARK7_HUMAN	RL23_HUMAN
	ADT2_HUMAN	RINI_HUMAN
	PSD11_HUMAN	PRS6B_HUMAN
		KPYM_HUMAN
		A2MG_HUMAN
		6PGD_HUMAN
		RLA0_HUMAN
		G3V5Z7_HUMAN
		Q5JXI8_HUMAN
		G8JLB6_HUMAN
		SMC2_HUMAN
		Q5JR95_HUMAN
		EF1B_HUMAN
		ACTG_HUMAN
		RS15A_HUMAN
		IF4A1_HUMAN
		SSBP_HUMAN
		F8W727_HUMAN
		H0YLU7_HUMAN
		HMGB1_HUMAN
		KINH_HUMAN
		YKT6_HUMAN
		RS27_HUMAN
		UBA1_HUMAN

		Q32Q12_HUMAN
		RL6_HUMAN
		MDHC_HUMAN
		J3KQ18_HUMAN
		E9PKT8_HUMAN
		SP16H_HUMAN
		COR1C_HUMAN
		A0A0U1RRM4_HUMAN

Supplementary Table 3

	Ykt6 Mutants	Abbreviations
1	Ykt6 - WT	Ykt6 Wild Type
2	Ykt6-3E	Ykt6 with three sites mutated to Glutamic acid (Phosphomimicking mutant)
3	Ykt6-3A	Ykt6 with three sites mutated to Alanine (Non-phosphorylatable mutant)
4	Ykt6-4E	Ykt6 with four sites mutated to Glutamic acid in *Drosophila* (Phosphomimicking mutant)
3	Ykt6-4A	Ykt6 with four sites mutated to Alanine in *Drosophila* (Non-phosphorylatable mutant)
5	C194A	Palmitoylation mutant
6	C195A	Farnesylation mutant
7	C194A/195A	Palmitoylation and Farnesylation double mutant
8	Ykt6-3E/C194A/195A	Phosphomimicking, Palmitoylation and Farnesylation mutant
9	F42A	Longin Domain Mutation

	Others	Abbreviations
1	Bio ID	Proximity dependent Biotin identification
2	BirA	Biotin protein ligase
3	EV	Extracellular vesicles
4	PKC	Protein kinase C
5	PDK1	Phosphoinositide-dependent kinase 1
6	CDK1	Cyclin dependent kinase 1
7	MVB	Multi vesicular bodies
8	ILV	Intraluminal vesicles
9	ER	Endoplasmic reticulum

3.3 Manuscript III: Characterization of Wnt-bearing small extracellular vesicles

Citation:

Pradhipa Karuna M[1], Wiebke Möbius[4], Britta Brügger[5] and Julia Christina Gross[1,2,3*]

Individual contributions to the article:
Applicant name: Pradhipa Karuna M (first author)

1. **Main and Supplementary Figures/Tables** (actively performed experiments and/or analyzed data)

   Main: 1A, 1B, 1C, 1D, 1F, 1G, 2A-J
   Supplementary: Table 1, Table 2, Table 3

2. **Writing and Intellectual Contributions**

   - Contributed to writing the entire manuscript such as introduction, results, discussion, materials and methods.
   - Contributed to figure arrangement and figure legends of all the figures.
   - Actively involved in experimental design and closely collaborated with Prof. Dr. Britta Brügger for large scale lipidomics experiments and data analysis. Worked together with Dr. Christof Lenz for large scale proteomic experiments and data analysis.

Characterization of Wnt-bearing small extracellular vesicles

Pradhipa Karuna M[1], Wiebke Möbius[4], Britta Brügger[5] and Julia Christina Gross[1,2,3*]

Affiliations:

[1] Developmental Biochemistry, University Medical Center Goettingen, Goettingen, Germany

[2] Hematology and Oncology, University Medical Center Goettingen, Goettingen, Germany

[3] Health and Medical University Potsdam, Potsdam, Germany

[4]Neurogenetics, Max Planck Institute of Experimental Medicine, Goettingen, Germany

[5]Heidelberg University Biochemistry Center (BZH), Heidelberg, Germany

*** Correspondence:**

Julia Christina Gross, Health and Medical University Potsdam, Potsdam, Germany, julia.gross@health-and-medical-university.de

Abstract

Small extracellular vesicles (sEVs) otherwise termed exosomes, are generated from intraluminal vesicles (ILVs) released after fusion of multivesicular endosomes (MVEs) with the plasma membrane. They act as messengers that transport proteins, lipids or nucleic acids to the extracellular space to maintain cellular homeostasis or to promote pathological conditions. Wnt, an essential morphogen for development, reaches the extracellular space by being loaded onto exosomes for long-range signalling. Different Wnt ligands are carried by different sub-populations of EVs depending on the cell type and the function. Using a conventional ultracentrifugation technique combined with immunomagnetic based pull-down assay, we discovered that Wnts are not carried by bonafide $CD63^+$, $CD81^+$, $CD9^+$, $Alix^+$ or $Syntenin^+$ exosome sub-types. Strikingly, Wnts were identified in the flow-through fraction after the pull-down of classical exosomal markers $CD63^+/CD81^+/CD9^+$. The flow-through fraction was enriched in exosomal vesicles as confirmed by transmission electron microscopy and lipidomic characterization. Furthermore, our proteomics characterization revealed a novel non-canonical sub-population of exosomes that could potentially carry Wnt proteins.

Keywords

Tetraspanins, Rabs, Annexins, Flowthrough, Exosomes

Introduction

Extracellular vesicles (EVs) are messengers that carry proteins, lipids or nucleic acids between cells to promote homeostasis or pathologies. They are broadly classified as exosomes or microvesicles, based on their size and origin. Exosomes are generated as intra-luminal vesicles (ILVs) formed by the inward budding of the limiting membranes of multi vesicular endosomes (MVEs). They are 30-100nm in diameter and are released by the fusion of MVEs with the plasma membrane. Microvesicles are generated by outward budding of the plasma membrane and subsequent release of vesicles into the extracellular space. They are 50-1000nm in diameter, but can also be larger. Even though exosomes and microvesicles have different modes of biogenesis, they share the common machinery of the endosomal system (Van Niel, D'Angelo, & Raposo, 2018). These machinery sort cargoes on the microdomains of MVEs for fusion with the plasma membrane, followed by the release of cargoes into the extracellular space. Exosomes are formed by ESCRT-dependent and ESCRT-independent machinery. The biogenesis and the abundance of exosomes are further dependent on the cell type and the extracellular signals from the target cells (Mathieu, Martin-Jaular, Lavieu, & Théry, 2019). For example, tumour cells communicate with the neighbouring cells through extracellular vesicles to promote tumour migration and metastatic niche formation (Peinado et al., 2017). On the other hand, a healthy cell communicates with nearby cells or tissues in an autocrine or paracrine manner to promote growth and development (Raposo & Stoorvogel, 2013). Therefore, cells secrete different sub-populations of exosomes depending on the protein sorting machinery as well as stimuli from their surrounding cells. Overall, exosome biogenesis is complex and is influenced by a plethora of signals in the microenvironment.

The cargoes that are sorted onto exosomes reach the endosomal system from the Golgi apparatus or are internalized at the plasma membrane. For example, Wnt proteins enter the endosomal system through endocytosis, are sorted onto MVEs and are released onto exosomes for long-range signalling (Gross, Chaudhary, Bartscherer, & Boutros, 2012; Linnemannstöns et al., 2020). As they are crucial morphogens for development and tissue morphogenesis, different exosomes carry different Wnts based on the cell type and the required function. For example, in breast cancer cells, exosomes carrying Wnt11 promote cell invasion and therefore metastasis through the Wnt-PCP pathway (Luga et al., 2012). Similarly, during neuronal regeneration, exosomes carry Wnt10b to promote axonal growth by activating mTOR signalling (Tassew et al., 2017). Even though several studies highlight the function of exosomes on carrying Wnts, it is still unclear if there are specific sub-population of exosomes involved in the transport of Wnt proteins to the target site. This is largely because exosomes are highly heterogeneous in nature.

In this study, we show for the first time that Wnts are not carried by bonafide CD63$^+$, CD81$^+$, CD9$^+$, alix$^+$ or syntenin$^+$ exosomes. Moreover, we characterized the lipidome of Wnt bearing vesicles, which revealed that the isolated fraction is enriched in exosomes in contrast to lipoprotein particles. To this end, mass spectrometry analysis revealed interesting non-canonical exosomal sub-populations that potentially carry Wnt.

Results

Wnts are secreted on a non-classical subpopulation of small EVs

Active Wnts are loaded onto exosomes for long-range signalling in *Drosophila* and mammalian cells (Gross et al., 2012). Exosomes are heterogeneous in nature and are characterized into different subtypes with distinct biological properties (Fig. 1A) (Kowal et al., 2016). To investigate if Wnts are sorted onto a specific exosomal subtype, we overexpressed tagged (Wnt-GFP) and untagged (Wnt-pCS2) Wnt3a in Hek293T cells, collected the conditioned media and isolated exosomes by ultracentrifugation (UC) at 100,000 g according to MISEV guidelines (Théry et al., 2018) (Fig. 1B, left part). Concordantly, we identified both untagged and tagged Wnts on exosomes in the UC fraction, along with conventional exosomal markers such as Alix, Syntenin and CD81 (Fig. 1C, D, lane 2). To identify if Wnts are sorted onto classical exosomal subpopulations such as tetraspanins, we performed an immunomagnetic based magnetic pull-down of the CD63$^+$, CD81$^+$ and CD9$^+$ carrying exosomes. Surprisingly, we did not find both tagged and untagged Wnts in the pull-down fraction (PD) (Fig. 1C, D, lane 3). This indicates that Wnts are not carried by the classical CD63$^+$, CD81$^+$ or CD9$^+$ exosomes along with Alix and Syntenin subtypes. We then collected the flow-through fraction (FT) left over after the pull-down and isolated exosomes by ultracentrifugation (Fig. 1B, right part). Expectedly, the exosomes isolated from this fraction do not carry CD81, indicating that the CD81$^+$ subtype of exosomes has efficiently been removed by pulldown, which further confirms the purity of the respective exosomal fractions. Strikingly, we identified both tagged and untagged Wnts in the flow-through fraction after ultracentrifugation (Fig. 1C, D lane 4). This indicates that Wnts are predominantly carried by the CD63$^-$, CD81$^-$ or CD9$^-$ exosome sub-types. Moreover, we also see that both the tagged and the untagged Wnts behave similarly where they are sorted onto the same exosomal sub-populations. This further confirms the functional similarity between wild-type and fluorescently tagged Wnt3a in exosomal secretion (Wesslowski et al., 2020). Taken together, we show that Wnts are not secreted on classical exosomal sub-populations and are present abundantly in the flow-through fraction.

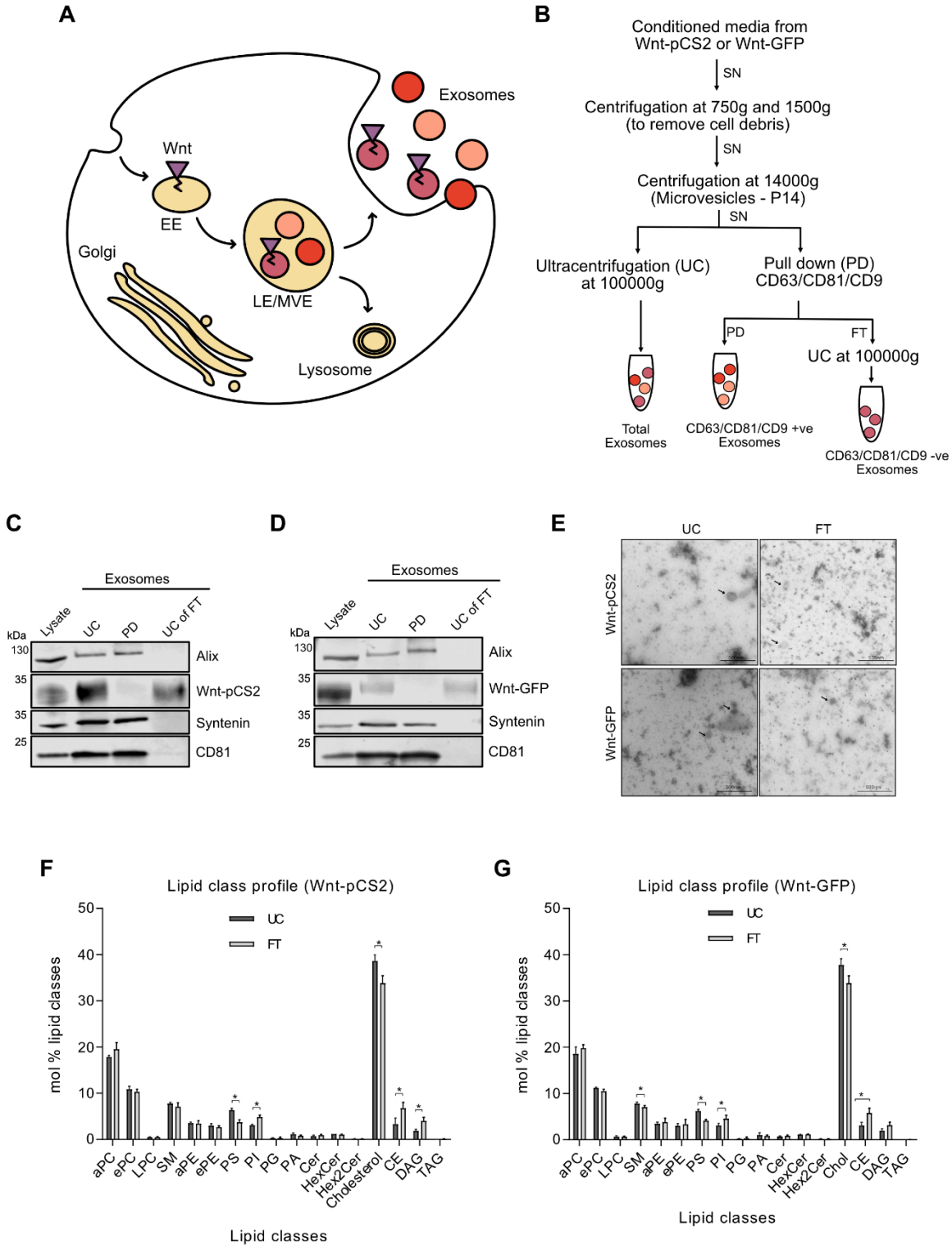

Figure 1: Wnts are secreted on non-classical subpopulations of small EVs. (A) Different subpopulations of exosomes in shades of red, generated as ILVs formed by the fusion of MVEs with the plasma membrane. **(B)** Scheme of sEV isolation from cell culture conditioned medium through stepwise serial centrifugation and immunomagnetic based pull-down assay. **(C)** Representative western blot of exosomal markers Alix, Syntenin and CD81 along with Wnt-pCS2 in cell lysates and exosomal fractions isolated by UC, PD and FT of UC, n=3. **(D)** Representative western blot of exosomal markers

Alix, Syntenin and CD81 along with Wnt-GFP in cell lysates and exosomal fractions isolated by UC, PD and FT of UC, n=3. **(E)** Electron microscopy images of 100,000g exosomal pellet of the UC and FT fraction from Wnt-pCS2 and Wnt-GFP. **(F, G)** Lipid class profile representing the percentage of lipid classes in the UC and FT fraction of Wnt-pCS2 and Wnt-GFP from three biological replicates. The lipid classes are as follows: a: diacyl, e: ether acyl, PC: phosphatidylcholine, LPC: lysophosphatidylcholine, SM: sphingomyelin, PE: phosphatidylethanolamine, PS: phosphatidylserine, PI: phosphatidylinositol, PG: phosphatidylglycerol, PA: phosphatidic acid, Cer: ceramide, HexCer: hexosylceramide, LacCer: lactosylceramide, CE: cholesterol ester, DAG: diacylglycerol, TAG: triacylglycerol.

Lipidomic characterization of Wnt bearing small EVs

In addition to exosomes, Wnts are known to be transported to long distances through association with lipoprotein particles. For example, Wnt5a associates with lipoprotein particles but not exosomal markers to regulate hindbrain morphogenesis in both mice and humans (Kaiser et al., 2019). Since we identified Wnts in the flow-through fraction, we next investigated if the fraction is composed of exosome vesicles or lipoprotein particles. We performed transmission electron microscopy (TEM) on the 100,000g pellet obtained by ultracentrifugation of supernatants before (UC) and after pulldown (FT) and were able to confirm the presence of exosome-like vesicles based on size and morphology in both UC and FT fraction (Fig. 1E). The lipid composition of exosomes reflects the endosomal system. They are therefore enriched in cholesterol, sphingomyelin, glycosphingolipids, and phosphatidylserine Interestingly, the lipid composition of ILVs depends on the maturation stage of the MVB, with cholesterol being high at the early ILV stages involved in exosome secretion (Skotland, Hessvik, Sandvig, & Llorente, 2019). To investigate the lipid composition of the flow-through fraction we performed a lipidomic characterization. The lipidome of UC and FT fraction revealed enrichment of cholesterol and sphingomyelin, compared to other lipid groups which confirm the presence of exosome vesicles in the fraction (Fig. 1F, G). In general, high levels of cholesterol esters (CE) and triacylglycerides (TAG) in exosome preparations indicate the presence of lipoprotein particles because CE and TAG make up the core of the lipid droplet. In addition, the presence of cardiolipin in the exosome preparation indicates mitochondrial membrane contaminations (Skotland, Sandvig, & Llorente, 2017). Our exosome preparation from tagged and untagged Wnts have low levels of cholesterol esters and triacylglycerides which further emphasizes the purity and composition of the isolated exosomes in the UC and the FT fraction (Fig. 1F, G).

Proteomic characterization of Wnt bearing small EVs

To identify the sub-populations of exosomes that carry Wnt, we performed a quantitative label-free data-independent acquisition (DIA) mass spectrometry analysis of the 100,000 g

exosome pellet obtained from ultracentrifugation (UC) and flow-through fraction (FT). The proteome was abundant in exosomes. Since Wnts were abundant in the exosomes from UC and FT fraction, we selected the top 1000 abundant proteins in the UC and FT fraction and first filtered out the non-vesicular proteins (Jeppesen et al., 2019). Furthermore, we filtered out the CD63, CD81, CD9 and IgG pull down proteome from the list (Based on (Kowal et al., 2016)), as the Wnts are not secreted on these classical exosome subtypes. We then filtered out the exosomal markers that are depleted in the FT fraction. The step-wise filtering of proteins is represented in the scheme (Fig. 2A), which resulted in exosomal sub-populations that could potentially carry Wnt proteins (Supplementary Table 1). There was a significant overlap of these Wnt-bearing exosomes from both tagged and untagged Wnts (Fig. 2B). A GO term enrichment of these markers revealed processes such as plasma membrane to endosome transport, protein localization to the cell periphery, secretion, cell cycle and Wnt signalling, among others (Fig. 2C, D).

Exosomes are heterogeneous in nature and we reasoned that the sub-type of exosomes that carry Wnts could perhaps belong to well-known non-classical exosome subtypes. Therefore, we further narrowed down the Wnt-bearing exosomal proteins by performing an overlap with the top EV markers as defined by Exocarta/Vesiclepedia and the GO terms associated with the extracellular vesicles. This led to a total of 55 exosomal proteins in Wnt-pCS2 and 43 proteins in Wnt-GFP (Fig. 2E). Since tagged and untagged Wnts behave similarly based on our previous findings, an overlap of these led to a final list of 41 exosomal sub-populations that could potentially carry Wnt (Fig. 2F, Supplementary Table 2). Based on the literature, we chose interesting candidates for further investigation and characterization (Fig. 2G). The candidates chosen are upregulated in several tumours. We reasoned that tumour cells up-regulate Wnt-bearing markers to promote uncontrolled proliferation. Annexin A2 is up-regulated in several tumours (Xi, Ju, & Wang, 2020). Annexins were categorized as exosome sub-populations devoid of CD63/CD81/CD9 (Kowal et al., 2016). Rac1 is a small GTPase that initiates several signalling pathways such as NFkB, Wnt/β-catenin and regulates cell adhesion, motility and polarity leading to cell proliferation (Kotelevets & Chastre, 2020). Rac1 correlated with aggressive tumours and are highly upregulated in colon cancers (Ji et al., 2015). Interestingly, many Rab proteins such as Rab1A, the Rab5 family and Rab14 were also present in the final list. Rab proteins regulate vesicle trafficking and exosome formation in the endocytic pathway (Blanc & Vidal, 2018).

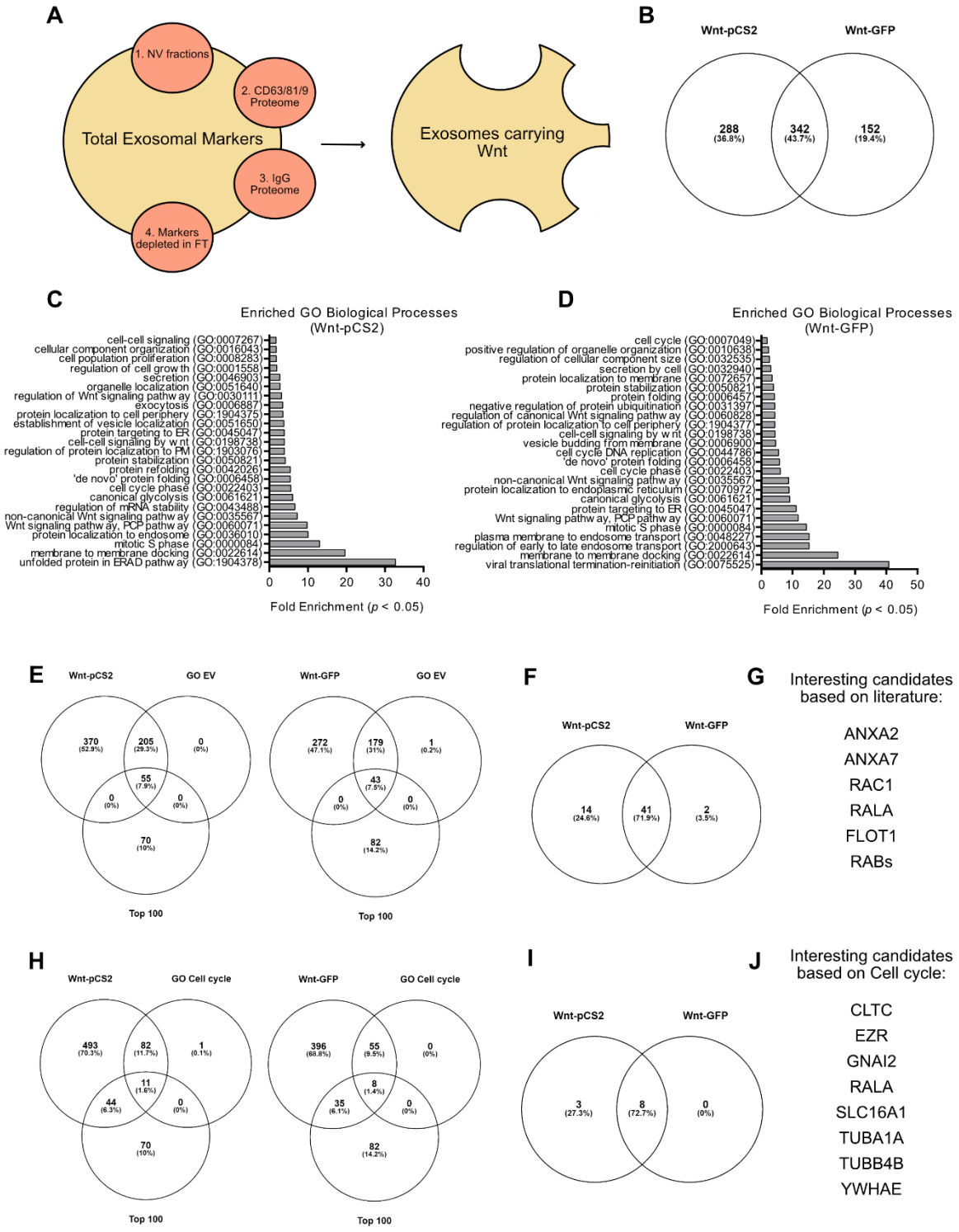

Figure 2: Proteomic characterization of Wnt bearing small EVs (A) Scheme representing the step-wise filtering of total exosomal markers to obtain the exosomal markers carrying Wnt. **(B)** Venn diagram representing an overlap of the filtered proteins from Wnt-pCS2 and Wnt-GFP. **(C, D)** Enriched GO Biological processes in Wnt-pCS2 or Wnt-GFP as determined by Fisher Exact Test with the Benjamini-Hochberg False Discovery Rate <0.05. **(E)** Venn diagram representing an overlap of the filtered proteins from Wnt-pCS2 or Wnt-GFP with Top EV markers and GO EVs. **(F)** Venn diagram representing an overlap of the final proteins from Wnt-pCS2 and Wnt-GFP. **(G)** List of interesting candidates based on

literature search. **(H)** Venn diagram representing an overlap of the filtered proteins from Wnt-pCS2 or Wnt-GFP with Top EV markers and GO Cell cycle. **(I)** Venn diagram representing an overlap of the final proteins from Wnt-pCS2 and Wnt-GFP. **(J)** List of interesting candidates based on cell cycle.

Interestingly, the GO term enrichment, apart from EV-related processes, also revealed an enrichment of cell cycle processes (Fig. 2C, D). The Wnt co-receptor LRP5/6 is a key Wnt signalling transducer and is under cell cycle control. (Davidson & Niehrs, 2010). Moreover, Mitotic Wnt signalling peaks at the G2/M phase of the cell cycle (Niehrs & Acebron, 2012). Therefore, secretion of Wnt-bearing exosomes could be cell cycle-dependent. Therefore, we performed an overlap of the potential Wnt-bearing exosomes with GO terms associated with the cell cycle as well as with top EV markers (Fig. 2H). This finally gave us a final list of 8 exosomal proteins that could potentially carry Wnt in a cell-cycle dependent manner (Fig. I, J, Supplementary Table 3). Understanding why Rabs, Annexins or other non-classical exosomal subtypes are involved in carrying Wnt proteins can give more insights into the regulation and trafficking of Wnt proteins. However, further characterization and validation these potential Wnt-bearing exosomes remains to be undertaken.

Discussion

In this study, we for the first time, have shown that Wnts are not secreted on classical well-characterized exosomal sub-populations such as CD63, CD81, CD9, Alix or Syntenin. Wnts were present in the flow-through after immunomagnetic pulldown of $CD63^+$, $CD81^+$ and $CD9^+$ exosomes predominantly. This implies that Wnts are not sorted onto well-known exosomal sub-populations and that exosomes are highly heterogeneous in nature. Even though tetraspanins, such as CD9, CD63, CD81 are widely used as bonafide exosomal markers, other subtypes devoid of these classical markers exist that carry important cargoes such as Wnt. Despite the traces of contaminants, our EM characterization confirms the presence of vesicles in the flow-through fraction. Complementing the EM analysis, our lipidomic characterization revealed that the flow-through fraction is indeed enriched in lipid classes that are associated with exosomal vesicles and not of the lipoprotein particles. Finally, proteomic analysis revealed non-canonical sub-populations of exosomal sub-types that could potentially carry Wnt proteins. Interestingly, these markers from both tagged and untagged Wnts were enriched in processes such as endocytosis, membrane-membrane docking, secretion, exocytosis, cell cycle and Wnt signalling. This confirms that active Wnts enter the endocytic pathway and are sorted onto exosomes.

Why Wnts are sorted onto a non-canonical sub-population of exosomes remains an interesting question. sEVs are categorized as sub-populations enriched in CD63/CD81/CD9 tetraspanins which are bonafide exosomes or sub-populations devoid of CD63/CD81/CD9 (Kowal et al., 2016). Based on our proteomic data, Wnts seem to be transported on exosomes devoid of CD63/CD81/CD9 tetraspanins. The sub-populations of exosomes devoid of tetraspanins are also known to be enriched in Annexins (Kowal et al., 2016). The Annexin family of proteins regulate autophagy and promote cell exocytosis. They are Ca^{2+} sensitive proteins that regulate vesicle fusion, aggregation and are involved in plasma membrane repair. Some of the other interesting candidates from our proteomic analysis include Rabs, RalA GTPase, Rac1 GTPase and Flotillins since most of them are up-regulated in several types of tumours. For example, Flotillins, which are lipid raft markers are closely associated with tumour development and metastasis (Liu et al., 2018). RalA is a GTPase known to promote breast cancer metastasis by harnessing the exosome biogenesis pathway. These GTPases secrete a different sub-type of EVs to promote metastatic niche formation (Ghoroghi et al., 2021). Since the tumour cells can hijack the cargo sorting of EVs, they might also have the ability to change the sub-type of secreted EVs. For example, the tumour cells could down-regulate the EVs that are necessary for cell adhesion and up-regulate EVs that promote growth and proliferation for example via Wnt proteins. Cell cycle progression involves the coordination of several growth-promoting signals. For example, the binding of Wnt proteins to the receptors promotes G1 to S progression of the cell cycle (Niehrs & Acebron, 2012). Therefore, in tumour cells, the sub-type of EVs carrying Wnt proteins can influence cell cycle progression to promote uncontrolled proliferation. Indeed, Wnt secretion and signalling components are mutated or up-regulated in several tumours (Wiese, Nusse, & van Amerongen, 2018). Unravelling the mechanism of sorting of Wnts onto different EV subtypes would provide more insights into the mechanism of tumour invasion and open up future perspectives of EV biomarker research.

Materials and Methods

Antibodies

The following antibodies were used for western blotting (WB): Wnt3a (1:1000; Western Blot (WB); Abcam), GFP (1:1000, WB, Molecular probes), Syntenin (1:1000, WB, Abcam), Alix (1:1000, WB, Santa Cruz), CD81 (1:1000, WB, Biolegend). Secondary antibodies were coupled to 680RD and 800 CW (1:20000, WB, Licor).

Cell culture and Transfection

Hek293T cells were maintained in DMEM (Gibco) supplemented with 10% fetal calf serum (Biochrom) at 37 °C in a humidified atmosphere with 5% CO_2. Cells were transiently transfected with Screenfect A (Screenfect) for plasmids Wnt-pCS2 and Wnt-GFP (Gross et al., 2012) according to the manufacturer's instructions. Cells were authenticated and checked regularly for mycoplasma contamination.

Extracellular vesicle purification

Extracellular vesicles were purified by differential centrifugation as described previously (Menck et al., 2017). In short, supernatants from mammalian cells were subjected to sequential centrifugation steps of 750 g, 1500g and 14,000g, before pelleting exosomes at 100,000g for 1h (Beckman). The supernatant was discarded, and exosomes were taken up in 1/100 of their original volume in 1X PBS. Exosome Pan Isolation kit (Miltenyi Biotec) was used for the immunomagnetic pull-down of exosomes as per the manufacturer's protocol.

Western blot analysis

Cell and sEV lysates in the SDS-PAGE sample buffer was boiled for 5 min before separating the protein on 4-12% gradient gels (Bolt Bis-Tris Plus Gels, Thermo Scientific). Protein was then transferred to PVDF membranes (Merck) and blocked with 5% (wt/vol) milk-TBST for 30 min. Membranes were incubated with primary antibodies overnight at 4 TBST at 4°C. After washing, membranes were incubated with fluorescently labelled secondary antibodies at room temperature in the dark and detected using Odyssey from Li-COR. Quantitative measurements were done with LiCOR image analysis software.

Mass Spectrometry

For large-scale Exosome isolation, cells were seeded and 24 h later transfected with Wnt3a-pCS2 or Wnt3a-GFP. Then, 72 h post-transfection, exosomes were isolated and the pellets were dissolved in 1X PBS buffer. Cells were washed with PBS twice, cell fractionated, and then boiled 5 min in non-reducing SDS sample buffer (300 mM Tris-HCl pH 6.8, 12% SDS, 0.05% Bromophenol blue, 60% Glycerol, 12 mM EDTA), run a short-distance (1.5 cm) on a 4–12% NuPAGE Novex Bis-Tris Minigel (Invitrogen). Gels were stained with Coomassie Blue for visualization purposes. Full lanes were sliced into 23 equidistant slices regardless of staining, short runs cut out as a whole and diced. After washing, gel slices were reduced with

dithiothreitol (DTT), alkylated with 2-iodoacetamide, and digested with trypsin overnight. Then, the resulting peptide mixtures were extracted, dried in a SpeedVac, reconstituted in 2% acetonitrile/0.1% formic acid/(v:v), and prepared for nanoLC-MS/MS as described previously [32]. For the generation of a peptide library for SWATH-MS, equal amount aliquots from each sample were pooled to a total amount of 80 µg and separated into eight fractions using a reversed-phase spin column (Pierce High pH Reversed-Phase Peptide Fractionation Kit, Thermo Fisher Scientific, Waltham, Massachusetts, United States. MS analysis Protein digests were separated by nanoflow chromatography. Then, 25% of gel slices or 1 µg aliquots of digested protein were enriched on a self-packed precolumn (0.15 mm ID × 20 mm, Reprosil-Pur120 C18-AQ 5 µm, Dr. Maisch, Ammerbuch-Entringen, Germany) and separated on an analytical RP-C18 column (0.075 mm ID × 250 mm, Reprosil-Pur 120 C18-AQ, 3 µm, Dr. Maisch) using a 30 to 90 min linear gradient of 5–35% acetonitrile/0.1% formic acid (v:v) at 300 nl/ min. SWATH-MS library generation was performed on a hybrid triple quadrupole-TOF mass spectrometer (TripleTOF 5600+) equipped with a Nanospray III ion source (Ionspray Voltage 2400 V, Interface Heater Temperature 150 ◦C, Sheath Gas Setting 12) and controlled by Analyst TF 1.7.1 software (SCIEX, Framingham, Massachusetts, MA, USA)build 1163 (all AB Sciex), using a Top30 data-dependent acquisition method with an MS survey scan of m/z 380–1250 accumulated for 250 ms at a resolution of 3.5 × 104 full widths at half maximum (FWHM). MS/MS scans of m/z 180–1500 were accumulated for 100 ms at a resolution of 17,500 FWHM and a precursor isolation width of 0.7 FWHM, resulting in a total cycle time of 3.4 s. Precursors above a threshold MS intensity of 200 cps with charge states 2+, 3+, and 4+ were selected for MS/MS, and the dynamic exclusion time was set to 15 s. MS/MS activation was achieved by CID using nitrogen as collision gas and the manufacturer's default rolling collision energy settings. Two technical replicates per reversed-phase fraction were analyzed to construct a spectral library. For quantitative SWATH analysis, MS/MS data were acquired using 100 variable size windows across the 400–1200 m/z range. Fragments were produced using rolling collision energy settings for charge state 2+, and fragments acquired over an m/z range of 180–1500 for 40 ms per segment. Including a 250 ms survey scan, this resulted in an overall cycle time of 4.3 s. Two replicate injections were acquired for each biological sample.

Mass Spectrometry Data Processing

For SWATH-MS analysis, protein identification was achieved using ProteinPilot Software version 5.0 (SCIEX, Framingham, Massachusetts, MA, USA) build 4769 (AB Sciex) at "thorough" settings. MS/MS spectra from the combined qualitative analyses were searched

against the UniProtKB Homo sapiens reference proteome (revision February 2017. 92,928 entries) augmented with a set of 51 known common laboratory contaminants to identify 597 proteins at a False Discovery Rate (FDR) of 1%. Spectral library generation and SWATH peak extraction were achieved in PeakView Software version 2.1 (SCIEX, Framingham, Massachusetts, MA, USA) build 11041 (AB Sciex) using the SWATH quantitation microApp version 2.0 SCIEX, Framingham, Massachusetts, MA, USA) build 2003. Following retention time correction on endogenous peptides spanning the entire retention time range, peak areas were extracted using information from the MS/MS library at an FDR of 1%. The 26 resulting peak areas were summed to peptide and protein area values, which were used for further statistical analysis.

Electron microscopy

Purified EVs were left to settle on carbon-coated grids. After washing with water, samples were stained with neutral uranyl acetate. After incubation with a 1:1 mixture of 4% uranyl acetate and 2% methylcellulose, grids were air-dried and visualized at 30 000X magnification using a transmission electron microscope (Zeiss EM900). Representative images from three biological replicates of Wnt-pCS2 and Wnt-GFP from UC and FT fraction were obtained. Particle size was determined compared to a size marker in Fiji.

Lipidomics

For large-scale Exosome isolation, cells were seeded and 24 h later transfected with Wnt3a-pCS2 or Wnt3a-GFP. Then, 72 h post-transfection, exosomes were isolated and the pellets were subjected to lipid extractions using an acidic liquid-liquid extraction method (Bligh, E. G.; Dyer, 1959), except plasmalogens, which were extracted under neutral conditions. To ensure that similar amounts of lipids were subjected to extractions, a test extraction was performed to determine the concentration of PC as a bulk membrane lipid and to adapt extractions volumes to similar total lipid amounts. Typically, a total lipid amount of approximately 2600 pmol (cells) or 2900 pmol (subcellular fractions) was subjected to extractions. Quantification was achieved by adding 1-3 internal lipid standards for each lipid class, with the standards resembling the structure of the endogenous lipid species. Of note, sample volumes were adjusted to ensure that all lipid standard to lipid species ratios were in a linear range of quantification. Typically, the range of standard to species ratios was within a range of >0.1 to <10. Following this approach, relative quantification of lipid species was performed. Lipid standards were added prior to extractions, using a master mix consisting of 50 pmol phosphatidylcholine (PC, 13:0/13:0, 14:0/14:0, 20:0/20:0; 21:0/21:0, Avanti Polar Lipids), 50

pmol sphingomyelin (SM, d18:1 with N-acylated 13:0, 17:0, 25:0, semi-synthesized (Özbalci, Sachsenheimer, & Brügger, 2013), 100 pmol deuterated cholesterol (D_7-cholesterol, Cambridge Isotope Laboratory), 30 pmol phosphatidylinositol (PI, 17:0/ 20:4, Avanti Polar Lipids), 25 pmol phosphatidylethanolamine (PE) and 25 pmol phosphatidylserine (PS) (both 14:1/14:1, 20:1/20:1, 22:1/22:1, semi-synthesized (Özbalci et al., 2013), 25 pmol diacylglycerol (DAG, 17:0/17:0, Larodan), 25 pmol cholesteryl ester (CE, 9:0, 19:0, 24:1, Sigma), and 24 pmol triacylglycerol (TAG, LM-6000/D5-17:0,17:1,17:1, Avanti Polar Lipids), 5 pmol ceramide (Cer, d18:1 with N-acylated 14:0, 17:0, 25:0, semi-synthesized or Cer d18:1/18:0-D3, Matreya) and 5 pmol glucosylceramide (HexCer) (d18:1 with N-acylated 14:0, 19:0, 27:0, semi-synthesized or GlcCer d18:1/17:0, Avanti Polar Lipids), 5 pmol lactosylceramide (Hex2Cer, d18:1 with N-acylated C17 fatty acid), 10 pmol phosphatidic acid (PA, 17:0/20:4, Avanti Polar Lipids), 10 pmol phosphatidylglycerol (PG, 14:1/14:1, 20:1/20:1, 22:1/22:1, semi-synthesized (Özbalci et al., 2013) and 5 pmol lysophosphatidylcholine (LPC, 17:1, Avanti Polar Lipids). The phosphatidylethanolamine plasmalogen (PE P-) standard mix consisted of 16.5 pmol PE P-Mix 1 (16:0p/15:0, 16:0p/19:0, 16:0p/ 25:0), 23.25 pmol PE P-Mix 2 (18:0p/15:0, 18:0p/19:0, 18:0p/25:0), 32.25 pmol PE P-Mix 3 (18:1p/15:0, 18:1p/19:0, 18:1p/25:0). Semi-synthesis of PE P- was performed as described in (Paltauf & Hermetter, 1994). The final $CHCl_3$ phase was evaporated under a gentle stream of nitrogen at 37°C. Samples were either directly subjected to mass spectrometric analysis, or were stored at -20°C before analysis, which was typically done within 1-2 days after the extraction. Lipid extracts were resuspended in 10 mM ammonium acetate in 60 µl methanol. 2 µl aliquots of the resuspended lipid extracts were diluted 1:10 in 10 mM ammonium acetate in methanol in 96-well plates (Eppendorf twin tec 96) before measurement. For cholesterol determinations, the remaining lipid extract was again evaporated and subjected to acetylation as described in (Liebisch et al., 2006). Samples were analyzed on a QTRAP 6500+ mass spectrometer (Sciex) with chip-based (HD-D ESI Chip, Advion Biosciences) electrospray infusion and ionization via a Triversa Nanomate (Advion Biosciences) as described. Data evaluation was done using LipidView (Sciex) and an in-house-developed software (ShinyLipids).

Acknowledgements

The authors thank the Proteomic facility at UMG and the Lipidomic facility in Heidelberg. Research in the lab of JCG is supported by the DFG-funded Research Center SFB1324/1 - project number 331351713 and GR4810/2-1, the Research program of the University Medical Center, University of Göttingen and a postdoctoral fellowship to K.L. by the Dorothea Schlözer Program, University of Göttingen.

Author Contributions

P.K.M. designed and carried out cell culture experiments, extracellular purification and data analysis. W.M performed EM analysis. B.B performed lipidomic analysis. P.K.M and J.C.G wrote the original draft along with reviewing and editing. J.C.G. conceived and supervised the study.

Competing Interests statement

The authors have no competing financial interests.

References

Blanc, L., & Vidal, M. (2018). New insights into the function of Rab GTPases in the context of exosomal secretion. *Small GTPases*, *9*(1–2), 95–106. https://doi.org/10.1080/21541248.2016.1264352

Bligh, E. G.; Dyer, W. J. (1959). A rapid method of total lipid extraction and purification. *Canadian Journal of Biochemistry and Physiology*, *37*(8), 911–917.

Davidson, G., & Niehrs, C. (2010). Emerging links between CDK cell cycle regulators and Wnt signaling. *Trends in Cell Biology*, *20*(8), 453–460. https://doi.org/10.1016/j.tcb.2010.05.002

Ghoroghi, S., Mary, B., Larnicol, A., Asokan, N., Klein, A., Osmani, N., … Hyenne, V. (2021). Ral GTPases promote breast cancer metastasis by controlling biogenesis and organ targeting of exosomes. *ELife*, *10*, 1–29. https://doi.org/10.7554/eLife.61539

Gross, J. C., Chaudhary, V., Bartscherer, K., & Boutros, M. (2012). Active Wnt proteins are secreted on exosomes. *Nature Cell Biology*, *14*(10), 1036–1045. https://doi.org/10.1038/ncb2574

Jeppesen, D. K., Fenix, A. M., Franklin, J. L., Higginbotham, J. N., Zhang, Q., Zimmerman, L. J., … Coffey, R. J. (2019). Reassessment of Exosome Composition. *Cell*, *177*(2), 428-445.e18. https://doi.org/10.1016/j.cell.2019.02.029

Ji, J., Feng, X., Shi, M., Cai, Q., Yu, Y., Zhu, Z., & Zhang, J. (2015). Rac1 is correlated with aggressiveness and a potential therapeutic target for gastric cancer. *International Journal of Oncology*, *46*(3), 1343–1353. https://doi.org/10.3892/ijo.2015.2836

Kaiser, K., Gyllborg, D., Procházka, J., Salašová, A., Kompaníková, P., Molina, F. L., … Bryja, V. (2019). WNT5A is transported via lipoprotein particles in the cerebrospinal fluid to regulate hindbrain morphogenesis. *Nature Communications*, *10*(1), 1–15. https://doi.org/10.1038/s41467-019-09298-4

Kotelevets, L., & Chastre, E. (2020). Rac1 signaling: From intestinal homeostasis to colorectal cancer metastasis. *Cancers*, *12*(3), 1–43. https://doi.org/10.3390/cancers12030665

Kowal, J., Arras, G., Colombo, M., Jouve, M., Morath, J. P., Primdal-Bengtson, B., … Théry, C. (2016). Proteomic comparison defines novel markers to characterize heterogeneous populations of extracellular vesicle subtypes. *Proceedings of the National Academy of Sciences of the United States of America*, *113*(8), E968–E977. https://doi.org/10.1073/pnas.1521230113

Liebisch, G., Binder, M., Schifferer, R., Langmann, T., Schulz, B., & Schmitz, G. (2006). High

throughput quantification of cholesterol and cholesteryl ester by electrospray ionization tandem mass spectrometry (ESI-MS/MS). *Biochimica et Biophysica Acta - Molecular and Cell Biology of Lipids*, *1761*(1), 121–128. https://doi.org/10.1016/j.bbalip.2005.12.007

Linnemannstöns, K., Witte, L., Pradhipa Karuna, M., Kittel, J. C., Danieli, A., Müller, D., … Gross, J. C. (2020). Ykt6-dependent endosomal recycling is required for Wnt secretion in the Drosophila wing epithelium. *Development (Cambridge)*, *147*(15). https://doi.org/10.1242/dev.185421

Liu, X. xu, Liu, W. dong, Wang, L., Zhu, B., Shi, X., Peng, Z. xuan, … Ren, C. ping. (2018). Roles of flotillins in tumors. *Journal of Zhejiang University: Science B*, *19*(3), 171–182. https://doi.org/10.1631/jzus.B1700102

Luga, V., Zhang, L., Viloria-Petit, A. M., Ogunjimi, A. A., Inanlou, M. R., Chiu, E., … Wrana, J. L. (2012). Exosomes mediate stromal mobilization of autocrine Wnt-PCP signaling in breast cancer cell migration. *Cell*, *151*(7), 1542–1556. https://doi.org/10.1016/j.cell.2012.11.024

Mathieu, M., Martin-Jaular, L., Lavieu, G., & Théry, C. (2019). Specificities of secretion and uptake of exosomes and other extracellular vesicles for cell-to-cell communication. *Nature Cell Biology*, *21*(1), 9–17. https://doi.org/10.1038/s41556-018-0250-9

Menck, K., Sönmezer, C., Worst, T. S., Schulz, M., Dihazi, H., Streit, F., … Boutros, M. (2017). Neutral sphingomyelinases control extracellular vesicles budding from the plasma membrane. *Journal of Extracellular Vesicles*, *6*(1). https://doi.org/10.1080/20013078.2017.1378056

Niehrs, C., & Acebron, S. P. (2012). Mitotic and mitogenic Wnt signalling. *EMBO Journal*, *31*(12), 2705–2713. https://doi.org/10.1038/emboj.2012.124

Özbalci, C., Sachsenheimer, T., & Brügger, B. (2013). Quantitative Analysis of Cellular Lipids by Nano-Electrospray Ionization Mass Spectrometry, *1033*, 3–20. https://doi.org/10.1007/978-1-62703-487-6

Paltauf, F., & Hermetter, A. (1994). Strategies for the synthesis of glycerophospholipids. *Progress in Lipid Research*, *33*(3), 239–328. https://doi.org/10.1016/0163-7827(94)90028-0

Peinado, H., Zhang, H., Matei, I. R., Costa-Silva, B., Hoshino, A., Rodrigues, G., … Lyden, D. (2017). Pre-metastatic niches: Organ-specific homes for metastases. *Nature Reviews Cancer*, *17*(5), 302–317. https://doi.org/10.1038/nrc.2017.6

Raposo, G., & Stoorvogel, W. (2013). Extracellular vesicles: Exosomes, microvesicles, and friends. *Journal of Cell Biology*, *200*(4), 373–383. https://doi.org/10.1083/jcb.201211138

Skotland, T., Hessvik, N. P., Sandvig, K., & Llorente, A. (2019). Exosomal lipid composition and the role of ether lipids and phosphoinositides in exosome biology. *Journal of Lipid Research*, *60*(1), 9–18. https://doi.org/10.1194/jlr.R084343

Skotland, T., Sandvig, K., & Llorente, A. (2017). Lipids in exosomes: Current knowledge and the way forward. *Progress in Lipid Research*, *66*, 30–41. https://doi.org/10.1016/j.plipres.2017.03.001

Tassew, N. G., Charish, J., Shabanzadeh, A. P., Luga, V., Harada, H., Farhani, N., … Monnier, P. P. (2017). Exosomes Mediate Mobilization of Autocrine Wnt10b to Promote Axonal Regeneration in the Injured CNS. *Cell Reports*, *20*(1), 99–111. https://doi.org/10.1016/j.celrep.2017.06.009

Théry, C., Witwer, K. W., Aikawa, E., Alcaraz, M. J., Anderson, J. D., Andriantsitohaina, R., …

Zuba-Surma, E. K. (2018). Minimal information for studies of extracellular vesicles 2018 (MISEV2018): a position statement of the International Society for Extracellular Vesicles and update of the MISEV2014 guidelines. *Journal of Extracellular Vesicles*, *7*(1). https://doi.org/10.1080/20013078.2018.1535750

Van Niel, G., D'Angelo, G., & Raposo, G. (2018). Shedding light on the cell biology of extracellular vesicles. *Nature Reviews Molecular Cell Biology*, *19*(4), 213–228. https://doi.org/10.1038/nrm.2017.125

Wesslowski, J., Kozielewicz, P., Wang, X., Cui, H., Schihada, H., Kranz, D., … Gross, J. C. (2020). eGFP-tagged Wnt-3a enables functional analysis of Wnt trafficking and signaling and kinetic assessment of Wnt binding to full-length Frizzled. https://doi.org/10.1074/jbc.RA120.012892

Wiese, K. E., Nusse, R., & van Amerongen, R. (2018). Wnt signalling: Conquering complexity. *Development (Cambridge)*, *145*(12), 1–9. https://doi.org/10.1242/dev.165902

Xi, Y., Ju, R., & Wang, Y. (2020). Roles of Annexin A protein family in autophagy regulation and therapy. *Biomedicine and Pharmacotherapy*, *130*(August), 110591. https://doi.org/10.1016/j.biopha.2020.110591

Supplementary Table 1

Wnt-pCS2 Filtered proteins (630)	Wnt-GFP Filtered proteins (494)
AARSD1	ABCF2
ABCE1	ACACA
ABCF1	ACE
ABCF2	ACOT7
ABCF3	ACSL1
ACACA	ACTB
ACOT7	ACTN1
ACSL1	ACTN4
ACTB	ACTR1A
ACTL6A	AGTRAP
ACTR1A	AHCY
ACTR2	AIMP1
ACTR3	ALDH16A1
ADAM10	ALDOA
ADAMTS1	AMY2A
ADH5	ANAPC7
ADSS2	ANO6
AGTRAP	ANP32E
AHCY	ANXA2
AHCYL1	ANXA7
AKR7A2	AP2A1
ALDH16A1	AP2A2
ALDH1A2	AP3B1
ALDH7A1	APEH
ALDH9A1	AQR
AMY2A	ARCN1
ANAPC2	ARF6
ANAPC5	ARHGDIA
ANAPC7	ARHGDIB
ANKFY1	ARL1
ANKRD28	ARL3
ANO6	ARPC1B
ANP32E	ARPC2
ANXA11	ARPC3
ANXA2	ARPC4-TTLL3
ANXA5	ATP1A1
ANXA6	ATP1B1
ANXA7	ATP1B3
AP2A1	ATP2B1
APAF1	ATP2B4
APRT	ATP5F1A
AQR	ATP5F1B
ARF4	ATP6V0A1
ARF6	ATP6V1A
ARL1	ATR
ARL2	B3GALT6
ARL3	B4GAT1
ARMC8	BAG6
ARPC4-TTLL3	BIRC6
ASCC3	BLMH
ASNA1	BST1
ASNS	BTAF1
ATP1A1	C17orf75
ATP1B3	C3
ATP5F1B	C4A
ATP6V0A1	C5
ATP6V0D1	CA2
ATR	CAB39
ATXN10	CAD
B4GAT1	CAP1
BAG6	CAPN1
BIRC6	CAPZB
BOP1	CBR1
BRAT1	CBS
BSG	CC2D1B
BUD23	CCT6A
C17orf75	CCT8
C3	CD1A
C4A	CD1B
C5	CD36
CA2	CD40
CAB39	CD44
CAD	CD97
CAP1	CDC123
CAPZA1	CDC40

CARM1	CDC42
CCS	CDK4
CCT3	CEP55
CCT6A	CHD4
CCT7	CLEC4A
CDC123	CLTC
CDK2	CMSS1
CDK4	CNP
CDK5	COCH
CDK9	COG2
CELF1	COL18A1
CEP55	COL6A1
CHD4	COPB1
CHST14	COPB2
CIAO1	COPG1
CIP2A	COPG2
CLUH	COPZ1
CNOT1	CPD
CNP	CPM
COCH	CPNE1
COG2	CPNE8
COL18A1	CPSF1
COPE	CPSF2
COPG1	CSNK1A1
COPZ1	CSNK2A1
CPNE1	CTNNA1
CPSF2	CTNNBL1
CPSF7	CTNND1
CSDE1	CXADR
CSK	CYBB
CSNK2A1	DARS
CSNK2A2	DCP1A
CSTF3	DCTN1
CTBP2	DCTN2
CTNNBL1	DDX18
CTNND1	DDX20
CTR9	DDX6
CXADR	DEK
DARS	DERA
DCAF7	DHX33
DCTN1	DHX37
DCTN2	DHX38
DCUN1D5	DNAJA1
DDB1	DNAJA2
DDX47	DNAJC7
DDX6	DNM2
DERA	DNMT1
DHX16	DPYSL2
DHX37	DSG2
DHX38	DYNC1I2
DHX40	DYNC1LI1
DIMT1	DYNLL2
DIPK2A	EDC4
DMWD	EEF1AKNMT
DNAAF5	EEF1B2
DNAJA1	EEF1E1
DNAJA2	EIF2B2
DNAJC7	EIF3A
DNM2	EIF3C
DRG1	EIF3D
DRG2	EIF3G
DSG2	EIF3K
DYNC1I2	EIF3L
DYNLL2	EIF3M
EEF1A2	EIF4A1
EEF1B2	EIF5A
EEF1E1	EIF6
EEF1G	ENO1
EFTUD2	EXOC4
EHD4	EXOC5
EIF2AK2	EXOSC6
EIF2B3	EZR
EIF2B4	F5
EIF2S1	FAM98A
EIF2S2	FANCI
EIF3C	FARSA
EIF3D	FBLN1
EIF3K	FERMT3
EIF3M	FLOT1
EIF5A	FUBP3

EIF6	FXR1
ELAC2	G3BP1
ELP1	G6PD
ELP2	GABARAPL2
ELP3	GDI2
EMG1	GEMIN4
ERCC6L	GEMIN5
EXOC5	GGT5
EXOSC3	GLIPR2
EXOSC4	GMPPA
EXOSC6	GNA11
EZR	GNA13
F5	GNAI2
FARSB	GNAI3
FBLN1	GNB1
FHL1	GNB4
FKBP5	GNL3
FLOT2	GSK3A
FXR1	GSN
G6PD	GSTP1
GABARAPL2	GSTZ1
GALK1	GTF2I
GARS1	GTF3C2
GBA	GTPBP4
GDI2	H1-2
GET4	HBA1;
GLA	HCK
GMDS	HEATR1
GMPS	HGH1
GNA11	HLA-DPB1
GNB2	HLA-DRA
GNE	HLA-H
GSK3B	HLTF
GSPT1	HMCES
GSTM3	HMGCS1
GTF2I	HNRNPA1
GTF3C1	HNRNPM
GTF3C4	HPRT1
GTPBP4	HSPA14
GYS1	HSPA1B
H1-2	HSPA6
H2AFY2	HSPB1
HACD3	HSPD1
HAT1	HTRA3
HBA1;	HVCN1
HBB	ICAM1
HBS1L	IDE
HDAC1	IDI1
HEATR3	IFT27
HELLS	IGSF8
HERC1	ILK
HGH1	INTS1
HNRNPA0	IPO4
HNRNPA2B1	IPO5
HP1BP3	IQGAP1
HSPA14	IRS4
HSPA1B	ISYNA1
HSPA4L	ITGA5
HSPB1	ITGAL
HSPH1	ITIH2
HTATSF1	ITIH3
IDI1	JUP
IGF2BP2	KARS1
IGF2BP3	KCTD12
IGSF8	KDM1A
IKBKB	KDM5C
ILK	KIF2A
INTS4	KIF5B
IPO11	KPNA2
IPO5	KRAS
IQGAP1	KRT3
IRS4	KRT8
ITGB1	LAMA1
ITIH2	LAMB1
ITIH3	LAMC1
JMJD6	LARP1
JUP	LCP1
KCTD12	LDHB
KIF11	LIG3
KIF2A	LLGL1

KIF5B	LMAN1
KIFBP	LMAN2
KPNA2	LNPEP
KRR1	LRRC8C
KRT9	LTF
LAMC1	LUC7L3
LANCL1	LYN
LAP3	MBTPS1
LARP1	MCM4
LARP7	MCMBP
LDHB	MDH2
LIG1	METTL5
LIMS1	MFGE8
LLGL1	MIF
LMAN1	MPP6
LMAN2	MPST
LRATD2	MRC1
LRBA	MSH3
LTF	MSN
LTN1	MTMR2
LTV1	MTR
LUC7L3	MYO1B
MAGED2	MYOF
MAP1S	NAP1L1
MAP2K7	NAT1
MAPK1	NCSTN
MARS	NF1
MAT2A	NID1
MAT2B	NID2
MBTPS1	NIFK
MCM2	NOB1
MCM5	NPEPPS
MCM6	NPM1
MCM7	NPTN
MCMBP	NRP1
MFGE8	NSUN2
MIF	NTMT1
MITD1	NUDT16L1
MOCS3	NUP107
MPG	NUP160
MPP2	NUP93
MPP6	OGFR
MPST	OLA1
MRE11	OSGEP
MSH2	PA2G4
MSH3	PABPC1
MSN	PAICS
MSTO1	PCSK6
MTOR	PCYT2
MTR	PDCD6
MVB12A	PDIA3
MYH10	PECAM1
MYO1B	PELP1
MYO1C	PFN1
MYO6	PGAM1
NAA15	PGK1
NANS	PHKB
NAP1L1	PI4KB
NARS1	PKM
NCAPD2	PLEC
NCAPH	PLS3
NEK9	PLXNB2
NELFB	PM20D2
NID1	PMM2
NID2	PMVK
NIFK	POLR3C
NOB1	POLR3D
NOC4L	POLR3E
NONO	PPIH
NOP2	PPP1CB
NPEPPS	PRDX2
NPM1	PRDX6
NSDHL	PRIM1
NSF	PRIM2
NTMT1	PRKAA1
NUDT16L1	PRKAR2A
NUP133	PRMT5
NUP155	PRPF19
NUP188	PRPF6
NUP43	PSAT1

NUP85	PSMA1
OGFR	PSMA2
OLA1	PSMA3
ORC2	PSMA4
OSGEP	PSMA5
OXSR1	PSMA6
P3H1	PSMA7
P4HA1	PSMB3
PABPC1	PSMB4
PAICS	PSMB5
PANK4	PSMB6
PAXBP1	PSMC1
PDCD4	PSMC3
PDCD6	PSMC4
PDS5A	PSMC5
PFN1	PSMC6
PFN2	PSMD12
PGAM1	PSMD2
PHKB	PSMD4
PI4KA	PSMD6
PI4KB	PSMD7
PLS3	PSMD8
POLR1C	PTAR1
POLR2B	PTGES3
POLR3C	PTPRE
POLR3D	PTX3
POLR3E	PUM3
POP1	PWP1
PPIA	QARS
PPM1G	RAB14
PPP1CB	RAB1A
PPP4C	RAB35
PPP6R3	RAB5A
PRDX2	RAB5B
PRIM1	RAB5C
PRKAA1	RAC1
PRKAR2A	RAC2
PRKRA	RACK1
PRMT5	RAD50
PRPF4	RAE1
PRPF6	RALA
PRPF8	RALB
PRPS1	RANBP1
PRPSAP1	RBBP7
PSMA1	RECQL
PSMA2	RFC5
PSMA3	RFTN1
PSMA4	RHOG
PSMA5	RNH1
PSMA6	RO60
PSMA7	RPA2
PSMB3	RPA3
PSMB4	RPL10A
PSMB5	RPL23
PSMB6	RPL23A
PSMC2	RPL24
PSMC4	RPL28
PSMC5	RPL30
PSMC6	RPL34
PSMD1	RPL36
PSMD12	RPL5
PSMD13	RPL7
PSMD3	RPL7A
PSMD4	RPL9
PSMD6	RPN1
PSMD7	RPP38
PTGES3	RPS10
PTX3	RPS11
PUM3	RPS12
QARS	RPS13
RAB1A	RPS14
RAB7A	RPS15A
RAD50	RPS17
RADX	RPS19
RANBP1	RPS24
RBBP4	RPS26
RBBP7	RPS27A
RCC1	RPS28
RCL1	RPS3A
RECQL	RPS4X

RFC4	RPS7
RFC5	RPS9
RHOT1	RRAS2
RO60	RRP12
RPA1	RTN3
RPL24	RTN4
RPL34	RTRAF
RPP38	RUVBL1
RPS13	RUVBL2
RPS24	SCAMP2
RPS27A	SCAMP3
RPS3A	SEC22B
RPS4X	SEC23IP
RPS7	SEH1L
RPS9	SEPTIN2
RPSA	SEPTIN7
RRAS2	SEPTIN9
RTCA	SERPINB1
RUVBL1	SERPINF1
RUVBL2	SETD3
SAMHD1	SF3A1
SCPEP1	SF3A3
SEC22B	SF3B1
SEH1L	SF3B2
SEPTIN2	SF3B3
SEPTIN7	SF3B6
SEPTIN9	SHMT1
SERPINC1	SIGLEC7
SERPINF1	SLC16A1
SF3A1	SLC1A5
SF3A3	SLC25A6
SF3B1	SLC44A1
SF3B3	SMARCC1
SH3GL1	SNAP23
SHMT1	SNRPA1
SLC16A1	SNRPB
SLC1A5	SNRPD3
SLC3A2	SPTAN1
SMAD3	SPTBN1
SMARCA4	SRBD1
SMARCA5	SRP72
SMARCC1	SRPK1
SNRNP70	SRRT
SNRPA1	SRSF7
SPATA5	SSRP1
SPTAN1	SUGP2
SPTBN1	SULT1A1
SRM	SUPT6H
SRP68	SYPL1
SRP72	TARBP1
SRSF1	TBC1D10B
SSRP1	TBCE
SULT1A1	TELO2
SUPT16H	TEX10
SUPT5H	THOC1
SUPT6H	THOP1
SYPL1	TKT
TAF2	TM9SF3
TARDBP	TOE1
TARS1	TPI1
TBC1D10B	TPM4
TBC1D9B	TPP2
TBCD	TRAPPC4
TCAF1	TRAPPC8
TCP1	TRPV2
TELO2	TSKU
TESK2	TTC30A
TEX10	TTC37
TFIP11	TUBA1A
THBS1	TUBB4B
THOC1	TUBB6
THOC6	TUBG1
THOP1	TUBGCP2
TIMP3	UBA6
TM9SF2	UBR5
TOE1	UCHL5
TPP2	UCKL1
TRAPPC11	UFL1
TRAPPC4	ULK3
TRAPPC8	UNC45A

TRIM25	USP5
TRIM28	USP7
TRIM32	UXS1
TRMT5	VAT1
TRMT6	VCAN
TSKU	VCL
TSR1	VPS36
TSTA3	VPS4A
TTC37	VTA1
TTC38	WDR26
TTC4	WDR6
TTLL12	WDR61
TUBG1	WDR74
U2AF1	WDR77
U2SURP	XPOT
UBA2	XRN2
UBA6	YTHDC2
UBE3C	YWHAE
UBR5	ZC3HAV1L
UCK2	
UGDH	
ULK3	
UMPS	
UNC45A	
USP13	
USP5	
UTP18	
UTP20	
UXS1	
VCAN	
VPS35	
VPS36	
VPS4A	
VTA1	
VTN	
WDR11	
WDR12	
WDR36	
WDR4	
WDR46	
WDR6	
WDR61	
WDR73	
WDR77	
WDR92	
XAB2	
XPNPEP1	
XPO5	
XPO7	
XRN2	
YARS	
YWHAE	
ZNRD2	
ACE	
ACTN1	
ACTN4	
AHSG	
ALDOA	
AP2A2	
ARHGDIA	
ARHGDIB	
ARPC1B	
ARPC2	
ATP1B1	
ATP2B1	
ATP2B4	
ATP5F1A	
ATP6V1A	
ATP6V1B2	
BST1	
CANX	
CAPN1	
CAPZB	
CCT8	
CD1A	
CD1B	
CD36	
CD40	
CD44	
CD97	

CDC42	
CLEC4A	
CLTC	
CPM	
CYBB	
DPYSL2	
EIF3L	
EIF4A1	
ENO1	
FERMT3	
FLOT1	
GGT5	
GLIPR2	
GNA13	
GNAI2	
GNAI3	
GNB1	
GNB4	
GSN	
HCK	
HLA-DPB1	
HLA-DRA	
HLA-H	
HSPA6	
HSPD1	
HVCN1	
ICAM1	
ITGA5	
ITGAL	
KRT3	
KRT8	
LCP1	
LNPEP	
LRRC8C	
LYN	
MRC1	
MYOF	
NCSTN	
NPTN	
NRP1	
PDIA3	
PECAM1	
PGD	
PGK1	
PKM	
PLEC	
PLXNB2	
PRDX1	
PSMD2	
PTPRE	
RAB14	
RAB35	
RAB5A	
RAB5B	
RAB5C	
RAC1	
RAC2	
RALA	
RALB	
RFTN1	
RHOG	
RNH1	
RPN1	
SERPINB1	
SIGLEC7	
SLC25A6	
SLC44A1	
SNAP23	
SYNGR2	
TPM4	
TRPV2	
TUBA1A	
TUBB4B	
TUBB6	
VCL	

Supplementary Table 2

Final list of Exosomal Proteins based on Top EV markers and GO Evs

Wnt-pCS2 Final proteins (55)	Wnt-GFP Final proteins (43)	Overlap (41)
ACTB	ACTB	ACTB
AHCY	ACTN1	AHCY
ANXA11	ACTN4	ANXA2
ANXA2	AHCY	ANXA7
ANXA5	ALDOA	ATP1A1
ANXA6	ANXA2	C3
ANXA7	ANXA7	CAP1
ATP1A1	ATP1A1	CCT6A
BSG	C3	EZR
C3	CAP1	GDI2
CAP1	CCT6A	IQGAP1
CCT3	CCT8	LDHB
CCT6A	CDC42	MFGE8
EHD4	CLTC	MSN
EZR	EIF4A1	PFN1
GDI2	ENO1	PRDX2
GNB2	EZR	RAB1A
IQGAP1	FLOT1	SLC16A1
ITGB1	GDI2	YWHAE
LDHB	GNAI2	ACTN1
MFGE8	GNB1	ACTN4
MSN	GSN	ALDOA
PFN1	IQGAP1	CCT8
PPIA	LDHB	CDC42
PRDX2	MFGE8	CLTC
RAB1A	MSN	EIF4A1
RAB7A	PFN1	ENO1
SLC16A1	PGK1	FLOT1
SLC3A2	PKM	GNAI2
TCP1	PRDX2	GNB1
THBS1	RAB14	GSN
YWHAE	RAB1A	PGK1
ACTN1	RAB5A	PKM
ACTN4	RAB5B	RAB14
ALDOA	RAB5C	RAB5A
CCT8	RAC1	RAB5B
CDC42	RALA	RAB5C
CLTC	SLC16A1	RAC1
EIF4A1	TKT	RALA
ENO1	TPI1	TUBA1A
FLOT1	TUBA1A	TUBB4B
GNAI2	TUBB4B	
GNB1	YWHAE	
GSN		
PGK1		
PKM		
PRDX1		
RAB14		
RAB5A		
RAB5B		
RAB5C		
RAC1		
RALA		
TUBA1A		
TUBB4B		

Supplementary Table 3

Final list of Exosomal Proteins based on Top EV markers and GO Cell cycle

Wnt-pCS2 Final proteins (11)	Wnt-GFP Final proteins (8)	Overlap (8)
ANXA11	CLTC	CLTC
EZR	EZR	EZR
ITGB1	GNAI2	GNAI2
SLC16A1	RALA	RALA
THBS1	SLC16A1	SLC16A1
YWHAE	TUBA1A	TUBA1A
CLTC	TUBB4B	TUBB4B
GNAI2	YWHAE	YWHAE
RALA		
TUBA1A		
TUBB4B		

3.4 Manuscript IV: Ykt6 modulates polyamine levels during cell cycle progression via the PDK1 pathway

Citation:

Pradhipa Karuna M[1], Adi Danieli-Mackay[1], Sabnam Parbin[1], Robert Koerner[1], Mona Honemann-Capito[1] and Julia Christina Gross[1,2,3*]

Individual contributions to the article:
Applicant name: Pradhipa Karuna M (first author)

1. **Main and Supplementary Figures/Tables** (actively performed experiments and/or analyzed data)

   Main: 1B, 1C, 1D, 1E, 1F, 1G, 2A-I, 3C, 4B, 4C, 4D, 4E, 5A-F, 6A-G
   Supplementary: S1A, B, E, F, S2A, B, S3C, D

2. **Writing and Intellectual Contributions**

   - Contributed to writing the entire manuscript such as introduction, results, discussion, materials and methods.
   - Contributed to figure arrangement and figure legends of all the figures.
   - Actively involved in experimental design and closely collaborated with Dr Gabriela Salinas for single-cell RNA sequencing experiments and data analysis.
   - Contributed to data analysis of metabolomics data.

Ykt6 modulates polyamine levels during cell cycle progression via the PDK1 pathway

Pradhipa Karuna M[1], Adi Danieli-Mackay[1], Sabnam Parbin[1], Robert Koerner[1], Mona Honemann-Capito[1] and Julia Christina Gross[1,2,3*]

Affiliations:

[1] Developmental Biochemistry, University Medical Center Goettingen, Goettingen, Germany

[2] Hematology and Oncology, University Medical Center Goettingen, Goettingen, Germany

[3] Health and Medical University Potsdam, Potsdam, Germany

* **Correspondence:**

Julia Christina Gross, Health and Medical University Potsdam, Potsdam, Germany, julia.gross@health-and-medical-university.de

Abstract

SNAREs play a crucial role in steering intracellular trafficking decisions. Ykt6 is a special SNARE protein that exists abundantly in the cytosolic pool in its inactive form, and upon stimuli is recruited to membranes to initiate vesicle fusion events. The promiscuity of the SNARE enables it to localize to diverse loci and regulate a multitude of processes. Here, we demonstrate a so far unfamiliar function of Ykt6 in cell cycle progression. We discovered that lack of Ykt6 affects cell growth and causes a delay in cell cycle progression. Employing a single-cell transcriptomic approach, complemented with flow cytometry, metabolomics and cell cycle synchronization techniques, we identified novel differentially expressed genes regulated by Ykt6. Interestingly, one of the down-regulated genes is SAT1, the rate-limiting enzyme in polyamine catabolism. The polyamines - putrescine, spermidine and spermine, regulated by a combination of synthesis, catabolism and transport, are indispensable for cellular growth and proliferation. We find putrescine to partially rescue the Ykt6 knockdown growth defects in human colon cancer cells. Furthermore, we dissected the molecular mechanism and the signalling pathway underlying the rescue by putrescine. This study elucidates a hitherto unknown role of Ykt6 in modulating the polyamine homeostasis during the cell cycle progression via the PDK1 signalling pathway.

Keywords

SNARE, SAT1, Putrescine, Metabolism, single-cell transcriptome

Introduction

SNARE (soluble N-ethylmaleimide-sensitive factor attachment protein receptor) proteins mediate vesicle fusion events that steer intracellular trafficking decisions. They are functionally categorized as v-SNARE (vesicle) or t-SNARE (target) based on their preferred localization (Ungar & Hughson, 2003) and structurally classified as R-SNARE (arginine) or Q-SNARE (glutamine) based on the conserved amino acids in the SNARE bundle complexes (Sutton, Fasshauer, Jahn, & Brunger, 1998). Typically, fusion events involve complexes formed between three Q-SNAREs donated by target organelles and one R-SNARE donated by the respective vesicle. SNAREs are evolutionarily conserved from yeast to human and unlike other SNAREs, Ykt6 is a special R-SNARE as it lacks a transmembrane domain. Ykt6 has an N-terminal longin domain and a C-terminal SNARE domain. The C-terminal has the consensus 'CCAIM' motif which can be palmitoylated and farnesylated at the cysteine residues respectively. One of the remarkable features of this SNARE is its ability to cycle between cytosol and membranes. A large pool of Ykt6 resides cytosolically in an auto-inhibited closed confirmation and upon activation, a conformation switch occurs which recruits Ykt6 to membranes to initiate vesicle fusion events (Fukasawa, Varlamov, Eng, Sollner, & Rothman, 2004; Wen et al., 2010). This gives an advantage to the SNARE to induce vesicle fusion events in diverse cellular compartments. However, the promiscuity of the SNARE also requires it to be tightly regulated, to prevent any fusion anomalies. For example, the longin domain indirectly regulates Ykt6 localization through intramolecular interactions with the SNARE domain to prevent promiscuous target interactions (Hasegawa, 2004). Another well-known regulatory mechanism is through phosphorylation of evolutionarily conserved residues in the SNARE domain (Malmersjö et al., 2016), where phosphorylation of Ykt6 triggers the open conformation which further determines its membrane recruitment and activity (Barz et al., 2020; McGrath et al., 2021; Pradhipa Karuna et al., 2020).

Ykt6 acts at the crossroads of secretory, endocytic and autophagy pathways and has a multifunctional role in diverse processes such as ER-Golgi trafficking (McNew et al., 1997; Zhang & Hong, 2001), exosomal Wnt secretion (Gross et al., 2012; Linnemannstöns et al., 2020), autophagosome-lysosome fusion (Bas et al., 2018; Gao et al., 2018; Nair & Klionsky, 2011). One of the intriguing roles of the SNARE is the ability to get recruited to organelles especially during stressful situations. Ykt6 adapts to nutrient stress in breast cancer cells by transport of leucine transporter to the plasma membrane (Saito et al., 2019), regulates autophagy under starvation conditions (Barz et al., 2020; McGrath et al., 2021), adapts to lysosomal stress in Parkinson's disease (Cuddy et al., 2019) and acts as a stress sensor in yeast (Dietrich et al., 2004). Since Ykt6 is involved in such crucial processes, it contributes to adapting to stress situations under physiological conditions, hijacked by cancer cells in its

favour. In fact, Ykt6 is up-regulated in p53-mutated breast tumours (Ooe et al., 2007) and metastatic tumours (Kluger et al., 2004). We set out to investigate if Ykt6 could play a potential role in regulating the cell cycle progression. The cell cycle is a precisely coordinated process, where the progression from one phase to another is tightly regulated by oscillating levels of cyclins and cyclin-dependent kinases. Important regulatory mechanisms occur during the G1 phase, where the cells ensure that they have enough nutrients and growth factors to help them grow and divide during the next phase. Amongst all the nutrients, growth factors and molecules required for a faithful cell cycle progression, polyamines are a category of small organic cations, that oscillates during the cell cycle and are essential for normal cell cycle progression (Nasizadeh et al., 2005; Ray et al., 1999).

The polyamines – putrescine, spermidine and spermine play an important role in regulating cellular growth and proliferation. SAT1 (spermidine/spermine N^1-acetyltransferase) is a key enzyme in polyamine catabolism, which catalyzes the acetylation of spermidine or spermine to generate N^1-acetylspermidine or N^1-acetylspermine, and N^1, $N^{1,2}$-diacetylspermine. These acetylated polyamines are then susceptible to either be exported out or converted back to putrescine or spermidine by N^1-acetylpolyamine oxidase (PAO) (Pegg, 2008). Therefore, overexpression of SAT1 leads to an overall depletion of spermidine and spermine while increasing the levels of putrescine and N^1-acetylspermidine. SAT1 has an important role in translation initiation (Lee et al., 2010) and its over-expression leads to rapid arrest in protein synthesis (Mandal et al., 2013).

In this study, we discovered a role of Ykt6 in regulating the cell cycle progression, where Ykt6 deficient cells show a significant G1 delay during the cell cycle progression and have reduced mitotic index, which makes them proliferate/divide slower. To deduce the so far unknown role of Ykt6 in the cell cycle, we used a single-cell transcriptomic approach and identified novel genes differentially regulated by Ykt6 in human colon cancer cell lines (HCT116). Notably, these genes were linked to membrane trafficking, metabolomic pathways and cell cycle processes. One of the identified genes SAT1, a key catabolic enzyme of the polyamine pathway, was down-regulated upon Ykt6 knockdown specifically in the G1 phase of the cell cycle. Remarkably, putrescine is able to partially rescue the growth defects caused by the loss of Ykt6 and putrescine is able to recruit Ykt6 to the membranes via the PDK1 signalling pathway. This study highlights a novel function of how Ykt6 could regulate the metabolic status of the cell by adapting the polyamine levels during cell cycle progression.

Results

Ykt6 KD reduces cell proliferation independently of apoptosis

Ykt6 is an essential gene in yeast (Ungermann et al., 1999) and is expressed ubiquitously in a variety of tissues (Catchpoole & Wanjin, 1999). We previously showed that Ykt6 knockdown causes growth defects *in vivo* (Linnemannstöns et al., 2020). To extend these findings in human cell culture, we used HCT116 colon cancer cells. In line with the *in vivo* data, we confirmed that knockdown of Ykt6 affects the cell's viability (Fig. 1A, S1A). We next monitored the rate of proliferation, which revealed that cells with Ykt6 knockdown proliferate much slower compared to their control counterparts (Fig. 1B). A similar pattern was observed in Hek293T cells (Fig. S1B). Since, we observed a delay in cell growth and proliferation, we next asked if knockdown of Ykt6 leads to apoptosis. Therefore, we performed an Annexin V-FITC/PI, a live and sensitive method that truly discriminates between nuclear debris and true apoptotic nuclei by staining phosphatidyl serine in the extracellular leaflet of the plasma membrane of apoptotic cells (Koopman et al., 1994). The cells were sorted into four regions, bases on PI vs Annexin-FITC stain, as represented by two-dimensional scatter plots (Fig. 1C, D). The plots are divided into four quadrants: viable cells negative to both the staining (Annexin V^-/PI^-), early apoptotic cells (Annexin V^+/PI^-), late apoptotic cells positive to both the staining (Annexin V^+/PI^+) and necrotic cells (Annexin V^-/PI^+). Tnfα, known to induce apoptosis was used as a positive control. Tnfα treated cells are less viable as seen in the scatter plots (Fig. 1D, left) and more apoptotic as represented in the Annexin V single scatter population (Fig. 1D, right) compared to the control cells (Fig. 1C). Interestingly, Ykt6 KD cells are less viable (Fig. 1E, F) as observed previously (Fig. 1A) but do not induce apoptosis (Fig. 1E). Comparing the early and late apoptotic cells separately revealed no significant increase in apoptosis with Ykt6 KD (Fig. 2G, H). Taken together, knockdown of Ykt6 leads to reduced growth and proliferation, but does not induce apoptosis.

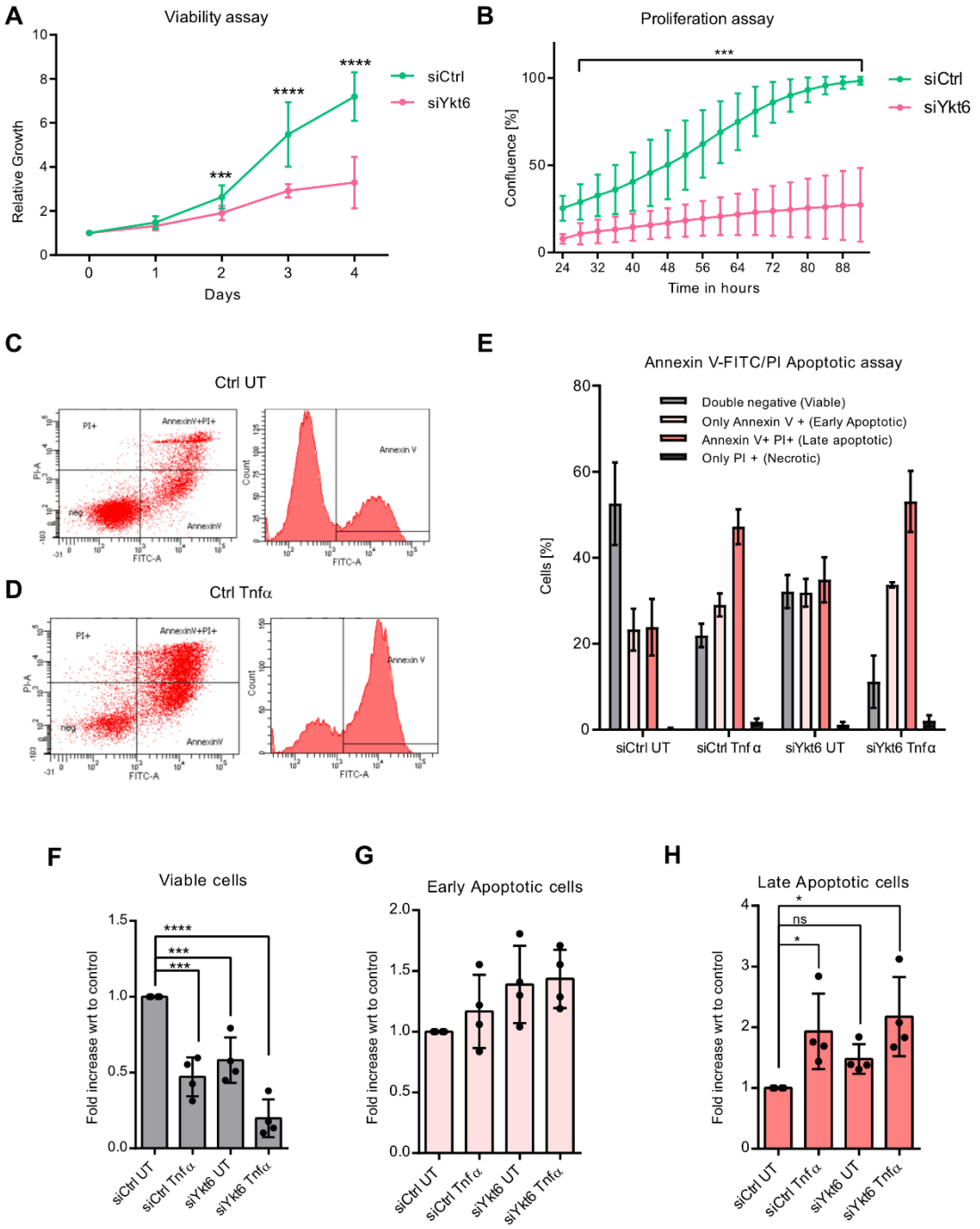

Figure 1: Ykt6 KD reduces cell proliferation independently of apoptosis. (A) Viability assay in HCT116 cells as measured by relative growth vs no. of days, normalized to day 0, in control or Ykt6 KD cells. **(B)** Rate of proliferation in HCT116 cells as measured by confluence percent vs time, in control or Ykt6 KD cells, n=3 **(C)** (left panel) Two dimensional scatter plot representing the population of cells gated into four quadrants and sorted based on PI vs Annexin V FITC staining, in the control untreated cells; (right panel) Population of cells gated and sorted based on only Annexin V FITC staining, in control untreated cells **(D)** (left panel) Two dimensional scatter plot representing the population of cells gated

into four quadrants and sorted based on PI vs Annexin V FITC staining, in the control cells treated with Tnfα (right panel); Population of cells gated and sorted based on only Annexin V FITC staining, in control cells treated with Tnfα **(E)** Percentage of cells sorted into: viable cells negative to both the staining (Annexin V^-/PI^-), early apoptotic cells (Annexin V^+/PI^-), late apoptotic cells (Annexin V^+/PI^+) and necrotic cells (Annexin V^-/PI^+), in control or Ykt6 KD in the presence or absence of Tnfα. **(F)** The percentage of viable cells from (F) normalized to the control, represented as fold increase. **(G, H)** The percentage of early apoptotic cells and late apoptotic cells from (E) normalized to the control, represented as a fold increase. All experiments were done with at least three biological replicates; *p<=0.05, **p<=0.01, ***p<=0.001, ****p<=0.0001

Ykt6 KD leads to G1 delay and reduced mitotic index

As Ykt6 KD cells grow and proliferate slower, we next monitored the cell cycle progression using flow cytometry. The cells are sorted into different cell cycle phases, along with the mitotic phase based on the PI (propidium iodide) staining that binds stoichiometrically to DNA (Fig. 2A) and MPM-2 antibody which stains the mitotic cells respectively (Riccardi & Nicoletti, 2006). The steady-state distribution of the cells in each cell cycle phase based on flow cytometry revealed that approximately 50% of the cells are in the G1 phase, 10% in the S phase, 40% in the G2/M phase and 2% of the cells are in mitotic phase (Fig. 2B). Interestingly, with Ykt6 KD we observe a small but significant increase in the percentage of cells in the G1 phase compared to the control cells, which is an indication of G1 delay (Fig. 2C). During the G1 phase of the cell cycle, the cells constantly monitor nutrient availability and growth factor levels that govern progression to the next phase (Lodish et al., 2004). In agreement, fewer cells are detected in the S phase (Fig. 1D) and G2/M phase compared to control cells (Fig. 1E). We reasoned that the G1 delay could be an indication of stress due to the lack of Ykt6. In response to replication errors, DNA damage, nutrient deprivation or other stresses, the cell cycle checkpoint is triggered, p53 is activated, which causes cell cycle arrest or cell death (Giono & Manfredi, 2006). Only the cells that meet the required criteria, get past the checkpoints to the following cell cycle phase. Hence, lesser cells enter the subsequent phases of the cell cycle with Ykt6 KD. Interestingly, although only a few percent of cells are in the mitotic phase, we observe a significant decrease in the percentage of cells in the M phase upon Ykt6 KD. This indicates a reduced mitotic index which explains the delay in proliferating/dividing cells (Fig. 1F). This is in line with the study, where Ykt6 overexpression leads to an increase in mitotic index and results in smaller cells (Thayanidhi et al., 2012). Concordantly, we observed that upon Ykt6 knockdown, the cells shift to a larger size fraction as measured by the flow cytometry (Fig. 1G, S1C, D). Taken together, we show that lack of Ykt6 slows down the growth and proliferative capacity of the cells, which is indicated as G1 delay and reduced mitotic index during the cell cycle progression.

The progression of the cell cycle relies on stress or damage sensors that signal mediator proteins, which in turn binds and regulates transcription factors to halt the cell cycle temporarily or permanently. p53, a tumour suppressor gene and a transcription factor can integrate stress signals from multiple pathways and regulate a plethora of genes by directly binding to them (Finlay, Hinds, & Levine, 1989). Few of the well-studied target effects include cell cycle arrest mainly mediated by CDKN1A or p21 or apoptosis, based on the encountered stress and cell type (Beauséjour et al., 2003; J. Chen, 2016). p21 is a universal cyclin-dependent kinase inhibitor and induces cell cycle arrest at the G1 phase by inhibiting cyclin-CDK complexes involved in the G1/S transition (Wade Harper, Adami, Wei, Keyomarsi, & Elledge, 1993). Having identified that Ykt6 KD does not induce apoptosis, we next asked if Ykt6 KD induces cell cycle arrest. Cell cycle arrest is measured by an increase in p21 levels both transcriptionally and translationally (Sekiguchi & Hunter, 1998; Xiong et al., 1993). Concordantly, we see that p21 protein levels were not increased upon Ykt6 KD (Fig. 2H, I). Taken together, knockdown of Ykt6 does not induce apoptosis or a visible cell cycle arrest, however, a repair mechanism might be involved, visible as a significant G1 delay and a reduced mitotic index.

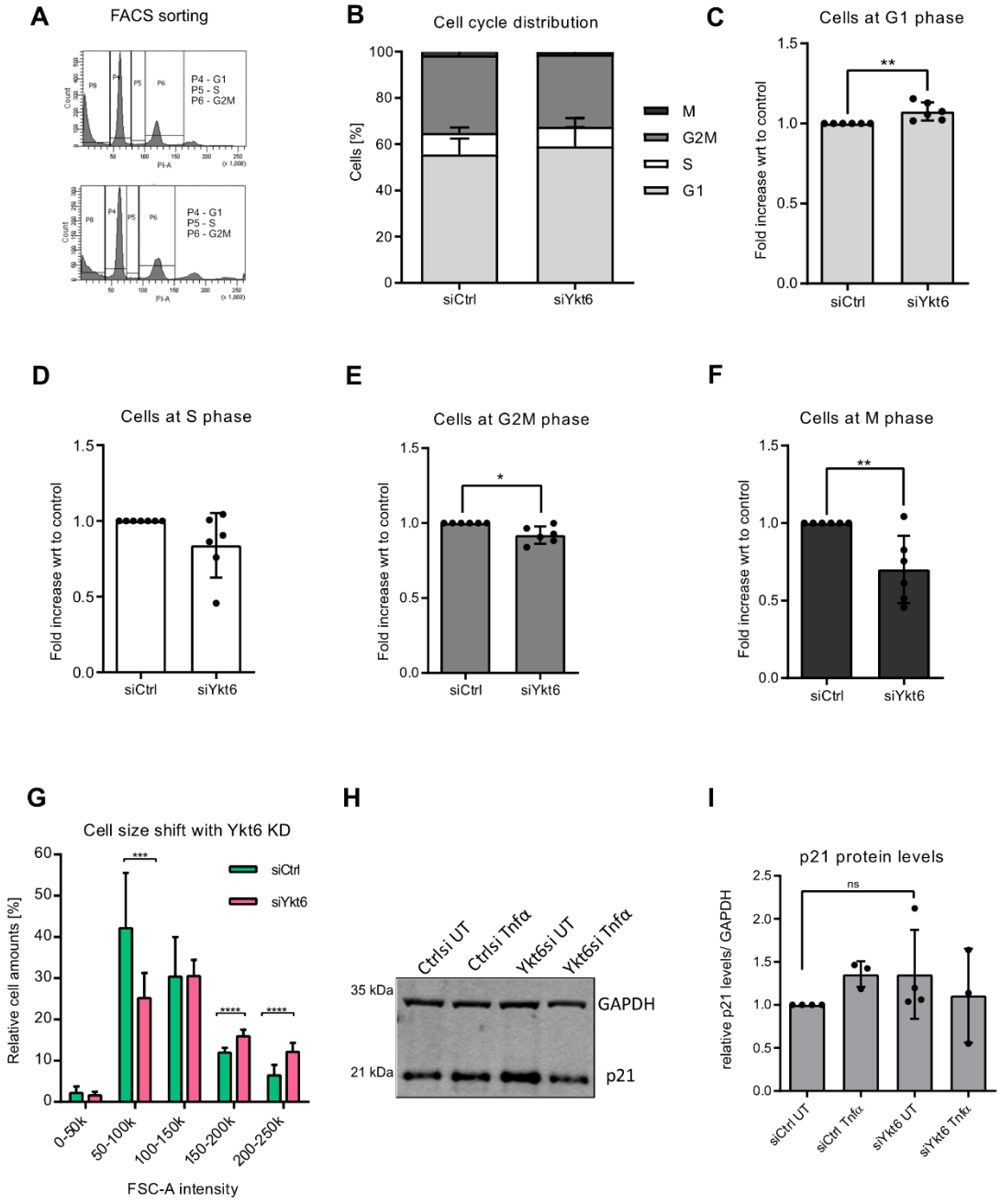

Figure 2: Ykt6 KD leads to G1 delay and reduced mitotic index. (A) The population of cells gated to sort for G1, S, G2/M phase using flow cytometry. **(B)** Percentage of cells sorted for G1, S, G2/M and M phase of the cell cycle using flow cytometry, n=6. **(C)** Percentage of cells sorted for G1 phase from (B) normalized to the control, represented as a fold increase. **(D-F)** Percentage of cells sorted for S, G2/M and M phase respectively from (B) normalized to control, represented as a fold increase **(G)** Cells sorted based on size bins as measured by the forward scatter intensity in the flow cytometry in control or Ykt6 KD cells, normalized to the control cells in each size bin. **(H)** Representative western blot of p21 levels in control or Ykt6 KD in the presence or absence of Tnfα **(I)** Quantification of WB from (H) normalized to the respective GAPDH levels, followed by normalization to the control UT sample. All experiments were done with at least three biological replicates; *p<=0.05, **p<=0.01, ***p<=0.001, ****p<=0.0001

Ykt6 shows stable expression levels during cell cycle phases

Ykt6 is highly expressed in neurons and over-expressed in metastatic tumours (Kluger et al., 2004; Ooe, Kato, & Noguchi, 2007). To investigate if Ykt6 is differentially expressed during the cell cycle, we synchronized HCT116 cells using double thymidine and CDK1 inhibitor RO-3306. In the double thymidine synchronization, the excess thymidine inhibits DNA synthesis, thereby arresting cells at the early S phase. After thymidine release, the cells progress through the subsequent cell cycle phases synchronously, where they enter the S phase in 0-2 hours, followed by the G2/M phase between 6-8 hours post-release (Fig. S3A) (Ma & Poon, 2016). In the RO-3306 synchronization, the cells are blocked at the G2/M border due to inhibition of CDK1 which is required for G2 to M transition and when released, the cells enter the M phase in 0-2 hours, followed by the G1 phase between 6-8 hours (Fig. S3B) (Vassilev et al., 1962). Ykt6 protein levels are stable throughout the cell cycle phases (Fig. 3A, B). Ykt6 mRNA levels did not show a significant difference in expression levels in the cell cycle phases by quantitative PCR (Fig. 3C). A significant portion of Ykt6 resides in membrane-associated particles that form aggregates, visible as a puncta in fluorescence microscopy (Thayanidhi et al., 2012). Using confocal microscopy, we explored the localization of Ykt6 in different cell cycle phases (Fig. 3D). The localization of Ykt6 was unchanged during the cell cycle phases as quantified by the total cellular fluorescence and the puncta number per cell (Fig. 3E, F). Using several different methods, we observe that Ykt6 is not differentially expressed or localized during cell cycle phases.

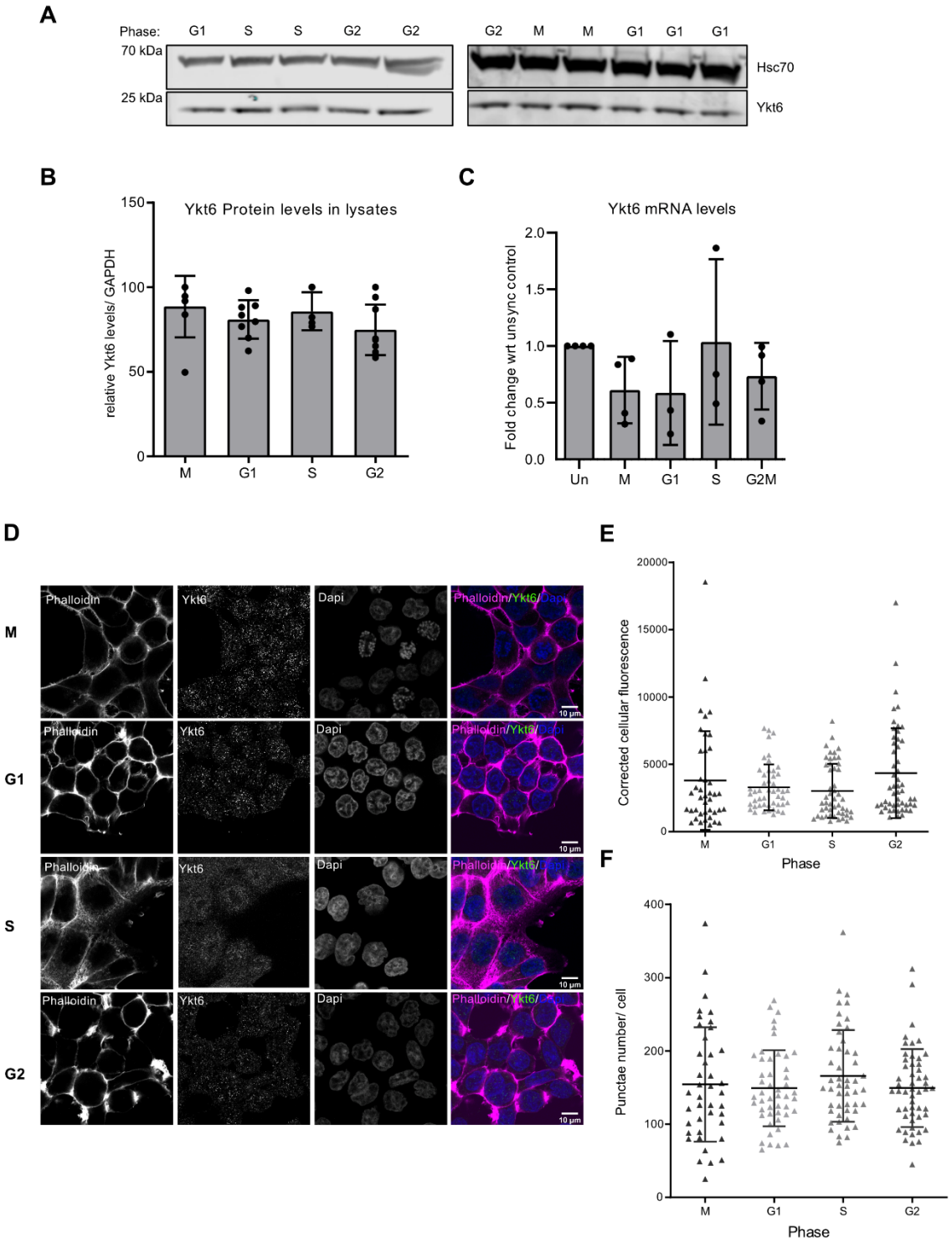

Figure 3: Ykt6 shows stable expression levels during cell cycle phases. **(A)** Representative western blot of Ykt6 during different cell cycle phases in synchronized cells. **(B)** Quantification of WB from (A) normalized to the respective Hsc70 levels. **(C)** Quantitative Real-time PCR (q-RT PCR) of Ykt6 expression levels in synchronized cells during different cell cycle phases normalized to β-actin levels, followed by normalizing to the unsynchronized control. **(D)** Representative immunofluorescence in

HCT116 cells stained for Ykt6, Phalloidin and Hoechst. Scale bar represents 10uM. **(E, F)** Quantification of corrected cellular fluorescence and puncta number per cell from (D).

Transcriptomic profiling of Ykt6 reveals novel differentially regulated genes

Although Ykt6 expression levels were unchanged throughout the cell cycle phases, the knockdown of Ykt6 affects the progression of the cell cycle. Ykt6 is involved in diverse functions such as Golgi growth (Shirakawa et al., 2020), nutrient stress adaptation (Saito et al., 2019) or trafficking of Wnt proteins (Gross, Chaudhary, Bartscherer, & Boutros, 2012), that could potentially occur during the G1 phase of the cell cycle. Therefore, we employed an unbiased single-cell transcriptomic approach to identify novel Ykt6-dependent expression patterns during the cell cycle progression. HCT116 treated with control or Ykt6 siRNA, reveal a heterogeneous population of single cells as represented by the tSNE plot (Fig. 4A). tSNE plot (t-Distributed Stochastic Neighbour Embedding) is a common pipeline used for visualizing the local structure of high-dimensional data in two dimensions (Kobak & Berens, 2019). A string network analysis, where the network interactions were increased by one level, revealed that the differentially regulated genes were primarily connected by cell cycle processes (Fig. 4B) (Szklarczyk et al., 2019). The 16 differentially genes are portrayed in the heat map based on their expression levels (Fig. 4C). Furthermore, the mRNA expression levels of these genes were analyzed using quantitative RT-PCR, which further validated the expression levels from the transcriptomic data (Fig. 4C, S2A).

We then performed a panther based enrichment analysis to investigate the pathways and processes these genes are connected to (J. E. Chen & Glover, 2016). The Reactome pathway analysis of upregulated genes revealed that membrane trafficking pathways (ER-Golgi, Golgi-ER) are enriched upon Ykt6 knockdown (Fig. 4D, S1E). This fits with the diverse trafficking role Ykt6 plays in the secretory pathway such as Wnt secretion (Gross et al., 2012) and with its essential role for proper Golgi function (Shirakawa et al., 2020). Other up-regulated genes include genes involved in the Interferon signalling pathway (IFI6 and ISG15), which are highly expressed post-infection known to regulate DNA-damage mediated apoptosis or misfolded protein degradation respectively (Huang, Wee, Gunaratne, Lane, & Bulavin, 2014; Qi et al., 2015). Apart from the antiviral activity, they have potent anti-mitogenic activity based on various stress stimuli (Olle Sangfelt, 2000). Many cytoskeletal and scaffolding genes such as AKAP12 and STMN1 that regulate cell migration and microtubule dynamics in the cell cycle are enriched as well (Akakura & Gelman, 2012; Han, Poppinga, & Schmidt, 2015; Rubin & Atweh, 2004). Interestingly, we observed that the ornithine decarboxylation pathway is upregulated, which is a key metabolic process involved in polyamine biosynthesis. The ornithine decarboxylase (ODC) enzyme activity oscillates during the cell cycle peaking at the

G1/S and G2/M boundary (Heby et al., 1981) and the first rate-limiting step in polyamine biosynthesis. All the down-regulated pathways and processes were related to cell cycle, cell cycle transition and cell cycle checkpoints (Fig. 4E, S1F). Therefore, single-cell transcriptomics revealed novel Ykt6-dependent genes majorly involved in membrane trafficking, cell cycle and metabolism.

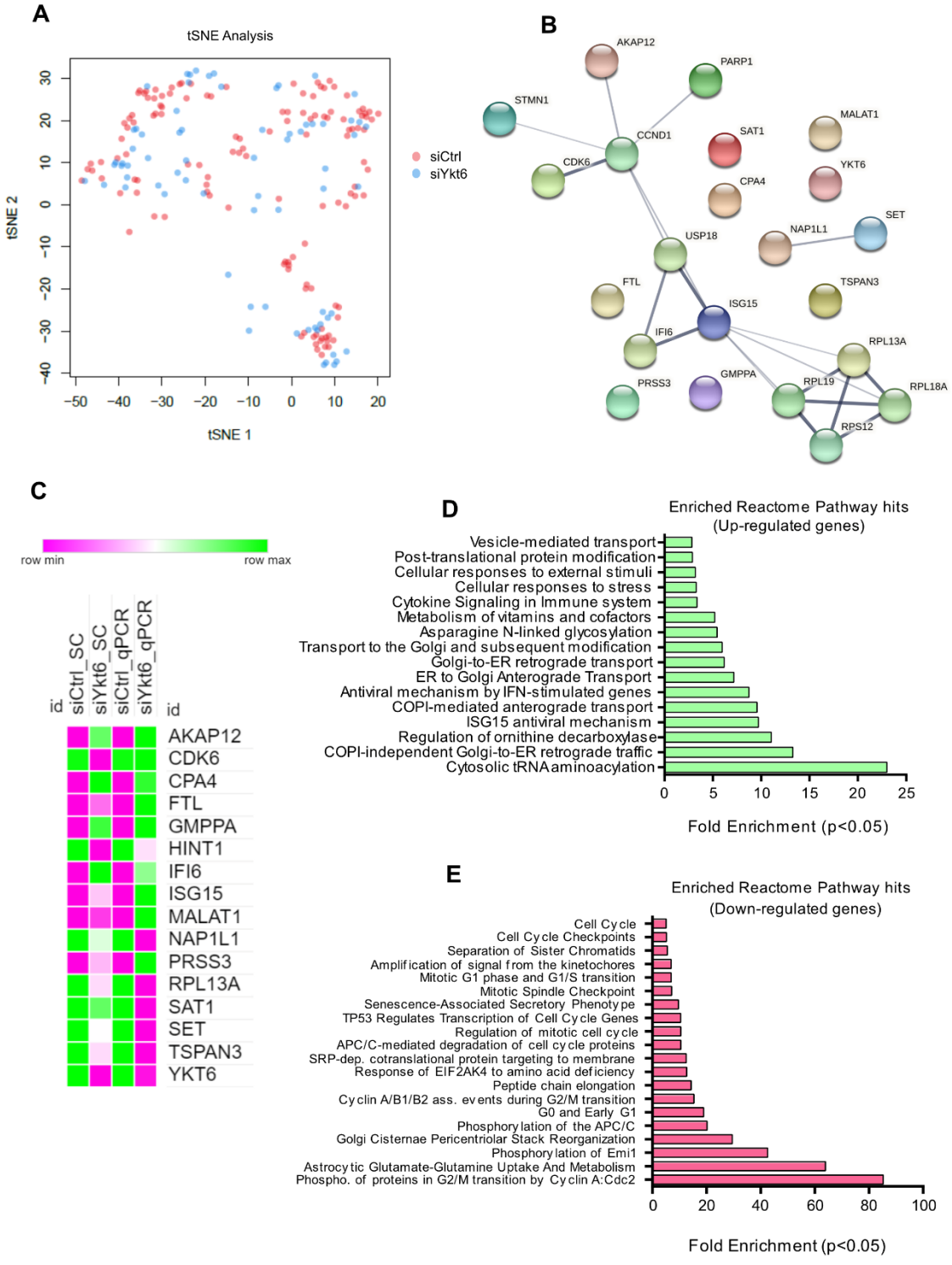

Figure 4: Transcriptomic profiling of Ykt6 reveals novel differentially regulated genes. **(A)** tSNE plot representing the distribution of single cells in control or Ykt6 KD samples in a two-dimensional space. **(B)** String network of differentially expressed genes with Ykt6 knockdown. **(C)** Heatmap representing the up or down-regulated genes based on the expression levels in Control or Ykt6 KD, as measure by quantitative PCR and single-cell RNA sequencing. **(D)** Enriched Reactome pathways of up-regulated genes with Ykt6 KD ($p<0.05$) as determined by Fisher Exact Test with the Benjamini-Hochberg False Discovery Rate <0.05. **(E)** Enriched Reactome pathways of down-regulated genes with Ykt6 KD ($p<0.05$) as determined by Fisher Exact Test with the Benjamini-Hochberg False Discovery Rate <0.05.

Ykt6 KD reduces SAT levels and leads to polyamine deficiency

Ykt6 was previously reported to adapt nutrient levels in cells during starvation, by trafficking leucine transporter (SLC7A5) to the plasma membrane to promote leucine uptake (Saito et al., 2019). Ykt6 is a potential regulator of GLUT4 trafficking in human cells (Morris et al., 2020) and is known to be involved in autophagosome-lysosome fusion especially during nutrient starvation (Barz et al., 2020). Therefore, we reasoned that Ykt6 could be involved in fine-tuning the metabolic requirements of the cell during cell cycle progression. Concordantly, one of the genes down-regulated with Ykt6 knockdown is a key metabolic enzyme involved in polyamine biosynthesis, SAT1. SAT1 (Spermidine/spermine N^1-acetyltransferase) catalyses the N^1-acetylation of spermidine and spermine and, by the successive activity of polyamine oxidase (PAO), spermine can be converted to spermidine and spermidine to putrescine, as represented in the scheme (Fig. 5A). SAT1 is considered the global polyamine rheostat and plays an important role in translation initiation and its overexpression inhibits protein synthesis (Mandal, Mandal, Johansson, Orjalo, & Park, 2013). Polyamines act at the G1/S of the cell boundary and depletion of polyamines leads to cell cycle delay at G1/S transition majorly and G2/M minorly (Ray et al., 1999; Yamashita et al., 2013). To determine the specific cell cycle phase where Ykt6 affects SAT1, we monitored the expression levels of SAT1 upon Ykt6 knockdown during different cell cycle phases. Upon Ykt6 KD, SAT1 was significantly down-regulated in unsynchronized cells in line with the transcriptomic data, however, the cell cycle synchronizers reduced the overall SAT1 expression levels during the cell cycle phases (Fig. 5B). Nevertheless, by normalizing each Ykt6 KD to its respective control in a specific cell cycle phase, we observed that SAT1 was down-regulated in the G1 and G2/M phase upon Ykt6 KD (Fig. 5C). These results indicate that lack of Ykt6 affects the cell cycle progression through SAT1 levels, which in turn would affect the polyamine levels. To investigate the polyamine levels upon Ykt6 knockdown, we performed metabolomic profiling. As expected, the polyamines putrescine, spermidine and spermine levels were lower in Ykt6 KD compared to the control as represented in the heatmap (Fig. 5D). Interestingly, the amino acids upstream of polyamine biosynthesis arginine and ornithine that feed into the polyamine biosynthetic

pathway are down-regulated as well (Fig. 5D). Therefore, the cells have reduced level of polyamines upon Ykt6 KD, possibly due to the requirement of Ykt6 in trafficking of the polyamine transporters. The down-regulation of SAT1 could be a compensatory mechanism to ensure enough reserves of spermidine and spermine for protein synthesis and cell growth.

Typically, SAT1 levels are maintained low, so the cells have enough spermidine and spermine for protein synthesis (Pegg, 2008). To deduce, if Ykt6 could affect the cell cycle progression via SAT1, we assessed protein synthesis levels in Ykt6 KD cells using puromycin labelling as a readout (Crossland, Smith, Atherton, & Wilkinson, 2017). We reasoned that Ykt6 KD cells that have lower levels of SAT1, should lead to increased protein synthesis compared to the control. In line with our hypothesis, the protein levels were increased significantly with Ykt6 knockdown (Fig. 5E, F). In mammalian cells, cell growth which majorly depends on protein synthesis continues, even when the cell cycle progression is blocked. This is indicated by an increased percentage of cells in the G1 phase and an increase in cell size (Faridi, Fawcett, Wang, & Roth, 2003). This is in line with our results, where Ykt6 KD cells reveal a delay in the G1 phase, increase in cell size and delay in proliferation. Taken together, we show that lack of Ykt6 leads to lower levels of SAT1 and polyamines, which leads to a delay in cell cycle progression.

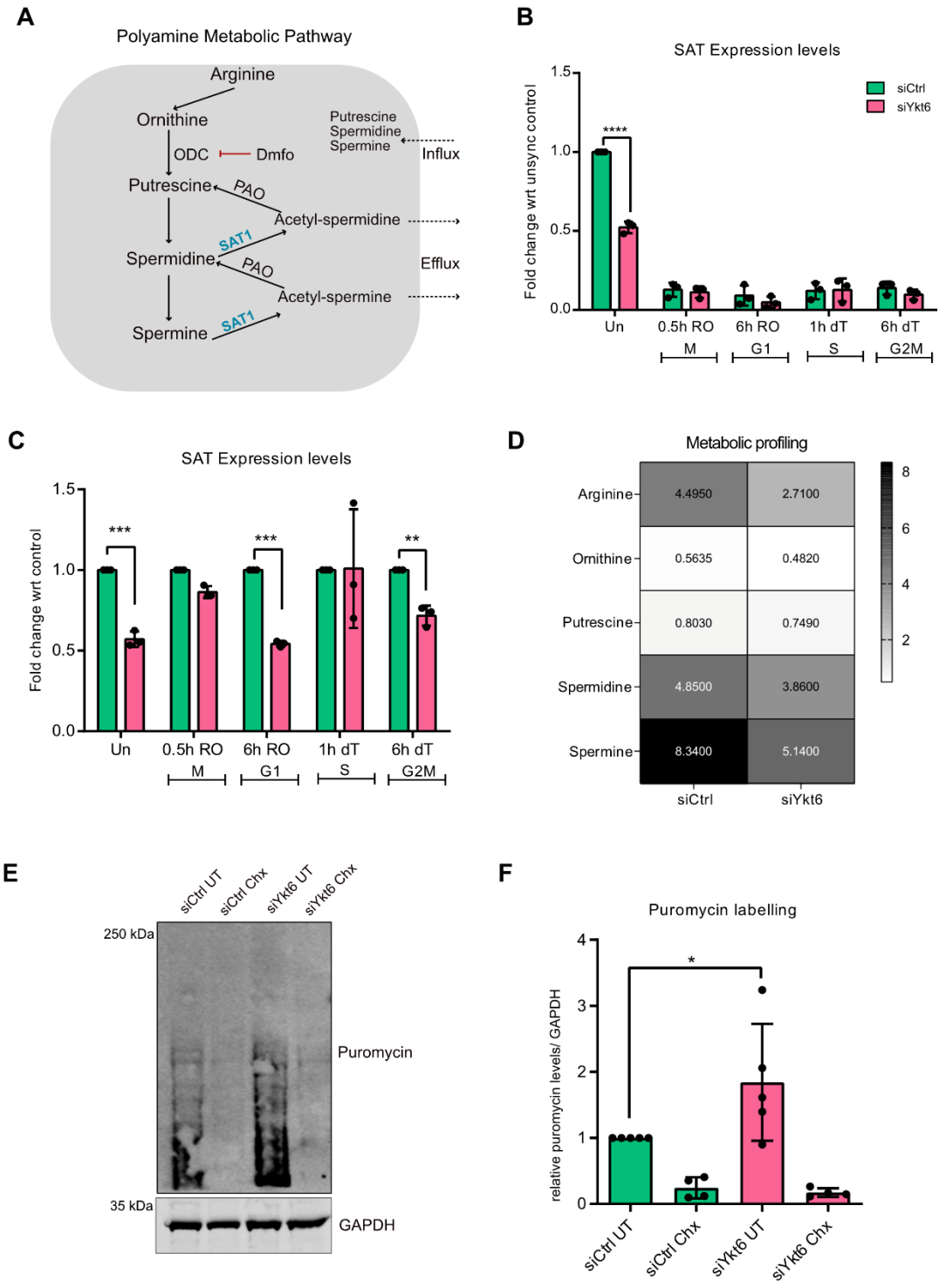

Figure 5: Ykt6 KD reduces SAT levels and leads to polyamine deficiency. (A) Scheme of polyamine biosynthetic pathway. **(B)** Quantitative Real-time PCR (q-RT PCR) of SAT1 expression levels in synchronized cells, normalized to β-actin levels, followed by normalizing with unsynchronized control. **(C)** Quantitative Real-time PCR (q-RT PCR) of SAT1 expression levels in synchronized cells during different cell cycle phases, normalized to β-actin levels, followed by normalizing with the respective control in each phase. **(D)** Metabolic profiling of HCT116 cells in control vs Ykt6 KD from two biological

replicates. **(E)** Representative western blot of puromycin levels, in control and Ykt6 KD cells treated with or without cycloheximide (Chx). **(F)** Quantification of WB from (E) normalized to the respective GAPDH levels, followed by normalization to the siCtrl UT sample.

Putrescine partially rescues the viability defects of Ykt6 KD via the PDK1 pathway

Since Ykt6 KD cells have reduced levels of polyamines, the cells could down-regulate SAT1 to ensure sufficient reserves of spermidine and spermine for cell growth and translation. We hypothesized that adding polyamines back to the Ykt6 KD cells could rescue the effect on cell growth and proliferation. To explore this, we performed a viability assay based on ATP quantitation, where we monitored the growth curve of control and Ykt6 KD cells at 24 and 48 hours after the addition of different polyamines, Dmfo (alpha-difluoromethylornithine), which inhibits polyamine biosynthesis and Tnfα as a positive control (Fig. S3C). Surprisingly, putrescine partially rescues the viability of Ykt6 KD at 24h and 48h (Fig. 6A, B, S3C). Putrescine can subsequently be metabolized into spermidine and spermine. Counter-intuitively, spermidine and spermine did not rescue the viability of the cells (Fig. 6A, S3D). The control or Ykt6 KD cells have a similar pattern with different treatments, except putrescine, which partially increases the viability of only Ykt6 KD cells and not the control (Fig. 6A, S3C). We further confirmed the rescue of viability by putrescine using Annexin V-FITC/PI staining as well, where the Ykt6 KD cells are more viable when treated with putrescine (Fig. 6C, D).

We next investigated the potential signalling pathway and the molecular mechanism underlying the rescue of Ykt6 KD phenotype with putrescine. Polyamine depletion was shown to induce PDK1 phosphorylation, which in turn increases its kinase activity (Keledjian, Marasa, Wang, & Rao, 2012). From our previous study, we identified PDK1 to phosphorylate Ykt6 *in vitro* (Pradhipa Karuna et al., 2020). Since polyamines act upstream of PDK1 signalling, we first investigated the effect of PDK1 on Ykt6 activity (Keledjian et al., 2012). Interestingly, inhibition of PDK1 by BX-795 inhibitor led to the membrane recruitment of Ykt6, whereas activating the kinase by PS-48 did not recruit the Ykt6 to membranes (Fig. 6E). Instead of inhibitors, we next activated or inhibited the PDK1 pathway further upstream with the addition or depletion of polyamines to understand the recruitment of Ykt6. To this end, we added the polyamines putrescine and spermine along with Dmfo. Again, adding putrescine, but not spermine led to the recruitment of Ykt6 via inhibiting the PDK1 pathway (Fig. 6F, G). Interestingly, polyamine homeostasis majorly depends on putrescine uptake, which is crucial for G1 to S phase transition (Martin, Ilett, & Minchin, 1991). Therefore, Ykt6 may be involved in the trafficking of polyamine transporters during the cell cycle progression. Taken together, we show that the growth delay of Ykt6 could be partially rescued by supplementing putrescine through the PDK1 signalling pathway.

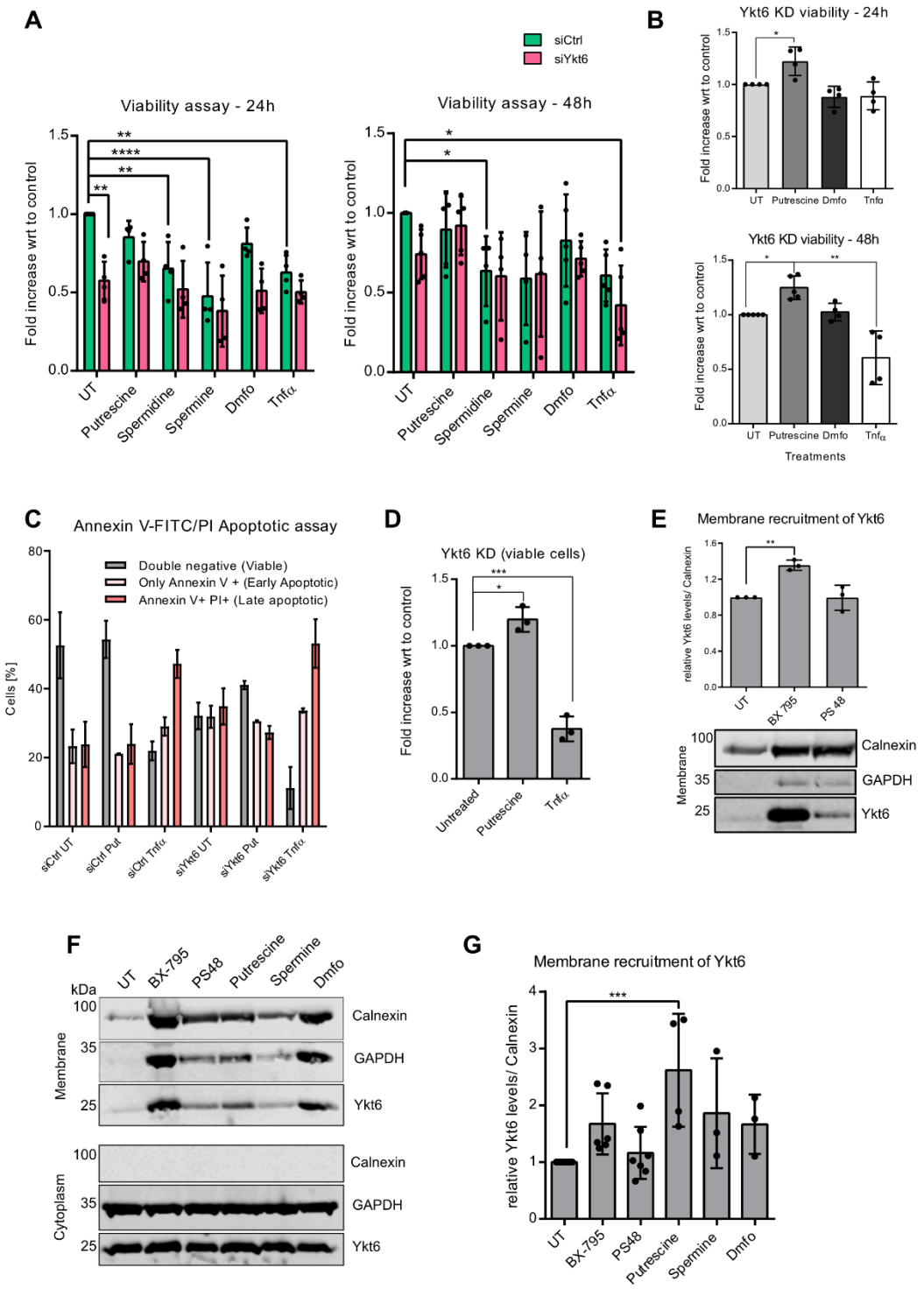

Figure 6: Putrescine rescues the viability defects of Ykt6 KD via the PDK1 pathway. (A) Viability assay representing the relative growth with different treatments: putrescine, spermidine, spermine, Dmfo and Tnfα in control and Ykt6 KD cells, normalized to control untreated cells represented as a fold increase, measured at 24 hours and 48 hours. **(B)** The relative growth of Ykt6 KD cells treated with putrescine, Dmfo and Tnfα at 24 and 48 hours normalized to the untreated Ykt6 KD cells, represented as a fold increase. **(C)** Percentage of cells sorted into viable cells negative to both the staining (Annexin

V^-/PI^-), early apoptotic cells (Annexin V^+/PI^-), late apoptotic cells (Annexin V^+/PI^+) and necrotic cells (Annexin V^-/PI^+), in control or Ykt6 KD cells with different treatments, putrescine or Tnfα. **(D)** Percentage of viable cells in Ykt6 KD from (C) normalized to the untreated Ykt6 KD cells, represented as a fold increase. **(E)** Representative western blot and quantification of Ykt6 in the membrane fraction with different treatments, normalized to Calnexin, which is a membrane marker. **(F)** Representative western blot of Ykt6 in cytosolic and membrane fraction with different treatments. **(G)** Quantification of WB from (F) normalized to the respective GAPDH or Calnexin levels, followed by normalization to the control UT sample.

Discussion

In this study, we have shown that Ykt6 is an essential SNARE for a faithful cell cycle progression and the lack of which impairs cell growth and proliferation, revealed as a G1 delay and reduced mitotic index phenotype. Since Ykt6 KD led to a cell cycle phenotype, a single cell transcriptomic approach is useful in the future to cluster individual cells into specific cell cycle phases based on the expression of cell cycle markers (Liu et al., 2017). Ykt6 deficient cells have lower levels of SAT1, which is a key metabolic enzyme and therefore low polyamine levels. Intriguingly, one of the polyamines which is also a catalytic product of SAT1, putrescine can partially rescue the growth defects caused by Ykt6 KD. Furthermore, putrescine triggers the open conformation of Ykt6, when the PDK1 signalling pathway is inhibited. Our results demonstrate the interplay between Ykt6 and polyamines, that govern the cell cycle progression through the PDK1 signalling pathway as depicted in the working model (Fig. 7). Taken together, we propose that Ykt6 could play a crucial role in modulating the polyamine homeostasis through the nutritional sensing PDK1 pathway, required for a proper cell cycle progression.

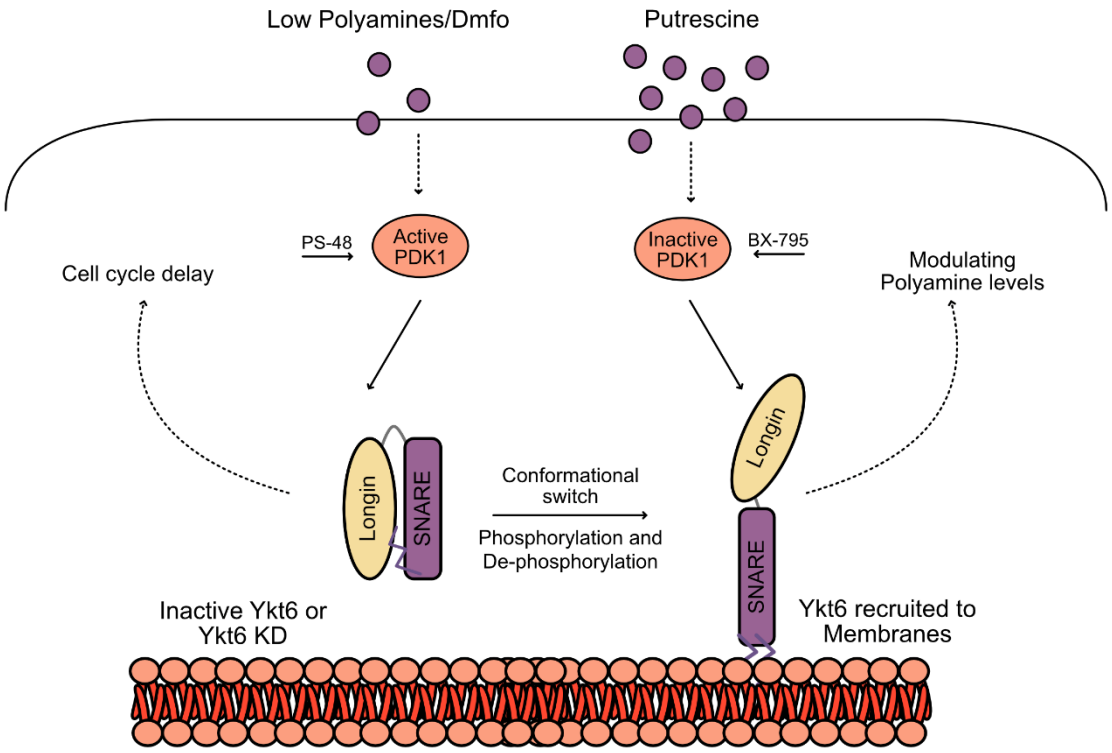

Figure 7: Working model of Ykt6 in modulating the polyamine levels during cell cycle progression.

Role of Ykt6 during cell cycle progression

Ykt6 is indispensable for cell growth *in vivo* and caused a visible delay in growth and proliferation in human colon cancer cells. Although it acts in diverse cellular processes, it remains unclear if Ykt6 has a dedicated function during cell cycle progression. Our finding revealed that Ykt6 has a canonical role during the cell cycle progression. Even though lack of Ykt6 causes cell cycle delay, it does not induce apoptosis or arrest the cell cycle. However, it remains unclear if Ykt6 KD cells exit the cell cycle and are in a non-diving quiescent like state. Nevertheless, based on our finding lack of Ykt6 causes a significant G1 delay, which could indicate that the cells are engaged in a repair mechanism or compensatory mechanism for the loss of Ykt6. In line with this, cell cycle-related genes involved in checkpoints, mitosis, cell cycle transition phase was down-regulated upon Ykt6 KD. However, none of the apoptotic or senescence genes was enriched in the transcriptome. Additionally, autophagy-related genes were not affected with Ykt6 KD, which further confirms its non-canonical role in autophagy (Matsui et al., 2018; Takáts et al., 2018). Concordantly, the membrane trafficking genes especially ER-Golgi and Golgi-ER transport are up-regulated, which could indicate that the up-regulation is a compensatory mechanism to rescue the trafficking role of Ykt6 in the secretory pathway. This is in line with the role of Ykt6 for proper Golgi function (Shirakawa et

al., 2020) and its role in the secretory pathway for example, in the secretion or recycling of Wnt proteins (Gross et al., 2012; Linnemannstöns et al., 2020). Cells spend most of the time in the G1 phase in constant communication with the external environment monitoring external and internal metabolic cues that govern the cell cycle progression. Since most of the key metabolic and regulatory processes occur during this phase, it was challenging the decipher the specific processes in the cell cycle where Ykt6 is required.

Ykt6 has a unique ability to act in stressful situations. Some of the studies where Ykt6 plays a role under cellular stress include trafficking of leucine transporter (SLC7A5) to the plasma membrane during nutritional starvation (Saito et al., 2019), lysosomal stress clearance in Parkinson's disease (Cuddy et al., 2019) and autophagosome-lysosome fusion under starvation (Takáts et al., 2018). It was also proposed as a stress sensor in yeast (Dietrich, Gurezka, Veit, & Ungermann, 2004). Since the majority of the protein resides in the cytoplasm, it can be triggered to be recruited to membranes by various unknown stimuli when required to act. Therefore, we reasoned that Ykt6 could be involved as a stress sensor or a valve that adapts to nutritional status during the cell cycle progression.

Role of Ykt6 as a stress sensor

Interestingly, our finding from the transcriptomic data linked Ykt6 to amino acid /polyamine metabolism. One of the down-regulated genes SAT1 is a key metabolic enzyme in polyamine biosynthesis and a gatekeeper of polyamine flux (Pegg, 2008). Polyamines are essential for cell growth and proliferation, lack of which causes G1 delay in the cell cycle (Fuller, Gerner, & Russell, 1977). Our finding by metabolic profiling further revealed that Ykt6 KD cells are deficient in all three polyamines, putrescine, spermidine (spd) and spermine (spm). The amino acids upstream of polyamines that feed into the polyamine biosynthetic pathway are arginine followed by ornithine. Interestingly, these amino acids were reduced as well upon Ykt6 knockdown. This indicates that overall Ykt6 KD cells have deficient metabolites compared to the control. Therefore, the cell down-regulates SAT1, to ensure enough reserves of spermidine and spermine for protein synthesis. This fits with our finding where Ykt6 KD cells have increased protein synthesis. Akt signalling pathway increases the mammalian cell size, by stimulating protein synthesis and inhibiting protein degradation (Faridi et al., 2003). In agreement, our findings reveal that Ykt6 knockdown cells are larger, which could be due to the increased protein synthesis.

Polyamines are required for the activation of elf5A, a major translation factor and polyamine depletion leads to growth delay (Zhang et al., 2019). The precursor for polyamine

biosynthesis is putrescine, which is further metabolized into spermidine and spermine sequentially. Depletion of polyamines leads to growth delay at G1/S and G2/M boundary (Ray, Zimmerman, Mccormack, Patel, & Johnson, 1999; Yamashita et al., 2013), which is in line with our findings where SAT1 is specifically down-regulated at the G1 and G2M phase of the cell cycle in Ykt6 KD cells. If the growth delay of Ykt6 KD cells is due to polyamine deficiency, we hypothesized that supplementing the cells with polyamines should rescue the phenotype. Strikingly, only putrescine was able to partially rescue the viability defects of Ykt6, but not spermidine (spd) or spermine (spm). Do the cells require more putrescine compared to spd/spm or does the intermediate enzymes or feedback mechanisms govern the uptake of different polyamines based on the cells requirement?

Interestingly, the polyamines enter and exit the cell via different transporters that are tightly regulated, where spd/spm have different transporters compared to putrescine. Spermidine and spermine are known to be transported via members of several SLC (solute carrier) transporters (Abdulhussein & Wallace, 2014; Moriyama, Hatano, Moriyama, & Uehara, 2020) and P-Type ATPases in mammalian systems (Vrijsen et al., 2020), whereas putrescine transporter occurs via SLC diamine exporter through Arginine/Putrescine exchange in mammals (Uemura et al., 2008) and by a putrescine-ornithine antiporter activity in E.coli (Kurihara et al., 2009; Terui et al., 2014). Even though the polyamines are added externally, the cells govern the uptake and excretion by regulating the transporters. The polyamine uptake depends on the growth status of the cell, where depletion of polyamines increases the affinity for putrescine, but not for spermidine (Corral & Wallace, 2020). Another interesting study revealed that putrescine uptake is cell cycle-dependent, required for G1 to S transition in mouse hepatocytes (Martin et al., 1991). This could explain why we observe rescue of Ykt6 KD growth effects with putrescine and not with spermidine or spermine. Therefore, our results further emphasize that Ykt6 could act as a sensor in modulating the polyamine levels during the cell cycle progression. Ykt6 promotes leucine uptake by transporting leucine transporter (SLC7A5) to the plasma membrane. Similarly, it is conceivable that Ykt6 regulates the polyamine levels directly by the trafficking of polyamine transporters.

Role of PDK1 in regulating Ykt6 activity

Several signalling pathways regulate polyamine uptake for example K-Ras negatively regulates putrescine transporter and SAT1 expression (Uemura et al., 2008). Another study reported that the level of polyamines induces the PDK1 activity which in turn suppresses apoptosis (Keledjian et al., 2012). PDK1 (phosphoinositide-dependent protein kinase-1) is a master kinase that is crucial for the phosphorylation and activation of Akt/PKB and many other

AGC kinases (protein kinases A, G and C) such as p70S6K (ribosomal protein S6 kinase), SGK (serum/glucocorticoid regulated kinase) and members of PKC family. PDK1 gets activated upon growth factors and polyamines and has several downstream effects in cell cycle progression, proliferation and protein translation (Cantley, 2002). PDK1 signalling axis is one of the most deregulated pathways in cancer. Lack of PDK1 led to a delay in the transition of cells from G1 to S and slowed the progression at the G2/M phase of the cell cycle (Nakamura et al., 2008). It acts downstream of the PI3K pathway, which is an important nutrient-sensing pathway (Luo, Manning, & Cantley, 2003). Since PDK1 was found to regulate Ykt6 activity, we reasoned that the PDK1 signalling pathway could be involved in sensing the polyamine levels, which in turn would recruit Ykt6 to modulate polyamine homeostasis during the cell cycle progression. One of the crucial regulatory mechanisms of Ykt6 is via phosphorylation of the SNARE domain. Many kinases are predicted to phosphorylate Ykt6 such as the PKC family of kinases (Malmersjö et al., 2016), PDK1 (Pradhipa Karuna et al., 2020), Protein kinase C iota type (PRKci) (McGrath et al., 2021) and Atg1 kinase (Barz et al., 2020) during autophagy. Phosphorylation of the SNARE drives the conformational switch of the Ykt6 from close to open confirmation, which recruits Ykt6 to the membranes. Once the phosphorylated SNARE is docked at the membranes, an additional dephosphorylation step is required which would enable the SNARE to initiate vesicle fusion events.

Counter-intuitively, inhibiting the PDK1 pathway, but not activating the pathway recruited Ykt6 to membranes. However, it is still unclear if the membrane recruited Ykt6 is active since an additional dephosphorylation step is required to activate the SNARE. Since PDK1 is in a constitutively active state, inhibiting the pathway could have several downstream effects that cause cellular stress, which in turn could activate Ykt6. To circumvent the use of artificial inhibitors, we activated or inhibited the pathway by adding or depleting polyamines. Our results indicate that putrescine led to strong membrane recruitment of Ykt6, which could occur by inhibiting the PDK1 pathway since polyamines act upstream of PDK1 (Keledjian et al., 2012). To modulate the polyamine levels, Ykt6 should undergo a conformation change from the closed state to an active membrane recruited state and facilitate the trafficking of polyamine transporters. The conformational switch of Ykt6 in turn could be regulated by the active or inactive state of PDK1.

Based on our findings, we propose that PDK1 could leverage Ykt6 by recruiting it to the membranes which in turn would modulate the polyamine homeostasis. It is plausible that Ykt6 modulates polyamine levels directly by trafficking the polyamine transporters similar to a study where Ykt6 traffics leucine transporter (Saito et al., 2019). In line with this, lack of Ykt6 leads to reduced polyamine levels that cause a delay in cell cycle progression. In our study, for the

first time, we show that Ykt6 modulates the polyamine homeostasis during the cell cycle progression via the PDK1 signalling pathway.

Materials and Methods

Antibodies

The following antibodies were used for western blotting (WB) or immunofluorescence (IF): Ykt6 (1:1000; Western Blot (WB); Santa Cruz), GAPDH (1:1000, WB, Millipore), Calnexin (1:1000, WB, Abcam), p21 (1:1000, WB, Cell signalling technology), Hsc 70 (1:1000, WB, Santa Cruz), Puromycin (1:25000, WB, Millipore). Secondary antibodies were coupled to Alexa Fluor 488,568,594 and 647 (1:500, IF, Invitrogen) and 680RD and 800 CW (1:20000, WB, Licor).

Cell culture and Transfection

Hek293T and HCT116 cells were maintained in DMEM (Gibco) supplemented with 10% fetal calf serum (Biochrom) at 37 °C in a humidified atmosphere with 5% CO_2. Cells were transiently transfected with Screenfect siRNA for siRNA and Screenfect A (Screenfect) for plasmids according to the manufacturer's instructions. Cells were authenticated and checked regularly for mycoplasma contamination.

Viability assay

Ykt6 effects on cell viability were measured by performing a CellTiter-Glo assay. Cells were seeded in a 96-well plate, reverse transfected with either Control or Ykt6 siRNA. The polyamines or inhibitors were added to the cells in the following concentrations: putrescine, spermidine and spermine in concentrations of 100µM, the inhibitors Dmfo at 500µM and, Tnfα at 15ng/ml. The viability was measured by luminometer at 24h and 48h post-treatment. Before measuring, 100 μl of the cell titer glow reagent (Promega) were added to each well (1:1). The plate was incubated on a shaker for 2 min at RT to allow cell lysis and then incubated at RT without shaking for 10 min to allow luminescence signal stabilization. The signal was measured using a luminometer and analyzed using MikroWin 2000 lite Version 4.43.

Real-time Proliferation assay

The cells were seeded in 96-well plates, reverse transfected with either Ctrl or Ykt6 siRNA. Cell proliferation is monitored by analyzing the occupied area (% confluence) of cell images over time. The cell confluence was scanned and measured every 4 hours by using the IncuCyte ZOOM Live Cell Analysis System (Essen Bioscience).

Cell cycle analysis using Flow cytometry

Cell cycle distribution and apoptosis were analysed using a Flow cytometer. For cell cycle analysis, cells were harvested and then fixed in 70% cold EtOH and stored at 4C until further use. The ethanol was removed by centrifuging at 400 g for 5 min. The pellet was re-suspended in 500µl 1X PBS and 0.25% Triton X-100 and incubated on ice for 15 min. Once again, samples were centrifuged and the pellet was incubated with 100µl of 1X PBS, 1% of BSA and primary antibody MPM-2 for 1 hour at RT. Following incubation, the tubes were centrifuged and the pellet was washed with 150 µl PBS with 1% BSA. The pellet was then resuspended in 100 µl PBS with 1% BSA and Alexa 488-conjugated goat anti-rabbit antibodies. The tube was incubated at RT for 30 min in the dark. The cells were then centrifuged and the pellet was resuspended in 400-900 µl RNase A solution (200 µg/ml in PBS), according to the pellet size. The tube was incubated in RT for 30 min in the dark. Before FACS analysis, 5 µl propidium iodide was added and the samples were analysed using a flow cytometer (BD Biosciences, San Jose, CA).

Apoptosis assay using Flow cytometry

For apoptosis analysis, FITC–Annexin V Apoptosis Detection Kit with PI (BioLegend, San Diego, CA). The cells were washed with 1x PBS and re-suspended with Annexin-V binding buffer. Post this, the cells were stained with Annexin-FITC and PI and incubated for 15 min at room temperature. The samples were analysed using a flow cytometer (BD Biosciences, San Jose, CA).

Cell cycle synchronization – RO 3306

Cells were seeded in 60 mm dishes, reverse transfected with control or Ykt6 siRNA if required, and incubated for 22 h. Then, RO-3306 solution (10 mM in DMSO) was added to a final concentration of 10 µM and the cells were incubated for 19-22 h. The cells were washed twice with PBS and a fresh medium was added before their harvest at different time points.

Cell cycle synchronization – Double Thymidine

Double Thymidine (100 mM in DMEM) and 2'-deoxycytidine (240 mM in water) solutions were freshly prepared. Cells were seeded in 60 mm dishes, reverse transfected with control or Ykt6 siRNA. Once the cells were attached in about 24 hours, thymidine solution was added for the first time to final concertation of 3 mM and was incubated for 14-16 h. The cells were then released from the thymidine block by washing with PBS and addition of fresh medium containing 24 µM 2'-deoxycytidine. Following 8-9 h of incubation, the cells were washed with PBS, thymidine solution was added for the second time and the cells were incubated for another 14-16 h. The cells were washed twice with PBS and a fresh medium containing 24 µM 2'- deoxycytidine was added to release to block. Following the second release, the cells were harvested at different time points.

Western Blotting

Cell and sEV lysates in the SDS-PAGE sample buffer was boiled for 5 min before separating the protein on 4-12% gradient gels (Bolt Bis-Tris Plus Gels, Thermo Scientific). Protein was then transferred to PVDF membranes (Merck) and blocked with 5% (wt/vol) milk-TBST for 30 min. Membranes were incubated with primary antibodies overnight at 4 TBST at 4°C. After washing, membranes were incubated with fluorescently labelled secondary antibodies at room temperature in the dark and detected using Odyssey from Li-COR. Quantitative measurements were done with LiCOR image analysis software.

Membrane Fractionation

As described previously (Baghirova, Hughes, Hendzel, & Schulz, 2015), Hek293T cells were seeded and transfected with Ykt6-WT plasmid. Then, 48 h post-transfection, cells were lysed on ice with 1 ml of Lysis buffer A (150 mM NaCl, 50 mM HEPES, 0.1% Saponin, 1 M Glycerol, and 1% PIC) and then centrifuged at 2000 g for 10 min at 4ºC. The supernatant (cytosolic fraction) was transferred to a new tube. The pellet was lysed in 1 ml of Lysis Buffer B (150 mM NaCl, 50 mM Hepes, 1% Igepal, 1 M Glycerol and 1% PIC) and incubated rotating for 30 min at 4ºC. Then, after being centrifuged at 7000 g for 10 min at 4ºC, the supernatant was transferred to a new tube (membrane fraction).

Puromycin labelling assay

Cells were reverse transfected with Control or Ykt6 siRNA, treated with Cycloheximide (20ug/ml) 48 hours post-transfection. The cells were harvested using Ripa lysis buffer 72 h post-transfection and labelled with puromycin (16ug/ml) for 1 hour before the harvest (Schmidt, Clavarino, Ceppi, & Pierre, 2009)

Immunostaining and Image Analysis

$2.0x10^4$ cells were seed in each well of an 8-wells slide in a final volume of 500µl. The cells were synchronized with the desired method (double thymidine or RO-3306). Following the release, the medium was removed and the cells were incubated with 100µl fixation solution (4% w/v PFA in PBS with 0.2% v/v Triton X-100) for 10 min at 37°C. Then, the fixation solution was replaced with blocking solution (5% w/v BSA in PBS with 0.05% v/v Triton X-100) and the cells were incubated for at least 30min. When needed, the cells were stored for up to three days at 4°C. For staining, the blocking solution was removed and the cells were incubated for 30min at RT with 50µl primary antibodies in the blocking solution. The cells were washed with 500µl PBS three times and incubated for 30min at RT in the dark with 50µl secondary antibodies and Alexa Fluor 647 phalloidin (Life Technologies, A22287, diluted 1:100) in blocking solution. The secondary antibody mixture was removed and the cells were incubated for 5min with Hoechst (1:500) in PBS. Following three washes with 500µl PBS the chambers of the slide were removed and one drop of Fluoromount G (SouthernBiotech, 0100-01) was pipetted on each well position. A coverslip was put on top of the slide and the Fluoromount G was left to dry overnight at RT in the dark. The stained samples were observed with the LSM780 confocal microscope (Zeiss) using a 63x objective and the ZEN 2.0 software.

Analysis of the Total Corrected Cellular Fluorescent (TCCF) intensity was modified based on the mentioned in (McCloy et al., 2014), using the software Fiji ((Fiji Is Just) ImageJ 2.0.0-rc-61/1.51n). In short, a figure was opened with Fiji, cells were outlined and set as Regions Of Interest (ROIs) with the ROI manager and the phalloidin staining channel. The channels were then split and the relevant channel was further processed. First, the Area, Integrated Density and Mean Gray Value of the ROIs were measured through the ROI manager. Then the image type was set to 8-bit and thresholded for 4.5-5.5% (closest possible to 5%) of the total intensity. The same Image was opened again in a “composite” mode and the measurement from the split channel was redirected to the relevant channel in the freshly opened figure through

Analyze and Set Measurement. Then the particles in each ROI were measured via the Analyze particle function (size: 5-Infinity pixel units, Circularity 0.00-1.00, 'Display Results' and 'Summarize' ticked). The percentage of intensity which is allocated to punctated Ykt6 was then calculated using the TCCF and the total corrected puncta intensity (TCPF) which was calculated with the same principle: TCPF= sum intensity of all puncta- (sum puncta area* mean background measurements), and the results were plotted using GraphPad Prism 5.

Single-cell RNA sequencing

A high-throughput full-length, single-cell RNA-seq approach was used with the SMART-Seq ICELL8 cx application. Cells were diluted for a final concentration of 1.4 cells/50 nl in a total volume of 1 ml in 1xPBS. Cell suspensions were fluorescently labelled with live/dead stain, Hoechst 33342 and propidium iodide (NucBlue™ Cell Stain Reagent, Thermo Fisher Scientific) for 15 min before their dispensing into the 5184 microchip nano wells (Takara Bio) using the ICELL8 system. CellSelect® Software (Takara Bio) was used to visualize and select wells containing single and live cells. Next, a full-Length cDNA synthesis by RT-PCR was done according to the SMART-Seq ICELL8 cx application protocol (Takara) by dispensing the reagents directly into the nano wells of the ICELL8 chip. P5 indexing primers were dispensed, with each of the 72 rows on the ICELL8 chip receiving a different index, in addition to Terra polymerase and reaction buffer. Transposase enzyme and reaction buffer (Tn5 mixture) were dispensed to selected wells, and the transposition reaction was performed. P7 indexing primers were dispensed to wells, with each of the 72 columns on the chip receiving a different index. Final Illumina libraries were amplified and pooled as they are extracted from the chip. Pooled libraries were purified and size selected using Agencourt AMPure XP magnetic beads (Beckman Coulter) to obtain an average library size of 800 bp. Library validation and quantification were done using the Fragment Analyzer by using the dsDNA 905 Reagent Kit (Advanced Bioanalytical) and the QuantiFluorTMdsDNA System from Promega. A typical yield for a library comprised of 1278 cells was 28.7 nM. Single-cell libraries were sequenced on the HiSeq 4000 (Illumina) to obtain on average ~ 0.5 Mio reads per cell (SE; 50bp).

For data analysis, bcl2fastq was used to retrieve fastq files with dual-indexed barcodes in their read headers and the resulting fastq files were used to associate reads with individual cells based on their barcodes, as well as quantify how many reads are in each cell using the mappa_demuxer.py script from Takara. The demultiplexed fastq file was then run through the analysis pipeline using the mappa_analysed.py script from Takara. In brief, the demultiplexed reads were trimmed for adapters using cutadapt version 2.5 and the reads kept after trimming were aligned to a custom human genome (hg38 version 99) using STAR 2.7. Next, the

uniquely mapped reads were counted for exons, genes (exons+introns) and mitochondrial chromosomes using featureCounts 1.6.4. TSNE analysis was used for clustering analysis.

Metabolomic profiling

The metabolic profiling of the cells was done using Biocrates p180 and Quant500 kit as per the manufacturer's protocol. In short, the cells were lysed with ice-cold phosphate buffer, followed by three freeze and thaw cycles. The samples were sonicated for 15 seconds, followed by freezing in liquid nitrogen and then thawed at 98C until clear. Then, the samples were centrifuged at 20,000g for 10 min at 4°C. The supernatant was transferred to a new Eppendorf and stored at -80°C until further use.

Real-time PCR

Total RNA was isolated from cells using Trizol reagent from Invitrogen. Equal amounts of RNA were reverse transcribes into cDNA. The resulting cDNA product was analyzed by real-time quantitative PCR using iQ SYBR Green Supermix and gene-specific primers. The primer sequences are listed in the table below. Transcript Ct-values were converted to fold change expression changes (2-ΔΔCt values) after normalization to housekeeping gene β-actin. Quantitative real-time PCR was performed using the CFX system (Bio-Rad).

Gene Name	Forward Primer	Reverse Primer
β-Actin	GAGCACAGAGCCTCGCCTTT	ACATGCCGGAGCCGTTGTC
YKT6	GTAGATACCAGAACCCACGA	CACCTCGCTCTAACAGAGAC
SAT1	ACTTCTCTTGCTTTCTATGCTG	TCACACCACCTTGTTGTTTATC
AKAP12	CGTCTCCTTCATTCGCAGGCT	GACAGGGGCAAGAGCCAAAAG
CPA4	TTCAATCGGCCTGTGGATGT	TCCGTTCTTGCCCTTCATTGT
FTL	CTCCTTCTTGCCAACCAAC	TTCCAGAGCCACATCATCG
IFI6	CCATCTATCAGCAGGCTCCG	CACCCCACTGCAAGTGAAGA
ISG15	GTGGACAAATGCGACGAACC	TCGAAGGTCAGCCAGAACAG
NAP1L1	GGAAGGGGAAGAAGAAGGAG	AGAAGGTAGACCAGTGCAG
STMN1	CGTCGAGGAGACAATAGGGG	CCGTCCCTTCAGACAATGGG
TSPAN3	AGCTGTAGGAGCCCTGCTTT	GCAGGATGATGACAAACGTGG

Statistics

All experiments were carried out at least in biological triplicates. All graphs depict the mean and error bars indicate standard deviation. Statistical significance was calculated by carrying out one-way ANOVA with Dunnett's multiple comparison test to compare a control mean with the other means or Student’s t-test where appropriate. The data that support the findings of this study are available from the corresponding author upon reasonable request.

Acknowledgements

The authors thank the NGS-Integrative Genomics (NIG), Institute of Human Genetics, UMG. Research in the lab of JCG is supported by the DFG-funded Research Center SFB1324/1 - project number 331351713 and GR4810/2-1, the Research program of the University Medical Center, University of Göttingen and a postdoctoral fellowship to K.L. by the Dorothea Schlözer Program, University of Göttingen.

Author Contributions

P.K.M. and A.D. designed and carried out cell culture experiments. P.K.M carried out data analysis. S.P and R.K performed quantitative PCR analysis. P.K.M and J.C.G wrote the original draft along with reviewing and editing. J.C.G. conceived and supervised the study.

Competing Interests statement

The authors have no competing financial interests.

References

Abdulhussein, A. A., & Wallace, H. M. (2014). Polyamines and membrane transporters. *Amino Acids*, *46*(3), 655–660. https://doi.org/10.1007/s00726-013-1553-6

Akakura, S., & Gelman, I. H. (2012). Pivotal Role of AKAP12 in the Regulation of Cellular Adhesion Dynamics: Control of Cytoskeletal Architecture, Cell Migration, and Mitogenic Signaling. *Journal of Signal Transduction*, *2012*, 1–7. https://doi.org/10.1155/2012/529179

Baghirova, S., Hughes, B. G., Hendzel, M. J., & Schulz, R. (2015). Sequential fractionation and isolation of subcellular proteins from tissue or cultured cells. *MethodsX*, *2*, e440–e445. https://doi.org/10.1016/j.mex.2015.11.001

Barz, S., Kriegenburg, F., Henning, A., Bhattacharya, A., Mancilla, H., Sánchez-Martín, P., & Kraft, C. (2020). Atg1 kinase regulates autophagosome-vacuole fusion by controlling SNARE bundling. *EMBO Reports*, *21*(12). https://doi.org/10.15252/embr.202051869

Beauséjour, C. M., Krtolica, A., Galimi, F., Narita, M., Lowe, S. W., Yaswen, P., & Campisi, J. (2003). Reversal of human cellular senescence: Roles of the p53 and p16 pathways. *EMBO Journal*, *22*(16), 4212–4222. https://doi.org/10.1093/emboj/cdg417

Cantley, L. C. (2002). The phosphoinositide 3-kinase pathway. *Science*, *296*(5573), 1655–1657. https://doi.org/10.1126/science.296.5573.1655

Catchpoole, D. R., & Wanjin, H. (1999). Characterization of the sequence and expression of a Ykt6 prenylated SNARE from rat. *DNA and Cell Biology*, *18*(2), 141–145. https://doi.org/10.1089/104454999315529

Chen, J. (2016). The cell-cycle arrest and apoptotic and progression. *Cold Spring Harbor Perspectives in Biology*, 1–16.

Chen, J. E., & Glover, G. H. (2016). Large-scale gene function analysis with PANTHER Classification System, *25*(3), 289–313. https://doi.org/10.1007/s11065-015-9294-9.Functional

Corral, M., & Wallace, H. M. (2020). Upregulation of polyamine transport in human colorectal cancer cells. *Biomolecules*, *10*(4). https://doi.org/10.3390/biom10040499

Crossland, H., Smith, K., Atherton, P. J., & Wilkinson, D. J. (2017). A novel puromycin decorporation method to quantify skeletal muscle protein breakdown: A proof-of-concept study. *Biochemical and Biophysical Research Communications*, *494*(3–4), 608–614. https://doi.org/10.1016/j.bbrc.2017.10.085

Cuddy, L. K., Wani, W. Y., Morella, M. L., Pitcairn, C., Tsutsumi, K., Fredriksen, K., … Mazzulli, J. R. (2019). Stress-Induced Cellular Clearance Is Mediated by the SNARE Protein ykt6 and Disrupted by α-Synuclein. *Neuron*, *104*(5), 869-884.e11. https://doi.org/10.1016/j.neuron.2019.09.001

Dietrich, L. E. P., Gurezka, R., Veit, M., & Ungermann, C. (2004). The SNARE Ykt6 mediates protein palmitoylation during an early stage of homotypic vacuole fusion. *EMBO Journal*, *23*(1), 45–53. https://doi.org/10.1038/sj.emboj.7600015

Faridi, J., Fawcett, J., Wang, L., & Roth, R. A. (2003). Akt promotes increased mammalian cell size by stimulating protein synthesis and inhibiting protein degradation. *American Journal of Physiology - Endocrinology and Metabolism*, *285*(5 48-5), 964–972. https://doi.org/10.1152/ajpendo.00239.2003

Finlay, C. A., Hinds, P. W., & Levine, A. J. (1989). The p53 proto-oncogene can act as a suppressor of transformation. *Cell*, *57*(7), 1083–1093. https://doi.org/10.1016/0092-8674(89)90045-7

Fukasawa, M., Varlamov, O., Eng, W. S., Sollner, T. H., & Rothman, J. E. (2004). Localization and activity of the SNARE Ykt6 determined by its regulatory domain and palmitoylation. *Proceedings of the National Academy of Sciences*, *101*(14), 4815–4820. https://doi.org/10.1073/pnas.0401183101

Fuller, D. J. M., Gerner, E. W., & Russell, D. H. (1977). Polyamine biosynthesis and accumulation during the G1 to S phase transition. *Journal of Cellular Physiology*, *93*(1), 81–88. https://doi.org/10.1002/jcp.1040930111

Giono, L. E., & Manfredi, J. J. (2006). The p53 Tumor Suppressor Participates in Multiple Cell Cycle Checkpoints. *Journal Cellular Physiology*, *211(3)*(May), 736–747. https://doi.org/10.1002/JCP

Gross, J. C., Chaudhary, V., Bartscherer, K., & Boutros, M. (2012). Active Wnt proteins are secreted on exosomes. *Nature Cell Biology*, *14*(10), 1036–1045. https://doi.org/10.1038/ncb2574

Han, B., Poppinga, W. J., & Schmidt, M. (2015). Scaffolding during the cell cycle by A-kinase anchoring proteins. *Pflugers Archiv European Journal of Physiology*, *467*(12), 2401–

2411. https://doi.org/10.1007/s00424-015-1718-0

Hasegawa, H. (2004). Intramolecular protein-protein and protein-lipid interactions control the conformation and subcellular targeting of neuronal Ykt6. *Journal of Cell Science*, *117*(19), 4495–4508. https://doi.org/10.1242/jcs.01314

Huang, Y. F., Wee, S., Gunaratne, J., Lane, D. P., & Bulavin, D. V. (2014). Isg15 controls p53 stability and functions. *Cell Cycle*, *13*(14), 2199–2209. https://doi.org/10.4161/cc.29209

Keledjian, K. M., Marasa, B. S., Wang, J. Y., & Rao, J. N. (2012). Induced PDK1 kinase activity suppresses apoptosis in intestinal epithelial cells by activating Akt signaling following polyamine depletion. *International Journal of Clinical and Experimental Medicine*, *5*(3), 221–228.

Kluger, H. M., Kluger, Y., Gilmore-Hebert, M., DiVito, K., Chang, J. T., Rodov, S., … Sapi, E. (2004). CDNA microarray analysis of invasive and tumorigenic phenotypes in a breast cancer model. *Laboratory Investigation*, *84*(3), 320–331. https://doi.org/10.1038/labinvest.3700044

Kobak, D., & Berens, P. (2019). The art of using t-SNE for single-cell transcriptomics. *Nature Communications*, *10*(1). https://doi.org/10.1038/s41467-019-13056-x

Koopman, G., Reutelingsperger, C. P. M., Kuijten, G. A. M., Keehnen, R. M. J., Pals, S. T., & Van Oers, M. H. J. (1994). Annexin V for flow cytometric detection of phosphatidylserine expression on B cells undergoing apoptosis. *Blood*, *84*(5), 1415–1420. https://doi.org/10.1182/blood.v84.5.1415.1415

Kurihara, S., Tsuboi, Y., Oda, S., Kim, H. G., Kumagai, H., & Suzuki, H. (2009). The putrescine importer puuP of escherichia coli K-12. *Journal of Bacteriology*, *191*(8), 2776–2782. https://doi.org/10.1128/JB.01314-08

Linnemannstöns, K., Witte, L., Pradhipa Karuna, M., Kittel, J. C., Danieli, A., Müller, D., … Gross, J. C. (2020). Ykt6-dependent endosomal recycling is required for Wnt secretion in the Drosophila wing epithelium. *Development (Cambridge)*, *147*(15). https://doi.org/10.1242/dev.185421

Liu, Z., Lou, H., Xie, K., Wang, H., Chen, N., Aparicio, O. M., … Chen, T. (2017). Reconstructing cell cycle pseudo time-series via single-cell transcriptome data. *Nature Communications*, *8*(1), 1–8. https://doi.org/10.1038/s41467-017-00039-z

Lodish, H., Berk, A., Matsudiara, P., A, K. C., Kreiger, M., Scott, M. P., … Darnell, J. (2004). *Molecular Cell Biology*. *W.H. Freeman 5th Edition*. https://doi.org/10.18772/22008014655.9

Luo, J., Manning, B. D., & Cantley, L. C. (2003). Targeting the PI3K-Akt pathway in human cancer: Rationale and promise. *Cancer Cell*, *4*(4), 257–262. https://doi.org/10.1016/S1535-6108(03)00248-4

Ma, H. T., & Poon, R. Y. C. (2016). Synchronization of HeLa cells. *Methods in Molecular Biology*, *1524*(June 2011), 189–201. https://doi.org/10.1007/978-1-4939-6603-5_12

Malmersjö, S., Di Palma, S., Diao, J., Lai, Y., Pfuetzner, R. A., Wang, A. L., … Meyer, T. (2016). Phosphorylation of residues inside the SNARE complex suppresses secretory vesicle fusion. *The EMBO Journal*, *35*(16), 1810–1821. https://doi.org/10.15252/embj.201694071

Mandal, S., Mandal, A., Johansson, H. E., Orjalo, A. V., & Park, M. H. (2013). Depletion of cellular polyamines, spermidine and spermine, causes a total arrest in translation and growth in mammalian cells. *Proceedings of the National Academy of Sciences of the*

United States of America, *110*(6), 2169–2174. https://doi.org/10.1073/pnas.1219002110

Martin, R. L., Ilett, K. F., & Minchin, R. F. (1991). Cell cycle–dependent uptake of putrescine and its importance in regulating cell cycle phase transition in cultured adult mouse hepatocytes. *Hepatology*, *14*(6), 1243–1250. https://doi.org/10.1002/hep.1840140646

Matsui, T., Jiang, P., Nakano, S., Sakamaki, Y., Yamamoto, H., & Mizushima, N. (2018). Autophagosomal YKT6 is required for fusion with lysosomes independently of syntaxin 17. *The Journal of Cell Biology*, jcb.201712058. https://doi.org/10.1083/jcb.201712058

McCloy, R. A., Rogers, S., Caldon, C. E., Lorca, T., Castro, A., & Burgess, A. (2014). Partial inhibition of Cdk1 in G2 phase overrides the SAC and decouples mitotic events. *Cell Cycle*, *13*(9), 1400–1412. https://doi.org/10.4161/cc.28401

McGrath, K., Agarwal, S., Tonelli, M., Dergai, M., Gaeta, A. L., Shum, A. K., … Caraveo, G. (2021). A conformational switch driven by phosphorylation regulates the activity of the evolutionarily conserved SNARE Ykt6. *Proceedings of the National Academy of Sciences of the United States of America*, *118*(12). https://doi.org/10.1073/pnas.2016730118

Moriyama, Y., Hatano, R., Moriyama, S., & Uehara, S. (2020). Vesicular polyamine transporter as a novel player in amine-mediated chemical transmission. *Biochimica et Biophysica Acta - Biomembranes*, *1862*(12), 183208. https://doi.org/10.1016/j.bbamem.2020.183208

Morris, S., Geoghegan, N. D., Sadler, J. B. A., Koester, A. M., Black, H. L., Laub, M., … Gould, G. W. (2020). Characterisation of GLUT4 trafficking in HeLa cells: Comparable kinetics and orthologous trafficking mechanisms to 3T3-L1 adipocytes. *PeerJ*, *2020*(3), 1–22. https://doi.org/10.7717/peerj.8751

Nakamura, K., Sakaue, H., Nishizawa, A., Matsuki, Y., Gomi, H., Watanabe, E., … Kasuga, M. (2008). PDK1 regulates cell proliferation and cell cycle progression through control of cyclin D1 and p27Kip1 expression. *Journal of Biological Chemistry*, *283*(25), 17702–17711. https://doi.org/10.1074/jbc.M802589200

Olle Sangfelt, S. E. and D. G. (2000). [Frontiers in Bioscience 5, d479-487, April 1, 2000] MECHANISMS OF INTERFERON-INDUCED CELL CYCLE ARREST Olle Sangfelt, Sven Erickson and Dan Grandér, (2), 479–487.

Ooe, A., Kato, K., & Noguchi, S. (2007). Possible involvement of CCT5, RGS3, and YKT6 genes up-regulated in p53-mutated tumors in resistance to docetaxel in human breast cancers. *Breast Cancer Research and Treatment*, *101*(3), 305–315. https://doi.org/10.1007/s10549-006-9293-x

Pegg, A. E. (2008). Spermidine/spermine-N1-acetyltransferase: A key metabolic regulator. *American Journal of Physiology - Endocrinology and Metabolism*, *294*(6). https://doi.org/10.1152/ajpendo.90217.2008

Pradhipa Karuna, M., Witte, L., Linnemannstoens, K., Choezom, D., Danieli-Mackay, A., Honemann-Capito, M., & Gross, J. C. (2020). Phosphorylation of ykt6 snare domain regulates its membrane recruitment and activity. *Biomolecules*, *10*(11), 1–19. https://doi.org/10.3390/biom10111560

Qi, Y., Li, Y., Zhang, Y., Zhang, L., Wang, Z., Zhang, X., … Huang, J. (2015). IFI6 inhibits apoptosis via mitochondrial-dependent pathway in dengue virus 2 infected vascular endothelial cells. *PLoS ONE*, *10*(8), 1–14. https://doi.org/10.1371/journal.pone.0132743

Ray, R. M., Zimmerman, B. J., Mccormack, S. A., Patel, T. B., & Johnson, L. R. (1999). Polyamine depletion arrests cell cycle and induces inhibitors p21(Waf1)/(Cip1), p27(Kip1), and p53 in IEC-6 cells. *American Journal of Physiology - Cell Physiology*,

276(3 45-3). https://doi.org/10.1152/ajpcell.1999.276.3.c684

Riccardi, C., & Nicoletti, I. (2006). Analysis of apoptosis by propidium iodide staining and flow cytometry. *Nature Protocols*, *1*(3), 1458–1461. https://doi.org/10.1038/nprot.2006.238

Rubin, C. I., & Atweh, G. F. (2004). The role of stathmin in the regulation of the cell cycle. *Journal of Cellular Biochemistry*, *93*(2), 242–250. https://doi.org/10.1002/jcb.20187

Saito, Y., Li, L., Coyaud, E., Luna, A., Sander, C., Raught, B., … Muthuswamy, S. K. (2019a). LLGL2 rescues nutrient stress by promoting leucine uptake in ER+ breast cancer. *Nature*, *569*(7755), 275–279. https://doi.org/10.1038/s41586-019-1126-2

Saito, Y., Li, L., Coyaud, E., Luna, A., Sander, C., Raught, B., … Muthuswamy, S. K. (2019b). LLGL2 rescues nutrient stress by promoting leucine uptake in ER + breast cancer. *Nature*, *569*(7755), 275–279. https://doi.org/10.1038/s41586-019-1126-2

Schmidt, E. K., Clavarino, G., Ceppi, M., & Pierre, P. (2009). SUnSET, a nonradioactive method to monitor protein synthesis. *Nature Methods*, *6*(4), 275–277. https://doi.org/10.1038/nmeth.1314

Sekiguchi, T., & Hunter, T. (1998). Induction of growth arrest and cell death by overexpression of the cyclin-Cdk inhibitor p21 in hamster BHK21 cells. *Oncogene*, *16*(3), 369–380. https://doi.org/10.1038/sj.onc.1201539

Shirakawa, R., Goto-Ito, S., Goto, K., Wakayama, S., Kubo, H., Sakata, N., … Horiuchi, H. (2020). A SNARE geranylgeranyltransferase essential for the organization of the Golgi apparatus . *The EMBO Journal*, *39*(8), 1–20. https://doi.org/10.15252/embj.2019104120

Sutton, R. B., Fasshauer, D., Jahn, R., & Brunger, A. T. (1998). Crystal structure of a SNARE complex involved in synaptic exocytosis at 2.4 A resolution. *Nature*, *395*(September), 347–353.

Szklarczyk, D., Gable, A. L., Lyon, D., Junge, A., Wyder, S., Huerta-Cepas, J., … Von Mering, C. (2019). STRING v11: Protein-protein association networks with increased coverage, supporting functional discovery in genome-wide experimental datasets. *Nucleic Acids Research*, *47*(D1), D607–D613. https://doi.org/10.1093/nar/gky1131

Takáts, S., Glatz, G., Szenci, G., Boda, A., Horváth, G. V., Hegedűs, K., … Juhász, G. (2018). Non-canonical role of the SNARE protein Ykt6 in autophagosome-lysosome fusion. *PLoS Genetics*, *14*(4), 1–23. https://doi.org/10.1371/journal.pgen.1007359

Terui, Y., Saroj, S. D., Sakamoto, A., Yoshida, T., Higashi, K., Kurihara, S., … Igarashi, K. (2014). Properties of putrescine uptake by PotFGHI and PuuP and their physiological significance in Escherichia coli. *Amino Acids*, *46*(3), 661–670. https://doi.org/10.1007/s00726-013-1517-x

Thayanidhi, N., Liang, Y., Hasegawa, H., Nycz, D. C., Oorschot, V., Klumperman, J., & Hay, J. C. (2012). R-SNARE ykt6 resides in membrane-associated protease-resistant protein particles and modulates cell cycle progression when over-expressed. *Biology of the Cell*, *104*(7), 397–417. https://doi.org/10.1111/boc.201100048

Uemura, T., Yerushalmi, H. F., Tsaprailis, G., Stringer, D. E., Pastorian, K. E., Hawel, L., … Gerner, E. W. (2008). Identification and characterization of a diamine exporter in colon epithelial cells. *Journal of Biological Chemistry*, *283*(39), 26428–26435. https://doi.org/10.1074/jbc.M804714200

Ungermann, C., Mollard, G. F. Von, Jensen, O. N., Margolis, N., Stevens, T. H., & Wickner, W. (1999). Complex on Isolated Vacuoles , Are Essential for Homotypic Fusion. *Cell*, *145*(7), 1435–1442.

Vassilev, L. T., Tovar, C., Chen, S., Knezevic, D., Sun, H., Heimbrook, D. C., … Memorial, R. P. (1962). Deoxyriboside Control and Synchronization of Mitosis. *Cell Cycle*, *1*(22), 682–683. https://doi.org/10.4161/cc.5.22.3463

Vrijsen, S., Besora-Casals, L., Van Veen, S., Zielich, J., Van Den Haute, C., Hamouda, N. N., … Vangheluwe, P. (2020). ATP13A2-mediated endo-lysosomal polyamine export counters mitochondrial oxidative stress. *Proceedings of the National Academy of Sciences of the United States of America*, *117*(49), 31198–31207. https://doi.org/10.1073/pnas.1922342117

Wade Harper, J., Adami, G. R., Wei, N., Keyomarsi, K., & Elledge, S. J. (1993). The p21 Cdk-interacting protein Cip1 is a potent inhibitor of G1 cyclin-dependent kinases. *Cell*, *75*(4), 805–816. https://doi.org/10.1016/0092-8674(93)90499-G

Wen, W., Yu, J., Pan, L., Wei, Z., Weng, J., Wang, W., … Zhang, M. (2010). Lipid-Induced Conformational Switch Controls Fusion Activity of Longin Domain SNARE Ykt6. *Molecular Cell*, *37*(3), 383–395. https://doi.org/10.1016/j.molcel.2010.01.024

Xiong, Y., Hannon, G. J., Zhang, H., Casso, D., Kobayashi, R., & Beach, D. (1993). P21 is a universal inhibitor of cyclin kinases. *Nature*, *366*(6456), 701–704. https://doi.org/10.1038/366701a0

Yamashita, T., Nishimura, K., Saiki, R., Okudaira, H., Tome, M., Higashi, K., … Igarashi, K. (2013). Role of polyamines at the G1/S boundary and G2/M phase of the cell cycle. *International Journal of Biochemistry and Cell Biology*, *45*(6), 1042–1050. https://doi.org/10.1016/j.biocel.2013.02.021

Zhang, H., Alsaleh, G., Feltham, J., Sun, Y., Napolitano, G., Riffelmacher, T., … Simon, A. K. (2019). Polyamines Control eIF5A Hypusination, TFEB Translation, and Autophagy to Reverse B Cell Senescence. *Molecular Cell*, *76*(1), 110-125.e9. https://doi.org/10.1016/j.molcel.2019.08.005

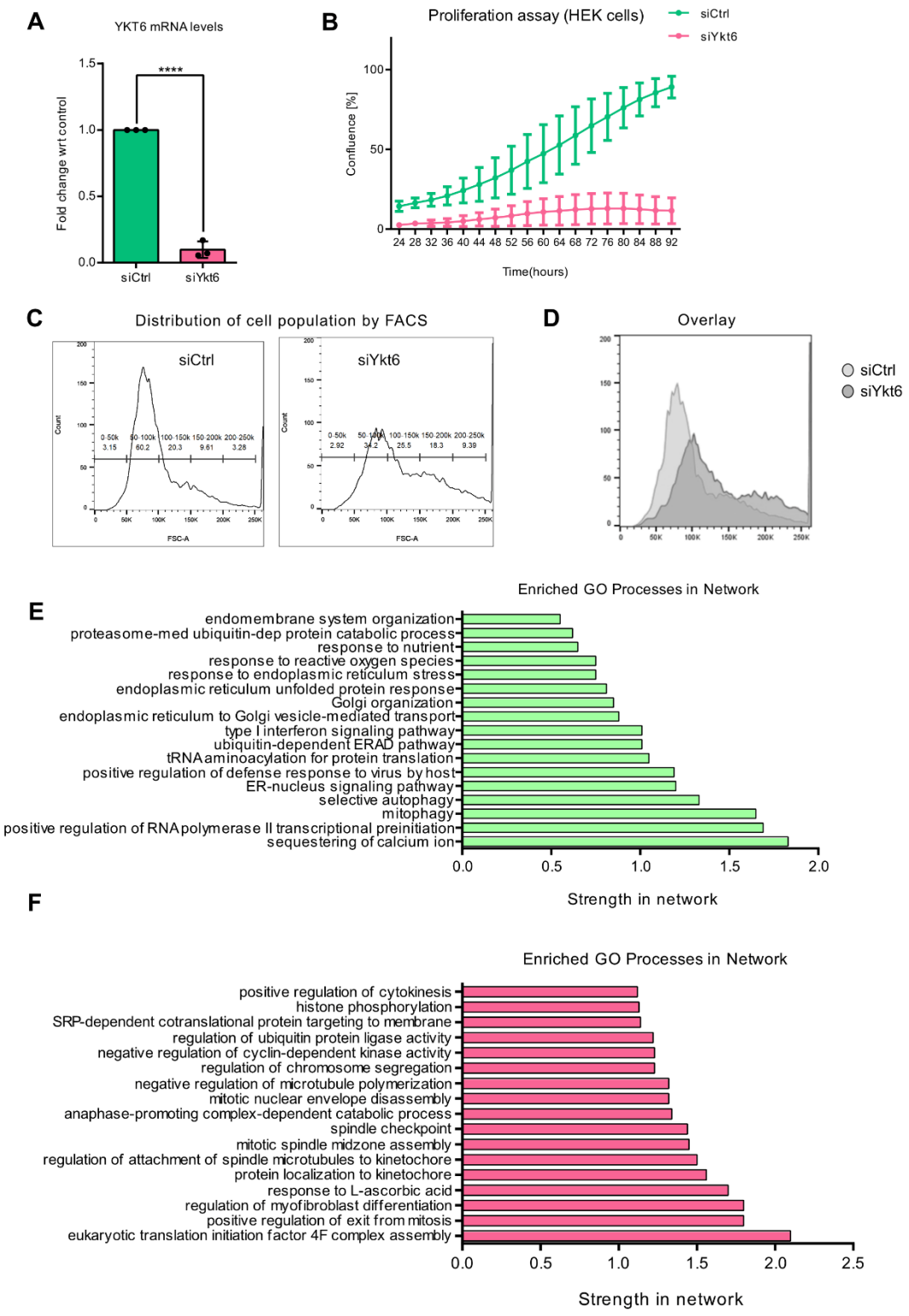

Figure S1: (A) Quantitative Real-time PCR (q-RT PCR) of Ykt6 expression levels, normalized to β-actin levels **(B)** Rate of proliferation in Hek293T cells as measured by the percentage of confluence vs time in control or Ykt6 KD cells. **(C)** Sorting of cells based on size bins as measured by forward-scatter intensity using flow cytometry in control vs Ykt6 KD cells. **(D)** Overlay of control vs Ykt6 KD cells from (C). **(E)** Enriched processes of up-regulated genes with Ykt6 KD in the string network **(F)** Enriched processes of down-regulated genes with Ykt6 KD in the string network.

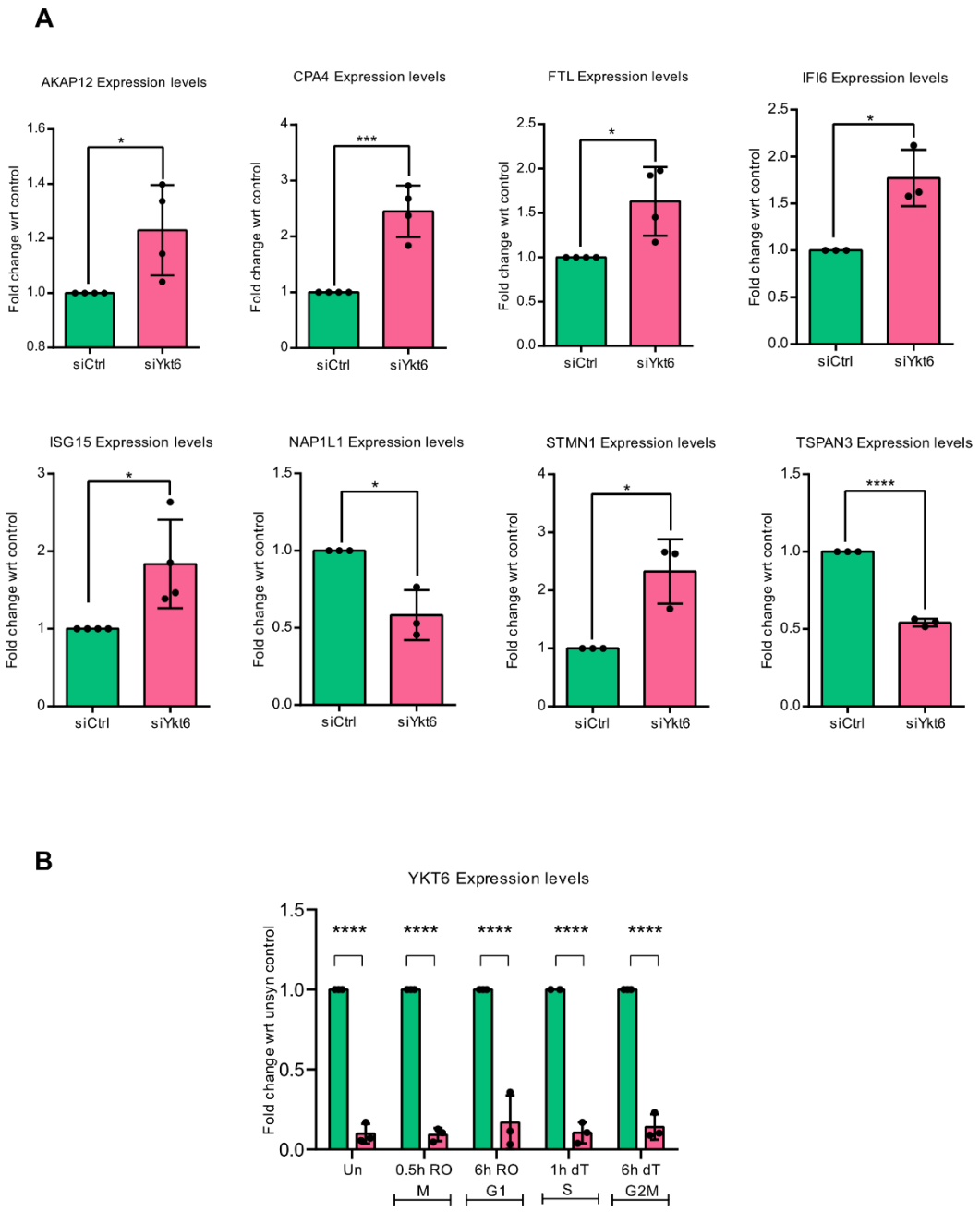

Figure S2: (A) Quantitative Real-time PCR (q-RT PCR) of AKAP12, CPA4, FTL, IFI6, ISG15, NAP1L1, STMN1, TSPAN3 expression levels, normalized to β-actin levels. **(B)** Quantitative Real-time PCR (q-RT PCR) of Ykt6 expression levels in synchronized cells during different cell cycle phases, normalized to β-actin levels, followed by normalizing with respective control in each phase.

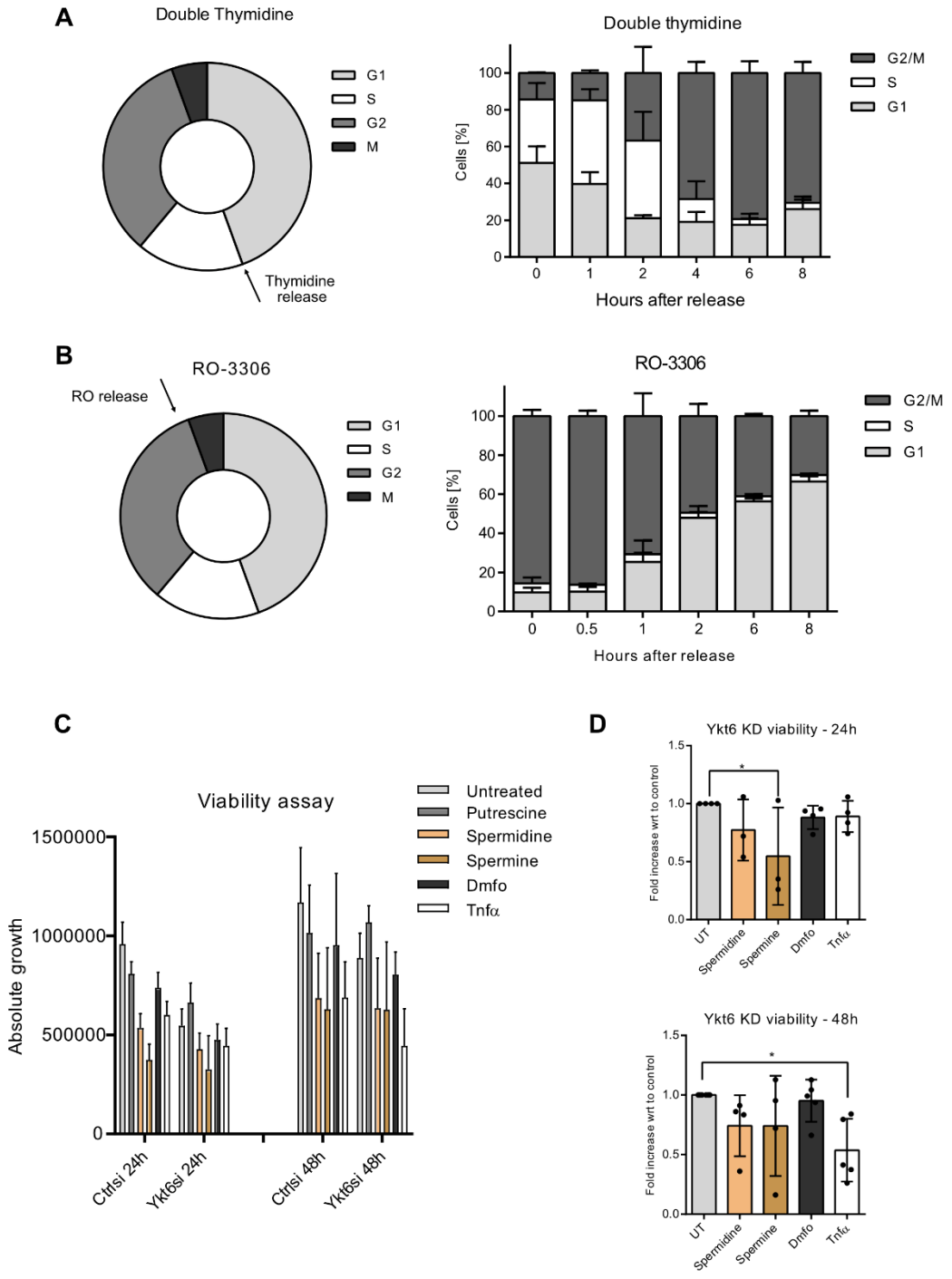

Figure S3: (A) Scheme of synchronization using Double thymidine block. The cells were treated with double thymidine and the cell cycle phases were analyzed at different time points post-release using flow cytometry **(B)** Scheme of synchronization using RO-3306. The cells were treated with RO-3306 and the cell cycle phases were analysed at different time points post-release using flow cytometry. **(C)** Viability assay representing the absolute growth in control or Ykt6 KD cells, with different treatments: putrescine, spermidine, spermine, Dmfo and Tnfα, measured at 24 hours and 48 hours. **(D)** The relative growth of Ykt6 KD cells treated with spermidine, spermine, Dmfo and Tnfα at 24 hours from (C) normalized to the untreated Ykt6 KD cells, represented as a fold increase.

4. Discussion

Ykt6 is highly conserved from yeast to humans and is an indispensable SNARE required for crucial fusion events at the crossroads of secretory, endocytic and autophagy pathways. Previously, we showed that lack of Ykt6 leads to growth defects *in vivo*. In this thesis, we identified that lack of Ykt6 leads to growth and proliferation delay in human colon cancer cells and embryonic kidney cells, which in turn leads to a delay during the cell cycle progression. Indeed, Ykt6 is implicated in a crucial trafficking role of cargoes that is required for cell growth and proliferation such as Wnt proteins. Wnts are secreted morphogens that induce development and patterning decisions. In this thesis, we dissected the molecular mechanism of Ykt6 in extracellular Wnt secretion, where Ykt6 is required for trafficking of Wnts at the sorting endosomal level for extracellular Wnt release. This is in line with the transcriptomic profiling that revealed novel Ykt6-dependent genes involved in membrane trafficking, cell cycle and metabolism. Interestingly, from our metabolic profiling, we identified that lack of Ykt6 leads to a lower level of polyamines and the precursor amino acids required for polyamine synthesis. Therefore, Ykt6 could be required for trafficking of the polyamine or amino acid transporters. Since Ykt6 is involved in the trafficking of growth factors like Wnt and possibly the polyamines, there should be a signalling pathway that regulates Ykt6. Ykt6 exists majorly in the cytoplasm but gets recruited to the membrane upon stimuli to initiate vesicle fusion events. In this thesis, we dissected that phosphorylation of the conserved residues in the SNARE domain of Ykt6 recruits it to the membranes. Using a combination of mutants in the longin and SNARE domain, we determined the activity of the membrane recruited Ykt6. Even though, phosphorylation recruits Ykt6 to the membranes, it is still inhibited to promote vesicle fusion events. The reason for this might be because a functional SNARE domain is required to initiate fusion events. Moreover, the cytosolic pool of Ykt6 could act as a reserve that gets recruited to membranes to traffic cargoes. We also identified PDK1 to phosphorylate Ykt6 *in vitro*. This would fit with its role in Wnt trafficking or polyamine homeostasis since PDK1 is an essential nutrient-sensing pathway. Therefore, the PDK1 axis could be involved in recruiting Ykt6 to the membranes based on upstream metabolic cues. Taken together, lack of Ykt6 leads to low extracellular Wnt levels and intracellular polyamine levels, which in turn could lead to a delay in growth and cell cycle progression.

Cells respond to extracellular and intracellular cues by modifying cargoes that are transported to the cell surface or secreted into the extracellular space. During stress situations, the cells modify the secreted factors or surface proteins through unconventional protein secretion (UPS) which is an alternative route in contrast to the classical bulk secretion pathway (Nuchel et al., 2021; Rabouille, 2017). Since Ykt6 has been proposed as a stress sensor in

yeast and acts at diverse cellular compartments, it could be employed by the UPS route under stress situations to adapt to the metabolic requirements of the cell. Overall, we propose a working model where Ykt6 could act as a valve in the trafficking of growth factors such as Wnt proteins and modulate metabolite levels such as polyamines required for cell growth, metabolism and proliferation. Since PDK1 is an important nutrient-sensing signalling axis, it could govern the conformation switch and hence the activity of Ykt6 based on upstream metabolic requirements as depicted in the overall working model Figure 6.

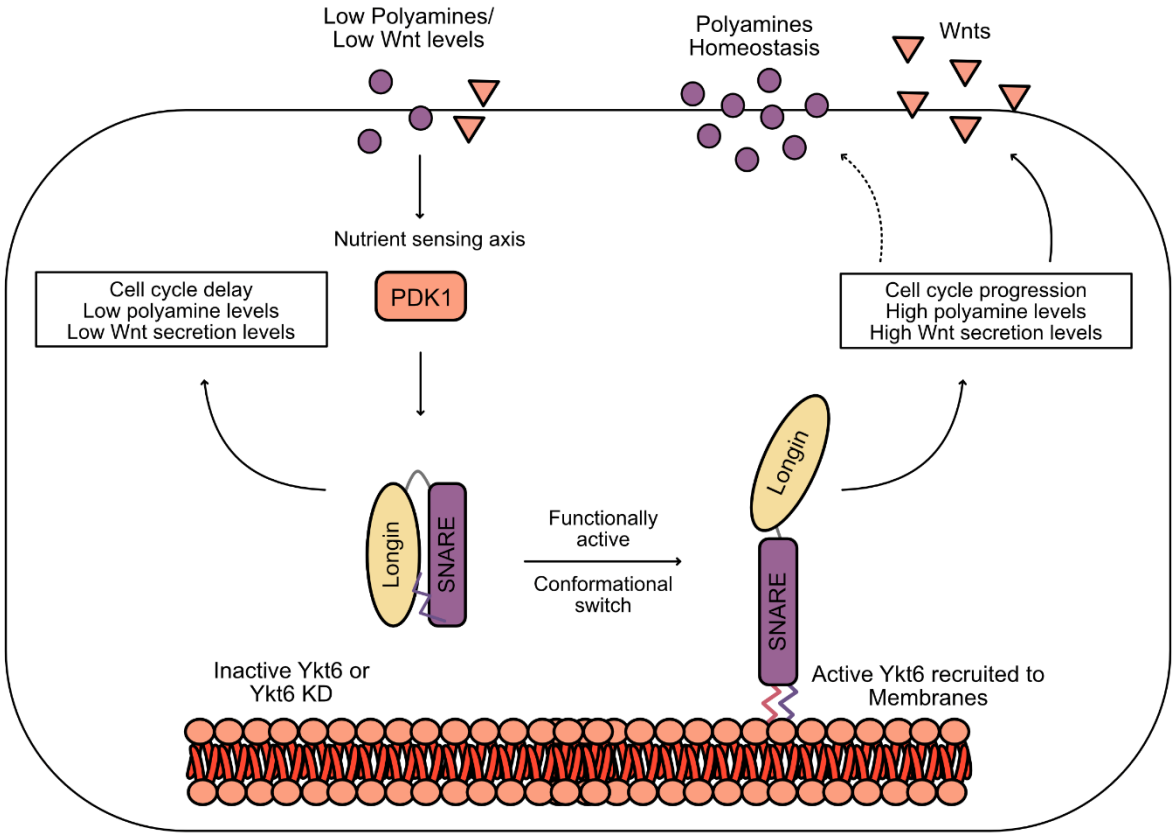

Figure 6: Working model of Ykt6 in the trafficking of Wnt proteins and modulating polyamine homeostasis. Inactive or knockdown of Ykt6 leads to lower extracellular Wnt and intracellular polyamine levels in contrast to active Ykt6 which gets recruited to membranes resulting in high Wnt or polyamine levels required for cell growth and proliferation.

4.1 Ykt6 regulates Wnt secretion at the endosomal level

Endocytic trafficking involves the transport of proteins or lipids between cellular compartments mediated by budding and the fusion of membrane-bound vesicles. SNARE proteins make up the core of membrane fusion machinery. Ykt6 is a versatile SNARE involved in multiple fusion events in diverse cellular compartments such as Golgi, endosomes and lysosomes. Endosomes act as a central station for sorting proteins for secretion, degradation or for recycling. The newly synthesized proteins or cargoes reach the endosomal system through the Golgi network or endocytosis. For example, Wnts are secreted morphogens that are trafficked through Golgi to the plasma membrane and reach the extracellular space. Once they reach the extracellular space, Wnts get endocytosed back into the cell, trafficked through ESCRT complexes, sorted onto vesicles and are released back into the extracellular space for secretion. Several studies exist to understand the mechanism and reason underlying Wnt endocytosis. Endocytosis is required for Wg trafficking and signalling in the *Drosophila* wing epithelium (Pfeiffer, Ricardo, Manneville, Alexandre, & Vincent, 2002). One of the reasons could be that Wnts need to be loaded onto extracellular vesicles for long-range signalling (Gross et al., 2012) or perhaps Wnts are additionally regulated at the endosomal level, to either be secreted or degraded.

It was previously shown that lack of Ykt6 reduces Wnt secretion on exosomes in *Drosophila* and mammalian cells (Gross et al., 2012). From our results, we see that knockdown of Ykt6 causes an intracellular accumulation of Wnt proteins (Manuscript I, Figure 1D) which indicates that Ykt6 is involved in a crucial fusion step of Wnt trafficking. At which step of the endocytic pathway does Ykt6 act in the trafficking of Wnt proteins? In the endocytic pathway, apart from protein sorting, the ESCRT machinery also plays a key role in the biogenesis of intraluminal vesicles (ILVs) in multivesicular endosomes (MVEs), which are sources of extracellular vesicle formation, otherwise called exosomes. The ESCRT-0 complex Hrs is recruited to endosomes via its FYVE domain that binds to phosphatidylinositol 3-phosphate (PI3-P), which is abundant in early endosomal membranes and MVBs (Urbé, Mills, Stenmark, Kitamura, & Clague, 2000). Our *in vivo* genetic analysis revealed that Ykt6 genetically interacts with Hrs and knockdown of Ykt6 increases Hrs-positive vesicles, but no changes were observed in MVB morphology (Manuscript I, Figure 4C, D). The transport from early (Rab5) to late endosome (Rab7) requires biogenesis of endosomal intermediates followed by the fusion with late endosomes. 2xFYVE-GFP that labels PI3P-containing endosomes mostly localizes to Rab7 endosomes. Concordantly, lack of Ykt6 also reduced FYVE-GFP positive endosomes, with decreased co-localization with Wg puncta, indicating that lack of Ykt6 reduces the pool of late PI3P-containing endosomes (Manuscript I, Figure

4E-H). This indicates that Ykt6 is required for fusion at the early endosomal level. This is in line with the Rab5Q88L assay results, where lack of Ykt6 decreases Wg trafficking to late endosomes, as Wg was seen outside of Rab5Q88L endosomes close to the membrane (Manuscript I, Figure 4I, J). Moreover, the lack of Ykt6 does not influence MVB biogenesis which also fits our previous finding where Ykt6 depletion increases sorting of exosomal marker CD63 from MVBs to lysosomes, but not its formation (Gross et al., 2012). Therefore, Ykt6 is required for a fusion step at the early endosomal level that facilitates trafficking of cargoes such as Wnt proteins to the late endosomes/MVBs and the lack of which could lead to degradation or accumulation of the cargoes.

Cargo sorting and vesicle trafficking in the endocytic pathway are regulated by Rab proteins that act as molecular switches. After entering the early endosomes, proteins or lipids can be directed to the late endosome/MVE for secretion or lysosome for degradation. Alternatively, they can be transported back to the plasma membrane via recycling endosomes mediated majorly by Rab4 and Rab11(Hu, Dammer, Ren, & Wang, 2015). Interestingly, the lack of Ykt6 led to an intracellular accumulation of both Wg and Rab4 at the plasma membranes that indicates that Ykt6 mediates Wg trafficking via Rab4 recycling endosomes (Manuscript I, Figure 6). Therefore, Ykt6 could mediate fusion events at the level of sorting endosomes upstream of MVB biogenesis. Why do cargoes such as Wnt be recycled via faster recycling endosomes instead of sorting into the MVBs remains unclear. Tissue morphogenesis depends on the endocytic recycling pathway, which can be clathrin-dependent (CDE) or clathrin-independent endocytic pathways (CIE). For example, recycling syndecans, a heparin sulphate proteoglycan requires ARF6, PIP2 and syntenin. Syntenin mutants cause accumulation of syndecans in the endosomes that block recycling and lead to impaired cell spreading (Zimmermann et al., 2005). E-cadherin once internalized, can be degraded or recycled which is crucial for the cells undergoing adhesion and morphogenesis (Grant & Donaldson, 2009). Similarly, Wg is an important morphogen whose directionality and secretion has to be tightly regulated. Wnts are known to spread via heparin sulphate proteoglycans like Dally and Dally-like protein (Dlp) (Han et al., 2005). Therefore, Wnts on the re-cycling endosomes could be an alternate route for reaching the target cell based on the cells requirement and the tissue type. In *Drosophila*, lack of Vamp7 led to an accumulation of Wg puncta in the Rab4-dependent recycling endosome which was Dlp positive (H. Gao, He, Lin, & Wu, 2017). Another study reported that in *Drosophila* embryos, recycling of Wnts sustain a high level of Wnt signalling which is required especially during development (Pfeiffer et al., 2002). Alternatively, it could be a mechanism to prevent degradation of the Wnts.

Since Ykt6 mediates Wnt trafficking at the early endosomal level, does it also regulate the endosomal trafficking of Wnts towards secretion or degradation based on the cell's metabolic requirements? Ykt6 was proposed as a stress sensor in yeast (Lars E.P. Dietrich et al., 2004). It is known to mediate crucial fusion events to adapt to the nutritional requirements of the cell. For example, under starvation conditions, Ykt6 mediates trafficking of leucine transporter to PM (Saito et al., 2019) and promotes autophagosome-lysosome fusion (Matsui et al., 2018; Takáts et al., 2018). The majority of Ykt6 exists in the cytosol and gets recruited to membranes upon unknown stimuli. We found that blocking endosomal acidification using bafilomycin or chloroquine led to the membrane recruitment of Ykt6 (Manuscript I, Figure 5). Since endosomes and lysosomes are acidic, it remains unclear to which de-acidified cellular compartment Ykt6 gets recruited to. The early endosomes are mildly acidic which enables the dissociation of receptors and ligands, where the receptors can be recycled. The ligands such as Wnts can be then directed for secretion or degradation (Hu et al., 2015) and passage through an acidic compartment is required for Wnt secretion. (Coombs et al., 2010). Endosomes could act as a central hub that senses Wnt signalling and fine-tunes Wnt secretion accordingly (Hemalatha, Prabhakara, & Mayor, 2016). An upstream signalling pathway could recruit Ykt6 to de-acidified endosomal compartments to mediate fusion events for extracellular Wnt release. Taken together, we show that the Ykt6-mediated fusion step at the sorting endosomal level regulates extracellular Wnt secretion levels and hence proper gradient formation.

4.2 Ykt6 phosphorylation determines its membrane recruitment and activity

Ykt6 has a unique structure and functional flexibility, which requires it to be tightly regulated to prevent any fusion anomalies. Even though there are several studies in understanding the regulation of the SNARE, the exact mechanism of the membrane recruitment and hence its activity is still not clear. The phosphorylation residues in the SNARE domain are conserved throughout the fungi, plant and animal kingdom (Malmersjö et al., 2016). Therefore, we identified and mutated these three conserved residues in humans and four residues in *Drosophila* to Alanine or Glutamate and generated non-phosphorylatable (Ykt6-4A/3A) or phosphomimicking mutant (Ykt6-4E/3E) respectively. How does phosphorylation of Ykt6 mechanistically regulate the conformation of Ykt6 to initiate vesicle fusion events? We used the phosphomimicking mutant to dissect the membrane recruitment and hence the activity of Ykt6. Our results from detergent fractionation and immunofluorescence microscopy revealed that Ykt6-3E associates primarily with membranes, whereas Ykt6-WT is present

predominantly in the cytoplasm (Manuscript II, Figure 2A, B, 3A). Since, the membrane recruited Ykt6 should be palmitoylated, which enables it to attach it to the membranes, we performed a pull-down of all the palmitoylated proteins using a click assay (Haberkant et al., 2016). Ykt6-3E was detected in the palmitoylated fraction, along with Wnt3A which is a positive control, whereas Ykt6-WT was below the detection threshold (Manuscript I, Figure 5C). Using different combinations of single and double mutations, in the longin domain (F42A), palmitoylation domain (C194) and farnesylation domain (C195), we aimed to determine the mechanism underlying the membrane recruitment of Ykt6 (Manuscript II, Figure 3A). Interestingly, we found that mutation in the longin domain (F42A) led to slight recruitment to membranes. The N-terminal longin domain interacts with the C-terminal SNARE domain and masks the lipid moieties to prevent the SNARE from binding to promiscuous targets (Haruki Hasegawa, Yang, Oltedal, Davanger, & Hay, 2004). Therefore, the interaction of the mutated longin domain with the SNARE domain could be distorted which leads to slight membrane recruitment. The non-phosphorylatable mutant does not associate with membranes, which further emphasizes the role of phosphorylation in membrane recruitment. Interestingly, all the combinations of double mutants which included the phosphomimicking mutant led to strong membrane recruitment (Manuscript II, Figure 3A). Therefore, phosphorylated Ykt6 is predominantly associated with the membranes. Since Ykt6 majorly exists in the cytoplasm, does the cytoplasmic fraction serve as a reserve pool, that gets recruited to membranes upon stimuli? Therefore, if more Ykt6 is present in this reserve pool, would more amounts of Ykt6 get recruited to membranes proportionally? Our results indicate that expressing increased amounts of Ykt6 WT, led to an expected linear increase of expression in overall cell lysates and the cytoplasmic fraction (Manuscript II, Figure 3C, D). However, this was not the case in the membrane fraction, where increased amounts of Ykt6 WT did not lead to increased membrane recruitment (Manuscript II, Figure 3E). This indicates that the cellular levels do not determine the membrane recruitment, but upstream stimuli or modifications in the SNARE domain determines the level of recruitment.

What are the kinases and hence the signalling pathways involved in phosphorylating Ykt6? Our finding from bead-based kinase screening revealed that Ykt6 was phosphorylated by PDK1 (phosphoinositide-dependent kinase 1) *in vitro* (Manuscript II, Figure 1D-F). This was intriguing because, PDK1 is an important nutritional sensing pathway, that acts downstream of the PI3K signalling pathway. PDK1 is activated or inhibited by upstream cues such as growth factors or nutrients. Ykt6 adapts the leucine levels by trafficking leucine transporter to the PM (Saito et al., 2019) and regulates extracellular Wnt levels by the trafficking of Wnt proteins (Linnemannstöns et al., 2020). Therefore, we hypothesized that PDK1 which is a growth factor-dependent kinase could phosphorylate and recruit Ykt6 to the membranes to

adapt to the metabolic demands of the cells based on upstream cues. Counter-intuitively, we see that inhibiting PDK1, but not activating it led to the membrane recruitment of Ykt6 (Manuscript IV, Figure 6E). However, it remains unclear if the membrane recruited Ykt6 is inhibited or activated. PDK1 is in a constitutively active state and inhibiting the pathway, could have other downstream effects that stress the cells, which in turn could recruit Ykt6 to adapt to stress. Indeed, other stressors such as blocking acidification by inhibiting the V-ATPase pumps also recruits Ykt6 to the membranes.

Indeed, another interesting question remains, if the phosphorylated membrane recruited Ykt6 initiates vesicle fusion events? Phosphorylation of Vamp8 within the SNARE domain reduces vesicle fusion *in vitro* and suppresses mast cell secretion in living cells. Phosphorylation is an inhibitory mechanism that allows the vesicles to dock but prevents the fusion with the plasma membranes (Malmersjö et al., 2016). *In Drosophila*, the lethality of a strong Ykt6 knockdown at the larval stage was rescued by overexpression of Ykt6-WT and non-phosphorylatable mutant Ykt6-4A, but not by the phosphomimicking mutant Ykt6-4E (Manuscript I, Figure 5J-O). Similarly, a mild knockdown of Ykt6 caused melanotic tumours and wing notches, a typical Wnt signalling and growth defect, which was rescued by re-expression of Ykt6-WT and 4A but not Ykt6-4E (Manuscript II, Table 2). In human Hek293T cells, Ykt6-3E was unable to rescue Wnt secretion, in contrast to Ykt6-WT and Ykt6-3A. Therefore, our results demonstrate a conserved physiological role of phosphorylation, essential for growth and development. Using our inducible RUSH system, we deduced that Ykt6 WT transports to Golgi together with Wnt3A, whereas Ykt6-3E led to a strong accumulation of Wnt3A at the plasma membrane (Manuscript II, Figure 2C-H). Our results from the Rab5QL assay determines that the phosphorylated Ykt6 hinders the endosomal fusion events, as Ykt6-3E yielded smaller endosomes (Manuscript II, Figure 5A, B). Furthermore, overexpression of Ykt6-3E reduced the Wnt secretion on exosomes. Complementing these findings, the proximity-dependent proteome revealed that only Ykt6 WT was proximal to processes such as ER-Golgi, Intra Golgi trafficking and autophagy, whereas the Ykt6 3E in the membrane fraction was proximal to PI3K/Akt signalling, protein folding and protein ubiquitination (Manuscript II, Figure 4). This indicates that a functional reserve pool of Ykt6 is required to adapt to the nutritional requirements of the cell, which is in line with a study where depalmitoylation of Ykt6 prevents it from entering the MVB pathway (Meiringer et al., 2008). Taken together, the phosphorylated Ykt6 is recruited to the membranes, however is still inhibited that prevents any vesicle fusion events.

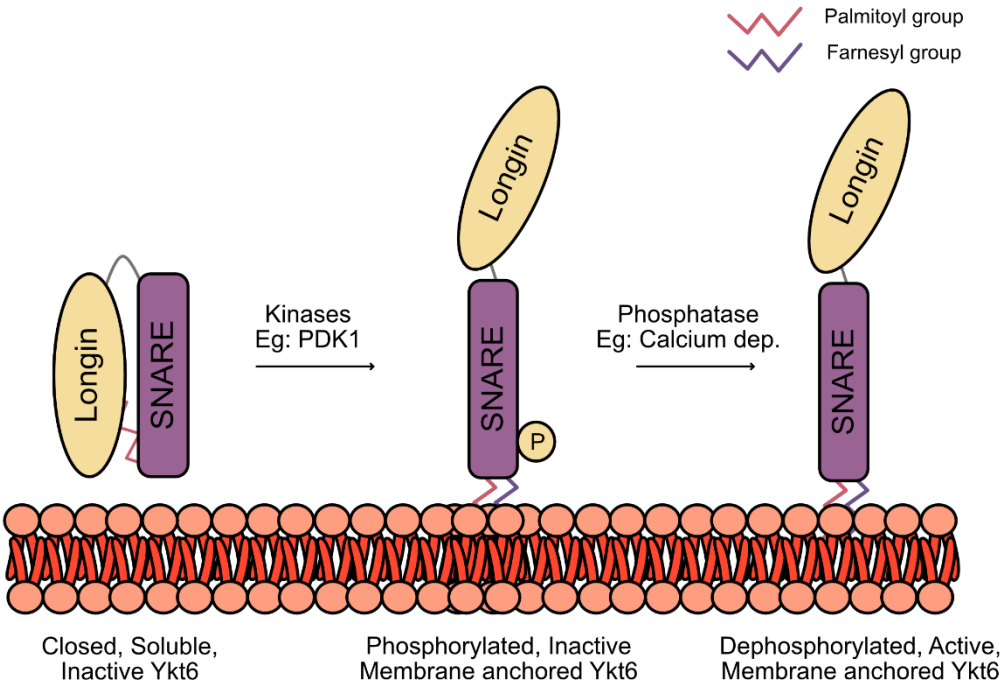

Figure 7: Model depicting three conformational states of Ykt6. The closed conformation of Ykt6 exists in the cytosol and is inactive. The phosphorylated Ykt6 associates primarily with membranes and is inhibited to initiate vesicle fusion events. The dephosphorylated Ykt6 associates primarily with membranes and is functionally active to initiate vesicle fusion events.

Since the phosphorylated Ykt6 is recruited to membranes, yet inhibited to initiate vesicle fusion, there should be involvement of phosphatases that activates the membrane recruited Ykt6. In fact, there are also other kinases known to phosphorylate Ykt6, Atg1 kinase in autophagy (Barz et al., 2020) and protein kinase C iota type (PRKCi) (McGrath et al., 2021). Interestingly, phosphorylated Ykt6 is sensitive to calcineurin (CaN), which is a Ca^{2+} dependent phosphatase (McGrath et al., 2021). In Parkinson's disease, α-synuclein triggers high levels of Ca^{2+} release which activates CaN. Interestingly, α-synuclein harnesses Ykt6 by inactivating it. Therefore, activating Ykt6 reduces α-synuclein toxicity through lysosomal stress clearance (Cuddy et al., 2019). Autophagy is known to be triggered by cytosolic Ca^{2+} signalling (Bootman, Chehab, Bultynck, Parys, & Rietdorf, 2018). Indeed, there are several signals including G-protein coupled receptors and receptor tyrosine kinase that increase calcium concentrations, most commonly via the PLC (phospholipase C) pathway. Therefore, the membrane recruited Ykt6, sensitive to CaN, could be regulated additionally by Calcium signalling pathways to initiate fusion events. For example, since Ykt6 plays a role in autophagy, Ykt6 could get recruited to membranes based on stimuli from signalling pathways and the rise of cytosolic Ca^{2+} levels could further trigger the vesicle fusion events. Therefore,

the membrane recruitment and hence the activity of Ykt6 is a two-step process, where the closed form of Ykt6 gets recruited to membranes upon phosphorylation and an additional de-phosphorylation is required to activate the membrane recruited Ykt6 to initiate vesicle fusion as depicted in the Figure 7.

4.3 Ykt6 acts as a stress sensor during cell cycle progression

Vesicle Trafficking involves the transport of cargoes or their receptors to their final destination which is crucial to activate several signalling pathways and to maintain metabolic homeostasis. The complex coordination and regulation of signalling pathways culminate in the progression of the cell cycle for growth, development and homeostasis. For example, the binding of Wnts to its receptors upregulates target genes such as cyclin D and c-myc that promote cell cycle progression (Niehrs & Acebron, 2012). Therefore, the cells must sustain continuous secretion of Wnts, to ensure steady active Wnt signalling. Endosomes are central hubs that regulate the duration, intensity and spatial patterning of morphogens that determines cell fate determination and migration. Wnts are additionally regulated at the endosomal level, loaded onto exosomes for long-range signalling (Linnemannstöns et al., 2020). Different exosomes carry different Wnts based on the cell type and function. For example, epididymal epithelium secretes high levels of Wnt2b on exosomes to induce Wnt/LRP6 signalling in sperm maturation (Koch, Acebron, Herbst, Hatiboglu, & Niehrs, 2015). In our study, for the first time, we show that Wnts are not secreted on classical exosomal sub-populations such as $CD63^{+}/CD81^{+}/CD9^{+}$ tetraspanins. They were predominantly identified in the flow-through fraction ($CD63^{-}/CD81^{-}/CD9^{-}$) which contained exosomal vesicles as characterized by electron microscopy and lipidomics (Manuscript III, Figure 1). Our proteomic characterization revealed several markers that could potentially carry Wnt. Interestingly, some of these markers such as Annexins, Rala, Rac1 and Flotillins are up-regulated in several tumours (Ghoroghi et al., 2021; Ji et al., 2015; Liu et al., 2018; Xi, Ju, & Wang, 2020). If these markers carry Wnt, then the tumours cells could specifically up-regulate the Wnt-bearing exosomal sub-populations to promote uncontrolled proliferation. Moreover, we also see an enrichment of cell-cycle dependent EV markers. The Wnt co-receptor LRP5/6 is a key Wnt signalling transducer and is under cell cycle control, where phosphorylation of the receptor is mediated by CDK14 during G2/M, which in turn increases the receptiveness of Wnt signalling (Davidson & Niehrs, 2010). For example, colon cancer cells secrete exosomes that reduce the mitotic duration to promote self-proliferation (Ren, Sun, Ma, Liu, & Wang, 2019). Therefore, secretion of Wnt-bearing exosomes could be cell-cycle dependent to promote mitogenic Wnt signalling in a healthy cell

or to promote metastatic niches in cancer cells. Since Ykt6 plays a crucial trafficking role in Wnt secretion and therefore Wnt signalling, we next asked if the lack of Ykt6 could affect the cell cycle progression.

Even though Ykt6 is an essential gene in yeast and well-studied in diverse cellular functions, its function during cell cycle progression is not well studied so far. Our studies revealed that lack of Ykt6 led to growth and proliferation delay in human colon cancer cells and embryonic kidney cells. The growth and proliferation defects are translated as G1 delay and reduced mitotic index during cell cycle progression (Manuscript IV, Figure 2). Even though Ykt6 could act at multiple trafficking events that occur during the cell cycle, it is still unclear if Ykt6 has a dedicated trafficking function that is crucial for cell cycle progression. Since Ykt6 knockdown also leads to reduced mitotic index, it is still unclear if these cells are in a quiescent-like state. In non-dividing cells, the quiescent state is favoured by up-regulating cell cycle arrest pathways or down-regulating mitogenic pathways (Hinze & Boucrot, 2018). Interestingly, our finding from Ykt6 knockdown does not reveal any cell cycle arrest, but simply a delay. If Ykt6 is involved in the trafficking of mitogens such as Wnt proteins, then the lack of Ykt6 could lead to a delay in cell proliferation. Therefore, it is plausible that lack of Ykt6 affects the trafficking of Wnt proteins which in turn could lead to a delay in cell cycle progression.

Cell cycle progression majorly depends on cell growth, which in turn relies on nutrient availability. Extracellular nutrient signals along with intracellular metabolites contribute to cell growth and therefore to an increase in cell size. mTOR is the master regulator that controls the cell growth by stimulating protein synthesis and, accordingly the cell size by sensing amino acids and growth-promoting signals (Fingar et al., 2002; Yuan, Xiong, & Guan, 2013). In our study, we observed that the knockdown of Ykt6 resulted in larger cell size (Manuscript IV, Figure 2G). An increase in cell size reflects an increased protein synthesis. In line with this, we identified that lack of Ykt6 leads to increased protein synthesis (Manuscript IV, Figure 5E, F). Why does the lack of Ykt6 lead to increased protein synthesis? Several pathways converge to promote cell growth and protein stabilization during cell cycle progression. The prominent Wnt/STOP pathway increases cellular protein levels and cell size, by inhibiting GSK3β-mediated protein degradation to promote cell growth (Acebron et al., 2014). Interestingly, 15% of the proteins are stabilized by Wnt/STOP signalling. Indeed, Ykt6 was also specified as one of the GSK3β targets. In the absence of Wnt signals, GSK3β phosphorylates several cytoplasmic target proteins. Does GSK3β phosphorylate Ykt6 as well? Though not strictly required, priming phosphorylation significantly increases the efficiency of substrate phosphorylation of most GSK3β targets by a factor of 100-1000X (Thomas et al., 1999). It would be interesting to investigate if GSK3β additionally phosphorylates a previously

phosphorylated Ykt6, as we identified a GSK3β phosphorylation motif in the longin domain at T55 position in the Ykt6 sequence. The PI3K/Akt pathway increases mammalian cell size by stimulating protein synthesis and inhibiting protein degradation (Faridi, Fawcett, Wang, & Roth, 2003). This indicates that Ykt6 plays an important role in protein synthesis and the lack of which affects cell growth, although the exact pathway involved in regulating the cell size in Ykt6 KD remains to be elucidated. In yeast cells, inactivation of cell cycle regulator genes results in large cell size where cell growth continues but cell division is blocked. Similarly, in mammalian cells, mTOR and PI3K-mediated cell growth continue even when the cell cycle progression is blocked with an increased percentage of cells in the G1 phase and increased cell size (Faridi et al., 2003). Therefore, cell growth and cell cycle progression are distinct processes in yeast as well as mammalian cells. This is in line with our findings where lack of Ykt6 leads to a delay in cell division that corresponds to an increased cell size due to increased protein synthesis.

How does the lack of Ykt6 increase protein synthesis? Based on our transcriptomic data, SAT1, a key catabolic enzyme in polyamine biosynthesis is down-regulated upon Ykt6 knockdown. Spermidine is required for the activation of the eukaryotic initiation factor (eIF5A), a major translation factor (Park, 2006). Depletion of polyamines leads to translation arrest and therefore cell growth delay/arrest (Mandal, Mandal, Johansson, Orjalo, & Park, 2013). Therefore, the cell compensates, the lack of Ykt6 by down-regulating SAT1, which in turn would prevent the catabolism of spermidine and spermine and lead to increased protein synthesis. Strikingly, our results from the metabolic profiling of Ykt6 KD revealed that the polyamines: putrescine, spermidine, spermine and, amino acids: arginine and ornithine involved in polyamine biosynthesis, are down-regulated upon Ykt6 knockdown (Manuscript IV, Figure 5D). Lack of polyamines leads to G1 delay during the cell cycle progression (Ray, Zimmerman, Mccormack, Patel, & Johnson, 1999). If the G1 delay observed with Ykt6 KD is due to a deficiency in polyamines, then polyamines should be able to rescue the Ykt6 KD phenotype. Indeed, we identified that putrescine, but not spermidine or spermine, partially rescued the growth effects of Ykt6 KD (Manuscript IV, Figure 6A, B). If the cells require spermidine and spermine, then why does only putrescine rescue the viability? Adding spermidine and spermine decreased the viability of the cells in both control and Ykt6 KD cells. Although polyamines are provided externally, the cells govern their uptake and transport. Polyamine levels are tightly regulated at the entry and exit of the cell by a combination of synthesis, catabolism and transport. Interestingly, putrescine has a different transporter (Uemura et al., 2008) in contrast to spermidine/spermine (Abdulhussein & Wallace, 2014). Therefore, the upstream signals involved in the uptake of these polyamines could be different. Moreover, spermidine and spermine are cytotoxic metabolites when provided in excess (Del

Rio et al., 2018). Interestingly, in colon cancer cells, polyamine depletion favoured uptake of putrescine rather than spermidine (Corral & Wallace, 2020). The uptake of polyamines also depends on the growth status of the cell. Interestingly, polyamine homeostasis majorly relies on putrescine uptake and sustaining high levels of intracellular putrescine is crucial for G1 to S phase transition during the cell cycle progression (Martin, Ilett, & Minchin, 1991). Therefore, it is plausible that Ykt6 could be involved in the trafficking of the polyamine transporters based on the cell growth status similar to the trafficking of leucine transporter under nutritional stress (Saito et al., 2019). In agreement, lack of Ykt6 results in low polyamine levels that cause a delay in the cell cycle, which can be partially rescued by supplementing putrescine. Therefore, the cell is compensating for the lack of Ykt6 by stimulating the uptake of putrescine, since the polyamine homeostasis majorly depends on putrescine.

Which signalling pathway is involved in stimulating the uptake of putrescine? Apart from being a precursor metabolite for spermidine, putrescine could have an essential function on its own which is not known so far. Polyamines coordinate with several signalling pathways to promote cell growth and proliferation. Putrescine stimulates the mTOR signalling pathway and therefore protein synthesis (Kong et al., 2014). Interestingly, depletion of polyamines by overexpression of SAT1 inhibits cell proliferation and migration via Akt/GSK3β/β-catenin signalling pathway in colorectal cancer cells (Wang et al., 2017). Polyamine depletion induces PDK1 activity, activates Akt, which in turn has several downstream effects on cell growth and proliferation. Since we identified PDK1 to phosphorylate Ykt6 *in vitro* and recruit Ykt6 to membranes, we reasoned that the PDK1 signalling pathway could regulate Ykt6 to modulate polyamine levels during cell cycle progression. Strikingly, we discovered that putrescine leads to membrane recruitment of Ykt6 via the PDK1 signalling pathway. Therefore, Ykt6 could be involved in mediating the trafficking of transporters involved in polyamine homeostasis during cell cycle progression required for cell growth and proliferation.

5. Summary of the findings and concluding remarks

In this study, we identified that Ykt6 regulates trafficking of Wnt proteins at the endosomal levels and the lack of which causes low extracellular Wnt levels. Furthermore, we discovered that lack of Ykt6 leads to lower polyamine levels, which could be due to the trafficking of the polyamine transporters. Since Ykt6 is involved in the crucial trafficking role of growth factors such as Wnt proteins and metabolites such as polyamines, the lack of Ykt6 leads to a delay in cell cycle progression and proliferation. Ykt6 exists predominantly in the cytosol and gets recruited to membranes to initiate fusion events. We also identified that phosphorylation of the Ykt6 SNARE domain regulates its membrane recruitment and activity. The key findings of the thesis are summarized as follows:

- It was previously shown Ykt6 is required for exosomal Wnt secretion (Gross et al., 2012). In this study, we aimed to understand at which step of Wnt trafficking does Ykt6 act. We identified that the lack of Ykt6 led to an increase in Hrs-positive vesicles and reduced the pool of PI3P containing late endosomes. Lack of Ykt6 led to a larger endosome in Rab5QL assay, where Wg localized outside the endosomes closed to the membrane. Therefore, lack of Ykt6 decreased Wg trafficking to late endosomes/MVEs. We also show that Ykt6 recycles Wg to the plasma membrane via Rab4 positive endosomes. Since Ykt6 is majorly present in the cytosol, it gets recruited to membranes to initiate fusion events. We further confirmed that Ykt6 attaches to the membranes via palmitoylation as revealed by the pull-down of palmitoylated proteins. Furthermore, we identified that de-acidification leads to membrane recruitment of Ykt6. Therefore, we propose that Ykt6 could get recruited to de-acidified compartments such as endosomes to traffic Wnt proteins and therefore extracellular Wnt release.
- We further identified that phosphorylation of the SNARE domain governs the membrane recruitment of Ykt6. By mutating the conserved phosphorylated sites, we identified that phosphorylated Ykt6 associates with membranes predominantly. Knockdown of Ykt6 leads to low Wnt secretion levels in humans and wing notches in *Drosophila*. However, the knockdown phenotype of Ykt6 was rescued with overexpression of Ykt6-WT and the non-phosphorylatable mutant, but not with the phosphomimicking mutant. Interestingly, we found that the cellular levels of Ykt6 do not determine the membrane recruitment of Ykt6, but rather an upstream stimulus involving modification of the SNARE domain. Furthermore, we identified Ykt6 to be phosphorylated by PDK1 *in vitro*, which is an essential nutrient-sensing pathway. Therefore, PDK1 could govern the conformational switch of Ykt6 based on upstream metabolic cues.

- Since lack of Ykt6 leads to growth defects *in vivo*, we set out to investigate the growth effects of Ykt6 in human cell culture. Our findings revealed that lack of Ykt6 leads to a delay in cell growth and proliferation. Interestingly, by flow cytometry, we identified that lack of Ykt6 increased the percentage of cells in the G1 phase which indicates a G1 delay and reduced the percentage of cells in the mitotic phase which indicates a reduced mitotic index. Therefore, Ykt6 has an essential role during cell cycle progression. Even though Ykt6 is not differentially expressed or localized throughout the cell cycle phases, single-cell transcriptomic characterization revealed novel Ykt6-dependent genes involved in membrane trafficking, cell cycle and metabolism. Interestingly, we identified SAT1, a key metabolic enzyme involved in polyamine homeostasis to be down-regulated upon Ykt6 KD specifically at the G1 phase. In line with this, all the metabolites/amino acids involved in polyamine synthesis were present in lower levels with Ykt6 KD. It could be plausible that Ykt6 is required for the trafficking of polyamine transporters similar to a study where Ykt6 traffics leucine transporter to the plasma membrane. Strikingly, one of the polyamines, putrescine, a catalytic product of SAT1, was able to partially rescue the growth defects caused by Ykt6 KD. Furthermore, putrescine led to membrane recruitment of Ykt6 in a PDK dependent manner. Since PDK1 is a nutrient-sensing pathway, it could regulate the membrane recruitment of Ykt6 to traffic growth factors such as Wnts or metabolites such as polyamines essential for cellular growth and proliferation.

Taken together, Ykt6 is a crucial SNARE involved in the trafficking of growth factors or cellular metabolites required during cell cycle progression. It acts at the crossroads of cell growth and metabolism. Therefore, we propose that Ykt6 acts as a valve by trafficking important cargoes to adapt to the metabolic requirements of the cell. Ykt6 can co-operatively act together with several important signalling pathways to adapt to stressful situations in the cell. For example, under stress situations, cells reshape the extracellular proteome and surface proteins via unconventional protein secretion (UPS) mediated by the mTORC1-GRASP55 signalling axis (Nuchel et al., 2021; Rabouille, 2017). This fits with the role of Ykt6, where it is involved in the trafficking of Wnt proteins in nutrient-replete conditions and involved in trafficking of leucine transporter to the PM under nutrient-depleted conditions (Gross et al., 2012; Saito et al., 2019). The PI3K-Akt-mTOR axis and Wnt signalling axis are important signalling pathways that are hyperactive in cancer. It is interesting to speculate if these pathways regulate the activity of Ykt6 or if Ykt6 regulates these pathways. Indeed, the signalling pathways and Ykt6 could be reciprocally regulated to adapt to the metabolic demands of the cell. Several important questions remain regarding the exact mechanism by which Ykt6 is recruited to different cellular compartments. The regulatory mechanism of Ykt6

is not simple as in the case of other SNAREs. Ykt6 has several layers of regulations such as phosphorylation and dephosphorylation that require coordination of several signaling pathways that culminate to activate Ykt6. Why cells should coordinate or employ important developmental pathways to activate a SNARE, still remains an exciting and puzzling question. Unravelling these questions would open future perspectives on therapeutics based on the activity of Ykt6. Due to its structural and functional flexibility, it has also been hijacked by cancer cells or neuronal cell to promote metastasis or protein aggregates during neurodegeneration respectively. The cancer cells or the neuronal cells activate Ykt6 by recruiting it to membranes which could increase the trafficking of growth factors and metabolites which in turn leads to unsupervised growth and proliferation. Moreover, the tumor cells associated increased aggressiveness, metastasis and immune-inhibitory phenotypes had a high expression of Ykt6 (Yang et al., 2021). In a similar fashion, farnesyl inhibitors or other molecules can be employed to activate Ykt6 at the membranes to adapt to cellular stress in a healthy cell. Ykt6 has the ability to co-ordinate extracellular nutritional status and intracellular metabolic needs to promote metabolic homeostasis required for a proper cell cycle progression. Therefore, Ykt6 could be activated in tissues or a system to sustain high levels of Wnt or polyamines essential for cell growth and division. Furthermore, Ykt6 could be used as a complementary drug target for cancer and neurodegenerative disorders to adapt to cellular metabolic stress or a promising biomarker in aggressive metastatic tumours.

Bibliography

(Overall Introduction and Discussion)

Abdulhussein, A. A., & Wallace, H. M. (2014). Polyamines and membrane transporters. *Amino Acids*, *46*(3), 655–660. https://doi.org/10.1007/s00726-013-1553-6

Acebron, S. P., Karaulanov, E., Berger, B. S., Huang, Y. L., & Niehrs, C. (2014). Mitotic Wnt Signaling Promotes Protein Stabilization and Regulates Cell Size. *Molecular Cell*, *54*(4), 663–674. https://doi.org/10.1016/j.molcel.2014.04.014

Acebron, S. P., & Niehrs, C. (2016). β-Catenin-Independent Roles of Wnt/LRP6 Signaling. *Trends in Cell Biology*, *26*(12), 956–967. https://doi.org/10.1016/j.tcb.2016.07.009

Alberts, B., Johnson, A., Lewis, J., Raff, M., Roberts, K., & Walter, P. (2002). *Molecular Biology of the Cell*. *4th edition. New York: Garland Science* (Vol. 1). Retrieved from https://www.ncbi.nlm.nih.gov/books/NBK21054/

Bartscherer, K., Pelte, N., Ingelfinger, D., & Boutros, M. (2006). Secretion of Wnt Ligands Requires Evi, a Conserved Transmembrane Protein. *Cell*, *125*(3), 523–533. https://doi.org/10.1016/j.cell.2006.04.009

Barz, S., Kriegenburg, F., Henning, A., Bhattacharya, A., Mancilla, H., Sánchez-Martín, P., & Kraft, C. (2020). Atg1 kinase regulates autophagosome-vacuole fusion by controlling SNARE bundling. *EMBO Reports*, *21*(12). https://doi.org/10.15252/embr.202051869

Beauséjour, C. M., Krtolica, A., Galimi, F., Narita, M., Lowe, S. W., Yaswen, P., & Campisi, J. (2003). Reversal of human cellular senescence: Roles of the p53 and p16 pathways. *EMBO Journal*, *22*(16), 4212–4222. https://doi.org/10.1093/emboj/cdg417

Bishop, J. M. (1988). The molecular genetics of cancer: 1988. *Leukemia*, *2*(4), 199–208.

Bootman, M. D., Chehab, T., Bultynck, G., Parys, J. B., & Rietdorf, K. (2018). The regulation of autophagy by calcium signals: Do we have a consensus? *Cell Calcium*, *70*(August 2017), 32–46. https://doi.org/10.1016/j.ceca.2017.08.005

Cantley, L. C. (2002). The phosphoinositide 3-kinase pathway. *Science*, *296*(5573), 1655–1657. https://doi.org/10.1126/science.296.5573.1655

Catchpoole, D. R., & Wanjin, H. (1999). Characterization of the sequence and expression of a Ykt6 prenylated SNARE from rat. *DNA and Cell Biology*, *18*(2), 141–145. https://doi.org/10.1089/104454999315529

Chen, J. (2016). The cell-cycle arrest and apoptotic and progression. *Cold Spring Harbor Perspectives in Biology*, 1–16.

Clevers, H., & Nusse, R. (2012). Wnt/β-catenin signaling and disease. *Cell*, *149*(6), 1192–1205. https://doi.org/10.1016/j.cell.2012.05.012

Coombs, G. S., Yu, J., Canning, C. A., Veltri, C. A., Covey, T. M., Cheong, J. K., … Virshup, D. M. (2010). WLS-dependent secretion of WNT3A requires Ser209 acylation and vacuolar acidification. *Journal of Cell Science*, *123*(19), 3357–3367. https://doi.org/10.1242/jcs.072132

Corral, M., & Wallace, H. M. (2020). Upregulation of polyamine transport in human colorectal cancer cells. *Biomolecules*, *10*(4). https://doi.org/10.3390/biom10040499

Cselenyi, C. S., Jernigan, K. K., Tahinci, E., Thorne, C. A., Lee, L. A., & Lee, E. (2008). LRP6 transduces a canonical Wnt signal independently of Axin degradation by inhibiting

GSK3's phosphorylation of β-catenin. *Proceedings of the National Academy of Sciences of the United States of America*, *105*(23), 8032–8037. https://doi.org/10.1073/pnas.0803025105

Cuddy, L. K., Wani, W. Y., Morella, M. L., Pitcairn, C., Tsutsumi, K., Fredriksen, K., … Mazzulli, J. R. (2019). Stress-Induced Cellular Clearance Is Mediated by the SNARE Protein ykt6 and Disrupted by α-Synuclein. *Neuron*, *104*(5), 869-884.e11. https://doi.org/10.1016/j.neuron.2019.09.001

Davidson, G., & Niehrs, C. (2010). Emerging links between CDK cell cycle regulators and Wnt signaling. *Trends in Cell Biology*, *20*(8), 453–460. https://doi.org/10.1016/j.tcb.2010.05.002

Davidson, G., Shen, J., Huang, Y. L., Su, Y., Karaulanov, E., Bartscherer, K., … Niehrs, C. (2009). Cell Cycle Control of Wnt Receptor Activation. *Developmental Cell*, *17*(6), 788–799. https://doi.org/10.1016/j.devcel.2009.11.006

DeBruine, Z. J., Xu, H. E., & Melcher, K. (2017). Assembly and architecture of the Wnt/β-catenin signalosome at the membrane. *British Journal of Pharmacology*, *174*(24), 4564–4574. https://doi.org/10.1111/bph.14048

Del Rio, B., Redruello, B., Linares, D. M., Ladero, V., Ruas-Madiedo, P., Fernandez, M., … Alvarez, M. A. (2018). Spermine and spermidine are cytotoxic towards intestinal cell cultures, but are they a health hazard at concentrations found in foods? *Food Chemistry*, *269*(June), 321–326. https://doi.org/10.1016/j.foodchem.2018.06.148

Dietrich, L. E P, & Ungermann, C. (2004). On the mechanism of protein palmitoylation. *EMBO Reports*, *5*(11), 1053–1057. https://doi.org/10.1038/sj.embor.7400277

Dietrich, Lars E.P., Gurezka, R., Veit, M., & Ungermann, C. (2004). The SNARE Ykt6 mediates protein palmitoylation during an early stage of homotypic vacuole fusion. *EMBO Journal*, *23*(1), 45–53. https://doi.org/10.1038/sj.emboj.7600015

Dietrich, Lars E.P., Peplowska, K., LaGrassa, T. J., Hou, H., Rohde, J., & Ungermann, C. (2005). The SNARE Ykt6 is released from yeast vacuoles during an early stage of fusion. *EMBO Reports*, *6*(3), 245–250. https://doi.org/10.1038/sj.embor.7400350

Faridi, J., Fawcett, J., Wang, L., & Roth, R. A. (2003). Akt promotes increased mammalian cell size by stimulating protein synthesis and inhibiting protein degradation. *American Journal of Physiology - Endocrinology and Metabolism*, *285*(5 48-5), 964–972. https://doi.org/10.1152/ajpendo.00239.2003

Fasshauer, D., Sutton, R. B., Brunger, A. T., & Jahn, R. (1998). Conserved structural features of the synaptic fusion complex: SNARE proteins reclassified as Q- and R-SNAREs. *Proceedings of the National Academy of Sciences of the United States of America*, *95*(26), 15781–15786. https://doi.org/10.1073/pnas.95.26.15781

Fidler, I. J., & George, P. (1980). The pathogenesis of cancer metastasis. *Nature*, *293*(January), 139–146.

Fingar, D. C., Salama, S., Tsou, C., Harlow, E., & Blenis, J. (2002). Mammalian cell size is controlled by mTOR and its downstream targets S6K1 and 4EBP1/eIF4E. *Genes and Development*, *16*(12), 1472–1487. https://doi.org/10.1101/gad.995802

Finlay, C. A., Hinds, P. W., & Levine, A. J. (1989). The p53 proto-oncogene can act as a suppressor of transformation. *Cell*, *57*(7), 1083–1093. https://doi.org/10.1016/0092-8674(89)90045-7

Fukasawa, M., Varlamov, O., Eng, W. S., Sollner, T. H., & Rothman, J. E. (2004). Localization

and activity of the SNARE Ykt6 determined by its regulatory domain and palmitoylation. *Proceedings of the National Academy of Sciences*, *101*(14), 4815–4820. https://doi.org/10.1073/pnas.0401183101

Gao, H., He, F., Lin, X., & Wu, Y. (2017). Drosophila VAMP7 regulates Wingless intracellular trafficking. *PLoS ONE*, *12*(10), 1–14. https://doi.org/10.1371/journal.pone.0186938

Gao, J., Reggiori, F., & Ungermann, C. (2018). A novel in vitro assay reveals SNARE topology and the role of Ykt6 in autophagosome fusion with vacuoles. *The Journal of Cell Biology*, *217*(10), 3670–3682. https://doi.org/10.1083/jcb.201804039

Gasnereau, I., Herr, P., Chia, P. Z. C., Basler, K., & Gleeson, P. A. (2011). Identification of an endocytosis motif in an intracellular loop of Wntless protein, essential for its recycling and the control of Wnt protein signaling. *Journal of Biological Chemistry*, *286*(50), 43324–43333. https://doi.org/10.1074/jbc.M111.307231

Ghoroghi, S., Mary, B., Larnicol, A., Asokan, N., Klein, A., Osmani, N., … Hyenne, V. (2021). Ral GTPases promote breast cancer metastasis by controlling biogenesis and organ targeting of exosomes. *ELife*, *10*, 1–29. https://doi.org/10.7554/eLife.61539

Giono, L. E., & Manfredi, J. J. (2006). The p53 Tumor Suppressor Participates in Multiple Cell Cycle Checkpoints. *Journal Cellular Physiology*, *211(3)*(May), 736–747. https://doi.org/10.1002/JCP

Glinka, A., Wu, W., Delius, H., Monaghan, A. P., Blumenstock, C., & Niehrs, C. (1998). Dickkopf-1 is a member of a new family of secreted proteins and functions in head induction. *Nature*, *391*(6665), 357–362. https://doi.org/10.1038/34848

Gonzalez, L., & Scheller, R. H. (1999). Regulation of membrane trafficking: Structural insights from a Rab/effector complex. *Cell*, *96*(6), 755–758. https://doi.org/10.1016/S0092-8674(00)80585-1

Gordon, M. D., & Nusse, R. (2006). Wnt signaling: Multiple pathways, multiple receptors, and multiple transcription factors. *Journal of Biological Chemistry*, *281*(32), 22429–22433. https://doi.org/10.1074/jbc.R600015200

Grant, B. D., & Donaldson, J. G. (2009). Pathways and mechanisms of endocytic recycling. *Nature Reviews Molecular Cell Biology*, *10*(9), 597–608. https://doi.org/10.1038/nrm2755

Grinnell, F. T. E. (2002). Ykt6p Is a Multifunctional Yeast R-SNARE That Is Required for Multiple Membrane Transport Pathways to the Vacuole. *Molecular Biology of the Cell*, *13*(November), 3915–3929. https://doi.org/10.1091/mbc.E02

Gross, J. C., Chaudhary, V., Bartscherer, K., & Boutros, M. (2012). Active Wnt proteins are secreted on exosomes. *Nature Cell Biology*, *14*(10), 1036–1045. https://doi.org/10.1038/ncb2574

Gupta, G. P., & Massagué, J. (2006). Cancer Metastasis: Building a Framework. *Cell*, *127*(4), 679–695. https://doi.org/10.1016/j.cell.2006.11.001

Haberkant, P., Stein, F., Höglinger, D., Gerl, M. J., Brügger, B., Van Veldhoven, P. P., … Schultz, C. (2016). Bifunctional Sphingosine for Cell-Based Analysis of Protein-Sphingolipid Interactions. *ACS Chemical Biology*, *11*(1), 222–230. https://doi.org/10.1021/acschembio.5b00810

Han, C., Yan, D., Belenkaya, T. Y., & Lin, X. (2005). Drosophila glypicans Dally and Dally-like shape the extracellular Wingless morphogen gradient in the wing disc. *Development*, *132*(4), 667–679. https://doi.org/10.1242/dev.01636

Hasegawa, H. (2004). Intramolecular protein-protein and protein-lipid interactions control the

conformation and subcellular targeting of neuronal Ykt6. *Journal of Cell Science*, *117*(19), 4495–4508. https://doi.org/10.1242/jcs.01314

Hasegawa, Haruki, Yang, Z., Oltedal, L., Davanger, S., & Hay, J. C. (2004). Intramolecular protein-protein and protein-lipid interactions control the conformation and subcellular targeting of neuronal Ykt6. *Journal of Cell Science*, *117*(19), 4495–4508. https://doi.org/10.1242/jcs.01314

He, X., Semenov, M., Tamai, K., & Zeng, X. (2004). LDL receptor-related proteins 5 and 6 in Wnt/β-catenin signaling: Arrows point the way. *Development*, *131*(8), 1663–1677. https://doi.org/10.1242/dev.01117

Hemalatha, A., Prabhakara, C., & Mayor, S. (2016). Endocytosis of Wingless via a dynamin-independent pathway is necessary for signaling in Drosophila wing discs. *Proceedings of the National Academy of Sciences of the United States of America*, *113*(45), E6993–E7002. https://doi.org/10.1073/pnas.1610565113

Herr, P., Hausmann, G., & Basler, K. (2012). WNT secretion and signalling in human disease. *Trends in Molecular Medicine*, *18*(8), 483–493. https://doi.org/10.1016/j.molmed.2012.06.008

Hinze, C., & Boucrot, E. (2018). Endocytosis in proliferating, quiescent and terminally differentiated cells. *Journal of Cell Science*, *131*(23), 1–10. https://doi.org/10.1242/jcs.216804

Hollstein, M., Sidransky, D., Vogelstein, B., & Curtis, C. (1991). p53 mutations in Human Cancers, (July), 49–54.

Hsiung, F., Ramirez-Weber, F. A., David Iwaki, D., & Kornberg, T. B. (2005). Dependence of Drosophila wing imaginal disc cytonemes on Decapentaplegic. *Nature*, *437*(7058), 560–563. https://doi.org/10.1038/nature03951

Hu, Y. B., Dammer, E. B., Ren, R. J., & Wang, G. (2015). The endosomal-lysosomal system: From acidification and cargo sorting to neurodegeneration. *Translational Neurodegeneration*, *4*(1), 1–10. https://doi.org/10.1186/s40035-015-0041-1

Huang, J., Papadopoulos, N., Mckinley, A. J., Farrington, S. M., Curtis, L. J., Wyllie, A. H., … Dunlop, M. G. (1996). APC mutations in colorectal tumors with mismatch repair deficiency. *Proceedings of the National Academy of Sciences of the United States of America*, *93*(17), 9049–9054. https://doi.org/10.1073/pnas.93.17.9049

Jho, E., Zhang, T., Domon, C., Joo, C.-K., Freund, J.-N., & Costantini, F. (2002). Wnt/β-Catenin/Tcf Signaling Induces the Transcription of Axin2, a Negative Regulator of the Signaling Pathway. *Molecular and Cellular Biology*, *22*(4), 1172–1183. https://doi.org/10.1128/mcb.22.4.1172-1183.2002

Ji, J., Feng, X., Shi, M., Cai, Q., Yu, Y., Zhu, Z., & Zhang, J. (2015). Rac1 is correlated with aggressiveness and a potential therapeutic target for gastric cancer. *International Journal of Oncology*, *46*(3), 1343–1353. https://doi.org/10.3892/ijo.2015.2836

Katanaev, V. L., Solis, G. P., Hausmann, G., Buestorf, S., Katanayeva, N., Schrock, Y., … Basler, K. (2008). Reggie-1/flotillin-2 promotes secretion of the long-range signalling forms of Wingless and Hedgehog in Drosophila. *EMBO Journal*, *27*(3), 509–521. https://doi.org/10.1038/sj.emboj.7601981

Kluger, H. M., Kluger, Y., Gilmore-Hebert, M., DiVito, K., Chang, J. T., Rodov, S., … Sapi, E. (2004). CDNA microarray analysis of invasive and tumorigenic phenotypes in a breast cancer model. *Laboratory Investigation*, *84*(3), 320–331. https://doi.org/10.1038/labinvest.3700044

Koch, S., Acebron, S. P., Herbst, J., Hatiboglu, G., & Niehrs, C. (2015). Post-transcriptional Wnt Signaling Governs Epididymal Sperm Maturation. *Cell*, *163*(5), 1225–1236. https://doi.org/10.1016/j.cell.2015.10.029

Komiya, Y., & Habas, R. (2008). Wnt signal transduction pathways, *4*(2), 68–75. Retrieved from www.landesbioscience.com

Kong, X., Wang, X., Yin, Y., Li, X., Gao, H., Bazer, F. W., & Wu, G. (2014). Putrescine stimulates the mTOR signaling pathway and protein synthesis in porcine trophectoderm cells. *Biology of Reproduction*, *91*(5), 1–10. https://doi.org/10.1095/biolreprod.113.113977

Lengauer, C., Kinzler, K. W., & Vogelstein, B. (1997). Genetic instability in colorectal cancers - Lengauer, Kinzler, Vogelstein.pdf. *Nature*, *15256*(1 995), 623–627.

Li, J., Yen, C., Liaw, D., Podsypanina, K., Bose, S., Wang, S. I., … Parsons, R. (1997). PTEN, a putative protein tyrosine phosphatase gene mutated in human brain, breast, and prostate cancer. *Science*, *275*(5308), 1943–1947. https://doi.org/10.1126/science.275.5308.1943

Linnemannstöns, K., Witte, L., Pradhipa Karuna, M., Kittel, J. C., Danieli, A., Müller, D., … Gross, J. C. (2020). Ykt6-dependent endosomal recycling is required for Wnt secretion in the Drosophila wing epithelium. *Development (Cambridge)*, *147*(15). https://doi.org/10.1242/dev.185421

Liu, X. xu, Liu, W. dong, Wang, L., Zhu, B., Shi, X., Peng, Z. xuan, … Ren, C. ping. (2018). Roles of flotillins in tumors. *Journal of Zhejiang University: Science B*, *19*(3), 171–182. https://doi.org/10.1631/jzus.B1700102

Lodish, H., Berk, A., Matsudiara, P., A, K. C., Kreiger, M., Scott, M. P., … Darnell, J. (2004). *Molecular Cell Biology*. *W.H. Freeman 5th Edition*. https://doi.org/10.18772/22008014655.9

Luo, J., Manning, B. D., & Cantley, L. C. (2003). Targeting the PI3K-Akt pathway in human cancer: Rationale and promise. *Cancer Cell*, *4*(4), 257–262. https://doi.org/10.1016/S1535-6108(03)00248-4

Lupashin, V. V., Pokrovskaya, I. D., McNew, J. A., & Waters, M. G. (1997). Characterization of a Novel Yeast SNARE Protein Implicated in Golgi Retrograde Traffic. *Molecular Biology of the Cell*, *8*(12), 2659–2676. https://doi.org/10.1091/mbc.8.12.2659

Malmersjö, S., Di Palma, S., Diao, J., Lai, Y., Pfuetzner, R. A., Wang, A. L., … Meyer, T. (2016a). Phosphorylation of residues inside the SNARE complex suppresses secretory vesicle fusion . *The EMBO Journal*, *35*(16), 1810–1821. https://doi.org/10.15252/embj.201694071

Malmersjö, S., Di Palma, S., Diao, J., Lai, Y., Pfuetzner, R. A., Wang, A. L., … Meyer, T. (2016b). Phosphorylation of residues inside the SNARE complex suppresses secretory vesicle fusion. *The EMBO Journal*, *35*(16), 1810–1821. https://doi.org/10.15252/embj.201694071

Mandal, S., Mandal, A., Johansson, H. E., Orjalo, A. V., & Park, M. H. (2013). Depletion of cellular polyamines, spermidine and spermine, causes a total arrest in translation and growth in mammalian cells. *Proceedings of the National Academy of Sciences of the United States of America*, *110*(6), 2169–2174. https://doi.org/10.1073/pnas.1219002110

Martin, R. L., Ilett, K. F., & Minchin, R. F. (1991). Cell cycle–dependent uptake of putrescine and its importance in regulating cell cycle phase transition in cultured adult mouse hepatocytes. *Hepatology*, *14*(6), 1243–1250. https://doi.org/10.1002/hep.1840140646

Matsui, T., Jiang, P., Nakano, S., Sakamaki, Y., Yamamoto, H., & Mizushima, N. (2018). Autophagosomal YKT6 is required for fusion with lysosomes independently of syntaxin 17. *The Journal of Cell Biology*, jcb.201712058. https://doi.org/10.1083/jcb.201712058

McGrath, K., Agarwal, S., Tonelli, M., Dergai, M., Gaeta, A. L., Shum, A. K., … Caraveo, G. (2021a). A conformational switch driven by phosphorylation regulates the activity of the evolutionarily conserved SNARE Ykt6. *Proceedings of the National Academy of Sciences of the United States of America*, *118*(12). https://doi.org/10.1073/pnas.2016730118

McNew, J. A., Søgaard, M., Lampen, N. M., Machida, S., Ye, R. R., Lacomis, L., … Söllner, T. H. (1997). Ykt6p, a prenylated SNARE essential for endoplasmic reticulum-golgi transport. *Journal of Biological Chemistry*, *272*(28), 17776–17783. https://doi.org/10.1074/jbc.272.28.17776

Meiringer, C. T. A., Auffarth, K., Hou, H., & Ungermann, C. (2008). Depalmitoylation of Ykt6 prevents its entry into the multivesicular body pathway. *Traffic*, *9*(9), 1510–1521. https://doi.org/10.1111/j.1600-0854.2008.00778.x

Mikels, A. J., & Nusse, R. (2006). Wnts as ligands: Processing, secretion and reception. *Oncogene*, *25*(57), 7461–7468. https://doi.org/10.1038/sj.onc.1210053

Morgan, D. O. (1995). Principles of CDK regulation. *Nature*, *374*(6518), 131–134. https://doi.org/10.1038/374131a0

Morris, S., Geoghegan, N. D., Sadler, J. B. A., Koester, A. M., Black, H. L., Laub, M., … Gould, G. W. (2020). Characterisation of GLUT4 trafficking in HeLa cells: Comparable kinetics and orthologous trafficking mechanisms to 3T3-L1 adipocytes. *PeerJ*, *2020*(3), 1–22. https://doi.org/10.7717/peerj.8751

Mulligan, K. A., Fuerer, C., Ching, W., Fish, M., Willert, K., & Nusse, R. (2012). Secreted Wingless-interacting molecule (Swim) promotes long-range signaling by maintaining Wingless solubility. *Proceedings of the National Academy of Sciences of the United States of America*, *109*(2), 370–377. https://doi.org/10.1073/pnas.1119197109

Naschberger, A., Orry, A., Lechner, S., Bowler, M. W., Nurizzo, D., Novokmet, M., … Rupp, B. (2017). Structural Evidence for a Role of the Multi-functional Human Glycoprotein Afamin in Wnt Transport. *Structure*, *25*(12), 1907-1915.e5. https://doi.org/10.1016/j.str.2017.10.006

Neumann, S., Coudreuse, D. Y. M., Van Der Westhuyzen, D. R., Eckhardt, E. R. M., Korswagen, H. C., Schmitz, G., & Sprong, H. (2009). Mammalian Wnt3a is released on lipoprotein particles. *Traffic*, *10*(3), 334–343. https://doi.org/10.1111/j.1600-0854.2008.00872.x

Niehrs, C., & Acebron, S. P. (2012). Mitotic and mitogenic Wnt signalling. *EMBO Journal*, *31*(12), 2705–2713. https://doi.org/10.1038/emboj.2012.124

Nuchel, J., Tauber, M., Nolte, J. L., Morgelin, M., Clara, T., Eckes, B., … Plomann, M. (2021). An mTORC1-GRASP55 signaling axis controls unconventional secretion to reshape the extracellular proteome upon stress, 1–19.

Nurse, P. (1990). Universal control mechanism regulating cell cycle timing of M-phase. *Nature*, *344*(April), 503–508. Retrieved from https://link.springer.com/content/pdf/10.1038/344503a0.pdf%0Ahttps://www.nature.com/articles/344503a0.pdf

Nurse, Paul. (2000). A long twentieth century of the cell cycle and beyond. *Cell*, *100*(1), 71–78. https://doi.org/10.1016/S0092-8674(00)81684-0

Nusse, R. (2005). Wnt signaling in disease and in development. *Cell Research*, *15*(1), 28–32. https://doi.org/10.1038/sj.cr.7290260

Ooe, A., Kato, K., & Noguchi, S. (2007). Possible involvement of CCT5, RGS3, and YKT6 genes up-regulated in p53-mutated tumors in resistance to docetaxel in human breast cancers. *Breast Cancer Research and Treatment*, *101*(3), 305–315. https://doi.org/10.1007/s10549-006-9293-x

Panáková, D., Sprong, H., Marois, E., Thiele, C., & Eaton, S. (2005). Lipoprotein particles are required for Hedgehog and Wingless signalling. *Nature*, *435*(7038), 58–65. https://doi.org/10.1038/nature03504

Park, M. H. (2006). The post-translational synthesis of a polyamine-derived amino acid, hypusine, in the eukaryotic translation initiation factor 5A (eIF5A). *Journal of Biochemistry*, *139*(2), 161–169. https://doi.org/10.1093/jb/mvj034

Pfeiffer, S., Ricardo, S., Manneville, J. B., Alexandre, C., & Vincent, J. P. (2002). Producing cells retain and recycle wingless in Drosophila embryos. *Current Biology*, *12*(11), 957–962. https://doi.org/10.1016/S0960-9822(02)00867-9

Port, F., & Basler, K. (2010). Wnt Trafficking: New Insights into Wnt Maturation, Secretion and Spreading. *Traffic*, *11*(10), 1265–1271. https://doi.org/10.1111/j.1600-0854.2010.01076.x

Port, F., Hausmann, G., & Basler, K. (2011). A genome-wide RNA interference screen uncovers two p24 proteins as regulators of Wingless secretion. *EMBO Reports*, *12*(11), 1144–1152. https://doi.org/10.1038/embor.2011.165

Port, F., Kuster, M., Herr, P., Furger, E., Bänziger, C., Hausmann, G., & Basler, K. (2008). Wingless secretion promotes and requires retromer-dependent cycling of Wntless. *Nature Cell Biology*, *10*(2), 178–185. https://doi.org/10.1038/ncb1687

Pradhipa Karuna, M., Witte, L., Linnemannstoens, K., Choezom, D., Danieli-Mackay, A., Honemann-Capito, M., & Gross, J. C. (2020). Phosphorylation of ykt6 snare domain regulates its membrane recruitment and activity. *Biomolecules*, *10*(11), 1–19. https://doi.org/10.3390/biom10111560

Pylypenko, O., Schönichen, A., Ludwig, D., Ungermann, C., Goody, R. S., Rak, A., & Geyer, M. (2008). Farnesylation of the SNARE Protein Ykt6 Increases Its Stability and Helical Folding. *Journal of Molecular Biology*, *377*(5), 1334–1345. https://doi.org/10.1016/j.jmb.2008.01.099

Rabouille, C. (2017). Pathways of Unconventional Protein Secretion. *Trends in Cell Biology*, *27*(3), 230–240. https://doi.org/10.1016/j.tcb.2016.11.007

Raposo, G., & Stoorvogel, W. (2013). Extracellular vesicles: Exosomes, microvesicles, and friends. *Journal of Cell Biology*, *200*(4), 373–383. https://doi.org/10.1083/jcb.201211138

Ray, R. M., Zimmerman, B. J., Mccormack, S. A., Patel, T. B., & Johnson, L. R. (1999). Polyamine depletion arrests cell cycle and induces inhibitors p21(Waf1)/(Cip1), p27(Kip1), and p53 in IEC-6 cells. *American Journal of Physiology - Cell Physiology*, *276*(3 45-3). https://doi.org/10.1152/ajpcell.1999.276.3.c684

Ren, R., Sun, H., Ma, C., Liu, J., & Wang, H. (2019). Colon cancer cells secrete exosomes to promote self-proliferation by shortening mitosis duration and activation of STAT3 in a hypoxic environment. *Cell and Bioscience*, *9*(1), 1–9. https://doi.org/10.1186/s13578-019-0325-8

Rhind, N., & Russell, P. (2012). Signaling pathways that regulate cell division. *Cold Spring*

Harbor Perspectives in Biology, *4*(10), 1–16. https://doi.org/10.1101/cshperspect.a005942

Rossi, V., Banfield, D. K., Vacca, M., Dietrich, L. E. P., Ungermann, C., D'Esposito, M., … Filippini, F. (2004). Longins and their longin domains: Regulated SNAREs and multifunctional SNARE regulators. *Trends in Biochemical Sciences*, *29*(12), 682–688. https://doi.org/10.1016/j.tibs.2004.10.002

Ruiz-Martinez, M., Navarro, A., Marrades, R. M., Viñolas, N., Santasusagna, S., Muñoz, C., … Monzo, M. (2016). YKT6 expression, exosome release, and survival in non-small cell lung cancer. *Oncotarget*, *7*(32), 51515–51524. https://doi.org/10.18632/oncotarget.9862

Sager, R. (1986). Genetic Suppression of Tumor Formation: A New Frontier in Cancer Research. *Cancer Research*, *46*(4), 1573–1580.

Saito, Y., Li, L., Coyaud, E., Luna, A., Sander, C., Raught, B., … Muthuswamy, S. K. (2019a). LLGL2 rescues nutrient stress by promoting leucine uptake in ER+ breast cancer. *Nature*, *569*(7755), 275–279. https://doi.org/10.1038/s41586-019-1126-2

Sakata, N., Shirakawa, R., Goto, K., Trinh, D. A., & Horiuchi, H. (2021). Double prenylation of SNARE protein Ykt6 is required for lysosomal hydrolase trafficking. *Journal of Biochemistry*, *169*(3), 363–370. https://doi.org/10.1093/jb/mvaa111

Sanchez-Vega, F., Mina, M., Armenia, J., Chatila, W. K., Luna, A., La, K. C., … Schultz, N. (2018). Oncogenic Signaling Pathways in The Cancer Genome Atlas. *Cell*, *173*(2), 321-337.e10. https://doi.org/10.1016/j.cell.2018.03.035

Sanderfoot, A. A., & Raikhel, N. V. (1999). The specificity of vesicle trafficking: Coat proteins and SNAREs. *Plant Cell*, *11*(4), 629–641. https://doi.org/10.1105/tpc.11.4.629

Senturk, E., & Manfredi, J. J. (2013). P53 and cell cycle effects after DNA damage. *Methods in Molecular Biology*, *962*(1), 49–61. https://doi.org/10.1007/978-1-62703-236-0_4

Sever, R., & Brugge, J. S. (2015). Signal transduction in cancer. *Cold Spring Harbor Perspectives in Medicine*, *5*(4). https://doi.org/10.1101/cshperspect.a006098

Shirakawa, R., Goto-Ito, S., Goto, K., Wakayama, S., Kubo, H., Sakata, N., … Horiuchi, H. (2020). A SNARE geranylgeranyltransferase essential for the organization of the Golgi apparatus . *The EMBO Journal*, *39*(8), 1–20. https://doi.org/10.15252/embj.2019104120

Steck, P. A., Pershouse, M. A., Jasser, S. A., Yung, W. K. A., Lin, H., Ligon, A. H., … Tavtigian, S. V. (1997). Identification of a candidate tumour suppressor gene, MMAC1, at chromosome 10q23.3 that is mutated in multiple advanced cancers. *Nature Genetics*, *15*(april), 356–362.

Stephen Paget. (1889). THE DISTRIBUTION OF SECONDARY GROWTHS IN CANCER OF THE BREAST. *The Lancet*, *7*(3), 91–93. https://doi.org/10.1007/s12307-014-0163-5

Strigini, M., & Cohen, S. M. (2000). Wingless gradient formation in the Drosophila wing. *Current Biology*, *10*(6), 293–300. https://doi.org/10.1016/S0960-9822(00)00378-X

Sutton, R. B., Fasshauer, D., Jahn, R., & Brunger, A. T. (1998). Crystal structure of a SNARE complex involved in synaptic exocytosis at 2.4 A resolution. *Nature*, *395*(September), 347–353.

Takáts, S., Glatz, G., Szenci, G., Boda, A., Horváth, G. V., Hegedűs, K., … Juhász, G. (2018). Non-canonical role of the SNARE protein Ykt6 in autophagosome-lysosome fusion. *PLoS Genetics*, *14*(4), 1–23. https://doi.org/10.1371/journal.pgen.1007359

Thayanidhi, N., Liang, Y., Hasegawa, H., Nycz, D. C., Oorschot, V., Klumperman, J., & Hay,

J. C. (2012). R-SNARE ykt6 resides in membrane-associated protease-resistant protein particles and modulates cell cycle progression when over-expressed. *Biology of the Cell*, *104*(7), 397–417. https://doi.org/10.1111/boc.201100048

Thomas, G. M., Frame, S., Goedert, M., Nathke, I., Polakis, P., & Cohen, P. (1999). A GSK3-binding peptide from FRAT1 selectively inhibits the GSK3-catalysed phosphorylation of Axin and β-catenin. *FEBS Letters*, *458*(2), 247–251. https://doi.org/10.1016/S0014-5793(99)01161-8

Tochio, H., Tsui, M. M. K., Banfield, D. K., & Zhang, M. (2001). An autoinhibitory mechanism for nonsyntaxin SNARE proteins revealed by the structure of Ykt6p. *Science*, *293*(5530), 698–702. https://doi.org/10.1126/science.1062950

Uemura, T., Yerushalmi, H. F., Tsaprailis, G., Stringer, D. E., Pastorian, K. E., Hawel, L., … Gerner, E. W. (2008). Identification and characterization of a diamine exporter in colon epithelial cells. *Journal of Biological Chemistry*, *283*(39), 26428–26435. https://doi.org/10.1074/jbc.M804714200

Ungar, D., & Hughson, F. M. (2003). SNARE Protein Structure and Function. *Annual Review of Cell and Developmental Biology*, *19*, 493–517. https://doi.org/10.1146/annurev.cellbio.19.110701.155609

Ungermann, C., Von Mollard, G. F., Jensen, O. N., Margolis, N., Stevens, T. H., & Wickner, W. (1999). Three v-SNAREs and Two t-SNAREs, Present in a Pentameric cis-SNARE Complex on Isolated Vacuoles, Are Essential for Homotypic Fusion. *The Journal of Cell Biology*, *217*(10), 3656–3669. https://doi.org/10.1083/jcb.201804028

Urbé, S., Mills, I. G., Stenmark, H., Kitamura, N., & Clague, M. J. (2000). Endosomal Localization and Receptor Dynamics Determine Tyrosine Phosphorylation of Hepatocyte Growth Factor-Regulated Tyrosine Kinase Substrate. *Molecular and Cellular Biology*, *20*(20), 7685–7692. https://doi.org/10.1128/mcb.20.20.7685-7692.2000

Van Niel, G., D'Angelo, G., & Raposo, G. (2018). Shedding light on the cell biology of extracellular vesicles. *Nature Reviews Molecular Cell Biology*, *19*(4), 213–228. https://doi.org/10.1038/nrm.2017.125

Veit, M. (2004). The human SNARE protein Ykt6 mediates its own palmitoylation at C-terminal cysteine residues. *Biochemical Journal*, *384*(2), 233–237. https://doi.org/10.1042/bj20041474

Wade Harper, J., Adami, G. R., Wei, N., Keyomarsi, K., & Elledge, S. J. (1993). The p21 Cdk-interacting protein Cip1 is a potent inhibitor of G1 cyclin-dependent kinases. *Cell*, *75*(4), 805–816. https://doi.org/10.1016/0092-8674(93)90499-G

Wang, C., Ruan, P., Zhao, Y., Li, X., Wang, J., Wu, X., … Xie, S. (2017). Spermidine/spermine N1-acetyltransferase regulates cell growth and metastasis via AKT/β-catenin signaling pathways in hepatocellular and colorectal carcinoma cells. *Oncotarget*, *8*(1), 1092–1109. https://doi.org/10.18632/oncotarget.13582

Weng, J., Yang, Y., & Wang, W. (2015). Lipid regulated conformational dynamics of the longin SNARE protein Ykt6 revealed by molecular dynamics simulations. *Journal of Physical Chemistry A*, *119*(9), 1554–1562. https://doi.org/10.1021/jp5075708

Wiese, K. E., Nusse, R., & van Amerongen, R. (2018). Wnt signalling: Conquering complexity. *Development (Cambridge)*, *145*(12), 1–9. https://doi.org/10.1242/dev.165902

Xi, Y., Ju, R., & Wang, Y. (2020). Roles of Annexin A protein family in autophagy regulation and therapy. *Biomedicine and Pharmacotherapy*, *130*(August), 110591. https://doi.org/10.1016/j.biopha.2020.110591

Yan, D., & Lin, X. (2009). Shaping morphogen gradients by proteoglycans. *Cold Spring Harbor Perspectives in Biology*, *1*(3), 1–17. https://doi.org/10.1101/cshperspect.a002493

Yang, Z., Yan, G., Zheng, L., Gu, W., Liu, F., Chen, W., … Xu, X. (2021). YKT6 , as a potential predictor of prognosis and immunotherapy response for oral squamous cell carcinoma, is related to cell invasion, metastasis, and CD8+ T cell infiltration . *OncoImmunology*, *10*(1), 1938890. https://doi.org/10.1080/2162402x.2021.1938890

Yuan, H. X., Xiong, Y., & Guan, K. L. (2013). Nutrient Sensing, Metabolism, and Cell Growth Control. *Molecular Cell*, *49*(3), 379–387. https://doi.org/10.1016/j.molcel.2013.01.019

Zhai, L., Chaturvedi, D., & Cumberledge, S. (2004). Drosophila Wnt-1 undergoes a hydrophobic modification and is targeted to lipid rafts, a process that requires porcupine. *Journal of Biological Chemistry*, *279*(32), 33220–33227. https://doi.org/10.1074/jbc.M403407200

Zhang, P., Wu, Y., Belenkaya, T. Y., & Lin, X. (2011). SNX3 controls Wingless/Wnt secretion through regulating retromer-dependent recycling of Wntless. *Cell Research*, *21*(12), 1677–1690. https://doi.org/10.1038/cr.2011.167

Zimmermann, P., Zhang, Z., Degeest, G., Mortier, E., Leenaerts, I., Coomans, C., … David, G. (2005). Syndecan recyling is controlled by syntenin-PIP2 interaction and Arf6. *Developmental Cell*, *9*(3), 377–388. https://doi.org/10.1016/j.devcel.2005.07.011

Abbreviations

µg	microgram
µl	microliter
AKAP12	A-kinase anchor protein 12
Akt/PKB	serine/threonine-protein kinase
AP2	Activator Protein 2
APC	Adenomatous polyposis coli
Atg1	Autophagy-related protein
ATPase	Adenosine triphosphate
BSA	Bovine serum albumin
C. *elegans*	*Caenorhabditis elegans*
CD	Cluster of differentiation
CDK	Cell-cycle dependent kinase
CDKN1A	Cyclin Dependent Kinase Inhibitor 1A
CPA4	Carboxypeptidase A4
Cys	Cysteine
DAPI	4’,6’–Diamidino-2-phenylindole
DMEM	Dulbecco’s Modified Eagle Medium
DNA	Deoxyribonucleic acid
EE	Early endosome
elf5A	eukaryotic translation initiation factor 5A
ER	Endoplasmic reticulum
ESCRT	Endosomal sorting complexes required for transport
EV	Extracellular vesicle
FACS	Fluorescence-activated cell sorting
FBS	Fetal bovine serum
FITC	Fluorescein isothiocyanate
FTL	Ferritin Light Chain
GMPPA	GDP-Mannose Pyrophosphorylase A
GSK3	Glycogen synthase kinase 3
GTPase	Guanosine triphosphate

h	hours
HINT1	Histidine Triad Nucleotide Binding Protein 1
HRS	Hepatocyte growth factor-regulated tyrosine kinase substrate
IFI6	Interferon Alpha Inducible Protein 6
ISG15	Interferon-stimulated gene 15
KD	Knockdown
kDa	Kilodalton
LE	Late endosome
LLG2	LLGL Scribble Cell Polarity Complex Component 2
LRP5/6	Lipoprotein receptor-related protein 6
Marcks	Myristoylated alanine-rich C-kinase substrate
min	minutes
mTOR	Mammalian target of rapamycin
MVB	Multi-vesicular body
NFkB	Nuclear factor ‘kappa-light-chain-enhancer’ of activated B-cells
Nrf2	Nuclear factor-erythroid factor 2-related factor 2
PBS	Phosphate-buffered saline
PH	Pleckstrin homology
PI3K	Phosphatidylinositol 3-kinase
PIP2	Phosphatidylinositol-4,5-bisphosphate
PIP3	Phosphatidylinositol-3,4,5-trisphosphate
PKC	Protein kinase C
PM	Plasma membrane
PRSS3	Serine Protease 3
PTEN	Phosphatase and Tensin Homolog deleted on Chromosome 10
Rac-1	Ras-related C3 botulinum toxin substrate 1
RalA	Ras-related protein Ral-A
Ras	Rat sarcoma virus
RPL13A	Ribosomal Protein L13a
RT	Room Temperature
Rtk	Receptor Tyrosine Kinase

SET	SET Nuclear Proto-Oncogen
siRNA	Small interfering RNA
SLC7A5	Solute Carrier Family 7 Member 5
Snap29	Synaptosome Associated Protein 29
SNARE	Soluble N-ethylmaleimide-sensitive-factor attachment receptor
SNX3	Sorting nexin-3
STMN1	Stathmin 1
Stx17	Syntaxin 17
TCF/LEF	T cell factor/lymphoid enhancer factor family
TGFβ	Transforming growth factor beta
TNFα	Tumor-necrosis factor α
Tsg101	Tumor Susceptibility 101
TSPAN3	Tetraspanin 3
UT	Untreated
VAMP7	Vesicle Associated Membrane Protein 7
VPS	Vacuolar protein sorting
VTPase	Vacuolar-type ATPase
Wg	Wingless
Wnt	Wingless-related integration site
Wnt/STOP	Wnt-dependent stabilization of protein